EDUCACIÓN
SECRETARÍA DE EDUCACIÓN PÚBLICA

TECNOLÓGICO NACIONAL DE MÉXICO

Tecnológico Nacional de México

Centro Nacional de Investigación y Desarrollo Tecnológico

Tesis de Doctorado

Modelación numérica de una habitación con una ventana con cubierta de material de cambio de fase

presentada por

Miguel Ángel Ché Pan

como requisito para la obtención del grado de

Doctor en Ciencias en Ingeniería Mecánica

Director de tesis

Dr. Efrain Simá Moo

Cuernavaca, Morelos, México. Junio de 2023.

cenidet
Centro Nacional de Investigación y Desarrollo Tecnológico

Cuernavaca, Mor., 03/agosto/2023
No. De Oficio: SAC/125/2023
Asunto: Autorización de impresión de tesis

MIGUEL ÁNGEL CHE PAN
CANDIDATO AL GRADO DE DOCTOR EN CIENCIAS
EN INGENIERÍA MECÁNICA
P R E S E N T E

Por este conducto, tengo el agrado de comunicarle que el Comité Tutorial asignado a su trabajo de tesis titulado **"Modelación numérica de una habitación con una ventana con cubierta de material de cambio de fase"**, ha informado a esta Subdirección Académica, que están de acuerdo con el trabajo presentado. Por lo anterior, se le autoriza a que proceda con la impresión definitiva de su trabajo de tesis.

Esperando que el logro del mismo sea acorde con sus aspiraciones profesionales, reciba un cordial saludo.

A T E N T A M E N T E
Excelencia en Educación Tecnológica®
"Conocimiento y tecnología al servicio de México"

EDUCACIÓN | TECNOLÓGICO NACIONAL DE MÉXICO
CENTRO NACIONAL DE INVESTIGACIÓN Y DESARROLLO TECNOLÓGICO
SUBDIRECCIÓN ACADÉMICA

CARLOS MANUEL ASTORGA ZARAGOZA
SUBDIRECTOR ACADÉMICO

C. c. p. Departamento de Ingeniería Mecánica
Departamento de Servicios Escolares

CMAZ/lmz

Centro Nacional de Investigación
y Desarrollo Tecnológico
Departamento de Ingeniería Mecánica

Cuernavaca, Mor., a 31 de julio de 2023

DR. CARLOS MANUEL ASTORGA ZARAGOZA
SUBDIRECTOR ACADÉMICO
PRESENTE

AT'n: DR. JORGE COLÍN OCAMPO
PRESIDENTE DEL CLAUSTRO DOCTORAL
DEL DEPARTAMENTO DE ING. MECÁNICA

Los abajo firmantes, miembros del Comité Tutorial del estudiante **Miguel Ángel Che Pan** manifiestan que después de haber revisado el documento de tesis titulado **"Modelación numérica de una habitación con una ventana con cubierta de material de cambio de fase"** realizado bajo la dirección Dr. Efraín Simá Moo, el trabajo se ACEPTA para proceder a su impresión.

ATENTAMENTE

DRA. YVONNE CHÁVEZ CHENA
CENIDET

DR. JESÚS ARCE LANDA
CENIDET

DR. MIGUEL ANGEL CHAGOLLA ARANDA
CENIDET

DRA. IVETT ZAVALA GUILLÉN
CICESE

DR. EFRAÍN SIMÁ MOO
CENIDET

c.c.p: Mtra. Ma. Elena Gómez Torres Jefa del Departamento de Servicios Escolares
c.c.p: Dr. Carlos Manuel Astorga Zaragoza Subdirector Académico
c.c.p: Expediente

Acknowledgement

To Consejo Nacional de Humanidades Ciencia y Tecnloogía (CONAHCyT) for the financial support provided.

Especially to my thesis advisor:

Jesus Perfecto Xamán Villaseñor †

For taking a leap of faith and giving me the opportunity to work under your tutelage. I will always be thankful for genuinely wanting for us your students to grow and become the best we could be. Despite always being busy, thank you for always taking the time to advise me and chat with me until night fell. I'm not sure if you considered me a friend, or if I was worthy, but, the one thing I'm certain of, is that I miss you...

*To my **mother** and **sisters** for their unconditional support at all stages of my life.*

*To my beloved **wife** for constantly bringing out the best of me. For her advises, support and love, and for making me a father of a beautiful child.*

To my friends from the lab who gave their support and help at time of joy and difficulty.

To the thesis advisor and reviewers, for their comments and suggestions throughout this project.

To Mrs. Rocío, who always did what was in her hands to help us.

To Centro Nacional de Investigación y Desarrollo Tecnológico (CENIDET), for giving me the opportunity to obtain my Ph.D grade.

Contents

Figures

Tables

Nomenclature

Symbol	Description
H	Length of the window system, m
G	Solar Irradiance, W m^{-2}
a_E, a_W, a_N, a_s, a_P	Discretized equation coefficients
b	independent term of the discretized equation
D_e, D_w, D_n, D_s	Diffusive fluxes, Kg m^{-1} s^{-1}]
F_e, F_w, F_n, F_s	Convective fluxes, Kg m^{-2} s^{-1}
J_e, J_w, J_n, J_s	Total fluxes,
S	Source term
P	Pressure, Pa
Pe	Peclet number
Pr	Prandtl number
C_P	Specific heat, J kg^{-1} C^{-1}
h_{out}	Outdoor convective heat transfer coefficient, W $m^{-2}K^{-1}$
h_{int}	Indoor convective heat transfer coefficient, W $m^{-2}K^{-1}$
q	Heat flux, W m^{-2}
S_g	Extinction coefficient, m^{-1}
T	Temperature, C
T_{amb}	Ambient temperature, K
T_g	Glass temperature, C
T_{PCM}	PCM temperature, C
T_{roof}	Roof temperature, C
T_{room}	Room temperature, C
T_{floor}	Floor temperature, C
T_{ground}	Ground temperature, C
T_{W2}	West wall temperature, C
T_{W3}	North wall temperature, C
T_{W3}	East wall temperature, C
t	Time, s

Symbol	Description
u, v	Components of velocity, $m\ s^{-1}$
x, y	Coordinates, m
dx, dy	Differential terms
N_x, N_y	Computational nodes
Greek	
α^*	Absortivity
ρ^*	Reflectivity
β	Thermal expansion coefficient
ε	Emisivity
Δ_t	Time step, s
Θ	Glass attenuation function
λ	Thermal conductivity, W $m^{-1}K^{-1}$
δx	Gap between nodes in the x axis
δy	Gap between nodes in the y axis
Δx	Thickness of the control volume in the x axis
Δy	Thickness of the control volume in the y axis
Γ	Diffusive transport coefficient
ϕ	Unknown variable
Subscrits	
$Cond$	Conduction
$Conv$	Convection
Int	Indoor
Out	Outdoor
Rad	Radiation
g	Glass
PCM	Phase Change Material

Abstract

In this research work the study of the thermal performance of a PCM shutter implemented in a window and how it affects the temperatures inside a room was carried out. A hybrid mathematical model was used to perform the evaluation where the mathematical model of the proposed window with the phase change material shading was solved using computational fluid dynamics whereas the mathematical model of the cavity representative of the room was developed by means of global energy balances.

The proposed system was subjected to the climate conditions of Mérida Yucatán in the Mexican Republic and the obtained results were compared against a conventional window thermal performance. For the study, the warmest and coldest day of each month of the year were selected to model the proposed system. The starting time for the simulations were between 05:00 to 07:00 hours and they extended up to 24:00 hours. It is worth mentioning that the starting hour of the simulations varied depending when the solar radiation started in each of the selected days. It was carried out this way to reduce the computational time load, and because at hours without solar radiation at the beginning of the day, variations in the ambient temperature are not significant. However, at hours without solar radiation during the night, the simulations continued in order to verify the effectiveness of the delay in the thermal inertia caused by the use of the PCM shutter.

The results showed that the behavior of the temperatures of the window with the PCM shutter compared to those of the conventional window, as well as the temperatures inside the room; were very similar regardless of the season of the year or whether it was the hottest or coldest day of the season. For all the analyzed days the heat fluxes showed a tendency to be linear when the PCM shutter was implemented, preventing the energy from flowing towards the outside ambient, provoking a rise in the temperatures in the inner surface of the window and in the room. Therefore, it was concluded that: the PCM shutter alone cannot benefit the temperatures inside the room since the rest of the room envelope elements showed higher temperatures than the window system for all the analyzed day and in both cases under study. However, because of the thermal storage capability of the PCM, although it raised the temperatures in the room and inner surface of the window, it shows to be a promising implementation as a shutter since it did reduce the total heat fluxes by around 87%. Therefore, its adequate implementation is worth to be further investigated.

Chapter 1

Introduction

The use of non-renewable energies such as fossil fuels which pollute the planet has taken a negative impact on the environment. Global warming and climate change that human kind has experienced worldwide over the last decades, are caused mainly by the greenhouse gases produced by burning fossil fuels. In recent decades particularly in the field of housing, energy consumption for air conditioning has greatly increased greatly due to the climatic changes experienced by our planet. According to the national energy balance conducted by the Ministry of Energy of México (SENER) in 2020 the residential sector consumed 21.90% of the total energy worldwide. In México, this sector represents 24.54% of the total production, and part of this consumption is destined for air conditioning systems **[1]**. These systems improve the thermal comfort inside buildings since approximately 70% of the Mexican territory has a warm climate (CONABIO) **[2]**, which negatively affects thermal comfort. The idea of using environmentally friendly systems in buildings that work with solar energy, arises to prevent the use of these air conditioning systems. The solar energy can be exploited by implementing passive solar systems. Among passive solar technologies, there are techniques focused on bioclimatic architecture. Bioclimatic architecture consists of designing the components of the building envelope (roof, walls, windows, floor) by taking advantage of the naturally available resources, such as solar radiation, vegetation, rain, wind, and considering the weather conditions. Consequently, research and investigation proposals focused on the study of building components for energy saving and its efficient use are topics of interest in the scientific field.

Among the different techniques focused on walls exist the Trombe walls, ventilated walls, double skin facades with plants, etc. **[3-6]** Also, there are techniques for ceilings, for example, ventilated roofs, green roofs, reflective roofs, photovoltaic roofs, composite ceilings with radiative transmitting barrier and evaporative roof cooling systems and the use of hollow block for roof construction **[7-13]**. Among the different passive technologies used in windows are double-glazed windows, low emissivity, and reflective glass, with solar control film, among others **[14-19]**. The windows and glass technologies have been investigated and developed to reduce room energy gains and losses. Some examples of the developed technologies are air gel, prismatic, vacuuming glasses, and phase change materials **[20]**. Recently the interest in using phase change material (PCM) has emerged since these materials can retain or store energy during the phase change process, which causes a delay in the energy that enters the building. Later, the stored energy is released when the weather conditions change during the day and night. Therefore, the use of

phase change materials is a viable alternative for thermal control in building envelopes, as well as in their internal components [**21, 22**].

The implementation of PCM in windows has been widely studied over the last decades, showing favorable results in its thermal performance. For example, **Ismail and Henriquez** [**23**] performed an experimental-theoretical study of a double glass window filled with a PCM in the space between the glass sheets. The results showed a decrease in the transmitted energy through the window with the PCM. Other investigations about the implementation of PCM in windows are parametric studies in which the characterization of the thermal properties, as well as the thickness and the type of PCMs, were varied to find the optimal values for each case of study. Also, there were comparisons of the thermal performance of windows filled with PCM against windows filled with absorbent gases and the optical properties of PCM glazed systems were also investigated [**24-30**].

Dong Li et al. [**31**] conducted a numerical study on the energy consumption of windows that contain nano-PCMs. The results show that the minimum energy consumption is obtained with a 1% concentration of 100 *nm* diameter nanoparticles. That same year these authors studied [**32**] the thermal and optical performance of a window filled with PCM nanoparticles. The results showed that the performance of a window filled with PCM paraffin dispersed in nanoparticles is more efficient than pure paraffin, regardless of the nanoparticle type. Another experimental study of a PCM-filled glaze's thermal and optical performance and its comparison with an air-filled glaze was carried out by **Chagyu Liu et al.** [**33**]. The results showed that the performance of a PCM-filled glaze improved, compared to the one filled with air and that the glass transmittance is 50% when the PCM is in the liquid state. That same year **Changyu Liu et al.** [**34**] developed a numerical model to determine the thermal and optical performance of a roof with multiple layers of PCM-filled glazing. The results showed that a 12-20 *mm* PCM thickness and 16-18 °C melting temperature are recommended when the influence of the design parameters of the PCM is considered on the thermal and optical performance of the glazed roof.

Based on what has been described above, PCMs and their different applications in glazing show promising results in terms of their thermal performance and the regulation of thermal comfort in buildings. However, the studies mentioned show the application of encapsulated PCMs between glasses, not as a shade, curtain, or window shutter. Considering that a partially open window shutter shows an increase in heat gain from 11.15 to 73.4% compared to a window with the blind fully closed and that it is more efficient to keep the blind completely closed using artificial lighting in the room [**35**], the applications of the PCMs as a filling for curtains or window shutters (shutter-PCM) look promising. However, the concept of shutter-PCM is yet to be studied in depth, and investigation in this direction is scarce.

Among the investigations carried out to study the thermal performance of a window shutter-PCM, **Alawadhi [36]**, reported a pioneering investigation of a two-dimensional model of a window with a PCM shutter whose numerical solution was obtained using the finite element method. The system's geometry consisted of a glass sheet in contact with the outside environment, an air gap, and the blind/shutter filled with a PCM in contact with the environment inside the room. The results showed that heat gain through the window was reduced by 23.3% when the blind had 0.03 *mm* thick PCM (P116). There is also the numerical analysis performed by **Wang and Zhao [37]**, who proposed a window system with an internal curtain containing a PCM. The authors used two PCMs, the RT28 paraffin, and the n-eicosane, with melting temperatures of 28 °C and 37 °C, respectively. Also, the authors proposed to use two virtual PCMs with the same thermophysical properties as the RT28 by changing their melting temperature to 29 (PCM29) and 30 °C (PCM30). The results showed that with a glass-curtain gap of 5 *cm*, the 5 *mm* thickness PCM29 had the best thermal performance because it reduced the energy gain by 16.2%, concluding that the melting temperature of the material plays a vital role in its performance. **Silva et al. [38]** experimentally analyzed the thermal performance of a window blind with a PCM subjected to the Mediterranean summer climate. A test box was built with a 7 *m* length, 2.35 *m* width, and 2.58 *m* height. The test box was divided into two compartments with the exact dimensions, with thermally insulated ceilings and walls and two windows on the south face of each compartment. The blind/shutter system was made of hollow aluminum blades behind a double glass window. Both glass sheets were 5 *mm* thick, and the space between them was 12 *mm*, with dimensions of 1.8 *m* long and 2.28 *m* high, with the difference that the aluminum blades contained a PCM in one compartment. The PCM used was the organic paraffin RT28HC. The results observed that the compartment with PCM reduced the maximum and minimum temperature values by 6 and 11% compared to the compartment without PCM. It was concluded that PCM is an alternative for thermal conditioning inside buildings. That same year **Silva et al. [39]** extended the analysis for a winter period in the Mediterranean. The results showed that the compartment with the PCM reached a maximum temperature reduction of 90% during the period in which the PCM stores' energy.

On the other hand, when the exterior and interior temperature fall below the solidification temperature of the PCM, it releases the stored energy and reduces the interior temperature by 35%. In 2016, **Silva et al. [40]** conducted a theoretical-experimental study of the thermal behavior of a window blind/shutter containing a PCM. A two-compartment test chamber was constructed, both with the exact dimensions. Aluminum blinds/shutters were installed in both compartments with the difference that in one of them, the blind/shutter was filled with a PCM, and in the other compartment, the blind is hollow (reference). Two theoretical models were presented, one for each compartment. The results showed that the maximum temperature differences between the numerical and experimental data for both compartments were 2.97 and 3.54 °C (a compartment with a PCM and reference, respectively). Also, the average temperature

inside the reference compartment varies from 15 to 46 °C and 18 to 42 °C for the PCM compartment. The authors concluded that the PCM compartment improved by regulating the indoor temperature by 8.7% for the warm-up period and 16.7% for the night period. In 2017 **Li et al.** [**41**] theoretically studied the heat transfer in an integrated double skin façade and a PCM blind system using the ANSYS Workbench software. The authors compared their proposed system with a conventional aluminum blind system. Their results showed that the proposed system was able to reduce the average air temperature and outlet temperature while improving the convective heat transfer between the cavity air and the blades. Also, compared with the aluminum blind, the PCM blind can absorb a large amount of excessive heat in the cavity. Later in 2019 **Li et al.** [**42**] extended their study by experimentally evaluating the integrated double skin façade and a PCM blind system. The authors developed a novel laminated composite phase change material (PCM) blind system with high thermal energy storage capacity and applied it in a typical double skin facade building. The results showed that the integrated PCM blind system was able to keep the average air temperature in the DSF below 35 °C during the monitored period in summer and showed no significant increase as compared with the ambient temperature. The surface temperature of the inner skin of the DSF was also reduced up to about 2.9 °C as compared with the external skin surface temperature thus reducing heat transfer into the building.

In recent years the PCM glazing researches have been focusing in the evaluation of multiple glazing windows filled with translucent PCM under different weather conditions [**43,45**], the effect of nanoparticles on the thermophysical and optical properties of nano-enhanced PCM [**46**], among other investigations [**47**]**.**

Based on the previous review, the studies regarding the use of PCM in curtains, blinds, or shaders for windows have slowed down. Since shutters can reduce heat gains on their own [**35**], the integration of PCM into the shutters seems promising for building energy savings. However, the double skin facades could be high cost. Therefore, the implementation of the PCM in a regular shutter could be more suitable for developing countries with warm climates such as México. Also, for building already built, in which the envelope materials were not suitable for the warm climate of México; the implementation of the PCM as a shutter is an alternative by installing it in front of the already existing window, without modifying its structure or the building. However, most studies that analyzed the thermal performance of a window shutter with a PCM, did not consider the interaction of the proposed system with the inside air of the cavity which is also interacting with the weather conditions thorough the envelope components [**36,37**] and regarding the experimental cases [**38-40**], the test boxes were insulated so the interactions of the weather conditions with the cavity and the proposed system were not taken into account. Hence, computational fluid dynamics, using the finite volume method and the cavity that represents the room and its envelope components were solved by the implementation of the global energy balance method. Also, additional to the studies carried out by **Alawadhi** [**36**] and **Wang and**

Zhao [**37**], among others, the present study considers the PCM filled shutter placed in the exterior of the proposed system, in contact with the outside ambient. The present investigation also takes into account the surface radiative exchange occurring within the air cavity in the window shutter-PCM system; additionally, the proposed system was coupled to a room in order to evaluate the effect of the use of the PCM on the room. The configuration that forms the window with the PCM had a configuration similar to that of the double window and the heat transfer modeling was carried out considering the glass sheet, the cover and the air trapped between them. Inside the room the effect of natural convection was considered. So that the complete system is made up of a room-window-PCM. The thermal evaluation was carried out under conditions of the warm weather of Mérida, Yucatán of the Mexican Republic. The thesis project was carried out in the facilities of the Department of Mechanical Engineering (DIM) of Cenidet and the infrastructure available in the DIM were used. The results were also compared with a typical window (transparent glass sheet).

1.1 Literature review

A bibliographic review of the studies done on thermal performance analysis of windows was carried out, as well as the implementation of a shading cover with phase change materials (PCM) to windows for use in rooms or buildings. The studies in which the windows are coupled to a room were also reviewed. These studies are relatively recent, and their data sheet is shown in the Appendix A **[15-65]**. Based on the literature review carried out, it was observed that there are several, numerical, experimental, or full-scale research for the thermal performance of several window configurations in which a phase change material was implemented, as well as studies of the coupling of a window with a room. However, to the date in the reported literature only in 10% of the studies, the PCM is encapsulated in a shutter, so this implementation needs to be further investigated. Also, there is still no history of studies carried out for the coupling of a window in which a PCM is implemented as a shader (window shutter) to a room under climatic conditions of the Mexican Republic. Furthermore, in the experimental studies in which a window with a PCM shutter is implemented in a chamber representing a room, the elements of the envelope (roof, walls, etc.) are insulated, so the energy provided by these elements to the room temperature was not taken into consideration when the evaluation of the thermal performance of the PCM shutter was carried out [**38-40**].

1.2 Goal

To study and analyze the heat transfer in a room coupled to a window with a shutter filled with a phase change material under warm weather conditions of the Mexican Republic.

1.3 Specific goals

1. To develop and implement a numerical code to simulate the transient heat transfer in a room coupled to a window with glazed elements.
2. To develop and implement a numerical code to model conjugate the heat transfer in a room coupled to a window with shading cover with a phase change material (PCM).
3. To Select a warm weather condition of the Mexican Republic.
4. To carry out the study of the thermal behavior of a room with a window with a PCM filled shutter under the selected climate conditions of Mexico.

1.4 Scope

To develop and implement a computational code using the finite volume method and the global energy balance formulation to model the conjugate heat transfer of a window with a shutter filled with a phase change material (PCM). The system is made up of a sheet of glass, a shutter and the air trapped between both walls. The shutter is considered of PCM. This PCM window-shutter model was coupled as a boundary condition to a natural convection model in a cavity, where the cavity represent a room. The study was carried out in transient state and in two dimensions for the window system with the PCM cover and one dimension for the room in which a three-dimension effects were considered. Climatic conditions of at least one state of Mexico was selected for characteristic days of the year as modeling information. It is intended to perform the thermal study with the selected weather conditions and different phase change materials. Finally, the thermal evaluation of the room-window system with and without PCM was performed using heat flux and temperature values. To carry out this work, the use of the in-house software developed in Cenidet was considered, in the numerical modeling of different thermal systems.

1.5 Thesis content

A short description of the contents of the thesis chapters is shown below:

Chapter 2. This Chapter explains the physical domain, and the mathematical models that represents the study cases established for the present document.

Chapter 3. This Chapter shows the methodology followed to solve the mathematical model established in Chapter 2, to carry on with the development and verification of the numerical code.

Chapter 4. This chapter shows the obtained results from the developed numerical code and also the its analysis and discussion were presented.

Chapter 5. This Chapter shows the conclusions of the results discussion and the recommendations for future research projects.

Chapter 2

Physical and mathematical model

To carry on with the thermal analysis of the proposed system it is necessary to establish a diagram which represents the physical domain of the room with the window shutter-PCM cover. Then through this physical domain model, to establish its mathematical formulation which represent the physical phenomena occurring in the system under study. Therefore, based, on both representations (physical and mathematical) it is possible to evaluate and understand the behavior of the proposed system. Therefore, in this chapter, the diagram for the room and window with the shutter-PCM altogether for the conjugate heat transfer (diffusion, convection and radiation) analysis is presented first, followed by a diagram for the physical phenomena occurring in all the elements of the system under analysis. Finally, the conservation equations that represent the heat transfer phenomena occurring.

2.1 Diagram of the physical domain for the study cases

The physical domain of the room and its components consist on the room that is H_Y high, H_X width and H_Z depth, the four vertical walls and the roof (T_g,T_{W2}, T_{W3}, T_{W4} and T_{roof} respectively) are interacting with the ambient temperature T_{ext} and with the air in the room (T_{room}). On the other hand, the floor (T_{floor}) is interacting with the temperature of the ground T_{ground} and with the room like the rest of the components mentioned. To know the thermal behavior of the room, a comparison between two configurations of the room will be carried out. Figure 2.1 shows the case study configurations as follows: a) a room with a glazed wall (single glass sheet) which is placed on the south face of the room and is considered as the conventional study case, and b) a room with a Phase Change Material (PCM) shutter that is in front of the glazed wall and works as a shader. The comparison will be carried out to know the room temperature difference and possible benefits when the PCM is implemented as a shader in the room glazed wall.

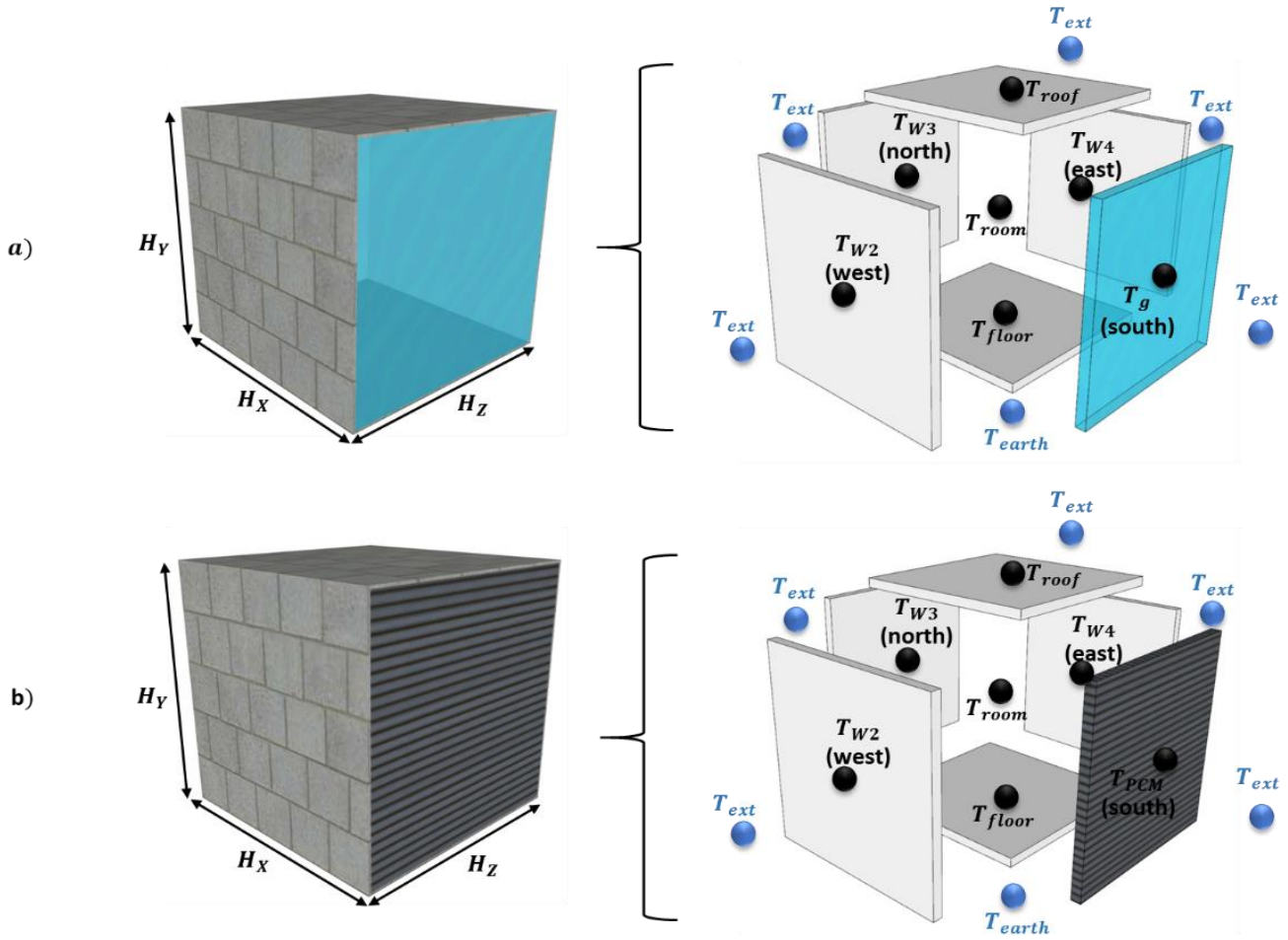

Figure 2.1.-Physical model for the case study configurations: a) room with a glazed wall on its south face and b) room with a shutter-PCM in front of the glazed wall.

As mentioned above, the physical domain under analysis is conformed by different envelope components (roof, walls, floor, and window shutter-PCM cover). However, the analysis was carried out using computational fluid dynamics (CFD) and global energy balances (GEB). The CFD is implemented to solve the conjugated heat transfer through the window shutter-PCM cover component and this component is coupled as a boundary condition to the GEB model which represents the room and the rest of the envelope elements.

2.1.1 Physical domain and heat transfer phenomena for the GEB model

Figure 2.2 shows the direction in which is considered that the energy flux travels through the room along the x, y, and z axes. Figure 2.2 shows that the energy flows from ambient conditions at the top of the system under analysis through the room, reaching the bottom of the ground below the floor of the room. Also is shown that the energy flows from the outside ambient conditions through the north wall (T_{W_3}), through the room (T_{room}) and the glazed wall

(T_g *or* T_{PCM} depending on the configuration under analysis) on the south face of the room until it reaches the outside ambient conditions. In the same way Figure 2.2 shows how the energy flux travel in the direction from the east wall (T_{W_4}) to the west wall (T_{W_2}).

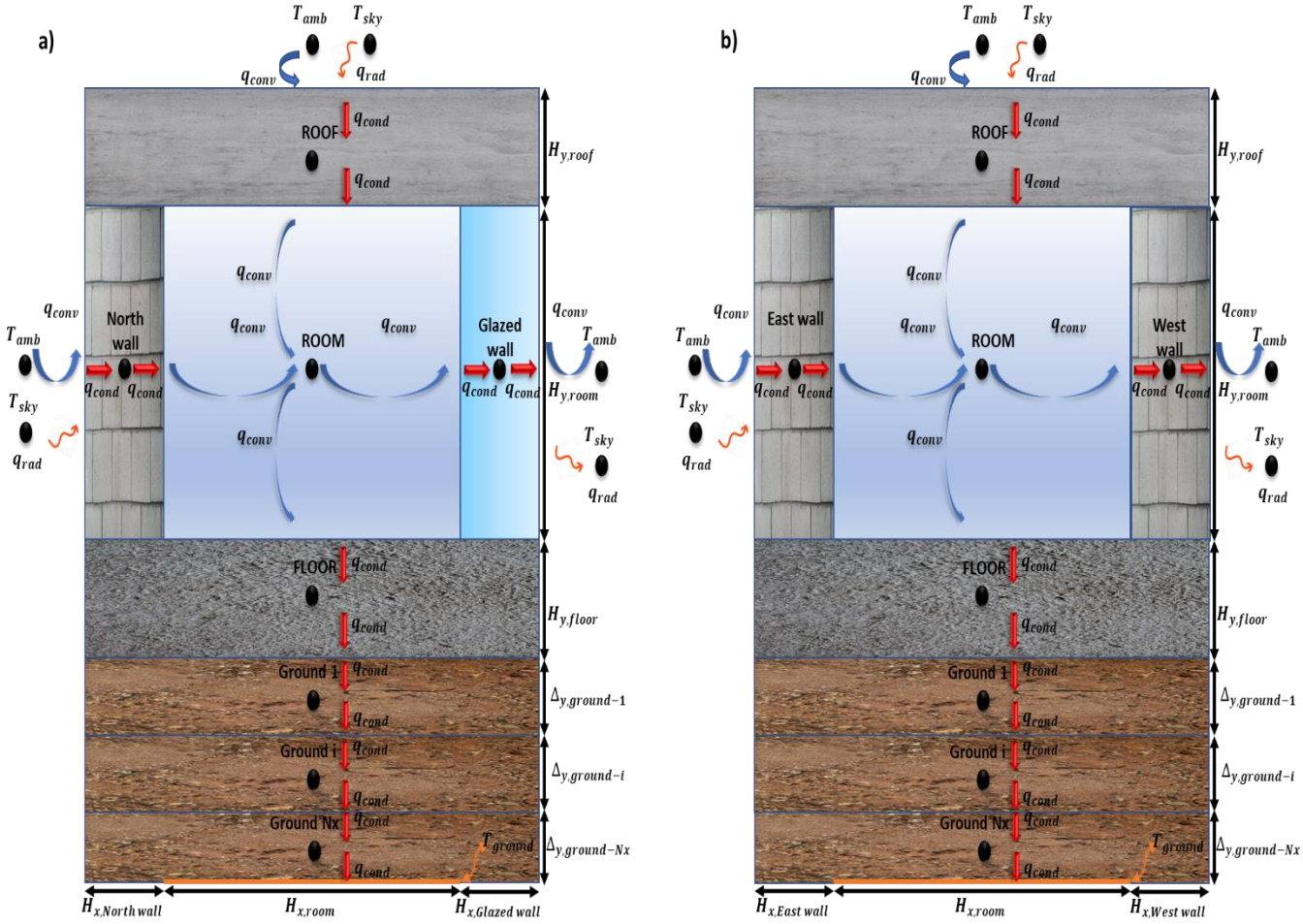

Figure 2.2 Direction of the heat flow travels through the room a) west side point of view, b) south side point of view.

2.1.2 Physical domain and heat transfer phenomena for the CFD model

Figure 2.3 shows the diagram of the 2D physical model for a window-Cover with PCM system represented by closed rectangular cavity of height H. The model is defined by an opaque wall (shading cover with a PCM) and a semi-transparent wall (clear glass), referred as W1 and W2, respectively. It is noted that W1 is the shading cover with $x3$ thickness in front of the clear glass in contact with the outside ambient at a temperature T_{amb}, and W2 is the inside glass whit $x1$ thickness in contact with the ambient inside the room at a temperature T_{room}. The horizontal walls are considered adiabatic, $x2$ is the gap between the glass and the curtain, and the fluid in the gap is air.

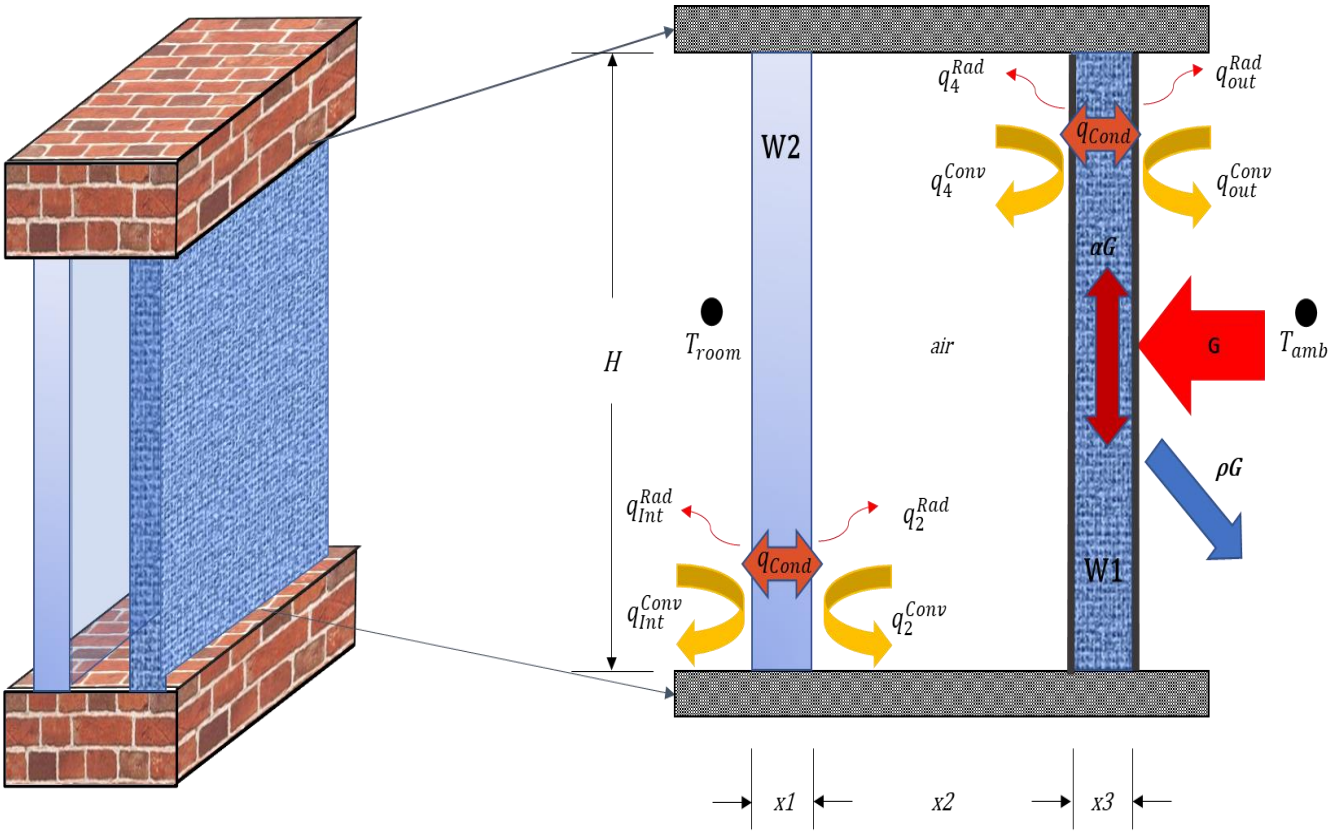

Figure 2.3 Physical model and heat transfer phenomena in the window-cover with PCM system

Figure 2.3 shows how solar radiation hits normal to surface W1, which is the opaque material that encapsulates the PCM. Due to its thin thickness, heat conduction is considered negligible, additionally it does not transmit any of the solar energy. However, a fraction of the solar energy is absorbed by the PCM, and the rest is reflected towards the outside. Due to the energy absorbed by W1 (cover with PCM), it has a variation on its internal energy bringing about a change of their temperature; as a consequence, the cover with PCM wall exchange thermal energy by radiation and convection with the surroundings, towards the air in the cavity (q_4^{conv} and q_4^{rad}) and the outside ambient (q_{out}^{conv} and q_{oout}^{rad}). The heat flux inside the air cavity causes the temperature of W2 to increase, and similarly as with W1, it induces convective and radiative heat flows inside the cavity ($q_2^{conv}$and q_2^{rad}) as well as towards the environment inside the room (q_{int}^{conv} and q_{int}^{rad}). On the other hand, due to the temperature difference between the two vertical surfaces W1 and W2, that form the cavity, a convective cell will arise between them.

2.2 Mathematical model

2.2.1 Equations of the room system by means of global energy balances

The mathematical model solved by the global energy balance method is a one-dimensional mathematical model; however, the considerations to call it a three-dimensional model is that the elements are accommodated as a 3D physical model cube with the room element in the center. This arrangement allows to know the temperature in the room with the contribution of all the other elements considered for this case. The mathematical model that describes the unsteady conjugate heat transfer through the roof, north wall, floor, east and west wall, and the room elements is given by the Equations (2.1-2.6) shown below, respectively:

$$\left(\frac{T_{sky}-T_{roof}}{\frac{1}{h^{rad}_{sky-roof}}}+\frac{T_{ext}-T_{roof}}{\frac{1}{h_{ext-roof}}+\frac{H_{x,roof}}{2\lambda_{roof}}}+\alpha_{roof}G\right)-\left(\frac{T_{roof}-T_{room}}{\frac{H_{x,roof}}{2\lambda_{roof}}+\frac{1}{h_{roof-room}}}+q^{rad}_{roof}\right)=\frac{\partial\left(\rho_{roof}C_{p_{roof}}T_{roof}\right)}{\partial t}Hy_{roof} \tag{2.1}$$

$$\left(\frac{T_{sky}-T_{W_3}}{\frac{1}{h^{rad}_{sky-W_3}}}+\frac{T_{ext}-T_{W_3}}{\frac{1}{h_{ext-W_3}}+\frac{H_{x,W_3}}{2\lambda_{W_3}}}+\alpha_{W_3}G\right)-\left(\frac{T_{W_3}-T_{room}}{\frac{H_{x,W_3}}{2\lambda_{W_3}}+\frac{1}{h_{W_3-room}}}+q^{rad}_{W_3}\right)=\frac{\partial\left(\rho_{w3}C_{p_{w3}}T_{w3}\right)}{\partial t}Hx_{w3} \tag{2.2}$$

$$\left(\frac{T_{room}-T_{floor}}{\frac{1}{h_{room-floor}}+\frac{H_{x,floor}}{2\lambda_{floor}}}+q_{floor}^{rad}\right)-\left(\frac{T_{floor}-T_{earth}}{\frac{H_{x,floor}}{2\lambda_{floor}}}\right) \tag{2.3}$$

$$=\frac{\partial\left(\rho_{floor}C_{p_{floor}}T_{floor}\right)}{\partial t}Hy_{floor}$$

$$\left(\frac{T_{sky}-T_{W_4}}{\frac{1}{h_{sky-W_4}^{rad}}}+\frac{T_{ext}-T_{W_4}}{\frac{1}{h_{ext-W_4}}+\frac{H_{x,W_4}}{2\lambda_{W_4}}}+\alpha_{W_4}G\right)-\left(\frac{T_{W_4}-T_{room}}{\frac{H_{x,W_4}}{2\lambda_{W_4}}+\frac{1}{h_{W_4-room}}}\right) \tag{2.4}$$

$$=\frac{\partial\left(\rho_{w4}C_{p_{w4}}T_{w4}\right)}{\partial t}Hx_{w4}$$

$$\left(\frac{T_{room}-T_{W_2}}{\frac{1}{h_{room-W_2}}+\frac{H_{x,W_2}}{2\lambda_{W_2}}}\right)-\left(\frac{T_{W_2}-T_{ext}}{\frac{H_{x,W_2}}{2\lambda_{W_2}}+\frac{1}{h_{ext-W_2}}}+\frac{T_{W_2}-T_{sky}}{\frac{1}{h_{sky-W_2}^{rad}}}+\alpha_{W_2}G\right) \tag{2.5}$$

$$=\frac{\partial\left(\rho_{w2}C_{p_{w2}}T_{w2}\right)}{\partial t}Hx_{w2}$$

$$\left(\frac{T_{W_4}-T_{room}}{\frac{H_{x,W_4}}{2\lambda_{W_4}}+\frac{1}{h_{W_4-room}}}+\frac{T_{roof}-T_{room}}{\frac{H_{x,roof}}{2\lambda_{roof}}+\frac{1}{h_{conv,roof-room}}}+\frac{T_{W_3}-T_{room}}{\frac{H_{x,W_3}}{2\lambda_{W_3}}+\frac{1}{h_{W_3-room}}}\right) \tag{2.6}$$

$$-\left(\frac{T_{room}-T_g}{\frac{1}{h_{room-g}}+\frac{H_{x,g}}{2\lambda_g}}+\frac{T_{room}-T_{floor}}{\frac{1}{h_{conv,room-floor}}+\frac{H_{x,floor}}{2\lambda_{floor}}}+\frac{T_{room}-T_{W_2}}{\frac{1}{h_{room-W_2}}+\frac{H_{x,W_2}}{2\lambda_{W_2}}}\right)$$

$$=\frac{\partial\left(\rho_{room}C_{p_{room}}T_{room}\right)}{\partial t}Hxy_{room}$$

The window shutter-PCM element, is considered as a known temperature value which is obtained by means of the CFD model.

2.2.2 Window-cover with PCM by means of CFD.

Since the proposed system of a window shutter-PCM is conformed by the shutter that encapsulates de PCM, the glass sheet and the air cavity which separates them, the governing equations that represents the conjugate heat transfer occurring in the system solved using a CFD model are shown below after the following considerations:

- The model is two-dimensional and in transient state.
- The flow is laminar.
- The fluid (air) is Newtonian and incompressible.
- The fluid is non-participant due to its low moisture content.
- The horizontal walls are adiabatic.
- The Boussinesq approximation is valid, since the density is considered constant in the momentum equation, taking its variation only in the term of body forces, this approximation is expressed by: $(\rho_\infty - \rho) = \beta\ (T - T_\infty)$
- The thermophysical properties of air and glass are constant and the optical properties independent of wavelength and temperature.

2.2.2.1 Laminar natural convection inside the cavity

Natural convection is a physical phenomenon that occurs by the movement of a fluid caused only by a change in its density; that is, the fluid of higher density descends, and that of lower density rises due to the arising buoyancy forces involved in the momentum equations. Therefore, the expressions that describe the convective phenomenon in the closed cavity of the system are the mass, momentum, and energy conservation equations in two dimensions presented below **[66]**:

Mass conservation equation:

$$\frac{\partial(\rho)}{\partial t} + \frac{\partial(\rho u)}{\partial x} + \frac{\partial(\rho v)}{\partial y} = 0 \qquad (2.7)$$

Momentum conservation equation in x-direction:

$$\frac{\partial(\rho u)}{\partial t} + \frac{\partial(\rho u u)}{\partial x} + \frac{\partial(\rho v u)}{\partial y} = \frac{\partial}{\partial x}\left(\mu \frac{\partial u}{\partial x}\right) + \frac{\partial}{\partial y}\left(\mu \frac{\partial u}{\partial y}\right) - \frac{dP}{dx} \qquad (2.8)$$

Momentum conservation equation in y-direction:

$$\frac{\partial(\rho v)}{\partial t}+\frac{\partial(\rho u.v)}{\partial x}+\frac{\partial(\rho v.v)}{\partial y}=\frac{\partial}{\partial x}\left(\mu\frac{\partial v}{\partial x}\right)+\frac{\partial}{\partial y}\left(\mu\frac{\partial v}{\partial y}\right)-\frac{dP}{dy}+\rho g\beta(T-T_{\infty}) \quad (2.9)$$

Energy conservation equation:

$$\frac{\partial(\rho T)}{\partial t}+\frac{\partial(\rho uT)}{\partial x}+\frac{\partial(\rho vT)}{\partial y}=\frac{\partial}{\partial x}\left(\frac{\lambda}{Cp}\frac{\partial T}{\partial x}\right)+\frac{\partial}{\partial y}\left(\frac{\lambda}{Cp}\frac{\partial T}{\partial y}\right) \quad (2.10)$$

Regarding the velocity components, there is a no-slip condition at the boundaries, meaning there is no relative movement between the surface and the layer of fluid in contact with it; therefore, the fluid velocity all along the boundary is zero. Additionally, the temperature boundary conditions are defined as follows: horizontal walls are adiabatic, and on the vertical walls, an energy balance is performed between the fluid and the corresponding wall. The mathematical expressions that represent the vertical boundary conditions are shown below:

Thermal boundary conditions:

$$\left(q_2^{conv}+q_2^{Rad}\right)=-\lambda_g\frac{\partial T_g}{\partial x} \quad \text{for} \quad x=x_1,\ \ 0\le y\le H \quad (2.11)$$

$$-\left(q_4^{conv}+q_4^{Rad}\right)=-\lambda_{PCM}\frac{\partial T_{PCM}}{\partial x} \quad \text{for} \quad x=x_1+x_2,\ \ 0\le y\le H \quad (2.12)$$

2.2.2.2 Mathematical model for the semi-transparent wall (W2)

Figure 2.3 shows the physical model for the semi-transparent wall "W2", where T_{room} is the temperature inside the room, and the $q's$ are the convective and radiative heat fluxes transferred to the inside of the room and to the interior of the cavity. The energy equation in transient state can be obtained by performing an energy balance on a differential element of the semi-transparent wall, and it describes the phenomenon of heat conduction through the glass as shown below:

$$\frac{\partial(\rho_g T_g)}{\partial t}=\frac{\partial}{\partial x}\left(\frac{\lambda_g}{Cp_g}\frac{\partial T_g}{\partial x}\right)+\frac{\partial}{\partial y}\left(\frac{\lambda_g}{Cp_g}\frac{\partial T_g}{\partial y}\right)+\frac{1}{Cp_g}\frac{\partial\Theta(x)}{\partial x} \quad (2.13)$$

Where: $\Theta(x)=Gexp\left[-S_g(x_1-x)\right]$ is the energy attenuation function by absorption and scattering, S_g is the glass extinction coefficient and x_1 is the glass thickness **[67]**. According to Figure 2.3, the mathematical expressions that represent the thermal boundary conditions for the semi-transparent wall are as follows:

$$-\lambda_g\frac{\partial T_g}{\partial x}=h_{int}\left(T_{int}-T_g\right)+\varepsilon_g^*\sigma(T_{int}^4-T_g^4) \quad \text{for } x=0,\ 0<y<H \quad (2.14)$$

$$-\lambda_g \frac{\partial T_g}{\partial x} = q_2^{conv} + q_2^{rad} \qquad \text{for } x = x_1,\ 0 < y < H \qquad (2.15)$$

2.2.2.3 Mathematical model for the PCM wall (W1)

The energy equation in transient state that describes the heat diffusion phenomena through the PCM can be obtained by performing an energy balance on a differential element of the wall W1 resulting in the equation shown below:

$$\frac{\partial(\rho_{PCM} Cp_{PCM} T_{PCM})}{\partial t} = \frac{\partial}{\partial x}\left(\lambda_{PCM} \frac{\partial T_{PCM}}{\partial x}\right) + \frac{\partial}{\partial y}\left(\lambda_{PCM} \frac{\partial T_{PCM}}{\partial y}\right) \qquad (2.16)$$

To analyze the thermal behavior of the phase change material in a system, different solution methods are applied, which are divided into two families: front tracking methods and the fixed domain methods **[68]**, **[69]**. For the present study the mathematical model of the PCM was solved by means of the effective heat capacity method (C_P effective), which is in the family of fixed domain methods **[70-72]**.

The horizontal surfaces are considered adiabatic, and the mathematical expressions that represent the boundary conditions for the vertical surfaces are:

$$-\lambda_{PCM} \frac{\partial T_{PCM}}{\partial x} = \left(q_4^{conv} + q_4^{rad}\right) \qquad \text{for } x = x_1 + x_2, 0 < y < H \qquad (2.17)$$

$$-\lambda_{PCM} \frac{\partial T_{PCM}}{\partial x} + \alpha^* G = h_{ext}(T_{PCM} - T_{ext}) + \varepsilon^* \sigma (T_{PCM}^4 - T_{ext}^4) \quad \text{for} \quad x = x_1 + x_2 + x_3, 0 < y < H \qquad (2.18)$$

2.2.2.4 Surface thermal radiation model

The net radiative method (radiosity-irradiosity method) **[67]** is applied in this study to find the heat fluxes resulting from the radiative exchange in the cavity. The surfaces of the cavity are supposed opaque and diffuse. The following energy balance gives the radiative heat flux for the jth element in each wall:

$$q_j^{rad} = q_j^{out}(x_j) - q_j^{in}(x_j) \qquad (2.19)$$

Where the radiosity for each jth element is defined as:

$$q_j^{out}(x_j) = \varepsilon_j^* \sigma T_j^4 + \rho_j^* q_j^{in}(x_j) \qquad (2.20)$$

And the irradiance is given by:

$$q_j^{in}(x_j) = \sum_{k=1}^{m} \int_{Ak} q_k^{out}(x_k)\, dF_{dA_j - dA_k} \tag{2.21}$$

Where $dF_{dAj-dAk}$ is the view factor solved by Hottel's crossed-string method **[67]** and is between the surface differential elements dA_j and dA_k and is defined as: the fraction of the radiant energy leaving surface j that is intercepted by surface k.

Now that the physical domain with its heat transfer phenomena and the mathematical model that represents them were established; the methodology to solve the problem of the room with the shutter-PCM window, will be described in Chapter 3.

Chapter 3

Numerical solution methodology

This chapter shows the methodology that was used for the solution of the mathematical model proposed in Chapter 2, the different numerical methods are described in a general way, and a detailed description is given for the methods used in this work. Afterwards, the solution of verification problems is presented to guarantee that the developed numerical code does not contain errors and provides reliable results. When the numerical code was finished a temporal and spatial mesh independence test was carried out, to verify that the results obtained from the numerical code are accurate enough without spending unnecessary computational time.

Since the proposed system of a room with a window shutter-PCM, was solved using two different techniques (CFD and GEB) and considering the window temperature a known value for the room. The first step is to show the solution methodology of the CFD model.

3.1 Solution of the CFD model

Conservation laws describe the phenomena that occur in fluid mechanics. The theoretical solution of the mathematical models formulated through the conservation laws can be classified as analytical and numerical. Analytical solutions are used for special cases in which the configurations are simple and take very restricted considerations, that is, for simple or ideal problems. Because for the mathematical models presented in Chapter 2.2.2, there are no analytical methods for the solution due to the problem's complexity. Therefore, it was decided to use a numerical method.

The numerical methods most used to solve the mass, momentum and energy conservation equations are three: finite difference (FDM), finite element (FEM) and finite volume (FVM).

The **FDM** is the oldest numerical method and was introduced by Euler in the 18th century. The starting point of the method is the conservative equation of one variable Φ in differential form. The unknown variable Φ is described by means of points on the nodes of a mesh (the solution domain is covered by a mesh). At each grid point the equation is approximated by replacing the partial derivatives by finite approximations using Taylor series expansion or fitted polynomials, which are used to obtain the finite difference approximations for the first and second derivative of Φ with respect to the coordinates in terms of the nodal values. The result is an algebraic approximation for Φ at each node of the mesh, in which the value of the variable at this node and at certain neighboring nodes appear as unknowns. The FDM can be applied to any type of mesh. However, the method is complicated when it is applied to non-regular meshes. The main

disadvantage of FDM is that it is non-conservative, that is, the conservation of mass does not hold unless special care is taken for it. Also, another significant disadvantage in complex flows is the restriction of simple geometries **[73]**.

The **FEM** is a generalization of the variational principle and weighted residuals methods. These methods are based on the idea that the solution for Φ_j of a differential equation can be represented as a combination of unknown lineal parameters as c_j and the appropriate functions of Φ_j for the entire domain. In summary the FEM stars with a solution proposal for Φ (function of c_j and Φ_j) this proposal is substituted in the conservation equations, but since the proposal does not satisfy the complete solution domain, then a residual value stays as result (If the approximation was exact, the residual would be zero). The following step is to minimize the residuals by multiplying them by a group of weighted functions and integrate them (setting the integrals equal to zero). As a result, a group of algebraic equations is obtained for unknown coefficients c_j, of the approximation functions **[73]**.

The **FVM** was developed initially as a special form of the finite difference formulation. The entire physical domain is subdivided into a finite number of contiguous control volumes (CV), and conservation equations are applied for each CV. At the center of each CV is a computational node in which the variables are calculated. An integral is made for each control volume, and the volume integrals are substituted by surface integrals by the Gauss divergence theorem. The surface integrals are approximated by using any available quadrature formula. Besides, an interpolation scheme is used to express the values of the variables on the surfaces of the CVs in terms of the nodal values and the neighboring nodes. As a result, an algebraic equation is obtained for each CV, in which values of the neighboring nodes appear.

The FVM can be applied to any type of mesh and therefore can be applied to complex geometries. The mesh defines only the boundaries of the control volumes. The method is conservative by construction, i. e., the properties of importance comply with conservation for each CV, so the surface integrals that represent convective and diffusive flows are the same for the interfaces (boundaries) of the adjacent CVs. The FVM approach is perhaps the simplest to understand and program. All the terms that need to be approximated have physical meaning, therefore, its application is popular among engineers. A disadvantage of the FVM lies in the difficulty to use high-order schemes in three dimensions, since the FVM requires two levels of approximation (interpolation and integration).

For this study, the finite volume method was chosen to solve the governing equations of the proposed system because this method by construction considers integral conservation of mass, momentum, and energy in each control volume. Furthermore, all terms that need to be approximated have physical meaning **[66]**.

3.1.1 Mesh generation of the FVM

3.1.1.1 Spatial mesh

Figure 3.1 shows the spatial discretization mesh representing the integration of the partial differential equations system. This is, the divisions in x_i over which the derivatives lie (spatial variations, etc.). For the present study, a non-uniform mesh is considered for the region with air. The control volumes of this mesh are thinner at the ends where the boundary layer phenomena are more intensely appreciated and thicker in the central part. The selection of the non-uniform mesh was because it adapts well to the geometry of the domain to be studied and allows the introduction of the appropriate boundary conditions, so the results are physically acceptable. On the other hand, if the mesh is adequate to the geometry and dense enough, the description of the physical phenomenon in that region is more approximate, however, the processing time also increases exponentially.

The distribution of the nodes (CV) was carried out by means of a hyperbolic trigonometric function expressed by equation (3.1), in which, k_x is an adjustment parameter that allows a narrowing in the regions in contact with the solid surfaces. In the present study, narrowing was performed only in the x direction **[74]**.

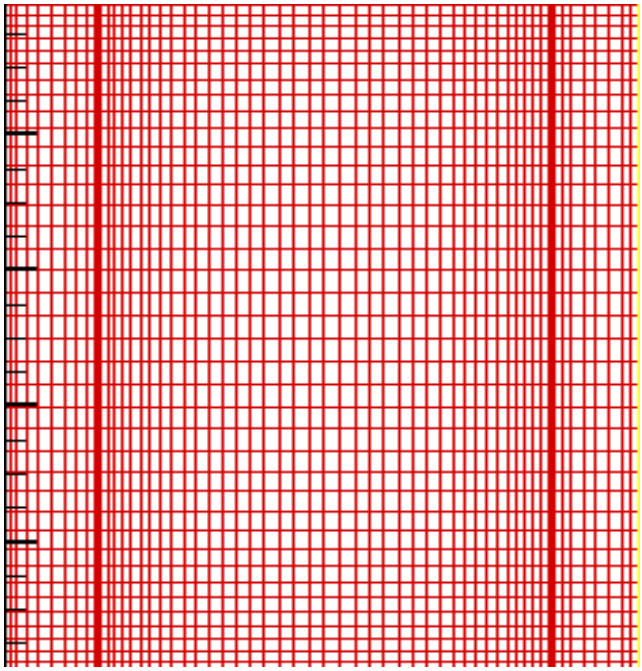

Figure 3.1 Discrete mesh.

$$x_i = \frac{L}{2}\left[1 - \frac{tanhk_x\left(\frac{2_i - 2}{N_x - 2}\right)}{tanhk_x}\right] \tag{3.1}$$

3.1.1.2 Temporal mesh

Time discretization is also a very important parameter in transient models. When the physical phenomenon reaches equilibrium conditions and shows a constant dynamic behavior over time, it is said that the phenomenon has reached the steady state (there are also phenomena that reach an oscillatory steady state or that do not reach the steady state). If the interest of the study is towards what happens in a certain time step (Δ_t), it is necessary to know what happens in the previous instants, so time is divided into time intervals to know the evolution of the model at each instant.

Temporal discretization likewise spatial discretization can be performed in "thicker" (longer) or "thinner" (shorter) time intervals. The thickness of the temporal mesh affects the convergence during the calculations. Therefore, the smaller the time step, the better convergence in the algorithm. However, using very short time steps increases the number of computations and consequently the computation time increases exponentially. In conclusion, to obtain the solution of a given problem, numerical methods have a compromise between computation time and the accuracy of results. Figure 3.2 shows an example of the temporal mesh used in the study.

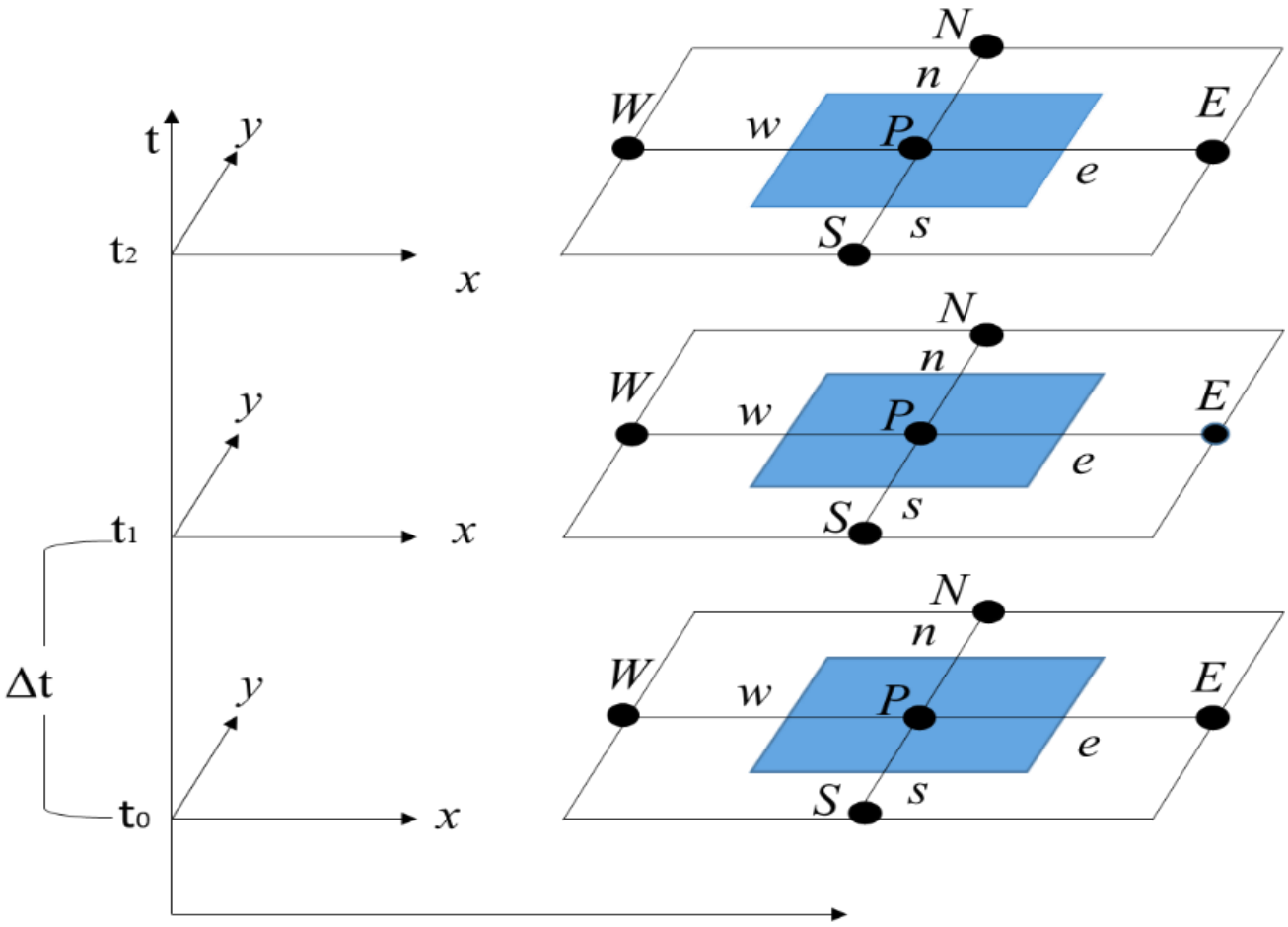

Figure 3.2 Temporal mesh.

3.1.2 Discretization of the conservation equations

Next, the discretization of the convection-diffusion equation of the variable Φ is shown, in order to present a notation of grouped coefficients, which will be useful to solve it. Finally, the numerical schemes used are described in general.

3.1.2.1 General two-dimension convection-diffusion equation

The differential equations that govern the processes under study, that is, continuity, momentum and energy, obey a generalized conservation principle, therefore, they can be compacted in a single expression called the generalized convection-diffusion equation which is shown below **[75]**.

$$\frac{\partial(\rho\phi)}{\partial t}+\frac{\partial(\rho u\phi)}{\partial x}+\frac{\partial(\rho v\phi)}{\partial y}=\frac{\partial}{\partial x}\left(\Gamma\frac{\partial\phi}{\partial x}\right)+\frac{\partial}{\partial y}\left(\Gamma\frac{\partial\phi}{\partial y}\right)+S \qquad (3.2)$$

The first term on the left side of the equation is the temporal term which represents the variation of the unknown variable Φ through time, the second and third terms are the advective components represented by the equation of continuity and momentum which involve transport due to flow movements, the first two terms on the right side of the equation are the diffusive terms represented by the Laplacian of Fourier's law and the last term on the right side is the source or heat generation term inside the CV in which all the terms that cannot be added to any of the terms described above are gathered together.

Table 3.1 shows the equivalences for the mass, momentum and energy conservation equations expressed in terms of Φ, Γ, and S with respect to the generalized equation.

Table 3.1 Equivalences of the generalized formulation.

Conservation equation	Variable (Φ)	Diffusive property (**Γ**)	Source term (**S**)
Mass	1	0	0
Momentum-x	u	μ	$-\frac{\partial P}{\partial x}$
Momentum-y	v	μ	$-\frac{\partial P}{\partial y}$
Energy	T	$\frac{\lambda}{C_p}$	0

3.1.2.2 Integration of the generalized equation

The starting point of the FVM is dividing the physical domain into CV where the spatial discretization will take place. Figure 3.3 shows a CV on a two-dimensional Cartesian mesh. This mesh was used for the discretization of the generalized equation and this CV represents a generic control volume of the spatial mesh and is related to its neighboring nodes; north (N), south (S), east (E), and west (W).

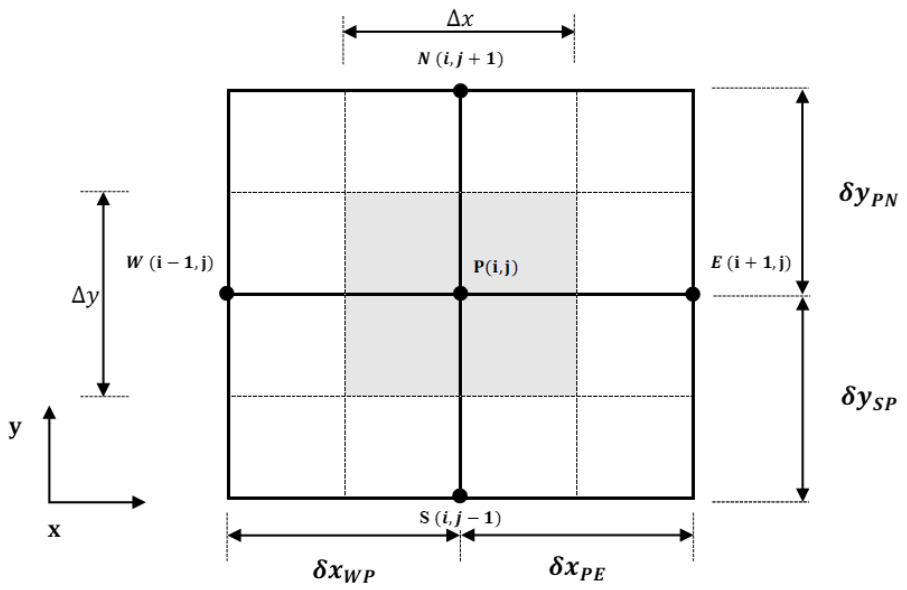

Figure 3.3 CV on a two-dimensional mesh

To obtain the discretized equation as mentioned above, it is necessary to use two levels of approximation (integration and interpolation). To obtain the discretized equation, it is necessary to carry out the spatial integration over the control volume of the previous figure, as well as the integration in time.

Integrating equation (3.2) in space over the geometric limits of the control volume and applying the midpoint rule, equation (3.3):

$$\int_s^n \int_w^e \frac{\partial(\rho\phi)}{\partial t}dxdy + \int_s^n \int_w^e \frac{\partial(\rho u\phi)}{\partial x}dxdy + \int_s^n \int_w^e \frac{\partial(\rho v\phi)}{\partial y}dxdy = \int_s^n \int_w^e \frac{\partial}{\partial x}\left[\Gamma\frac{\partial\phi}{\partial x}\right]dxdy + \int_s^n \int_w^e \frac{\partial}{\partial y}\left[\Gamma\frac{\partial\phi}{\partial y}\right]dxdy + Sdxdy \quad (3.3)$$

By solving the integral, equation (3.4) is obtained.

$$\frac{\partial(\rho\phi)}{\partial t}dxdy + [(\rho u\phi)e - (\rho u\phi)w]\Delta y + [(\rho v\phi)n - (\rho v\phi)s]\Delta x = \left[\Gamma\frac{\partial\phi}{\partial x}\Big|_e - \Gamma\frac{\partial\phi}{\partial x}\Big|_w\right]\Delta y + \left[\Gamma\frac{\partial\phi}{\partial y}\Big|_s - \Gamma\frac{\partial\phi}{\partial y}\Big|_n\right]\Delta x + S\Delta x\Delta y \quad (3.4)$$

Equation (3.4) has not yet been integrated over time, to account for the variation of Φ through the time $t(n)$ to $t + \Delta_t(n+1)$, the following expression is used:

$$\int_t^{t+\Delta t} \phi dt = [f\phi^{n+1} + (1-f)\phi^n]\Delta t \quad (3.5)$$

Where:

If $f = 0.0$ we have the explicit schema.

If $f = 0.5$ we have the Crank-Nicolson schema.

If $f = 1.0$ we have the implicit schema.

In this thesis was considered $n+1$ (implicit method) as the time instant of the properties evaluation. Finally, following the consideration $f = 1$, the result of the time integration of equation (3.4) in the control volume is:

$$\frac{\left|(\rho\phi)_p^{n+1} - (\rho\phi)_p^n\right|}{\Delta t}\Delta x\Delta y + [(\rho u\phi)e - (\rho u\phi)w]\Delta y + [(\rho v\phi)n - (\rho v\phi)s]\Delta x = \left[\Gamma\frac{\partial\phi}{\partial x}\Big|_e - \Gamma\frac{\partial\phi}{\partial x}\Big|_w\right]\Delta y + \left[\Gamma\frac{\partial\phi}{\partial y}\Big|_s - \Gamma\frac{\partial\phi}{\partial y}\Big|_n\right]\Delta x + S\Delta x\Delta y \quad (3.6)$$

For the simplification of the previous equation, the following terms are defined to help compact the equation.

Convective fluxes through the faces of the control volume.

$$\begin{aligned} F_e &= (\rho u)_e\Delta y \\ F_w &= (\rho u)_w\Delta y \\ F_n &= (\rho v)_n\Delta x \\ F_s &= (\rho v)_s\Delta x \end{aligned} \quad (3.7)$$

Diffusive terms through the control volume:

$$\begin{aligned} D_e &= \frac{\Gamma}{(\delta x)e}\Delta y \\ D_w &= \frac{\Gamma}{(\delta x)w}\Delta y \\ D_n &= \frac{\Gamma}{(\delta x)n}\Delta x \\ D_s &= \frac{\Gamma}{(\delta x)s}\Delta x \end{aligned} \quad (3.8)$$

Peclet Numbers:

$$P_e = \frac{F_e}{D_e}\Delta y$$
$$P_w = \frac{F_w}{D_w}\Delta y$$
$$P_n = \frac{F_n}{D_n}\Delta x \qquad (3.9)$$
$$P_s = \frac{F_s}{D_s}\Delta x$$

Finally, total fluxes through the faces of the control volume (convection plus diffusion):

$$J_e = \left[(\rho u\phi)_e - \left(\Gamma\frac{\partial\phi}{\partial x}\right)_e\right]\Delta y$$
$$J_w = \left[(\rho u\phi)_w - \left(\Gamma\frac{\partial\phi}{\partial x}\right)_w\right]\Delta y$$
$$J_n = \left[(\rho v\phi)_n - \left(\Gamma\frac{\partial\phi}{\partial x}\right)_n\right]\Delta x \qquad (3.10)$$
$$J_s = \left[(\rho v\phi)_s - \left(\Gamma\frac{\partial\phi}{\partial x}\right)_s\right]\Delta x$$

When equation (3.10) is replaced into equation (3.6) considering $n = 0$, the following expression is obtained.

$$\frac{\left|(\rho\phi)_p - (\rho\phi)_p^0\right|}{\Delta t}\Delta x\Delta y + (J_e - J_w) + (J_n - J_s) = S\Delta x\Delta y \qquad (3.11)$$

The continuity equation is introduced to ensure the convection-diffusion equation convergence and that each discrete equation complies with the conservation principle. Therefore, it is ensured that the final solution obtained through the iterative process complies with the principle of conservation of mass.

$$\frac{\left|\rho_p - \rho_p^0\right|}{\Delta t}\Delta x\Delta y + (F_e - F_w) + (F_n - F_s) = 0 \qquad (3.12)$$

Now multiplying equation (3.12) by ϕ_p and by subtracting the resulting equation from equation (3.11), the equation that will finally be used as discrete was reached:

$$(\phi_p - \phi_p^0)\,\frac{\rho_p^0}{\Delta t}\Delta x\Delta y + [(J_e - F_e\phi_P) - (J_w - F_w\phi_P)] + [(J_n - F_n\phi_P) - (J_s - F_s\phi_P)] = S\Delta x\Delta y \tag{3.13}$$

The previous development shows how to convert differential equations to discrete equations. Now it will be shown how to convert the discrete equation to a notation of grouped coefficients, i. e., express the variable of a node P as a function of the variable of the neighboring nodes E, W, N, S and as a function of other parameters that encompass the source term. Therefore, the generalized scheme formulation was used to evaluate the following terms **[75]**:

$$\begin{aligned}(J_e - F_e\phi_P) &= a_E(\phi_P - \phi_E)\\ (J_w - F_w\phi_P) &= a_W(\phi_W - \phi_P)\\ (J_n - F_n\phi_P) &= a_N(\phi_P - \phi_N)\\ (J_s - F_s\phi_P) &= a_S(\phi_S - \phi_S)\end{aligned} \tag{3.14}$$

Then, by replacing equation (3.14) into equation (3.15) the generalized diffusion convection equation in grouped coefficient notation, is obtained:

$$a_p\phi_p = a_E\phi_E + a_W\phi_W + a_N\phi_N + a_S\phi_S + b \tag{3.15}$$

Where:

$$\begin{aligned}a_E &= D_eA(|P_e|) + \max[-F_e, 0]\\ a_W &= D_wA(|P_w|) + \max[F_w, 0]\\ a_N &= D_nA(|P_n|) + \max[-F_n, 0]\\ a_S &= D_sA(|P_s|) + \max[F_s, 0]\\ a_P &= a_E + a_W + a_N + a_S + (F_e - F_w) + (F_n - F_s)\\ b &= a_p^0\phi_p^0 + S\Delta x\Delta y\end{aligned} \tag{3.16}$$

Where $A(|P_e|)$ is a function proposal to generalize the approximation schemes (upwind, centered, power law, exponential and hybrid) **[75]**. The difference between the approximation schemes lies in how they evaluate certain properties at the CV boundaries.

3.1.2.3 Numerical schemes

To evaluate $A(|P_e|)$ the dependent variables values at the borders of the control volumes must be known. This allows the calculation of the total flows through them. This is achieved through approximation schemes, which can be of low or high order. Patankar (1980) **[75]** makes use of low order schemes such as: upwind, hybrid, and power law.

In all the equations it is necessary to know the values of the variables at the interfaces of the control volumes, to calculate the flows and therefore, the necessary coefficients for the solution of the variable Φ at point P.

Calculating the necessary relations for the variables in the interface of the control volumes is one of the main difficulties when using the finite volume method, so convergence of the algorithm, as well as results accuracy, depends on the way to calculate the variable in the control volume interface.

The difference between the approximation schemes lies in the selection of the type of approximation of the convective terms. Depending on the type of approximation, there may be convergence and/or accuracy problems. For the diffusive term's approximation, it is recommended to use a centered interpolation. It has been analytically shown that the best approximation for diffusive terms is a centered difference **[66]**. On the other hand, the approximations for the convective terms are more complicated, depending on the type of approximation, convergence problems and even unreal or illogical solutions can be reached.

Low-order schemes take one or two nodal points to approximate the value at the control volume interface. A brief summary of the low-order schemes is shown below:

- **Up wind**

Approximates the value of the variable at the border of the CV with the nodal value immediately at the border, according to the flow direction. It provides physically acceptable results, but with low accuracy. To improve the accuracy of the results, a denser mesh has to be used, but it has a good behavior for convergence since it is not oscillatory.

- **Centered**

Uses the average values of the two closest nodes to the boundary in order to approximate the variable. It works well for problems at low speeds, but it is not advisable for highly convective situations, since it does not adequately represent the convective transport properties.

- **Hybrid**

It combines the characteristics of the centered scheme and the upwind scheme. It approaches with a centered scheme for low speeds and for high speeds it uses the characteristics of the upwind scheme.

- **Exponential**

It was developed according to the analytical (exact) solution of the one-dimensional steady-state problem, so it produces the exact solution for any value of the Peclet number and for any number of grid points in this type of problem. However, the exponential scheme is not widely used or recommended in multidimensional convection-diffusion problems, because it is not exact in this type of problem, in addition to taking too much computation time.

- **Power law**

This scheme was developed by Patankar (1980) **[75]** and is a modification of the hybrid scheme based on the exponential scheme. This formulation assumes that the differentiation of the diffusion is zero when the Peclet number is greater than 10. If $0 < P_e < 10$ the flow is evaluated by a polynomial expression. This scheme has the same accuracy in the results as the exponential scheme, but, in addition, it improves convergence, which is why it was once the most widely used and recommended in diffusion convection problems.

Table 3.2 Function $A(|P|)$ for different schemes.

Scheme	$\boldsymbol{A(\lvert P\rvert)}$
Upwind	1.0
Centered	$1 - 0.5\lvert P\rvert$
Hybrid	$Max[1 - 0.5\lvert P\rvert]$
Exponential	$\lvert P\rvert/(exp(\lvert P\rvert) - 1)$
Power law	$\mathrm{Max}[0, (1 - 0.1\lvert \mathrm{P}\rvert)^5$

3.1.3 Semi Implicit Method for Pressure Linked Equations (SIMPLE) algorithm.

When solving fluid flow problems, it may occur that the velocity field is known, so the use of the governing equations is simplified. However, there is also the case where the velocity field is unknown. Therefore, the velocity components (u, v, w) become dependent variables in such a way that to solve the governing equations the following difficulties arise:

- The momentum equation has a convective term, which is highly non-linear.
- The momentum and continuity equations are strongly coupled due to the velocity components that appear in them, which forms a system of partial differential equations.

Therefore, an important complexity arises when estimating the role of pressure in the momentum equations, since there is no transport equation for pressure **[76]**. Hence, the problem in the numerical solution of fluid dynamics is to solve the pressure gradient term of the momentum equation.

The SIMPLE algorithm is a sequential solution technique for coupling the mass and momentum conservation equations, in which the primary variables (velocities and pressure) are used. Among the problems that are found in the SIMPLE algorithm, is the representation of the pressure gradient in the motion equations. Patankar (1980) **[75]** has shown that the solution of the

momentum equations, discretized in the same computational nodes, can lead to an oscillatory pressure distribution that does not correspond to the real solution. To overcome this, the alternative is to use offset meshes. Other problems may be the treatment of the boundary conditions of the pressure correction equation (P') and the inconsistency of having to use under-relaxation for pressure (P), this inconsistency is overcomed by modifying the algorithm SIMPLE (SIMPLEC) proposed by Van Doormaal and Raithby (1984) **[77]**.

In the development of the SIMPLE algorithm, Patankar, and Spalding (1972) **[78]** used the idea of the staggered mesh and the concept of a predictor-corrector step for the coupling of velocity and pressure.

3.1.3.1 Staggered grid

One of the main aspects when coupling the mass and momentum equations is to use superimposed meshes that depends on the calculated variable. Hence, three or four superimposed meshes are used for the case of two and three dimensions respectively.

All the scalar variables (pressure, temperature, turbulent kinetic energy, among others) are placed or stored in the main or centered mesh. The velocity components u, v, w are stored in the x, y, z shifted meshes, respectively. The mesh displacement arrangement is such that the borders or interface of its control volumes coincide with the nodal points of the main mesh.

An important advantage of using displaced (staggered) meshes is having the representative center of the staggered mesh node on the border of the CV of the centered mesh node, since information on the flows is needed in the borders of the CV to solve the variables on the centered mesh, and the fact of having the velocity nodes in these borders avoids the need to interpolate the values. Therefore, more accurate correct results are obtained. Figure 3.4 shows how the displacement of the meshes for two dimensions works.

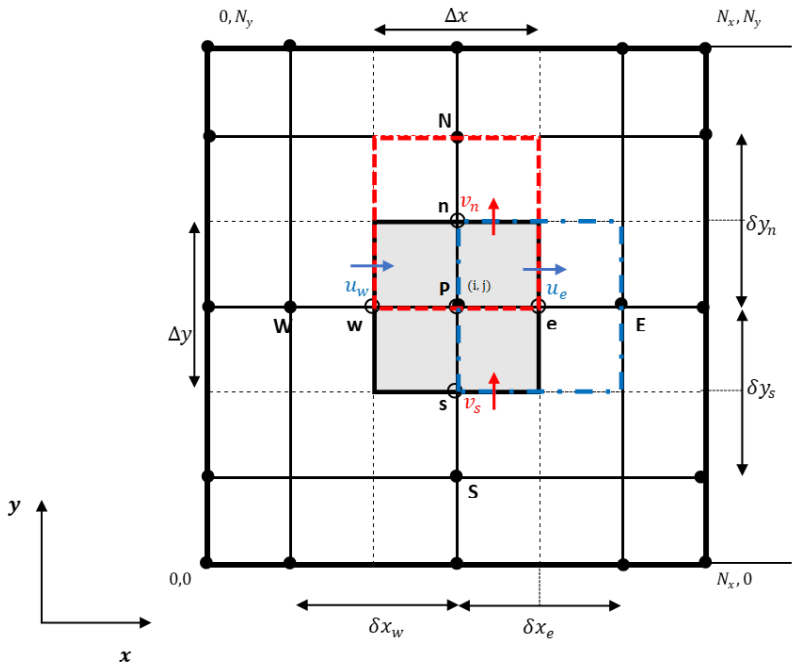

Figure 3.4 Staggered mesh: CV for scalar variables (black), velocity u (blue), and for velocity v (red).

3.1.3.2 SIMPLE algorithm formulation

The algorithm used in this study was the SIMPLEC algorithm, which belongs to the SIMPLE algorithm family, these algorithms use a sequential form for the solution of the global system of the Navier-Stokes equations.

The structure of the algorithm is basically composed by two parts: a) the assumption of a pressure field that facilitates obtaining a velocity distribution and b) the correction of these distributions by iteratively complying with the continuity equation until reaching a correct solution.

The first step to of the SIMPLE algorithm is to decompose the momentum equations source term, so the pressure appears explicit as shown below:

$$b^u = (p_P - p_E)\Delta_y + b_1^u$$
$$b^v = (p_P - p_N)\Delta_x + b_1^v \quad (3.17)$$

Where Δ_i is the i face of the CV area.

Considering equation 3.17, the discretized momentum equations for two dimensions in lumped coefficient notation can be written as:

$$a_e u_e = \sum a_{neighbours} u_{neighbours} + (p_P - p_E)\Delta_y + b_1^u$$
$$a_n v_n = \sum a_{neighbours} v_{neighbours} + (p_P - p_N)\Delta_x + b_1^v \quad (3.18)$$

To solve the momentum equations, an initial field p^* must be assumed, so this field can be used to obtain a "proposed" velocity field u^*, v^* through the following equations:

$$a_e u^*{}_e = \sum a_{neighbours} u^*{}_{neighbours} + \left(p^*{}_P - p^*{}_E\right)\Delta_y + b_1^u$$
$$a_n v^*{}_n = \sum a_{neighbours} v^*{}_{neighbours} + \left(p^*{}_P - p^*{}_N\right)\Delta_x + b_1^v \quad (3.19)$$

The velocity field obtained cannot comply with continuity unless the proposed pressure field is correct. Therefore, P' is designated as a pressure correction for P, in such a way that it provides a velocity field u^*, v^* that successively approaches the value that satisfies the continuity equation. Therefore, the correct pressure distribution is obtained with equation (3.20).

$$p = p^* + p' \quad (3.20)$$

Faced with this new pressure, velocity correction equations are also proposed:

$$u = u^* + u'$$
$$v = v^* + v' \quad (3.21)$$

If the assumed velocity equations (3.19) are subtracted from the momentum equations (3.18) for the correct velocities, a new momentum equation for the velocity corrections is obtained, according to equations (3.21), as a function of the corrected pressure field (the source term was eliminated, since it is the same for the two equations). The new momentum equation for the velocity corrections is given as:

$$a_e u'_e = \sum a_{neighbours} u'_{neighbours} + \left(p'_P - p'_E\right)\Delta y$$
$$a_n v'_n = \sum a_{neighbours} v'_{neighbours} + \left(p'_P - p'_N\right)\Delta x \quad (3.22)$$

In the above equations it can be seen that any nodal point depends on the pressure and the velocity correction at the neighboring points. At this point the approximation of vanishing the $\sum a_{neighbours} u'_{neighbours}$ y $\sum a_{neighbours} v'_{neighbours}$ terms is introduced in order to simplify the relationship between velocity and pressure correction. The omission of these terms is the main approximation of the SIMPLE algorithm (justification for the omission of the summations is given in detail by Patankar, 1980 [**75**]). Then equations (3.22) can be reduced to:

$$u'_e = d_e\left(p'_P - p'_E\right)$$
$$v'_n = d_n\left(p'_P - p'_N\right) \quad (3.23)$$

d_e and d_n coefficients represent the relationship between velocities and pressure corrections. These coefficients vary depending on the variant of the SIMPLE algorithm family.

The SIMPLE algorithm assumes that the correction velocities of any P node depends only on the variation of the correction pressure. This criterion is true as the iterative process approaches the correct velocities, since these tend to zero. Hence, the d_e and d_n expressions change to

$$d_e^u = \frac{\Delta y}{a_e}$$
$$d_n^v = \frac{\Delta x}{a_n} \tag{3.24}$$

In the case of the SIMPLEC (SIMPLE-Consistent) algorithm, the concept is exactly the same as in the SIMPLE algorithm, the difference consists in how it considers the relationship for velocity and pressure corrections, i. e., the values of d_e^u y d_n^v are different. In this case it is not necessary to under-relax the values of the correction pressure p', avoiding the difficulty of choosing an optimal value for the relaxation factor and therefore an improvement in the calculation time is obtained. The procedure is presented below:

From the momentum equations (3.22) for the correction velocities, the sum of the neighboring coefficients multiplied by the correction speed is subtracted from both sides of the equation. This can be expressed as follows from equations (3.22):

$$\begin{aligned}(a_e - \sum a_{neighbours})u'_e &= \sum a_{neighbours}(u'_{neighbours} - u'_e) + (p'_P - p'_E)\Delta y \\ &= (p'_P - p'_E)\Delta y \\ (a_n - \sum a_{neighbours})v'_n &= \sum a_{neighbours}(v'_{neighbours} - v'_n) + (p'_P - p'_E)\Delta y \\ &= (p'_P - p'_E)\Delta y\end{aligned} \tag{3.25}$$

The previous equations are as valid as the expressions of equations (3.22), here the approximation made by the SIMPLEC algorithm is to assume that the sums of the coefficients multiplied by the differences in correction velocities in each control volume is null. That is, if the pressure P is modified by P', the velocity u will respond to a change through u_e, which is a response from its neighboring points $u_{neighbours}$, all these velocity changes could be of the same order. The approximation of the SIMPLE algorithm is that the term $\sum a_{neighbours}u'_{neighbours}$ can be ignored in equation (3.22), while a term of similar magnitude from the left-hand side of the equation can be retained the term $\sum a_{neighbours}u_e$ appears on the left-hand side when the a_p

term of the generalized convection-diffusion equation (3.16) is substituted into equation (3.22) can be seen as an inconsistency.

Therefore, the approximation of the SIMPLEC algorithm is more appropriate since the correction velocity u is the result of its neighboring velocities and therefore, the term $\sum a_{neighbours}\left(u'_{neighbours} - u'_{e}\right)$ can be considered null. Hence, the expressions for the coefficients d_e^u and d_d_n^v of the SIMPLEC algorithm are:

$$d_e^u = \frac{\Delta y}{a_e^u - \sum a_{vecinos}^u} \qquad y \qquad d_n^v = \frac{\Delta y}{a_n^v - \sum a_{vecinos}^v} \tag{3.26}$$

Knowing the correction velocities, the real velocities can be calculated from the relations (3.21) as:

$$\begin{aligned} u_e &= u_e^* + d_e^u\left(p'_P - p'_E\right) \\ v_n &= v_n^* + d_n^v\left(p'_P - p'_N\right) \end{aligned} \tag{3.27}$$

Next, the continuity equation is integrated into a CV on the centered mesh (main mesh), to determine the appropriate information for pressure correction.

$$\frac{\left|\rho'_p - \rho'^0_p\right|}{\Delta t}\Delta x\Delta y + [(\rho' u)e - (\rho' u)w]\Delta y + [(\rho' v)n - (\rho' v)s]\Delta x = 0 \tag{3.28}$$

The previous equation can be expressed as a function of the correction pressure through equations (3.27) as:

$$a_P P'_P = a_E P'_E + a_W P'_W + a_N P'_N + a_S P'_S + b \tag{3.29}$$

Where:

$$\begin{aligned} a_E &= \rho_e d_e^u \Delta y \\ a_W &= \rho_w d_w^u \Delta y \\ a_N &= \rho_n d_n^v \Delta x \\ a_S &= \rho_s d_s^v \Delta x \\ a_P &= a_E + a_W + a_N + a_S \end{aligned} \tag{3.30}$$

$$b = \frac{(\rho_p^0 - \rho)}{\Delta x}\Delta x\Delta y + [(\rho u^*)_w - (\rho u^*)_e]\Delta y + [(\rho v^*)_s - (\rho v^*)_n]\Delta x$$

Velocities in the b (source) term of the pressure correction equation are the assumed velocities, that is, the continuity equation integrated into the CV in terms of the estimated velocities with changed sign. If the b term is zero, this means that the estimated velocities in conjunction with the available value of $(\rho_p^0 - \rho)$ satisfy the continuity equation and therefore no pressure correction is needed. The b term represents a source term in the pressure correction equation, which must vanish to zero during the iterative process.

The density value will be available only at the nodes of the main mesh (centered mesh), so the densities at the interface of the main control volume such as ρ_e must be approximated by some interpolation.

3.1.3.3 Boundaries discretization

All numerical solutions to fluid flow problems are defined in terms of the initial and boundary conditions. It is important to correctly specify the conditions and understand their role in the numerical algorithm. In transient problems the initial values of all flow variables need to be specified in all solution nodes of the flow domain.

In the border nodes on a centered grid, the control volume represents a volume and a null mass. Rather, it does not represent a real control volume, i. e. it is adjacent to the last control volume of the domain under study. For the case of border nodes on a staggered mesh, corresponds, a CV with smaller dimensions than the main CV, for the case of a uniform mesh the volume for the border node is exactly half the contiguous volume. For all the border nodes it is necessary to indicate which type of boundary condition prevails over them, if not, it will not be possible to solve the equations that need this information. The most common boundary conditions are Dirichlet, Neumann, and Robin conditions.

3.1.3.3.1 Dirichlet conditions (1st class)

This type of condition defines a value of the variable on the border nodes independently of the neighboring nodes, that is, the treatment of the coefficients is such that the node always maintains a constant value of the variable. From the algebraic equation in grouped coefficient notation equation (3.I5) it is established that $\Phi = f(x, y)$, so it can be concluded:

$$a_p = 1$$
$$a_E = a_W = a_N = a_S = 0 \qquad (3.31)$$
$$b = \phi_{boundary}$$

3.1.3.3.2 Von Neumann conditions (2nd class)

In this case, a gradient of the variable Φ is imposed perpendicular to the border in a similar way to the 1st class condition, it can be a function of space or time, that is:

$$\frac{\partial \phi}{\partial n} = f(x) \qquad (3.32)$$

For the present study, the boundary conditions for the horizontal walls are considered to be thermally insulated, this is $f(x) = 0$ as an example if an approximation is carried out for the boundary the following is obtained:

$$\frac{\phi_w - \phi_p}{(\delta x)_e} = 0 \tag{3.33}$$

3.1.3.3.3 Robin conditions (3rd class)

This type of boundary condition combines the first and second class boundary conditions and establishes that the analyzed boundary is governed by an inhomogeneous first-order differential equation that can be expressed as follows:

$$a\frac{\partial \phi}{\partial n} + b\phi = f(x) \tag{3.34}$$

Where a and b are different constants, for the case of a convective boundary the values of the constants will be $a = \lambda$ thermal conductivity, $b = h$ which is the convective heat transfer coefficient, and $f(x) = h\phi_{ambient}$ in such a way that:

$$\lambda\frac{\partial \phi}{\partial n} = h(\phi - \phi_{ambient}) \tag{3.35}$$

By discretizing the previous equation:

$$\lambda\frac{\phi_p - \phi_W}{\delta x_w} = h(\phi - \phi_{ambient}) \tag{3.36}$$

Rewriting:

$$\left(\frac{\delta x_w}{\lambda} + h\right)\phi_p = \left(\frac{\delta x_w}{\lambda}\right)\phi_W + h\phi_{ambient} \tag{3.37}$$

Where:

$$\begin{gathered} a_P = \frac{\delta x_w}{\lambda} + h \\ a_W = \frac{\delta x_w}{\lambda} \\ a_E = a_N = a_S = 0 \\ b = h\phi_{ambient} \end{gathered} \tag{3.38}$$

3.1.3.4 Solution method of the system of algebraic equations

There are two solution techniques for algebraic equations: direct methods and indirect or iterative methods. Examples of direct methods are the inversion of the coefficient matrix by Cramer's rule and Gaussian elimination (GE). Iterative methods include the Gauss-Seidel (GS) method, the line-by-line (LBL) method. The incomplete factorization (ILU) method and the conjugate gradient (CG) method, among others **[73]**.

Iterative methods are based on the repeated application of simple algorithms, which normally converge after a number of iterations. The number of operations for each iteration cycle is of the order of N, unlike direct methods, it is not possible to know a priori the number of iterations that will be necessary to obtain convergence, nor is it possible to guarantee convergence unless the system of equations satisfies a certain criterion. The main advantage of iterative methods is that only non-zero coefficients need to be stored in memory.

By discretizing the partial differential equations, a system of algebraic equations is obtained, which were solved by the iterative method of Gauss-Seidel line of implicit alternating directions (Line Gauss Seidel Alternating-Direction Implicit., LGS-ADI). The LGS-ADI method is a combination of the -by- (LBL) method with the Gauss-Seidel (GS) method used interchangeably. The coefficient matrix of the system of equations is penta-diagonal for the two dimensions case. In this type of matrices, the number of zero spaces is high and considerable memory space is needed to store them. Therefore, it is concluded that iterative methods are generally cheaper than direct methods **[66]**.

3.1.3.5 Convergence criterion

When using iterative methods to solve a system of equations, it must be considered that, when the solution of the problem tends to converge, the solution approaches the real solution asymptotically. It must also be considered that the numerical solution after a certain number of iterations no longer changes, and does not allow obtaining an improvement of the results towards the real solution, this is due to the errors involved in the truncations of the approximations, i. e., depending on the approximations used in the discretization process of the differential equations, certain results will be obtained and an improvement cannot be requested unless more exact approximations are used. This is why it is necessary to establish a convergence criterion of the iterative process from which the sufficiently convergent solution is considered. The residuals of the variables were calculated using the root mean square deviation (Equation (3.39)) for the entire solution domain.

$$\sum \geq R_{\phi}^{k} = \sqrt{\sum_{VC} \left(\left| (a_P \phi_i)^k - \left(\sum a_{vecinos} \phi_{vecinos} + b \right)^k \right| \right)^2} \qquad (3.39)$$

In solving the conservation equations of this study, it was established that the residual for all variables (velocities, pressure and temperature) was less than or equal to 10^{-10}.

3.1.3.6 Global algorithm of the iterative process

To solve the equations of mass and momentum, the SIMPLEC algorithm was implemented, and a summary of the procedure is presented below.

1. Starts with an estimated pressure field: P^*.
2. The momentum conservation equations are solved to obtain: u^* and v^*.
3. The pressure correction equation is solved to obtain: P'.
4. The pressure correction field P is used to correct the pressure field given by: $P = P^* + P'$.
5. Calculate the velocity components with the velocity correction values (determined with P) given by:

$$u = u^* + u$$

$$v = v^* + v$$

6. Solve other discretized conservation equations.
7. The convergence criterion is applied. If the criterion is reached, the results are printed, otherwise it continues with the next step.
8. Finally, in case of continuing with the iteration process, the pressure P becomes the estimated pressure P' and all the steps are repeated again until the solution converges.

A flowchart of the SIMPLEC algorithm is shown in Figure (3.5). It can be seen that for the SIMPLEC algorithm technique, the solution of the equations of conservation of mass and momentum is obtained sequentially.

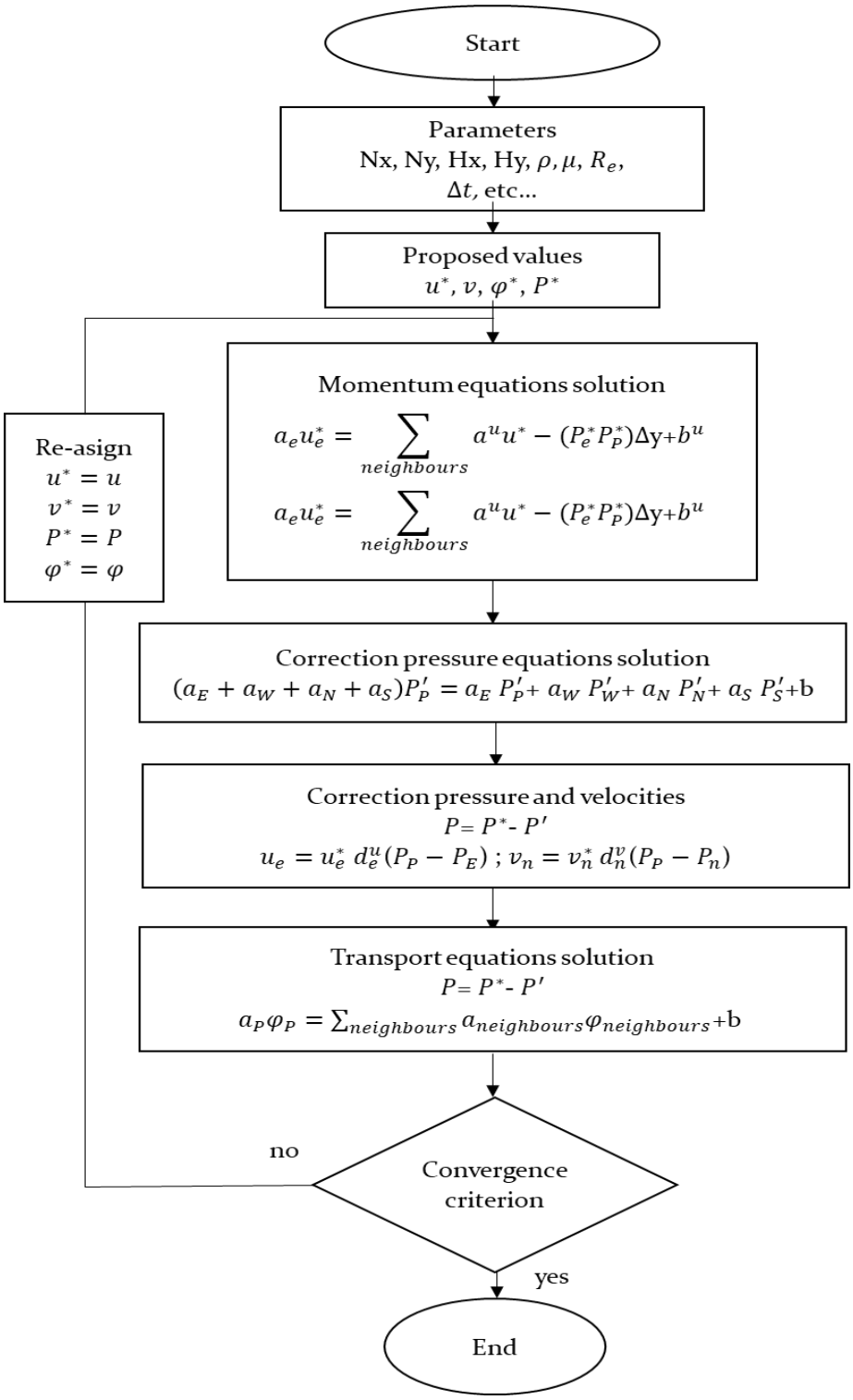

Figure 3.5 Flowchart for the SIMPLEC algorithm.

3.1.4 Solution method for the surface radiative exchange in the air cavity

The Radiosity-Irradiation Method (RIM) or net radiation method is applied in this study [**67**]. The method divides the cavity into N isothermal surfaces; the irradiance, radiosity, and view factors are considered uniform on each surface. An energy balance is carried out in each computational node of the surface under analysis, giving the expression:

$$q_{rad}^{total} = q_{out}^{rad} - q_{in}^{rad} \tag{3.40}$$

Considering that the energy that leaves the surface is composed of the emitted energy by the surface plus the reflected energy from the heat fluxes that impinge on the surface:

$$q_{out}^{rad} = \varepsilon\sigma T^4 + \rho q_{int}^{rad} \tag{3.18}$$

Where ε is the surface emissivity and ρ is the reflectivity which is obtained from the relation $\rho = 1 - \varepsilon$ used for opaque surfaces. The term q_{in}^{rad} encompasses the portions of energy leaving the other surfaces of the cavity $\left(q_{out'_s}^{rad}\right)$ with which the surface interacts in which the energy balance for net radiation is performed. Therefore, the flow of energy that falls on the surface under analysis also contains part of the energy q_{out}^{rad} of this surface that is reflected in the other surfaces and returns. Hence, the incident energy q_{in}^{rad} is expressed as:

$$q_{in}^{rad} = \sum F_v q_{out}^{rad} \tag{3.42}$$

Replacing expressions (3.41) and (3.42) into equation (3.40), the equation for the resulting radiative energy flux is as follows:

$$q_{rad}^{total} = \left(\varepsilon\sigma T^4 + \rho q_{int}^{rad}\right) - \sum F_v q_{out}^{rad} \tag{3.193}$$

Where F_v is the view factors, which can be determined from some approximation or by Hottels's crossed-string method for the two dimensions case [**67**]. Therefore, the resulting radiative fluxes for each cavity surface are called $q_{rad}^1, q_{rad}^2, q_{rad}^3, q_{rad}^4$ for the south, west, north and east surfaces, respectively.

An RIM flowchart for calculating radiative heat transfer between cavity walls is shown in Figure 3.6.

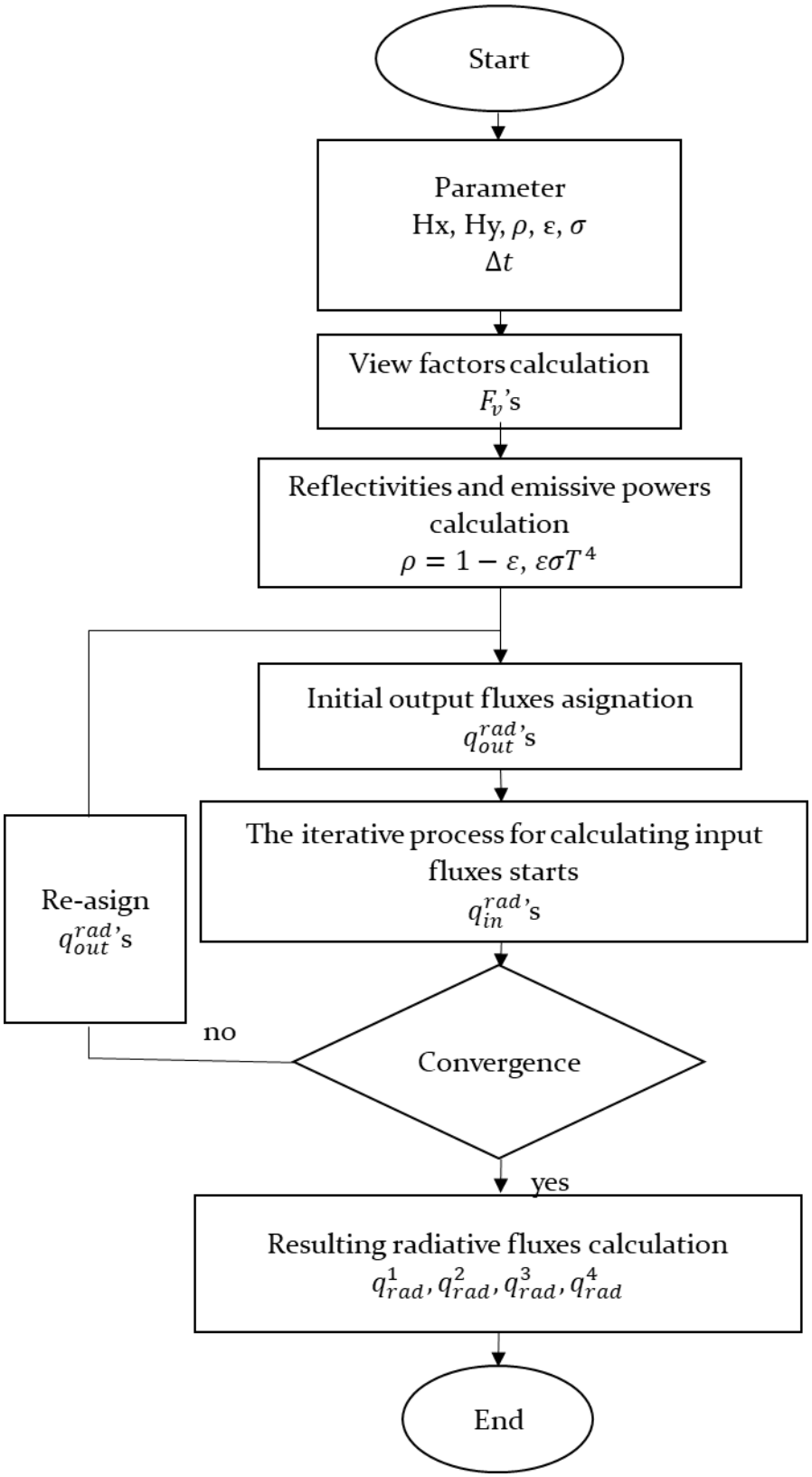

Figure 3.6 Flowchart for radiative Surface exchange in the cavity.

3.1.5 Solution method of the conductive model for the semi-transparent wall

The mathematical model for heat conduction was presented in the previous chapter (section 2.2.2.2). It is observed in this model that there are no terms for convective flows since it is a solid medium. Also, in this case the general discretized equation obtained for the convection-diffusion equation shown previously can be applied. This becomes valid for the conductive model of the semi-transparent wall, if the F's cancel out, with this consideration equation 3.15 reduces to:

$$a_p T_p = a_E T_E + a_W T_W + a_N T_N + a_S T_S + b \tag{3.420}$$

Where:

$$a_E = \frac{(\lambda/C_P)}{\delta x_e}\Delta y$$

$$a_W = \frac{(\lambda/C_P)}{\delta x_w}\Delta y$$

$$a_N = \frac{(\lambda/C_P)}{\delta x_n}\Delta x \tag{3.45}$$

$$a_S = \frac{(\lambda/C_P)}{\delta x_s}\Delta x$$

$$a_P = a_E + a_W + a_N + a_S$$

$$b = \rho_p^0 \frac{\Delta x \Delta y}{\Delta t} T_p^0 + \frac{1}{C_P} G\left(\exp[-S(H_x - x_i)] - \exp\left[-S_g(H_x - x_{i-1})\right]\right)\Delta y$$

The system of algebraic equations generated by equation (3.44) was solved by the LGS-ADI method, in which an unnormalized residual less than or equal to, was used to finish the iterative solution process.

3.1.6 Solution method of the conductive model for the phase change material

Because PCM materials change state as a function or with respect to their temperature over time, they must be treated mathematically in a special way compared to conventional systems. In order to analyze the thermal behavior of phase change materials in a system, different solution methods are applied, which are divided into two families: front tracking methods and fixed-domain methods **[68]**, **[69]**. The front tracking methods consist of having a diffusive governing equation for each phase of matter, for example, the solid and liquid phase (Equation (3.46) and (3.47) respectively) and an interface condition (Equation (3.48)).

Solid phase equation:

$$\frac{\partial(\rho_{sol} C_{p_{sol}} T_{sol})}{\partial t} = \frac{\partial}{\partial x}\left(\lambda_{sol}\frac{\partial T}{\partial x}\right) + \frac{\partial}{\partial x}\left(\lambda_{sol}\frac{\partial T}{\partial x}\right) \quad (3.46)$$

Liquid phase equation:

$$\frac{\partial(\rho_{liq} C_{p_{liq}} T_{liq})}{\partial t} = \frac{\partial}{\partial x}\left(\lambda_{liq}\frac{\partial T}{\partial x}\right) + \frac{\partial}{\partial x}\left(\lambda_{liq}\frac{\partial T}{\partial x}\right) \quad (3.217)$$

Interphase condition:

$$\lambda_i \frac{\partial T_i}{\partial n} - \lambda_i \frac{\partial T_i}{\partial n} = \rho h_i \frac{\partial S_i}{\partial t} \quad (3.48)$$

The fixed domain methods consist of using a single equation for both phases of the matter, and these methods are:

- Effective heat capacity method (C_p effective).
- Phase change liquid fraction method.
- H enthalpy method.
- Assumed heat flow method.
- Carman-Koseny method.

For the present study, the mathematical model of the PCM was solved using the C_p effective method, which is in the family of fixed-domain methods **[70-72]**. The C_p effective method was selected because of its less complicated implementation and the easy access to the information needed for the materials properties. In this method the phase change process occurs within the heat capacity term by adding the latent heat while the phase change from solid to liquid takes place. Thus, the C_p effective includes the energy stored as sensible and latent heat of the PCM. This can be expressed as a temperature dependent property. Therefore, to treat the PCM with the C_p effective, the chain rule is applied to the temporal term to the heat conduction equation in transitory state as follows:

$$\frac{\partial(\rho C_p T)}{\partial t} = T\frac{\partial(\rho C_p)}{\partial t} + \rho C_p \frac{\partial(T)}{\partial t} \quad (3.49)$$

Considering that the properties (ρ, C_p) are constant, the first term on the right-hand side of the equality is considered zero, so the equation can be rewritten like this:

$$\frac{\partial(\rho Cp\mathrm{T})}{\partial t} = \rho Cp\frac{\partial(\mathrm{T})}{\partial t} \quad (3.50)$$

Replacing equation (3.50) into the heat conduction equation

$$\rho Cp\frac{\partial(\mathrm{T})}{\partial t}=\frac{\partial}{\partial x}\left[\lambda\frac{\partial T}{\partial x}\right]+\frac{\partial}{\partial y}\left[\lambda\frac{\partial T}{\partial y}\right] \tag{3.51}$$

And adding $\rho h_{ls}\frac{\partial(\mathrm{F}_{pcm,l})}{\partial t}$ in the time term equation (3.51) becomes:

$$\rho\left(C_p\frac{\partial(T)}{\partial t}+h_{ls}\frac{\partial\left(\mathrm{F}_{pcm,l}\right)}{\partial t}\right)=\frac{\partial}{\partial x}\left(\lambda\frac{\partial T}{\partial x}\right)+\frac{\partial}{\partial x}\left(\lambda\frac{\partial T}{\partial x}\right) \tag{3.52}$$

where:

$\mathrm{F}_{pcm,l}=\left(\frac{T-T_S}{T_L-T_S}\right)^m$ is the liquid fraction of phase change for $0\ \leq\ f_{pcm,l}\ \leq\ 1$ and if $m=1$ the model is linear.

Applying the chain rule to the term $\frac{\partial(\mathrm{F}_{pcm,l})}{\partial t}$ it is rewritten as follows:

$$\frac{\partial(\mathrm{f}_{pcm,l})}{\partial t}=\frac{\partial(\mathrm{f}_{pcm,l})}{\partial T}\frac{\partial T}{\partial t} \tag{3.53}$$

Replacing equation (3.53) into (3.52) and factoring $\frac{\partial T}{\partial t}$ the equation becomes:

$$\underbrace{\rho\left(C_p+\frac{h_{ls}}{\Delta T}\right)}_{C_p\ Effective}\frac{\partial T}{\partial t}=\frac{\partial}{\partial x}\left(\lambda\frac{\partial T}{\partial x}\right)+\frac{\partial}{\partial x}\left(\lambda\frac{\partial T}{\partial x}\right) \tag{3.54}$$

This last equation being the mathematical model of the C_p effective method. To obtain the discretized equation from Equation (3.54), it is necessary to carry out the spatial integration over the control volume. Likewise, the temporal integration for time $t=t_0$ until $t=t+\Delta_t$:

$$\begin{aligned}&\int_t^{t+\Delta t}\int_s^n\int_w^e\rho\left(C_p+\frac{h_{ls}}{\Delta T}\right)\frac{\partial(\mathrm{T})}{\partial t}dxdydt\\&=\int_t^{t+\Delta t}\left(\int_s^n\int_w^e\frac{\partial}{\partial x}\left[\lambda\frac{\partial T}{\partial x}\right]dxdy+\int_s^n\int_w^e\frac{\partial}{\partial y}\left[\lambda\frac{\partial T}{\partial y}\right]dxdy\right)dt\end{aligned} \tag{3.55}$$

Integrating and using the midpoint rule spatially between the limits "w, e", and “s" respectively, which are the boundaries of the control volume we obtain:

$$\int_{t}^{t+\Delta t} \rho\left(C_p + \frac{h_{ls}}{\Delta T}\right)\frac{\partial(\mathrm{T})}{\partial t}\Delta x\Delta y = \int_{t}^{t+\Delta t}\left(\left[\left[\lambda\frac{\partial T}{\partial x}\right]_e - \left[\lambda\frac{\partial T}{\partial x}\right]_w\right]\Delta y + \left[\left[\lambda\frac{\partial T}{\partial y}\right]_n - \left[\lambda\frac{\partial T}{\partial y}\right]_s\right]\Delta x\right)dt \tag{3.56}$$

Next, an implicit discretization scheme is used to integrate the equation (3.56) over time to maintain its stability since PCMs present numerical instability. Therefore, the equation changes to:

$$\rho\left(C_p + \frac{h_{ls}}{\Delta T}\right)\left(T_P - T_P{}^0\right)\Delta y\Delta x = \left\{\left[\left[\lambda\frac{\partial T}{\partial x}\right]_e - \left[\lambda\frac{\partial T}{\partial x}\right]_w\right]\Delta y + \left[\left[\lambda\frac{\partial T}{\partial y}\right]_n - \left[\lambda\frac{\partial T}{\partial y}\right]_s\right]\Delta x\right\}\Delta t \tag{3.57}$$

To calculate the gradients T at the interfaces, a linear approximation is used (this approximation is known as central difference scheme). For this, the Taylor series is used, with which the high order terms Δx^2 (truncation error) are neglected, and the following expressions are obtained.

$$\left.\frac{\partial T}{\partial x}\right|_e = \frac{T_P - T_E}{\delta X_{PE}}$$

$$\left.\frac{\partial T}{\partial x}\right|_w = \frac{T_w - T_P}{\delta X_{WP}} \tag{3.58}$$

$$\left.\frac{\partial T}{\partial y}\right|_n = \frac{T_P - T_n}{\delta X_{Pn}}$$

$$\left.\frac{\partial T}{\partial y}\right|_s = \frac{T_s - T_p}{\delta y_{Ps}}$$

Replacing the expressions of equation (3.58) into equation (3.57), we obtain:

$$\underbrace{\left[\rho\left(C_p + h_{ls}\frac{\partial\left(\mathrm{F}_{pcm,l}\right)}{\partial t}\right)\frac{\Delta x\Delta y}{\Delta t}\right]}_{a_p} T_p - \underbrace{\left[\rho\left(C_p + h_{ls}\frac{\partial\left(\mathrm{F}_{pcm,l}\right)}{\partial t}\right)\frac{\Delta x\Delta y}{\Delta t}\right]}_{b} {T_P}^0$$

$$= \underbrace{\frac{\left.\frac{\lambda_e}{Cp}\right|_e}{\delta X_{PE}}\Delta y}_{a_e} T_E + \underbrace{\frac{\left.\frac{\lambda_e}{Cp}\right|_w}{\delta X_{PW}}\Delta y}_{a_w} T_W + \underbrace{\frac{\left.\frac{\lambda_e}{Cp}\right|_n}{\delta X_{PN}}\Delta x}_{a_n} T_N \qquad (3.59)$$

$$+ \underbrace{\frac{\left.\frac{\lambda_e}{Cp}\right|_s}{\delta X_{PS}}\Delta x}_{a_s} T_S + \underbrace{\rho\frac{\Delta x\Delta y}{\Delta t}}_{b}$$

In this way, the discrete equation for grouped coefficients is as follows:

$$a_p T_p = a_E T_E + a_W T_W + a_N T_N + a_S T_S + b \qquad (3.60)$$

3.1.7 General solution process for the mathematical model of the window system with PCM-shutter

1. The starting parameters and conditions are entered (dimensions, material, type of fluid, etc.)
2. The computational mesh is generated on which the equations of the mathematical model are solved.
3. View factors for radiative exchange in the cavity are calculated.
4. The radiative exchange model is solved to determine the net radiative heat fluxes at the differential surfaces in the cavity.
5. The heat conduction in the semi-transparent wall is solved.
6. The physical properties of the PCM are calculated.
7. The heat conduction in the PCM wall is solved.
8. The velocity and pressure field are determined using the SIMPLE algorithm.
9. The energy equation for the cavity is solved.
10. The solutions are evaluated by means of a convergence criterion for each time step, while this criterion is not met, steps 6 onwards are repeated.
11. If the criterion is met, then the result are printed.
12. The solutions are evaluated by means of a temporary convergence criterion, while this criterion is not met, steps 8 onwards are repeated.

13. If the temporal convergence criterion is met, the results are printed and the simulation ends.

Figure 3.7 presents the flowchart that represents the general solution procedure.

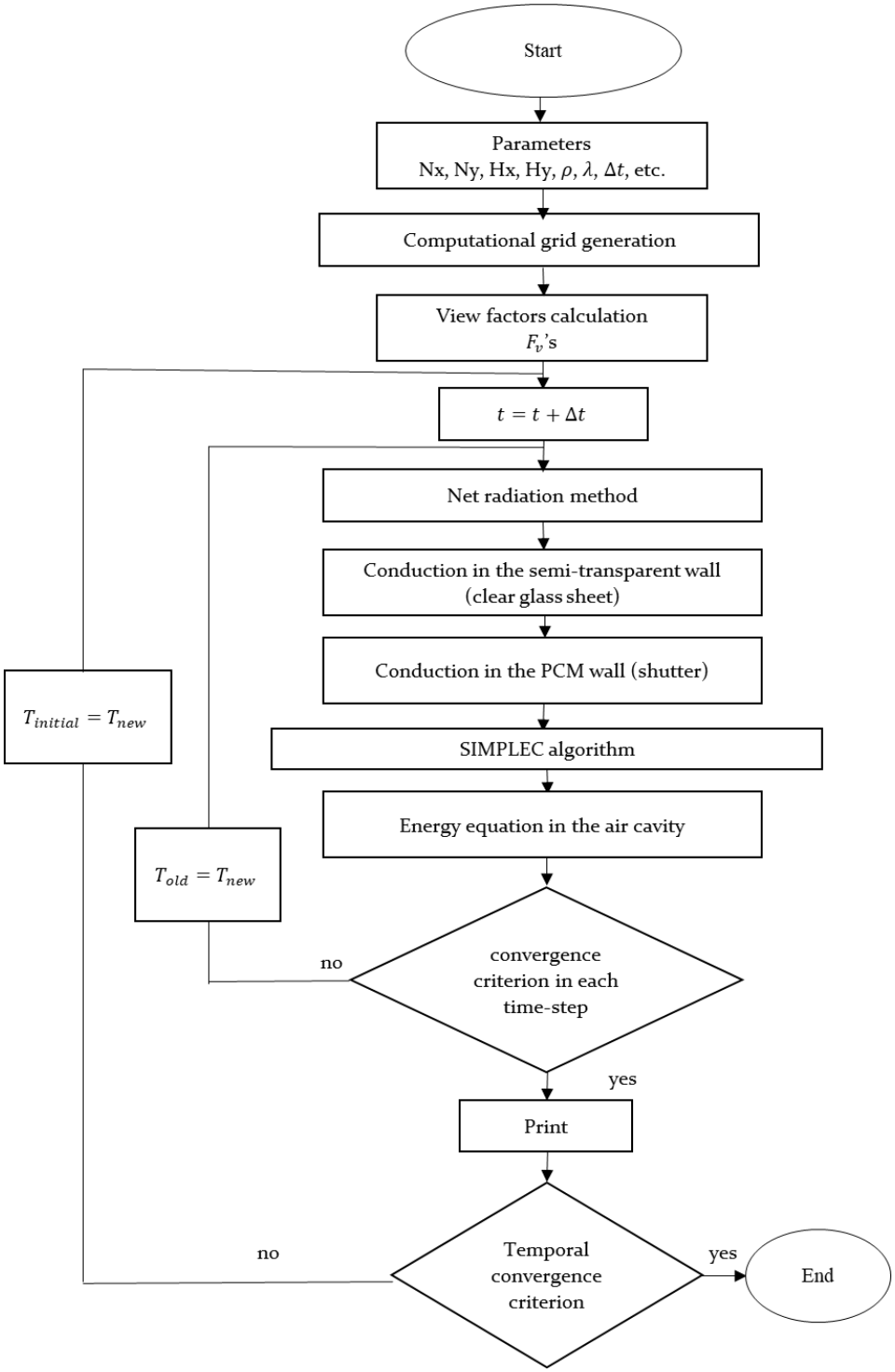

Figure 3.7 General flowchart for window with PCM solution.

3.2 Solution of the GEB model

As mentioned above, this study, considers a hybrid solution methodology in which the proposed system of window shutter PCM is solved by means of CFD using the FVM. This proposed system was coupled to a GEB model (representative of the room). Energy balances are applied with the objective of determining from a general point of view the amount of energy that is exchanged and accumulated in a system as a temperature difference consequence, i. e., determine the heat transfer global effects, without paying special interest in detailed analysis of the phenomena involved. Therefore, less detailed results are obtained, but the computational time is drastically reduced, which provides the opportunity to carry out a complete study that pays attention to a greater number of desired parameters to evaluate the thermal performance of the windows as needed.

The GEB method is based on the energy conservation law, which establishes that the exchange of the thermal flow or heat exchange in a system is equivalent to the difference between the heat that enters the system and the heat that leaves, plus the heat exchange within the system, Equation (3.61) **[79]**.

3.2.1 Energy balance development for the envelope elements

To determine the exchanged and accumulated energy in a system an energy balance is carried out on the element of interest. Equation (3.61) show the general energy balance for any element in unsteady state, where the heat flux that enters the element minus the heat flux that leaves it, is equal to the heat flux stored within it.

$$q_{in} - q_{out} = q_{stored}$$

$$q_{in} - q_{out} = \frac{\partial(\rho C_p T_1)}{\partial t} Hx_{element} \tag{3.61}$$

Since $q_{stored} = \frac{\partial(\rho C_p T_1)}{\partial t} Hx_{element}$, only the transitory term is considered in order to transform the differential term into an algebraic term.

$$\frac{\partial(\rho C_p T)}{\partial t} Hx_{element}$$

$$\frac{\rho C_p Hx}{\partial t}(T - T^0) = a_p^0(T - T^0) \tag{3.62}$$

Where $Hx_{element}$ is the thickness of the element under analysis.

3.2.1.1 Energy balance on the roof element

As shown in Figure 2.2, the roof element is interacting with the T_{ext}, T_{sky}, G and the T_{room} so considering an energy flux with a downwards direction the balance takes the form shown in Equation (3.63) below:

$$q_{in} = \frac{T_{sky} - T_{roof}}{\frac{1}{h^{rad}_{sky-roof}}} + \frac{T_{ext} - T_{roof}}{\frac{1}{h_{ext-roof}} + \frac{H_{x,roof}}{2\lambda_{roof}}} + \alpha_{roof} G$$

$$q_{out} = \frac{T_{roof} - T_{room}}{\frac{H_{x,roof}}{2\lambda_{roof}} + \frac{1}{h_{roof-room}}} + q^{rad}_{roof} \tag{3.63}$$

Where q_{in} and q_{out} are the energy fluxes that enter and exit the element, G is the solar radiation, λ_{roof} is the conductivity of the solid element, α_{roof} the absortance of the roof, $H_{x,roof}$ its thickness, $h_{ext-roof}$ is the convective heat transfer coefficient (CHTC) between the solid element and the fluid element, $h^{rad}_{sky-roof}$ is the radiative heat transfer exchange between the surface of the element and the sky and q^{rad}_{roof} is the non-participating radiative heat flux between the surface of the element and the surface of the rest of elements inside the room. Considering that $q_{in} - q_{out} = q_{stored}$ then:

$$\left(\frac{T_{sky} - T_{roof}}{\frac{1}{h^{rad}_{sky-roof}}} + \frac{T_{ext} - T_{roof}}{\frac{1}{h_{ext-roof}} + \frac{H_{x,roof}}{2\lambda_{roof}}} + \alpha_{roof} G \right) - \left(\frac{T_{roof} - T_{room}}{\frac{H_{x,roof}}{2\lambda_{roof}} + \frac{1}{h_{roof-room}}} + q^{rad}_{roof} \right) = a^0_p (T_{roof} - T^0_{roof}) \tag{3.64}$$

$$\left(\frac{T_{sky} - T_{roof}}{a_0} + \frac{T_{ext} - T_{roof}}{a_1} \right) + \alpha_{roof} G - \left(\frac{T_{roof} - T_{room}}{a_2} \right) + q^{rad}_{roof} = a^0_p (T_{roof} - T^0_{roof})$$

$$\left(\frac{a_1 T_{sky} - a_1 T_{roof} + a_0 T_{ext} - a_0 T_{roof}}{a_0 a_1} + a_0 a_1 \alpha_{roof} G\right)$$

$$- \left(\frac{T_{roof} - T_{room}}{a_2} + q_{roof}^{rad}\right) = a_p^0 (T_{roof} - T_{roof}^0)$$

$$a_1 a_2 T_{sky} - a_1 a_2 T_{roof} + a_0 a_2 T_{ext} - a_0 a_2 T_{roof} + a_0 a_1 a_2 \alpha_{roof} G - a_0 a_1 T_{roof} \quad (3.65)$$

$$- a_0 a_1 T_{room} + a_0 a_1 a_2 q_{roof}^{rad} = a_0 a_1 a_2 a_p^0 (T_{roof} - T_{roof}^0)$$

Developing the equation, the mathematical model for the roof element in lumped coefficient notation is as shown in Equation (3.66):

$$\begin{aligned} &\left(a_1 a_2 + a_0 a_2 + a_0 a_1 + a_0 a_1 a_2 a_p^0\right) T_{roof} - a_0 a_1 T_{room} \\ &= a_1 a_2 T_{sky} + a_0 a_2 T_{ext} + a_0 a_1 a_2 \alpha_{roof} G + a_0 a_1 a_2 q_{roof}^{rad} \\ &+ a_0 a_1 a_2 a_p^0 T_{roof}^0 \end{aligned} \quad (3.66)$$

This process is the same for the rest of the envelope elements. Detailed development is shown in appendix B.

3.2.2 Energy balance development for the room

The room element is interacting with the T_{roof} and the T_{floor} as well with T_{W_3} and the T_g and also with T_{W_4} and the T_{W_2} so considering an energy flux with downwards and left to right direction following the analogies of the previous balances the energy balance of the room element is as follows below in Equation (3.67):

$$\begin{aligned} q_{in} &= \frac{T_{W_4} - T_{room}}{\frac{H_{x,W_4}}{2\lambda_{W_4}} + \frac{1}{h_{W_4-room}}} + \frac{T_{roof} - T_{room}}{\frac{H_{x,roof}}{2\lambda_{roof}} + \frac{1}{h_{conv,roof-room}}} + \frac{T_{W_3} - T_{room}}{\frac{H_{x,W_3}}{2\lambda_{W_3}} + \frac{1}{h_{W_3-room}}} \\ q_{out} &= \frac{T_{room} - T_g}{\frac{1}{h_{room-g}} + \frac{H_{x,g}}{2\lambda_g}} + \frac{T_{room} - T_{floor}}{\frac{1}{h_{conv,room-floor}} + \frac{H_{x,floor}}{2\lambda_{floor}}} + \frac{T_{room} - T_{W_2}}{\frac{1}{h_{room-W_2}} + \frac{H_{x,W_2}}{2\lambda_{W_2}}} \end{aligned} \quad (3.67)$$

considering that $q_{in} - q_{out} = q_{stored}$ then:

$$\frac{T_{W_4}-T_{room}}{c_0}+\frac{T_{roof}-T_{room}}{c_1}+\frac{T_{W_3}-T_{room}}{c_2}-\frac{T_{room}-T_g}{c_3}+\frac{T_{room}-T_{floor}}{c_4}+\frac{T_{room}-T_{W_2}}{c_5}=a_p^0(T_{room}-T_{room}^0) \tag{3.68}$$

Developing the equation:

$$\frac{c_1c_2T_{W_4}-c_1c_2T_{room}+c_0c_2T_{roof}-c_0c_2T_{room}+c_0c_1T_{W_3}-c_0c_1T_{room}}{c_0c_1c_2}$$

$$-\frac{c_4c_5T_{room}-c_4c_5T_g+c_3c_5T_{room}-c_3c_5T_{floor}+c_3c_4T_{room}-c_3c_4T_{W_2}}{c_3c_4c_5}$$

$$=a_p^0(T_{room}-T_{room}^0)$$

$$\begin{aligned}c_1c_2c_3c_4c_5T_{W_4}-c_1c_2c_3c_4c_5T_{room}+c_0c_2c_3c_4c_5T_{roof}-c_0c_2c_3c_4c_5T_{room}\\+c_0c_1c_3c_4c_5T_{W_3}-c_0c_1c_3c_4c_5T_{room}-c_0c_1c_2c_4c_5T_{room}\\-c_0c_1c_2c_4c_5T_g+c_0c_1c_2c_3c_5T_{room}-c_0c_1c_2c_3c_5T_{floor}\\+c_0c_1c_2c_3c_4T_{room}-c_0c_1c_2c_3c_4T_{W_2}\\=c_0c_1c_2c_3c_4c_5a_p^0(T_{room}-T_{room}^0)\end{aligned} \tag{3.69}$$

the mathematical model for the room element in lumped coefficient notation is as shown in Eq (3.70):

$$\begin{aligned}&-c_1c_2c_3c_4c_5T_{W_4}-c_0c_2c_3c_4c_5T_{roof}-c_0c_1c_3c_4c_5T_{W_3}+\big(c_1c_2c_3c_4c_5+\\&c_0c_2c_3c_4c_5+c_0c_1c_3c_4c_5+c_0c_1c_2c_4c_5+c_0c_1c_2c_3c_5+c_0c_1c_2c_3c_4+\\&c_0c_1c_2c_3c_4c_5a_p^0\big)T_{room}-c_0c_1c_2c_4c_5T_g-c_0c_1c_2c_3c_5T_{floor}-c_0c_1c_2c_3c_4T_{W_2}=\\&c_0c_1c_2c_3c_4c_5a_p^0T_{room}^0\end{aligned} \tag{3.70}$$

The matrix notation for the equations of all elements is as follows:

$$\begin{bmatrix} (FF) & 0 & 0 & -f_0f_1 & 0 & 0 & 0 \\ 0 & (AA) & 0 & -a_0a_1 & 0 & 0 & 0 \\ 0 & 0 & (BB) & -b_0b_1 & 0 & 0 & 0 \\ -c_1c_2c_3c_4c_5 & -c_0c_2c_3c_4c_5 & -c_0c_1c_3c_4c_5 & (CC) & -c_0c_1c_2c_4c_5 & -c_0c_1c_2c_3c_5 & -c_0c_1c_2c_3c_4 \\ 0 & 0 & 0 & -d_2d_0 & (DD) & 0 & 0 \\ 0 & 0 & 0 & -e_2 & 0 & (EE) & 0 \\ 0 & 0 & 0 & -g_2g_0 & 0 & 0 & (GG) \end{bmatrix}$$

$$* \begin{bmatrix} T_{W_4} \\ T_{roof} \\ T_{W_3} \\ T_{room} \\ T_g \\ T_{floor} \\ T_{W_2} \end{bmatrix} = \begin{bmatrix} f_1f_2T_{sky} + f_0f_2T_{ext} + f_0f_1f_2\alpha_{W_4}G + f_0f_1f_2a_p^0T_{W_4}^0 \\ a_1a_2T_{sky} + a_0a_2T_{ext} + a_0a_1a_2\alpha_{roof}G + a_0a_1a_2a_p^0T_{roof}^0 \\ b_1b_2T_{sky} + b_0b_2T_{ext} + b_0b_1b_2\alpha_{W_3}G + b_0b_1b_2a_p^0T_{W_3}^0 \\ c_0c_1c_2c_3c_4c_5a_p^0T_{room}^0 \\ d_1d_2T_{sky} + d_1d_0T_{ext} + d_1d_2d_0\alpha_{roof}G + d_1d_2d_0a_p^0T_g^0 \\ e_1T_{earth} + e_1e_2a_p^0T_{floor}^0 \\ g_1g_2T_{sky} + g_1g_0T_{ext} + g_1g_2g_0\alpha_{W_2}G + g_1g_2g_0a_p^0T_{W_2}^0 \end{bmatrix} \quad (3.71)$$

3.2.3 General solution process for the mathematical model of the room and its envelope elements

The computational model was written using Fortran language and given de much simpler complexity of its solution, compared with the CFD model, Figure 6.7 shows the flowchart for the code that solves the conjugate heat transfer in the cubic cavity representative of the room.

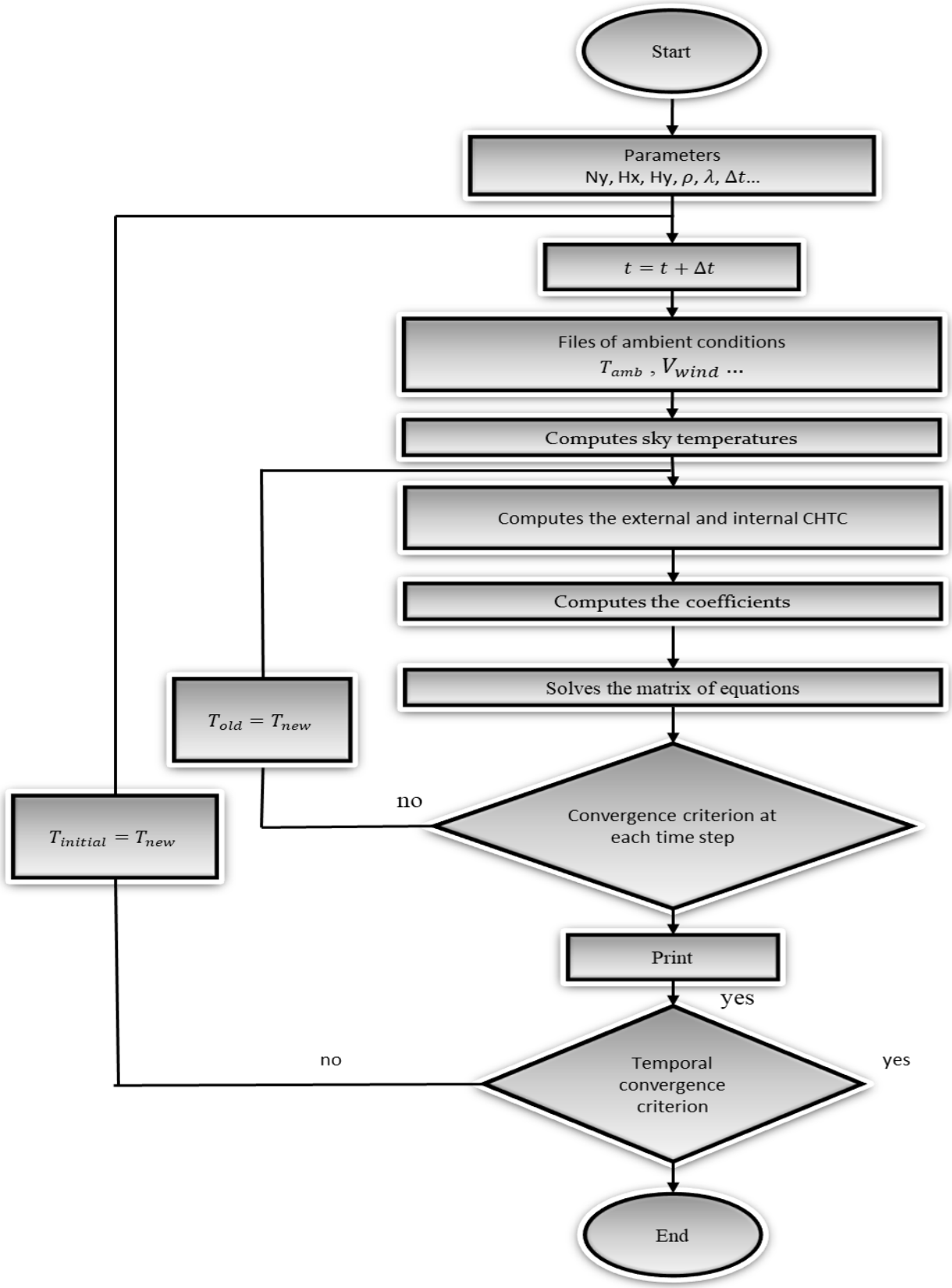

Figure 3.8 General flowchart for the room representative cubic cavity solution.

3.3 Verification of the numerical codes of the CFD and GEB models

Verification problems are presented for the computational numerical code developed to solve the CFD and the GEB models. Verification troubleshooting is carried out in order to verify that the developed numerical code does not contain errors and provides reliable results. The verification process is also a crucial step towards the coupling of both methodologies (CFD and GEB)

3.3.1 CFD model

The CFD model verification process was carried out by solving case studies reported in the literature. As this model is two-dimensional, the developed numerical code was adequate to all the previously mentioned two-dimensional problems. Once the code is adapted to the reference cases, its results will be compared to the cases reported in the literature.

3.3.1.1 Heat transfer in a differentially heated cavity

The problem of a differentially heated cavity through its vertical walls is solved. It is considered that inside the cavity there is dry air, which is a Newtonian and incompressible fluid whose flow is in a laminar regime. The geometry is formed of two isolated or adiabatic horizontal walls and two isothermal vertical walls (T_H and T_C), and the boundary conditions of the four walls is non-slip. The fluid has the following properties: $\lambda = 25.63x10^{-3}W/(K \cdot m), \rho = 1.2047kg/m^3, Cp = 1.004kJ/(K \cdot kg), \mu = 1.817x10^{-05}\ kg/s \cdot m, \beta = 3.411x10^{-3}K^{-1}, g = 9.81\ m/s^2, Pr = 0.712.$ The following Rayleigh numbers were considered: 10^3, 10^4, 10^5, 10^6. Because it is a widely known problem, it is used to validate numerical codes and the obtained numerical solution is compared with the reference data reported by De Vahl Davis in 1983 [**80**].

The movement of the fluid in this problem occurs due to the buoyancy term which represents the change in density caused by the temperature difference between the vertical walls. For the buoyancy term, the Boussinesq approximation $\left((\rho_\infty - \rho) = \beta(T - T_\infty)\right)$ is used, which allows considering the properties constant in the entire domain except in the buoyancy term, where the change in temperature in the fluid causes a change in its density and its movement; is based on assuming that the difference in inertia is negligible but gravity is strong enough to cause a significant difference in the specific weight of the fluid.

The mathematical model for the problem is given by the conservation equations of mass, momentum, and energy (2.7-2.10).

To verify the obtained results, it is also necessary to make the results dimensionless for the length and velocity scales, leaving H y $\sqrt{g\beta\Delta T\ H}$ respectively. The problem in dimensionless form as a function of the Rayleigh number (Ra) is given by $Ra = \rho g\beta\Delta T\ H^3\ /\ \alpha v$ and the Prandtl number

(Pr) by $Pr = \nu/\alpha$, where ν is the kinematic viscosity and α is the thermal diffusivity. As can be seen, the dimension of the cavity (H) is not specified, because it is determined based on the Rayleigh number. Also $\Delta T = T_H - T_C$ is the temperature difference between the isothermal walls and the dimensionless temperature is defined as $T^* = (T - T_C)/\Delta T$

The problem was solved using the SIMPLE algorithm in a steady state and with a 61x61 mesh. The values of the average, maximum and local minimum Nusselt number in the hot wall of the cavity and the dimensionless velocities in the center of the cavity are compared. The comparison is made by means of the maximum dimensionless velocity components (equation (3.72)) and the average Nusselt numbers (equations (3.73) and (3.74)), maximum and minimum in the hot wall of the cavity.

$$u^*{}_{max} = \frac{u_{max}}{\sqrt{g\beta\Delta T\, H}} \qquad v^*{}_{max} = \frac{v_{max}}{\sqrt{g\beta\Delta T\, H}} \tag{3.72}$$

The local Nusselt number on the hot wall is defined by the ratio of heat flow by local convection to heat flow by conduction, that is:

$$Nu_y = \frac{q_{conv}}{q_{cond}} = \frac{-\lambda \dfrac{\partial T}{\partial x}}{-\lambda \dfrac{T_H - T_C}{H}} = \frac{T_H - T_y}{T_H - T_C} \cdot \frac{H}{\Delta x} \tag{3.73}$$

Where T_y is the temperature of the fluid at y position and Δx is the horizontal difference at which this temperature is calculated with respect to the hot vertical wall. Finally, the mean Nusselt number is the result of integration over the entire vertical wall of the local Nusselt number:

$$Nu_{mean} = \frac{1}{H}\int_0^H Nu_y dy \tag{3.74}$$

The data presented in Table 3.2 refer to the average, maximum and minimum values of the Nusselt (Nu) taken from the hot wall of the cavity; the maximum dimensionless velocities u and at the center of the cavity are also presented in Table 3.3. Table 3.2 that that the results obtained in this work are satisfactory.

Table 3.3 Comparison of the results against those reported in the literature

Parameters	De Vahl Davis	This study	Error (%)
		Ra=10^3	
u_{max}	0.13	0.13	2.1
u_{max}	0.14	0.13	1.4
Nu_{max}	1.5	1.5	0.4
Nu_{min}	0.7	0.7	0.3
Nu_{mean}	1.1	1.1	0.2
		Ra=10^4	
u_{max}	0.2	0.2	0.0
u_{max}	0.2	0.2	0.0
Nu_{max}	3.5	3.5	0.0
Nu_{min}	0.5	0.5	0.0
Nu_{mean}	2.2	2.2	0.0
		Ra=10^5	
u_{max}	0.1	0.1	0.0
u_{max}	0.2	0.2	0.0
Nu_{max}	0.7	7.8	0.0
Nu_{min}	7.3	0.6	0.1
Nu_{mean}	4.5	4.5	0.0
		Ra=10^6	
u_{max}	0.0	0.0	0.0
u_{max}	0.2	0.2	0
Nu_{max}	18	18	0.0
Nu_{min}	0.9	0.7	0.2
Nu_{mean}	8.8	9.0	0.2

With the results shown in Table 3.3, there are small deviations in the results presented in this work compared with those reported in the literature, so it can be concluded that the developed code presents reliable and satisfactory results for this case.

3.3.1.2 Conjugate heat transfer in a differentially heated cavity with opaque conductive wall

The problem of conjugate heat transfer (conduction-convection) is solved in a differentially heated square cavity that is in contact with a wall with a thickness H_{xw}. The main objective is to analyze the effect of wall conduction on the convective flow of the cavity. It is considered that

inside the cavity there is dry air which is a Newtonian and incompressible fluid whose flow is in a laminar regime with constant properties (the Boussinesq approximation applies). The square cavity, which has two isolated or adiabatic horizontal walls with length H_x and two isothermal vertical walls (T_H y T_C) with length H_y and that is in contact with a wall of thickness H_{xw}; the boundary conditions of the four walls are non-slip. For the fluid it is considered, $Pr = 0.712$ and the Grashof number was varied (10^3, 10^5 y 10^6).

The equations that govern the phenomenon are the equations of mass, momentum and energy, finally the problem in a dimensionless form is a function of the Grashof number ($Gr = g\beta\Delta T\, H^3 / \upsilon^2$). For the numerical verification of the developed code, the obtained result was compared with those obtained by Kaminski and Prakash (1986) **[81]**.

Table 3.4 shows the average Nusselt numbers obtained for the Grashof values taken into consideration for this problem for a thickness ratio ($\frac{H_{XW}}{H_X}$) of 0.2 and 0.4 and for the conductivity ratio ($\frac{K_W H_X}{K H_{XW}}$) of 5, 25, 50 and 5000, comparing them with the reported in the literature.

Table 3.4 Comparison of the average Nusselt number for different Grashof numbers.

$\frac{K_W H_X}{K H_{XW}}$	$\frac{H_{XW}}{H_X} = 0.2$			$\frac{H_{XW}}{H_X} = 0.4$		
	Kaminski and Prakash (1986)	This study	Error (%)	Kaminski and Prakash (1986)	This study	Error (%)
				Ra10^3		
5	0.87	0.88	1.15	0.87	0.88	1.15
25	1.02	1.04	1.96	1.02	1.04	1.96
50	1.04	1.06	1.92	1.04	1.06	1.92
500	1.06	10.9	2.83	1.06	1.09	2.83
				Ra10^4		
5	2.08	2.11	1.44	2.08	2.11	1.44
25	3.42	3.48	1.75	3.41	3.47	1.76
50	3.72	3.78	1.61	3.71	3.77	1.62
500	4.08	4.14	1.47	4.08	4.14	1.47
				Ra10^5		
5	2.87	2.87	0.00	2.87	2.87	0.00
25	5.89	5.91	0.34	5.88	5.9	0.34
50	6.81	6.81	0.00	6.8	6.8	0.00
500	7.99	7.96	0.38	7.99	7.96	0.38

From Table 3.4 it is concluded that when the thickness ratio changes, there is no significant difference, but there is when the conductivity ratio changes. Considering that the highest percentage deviation is 2.83% for a Grashof of 10^3 which is not significant, therefore, it is concluded that the developed numerical code provides reliable results.

3.3.1.3 Heat transfer in a differentially heated cavity in transient state

The problem of a differentially heated cavity through its vertical walls is solved (section 3.3.1.1). It is considered that inside the cavity there is dry air which is a Newtonian and incompressible fluid whose flow is in a laminar regime. The geometry is composed of two isolated or adiabatic horizontal walls and two isothermal vertical walls (T_H and T_C); the boundary conditions of the four walls are non-slip. The phenomenon's evolution over time is considered. The results are compared with those obtained by Leal et al. (2000) **[82]**. Figures 3.9 and 3.10 show the dimensionless velocity distribution and temperature components respectively, at the middle of the cavity for Rayleigh numbers between 10^3 and 10^6, $P_r = 0.71$ and $T_0 = T_C$.

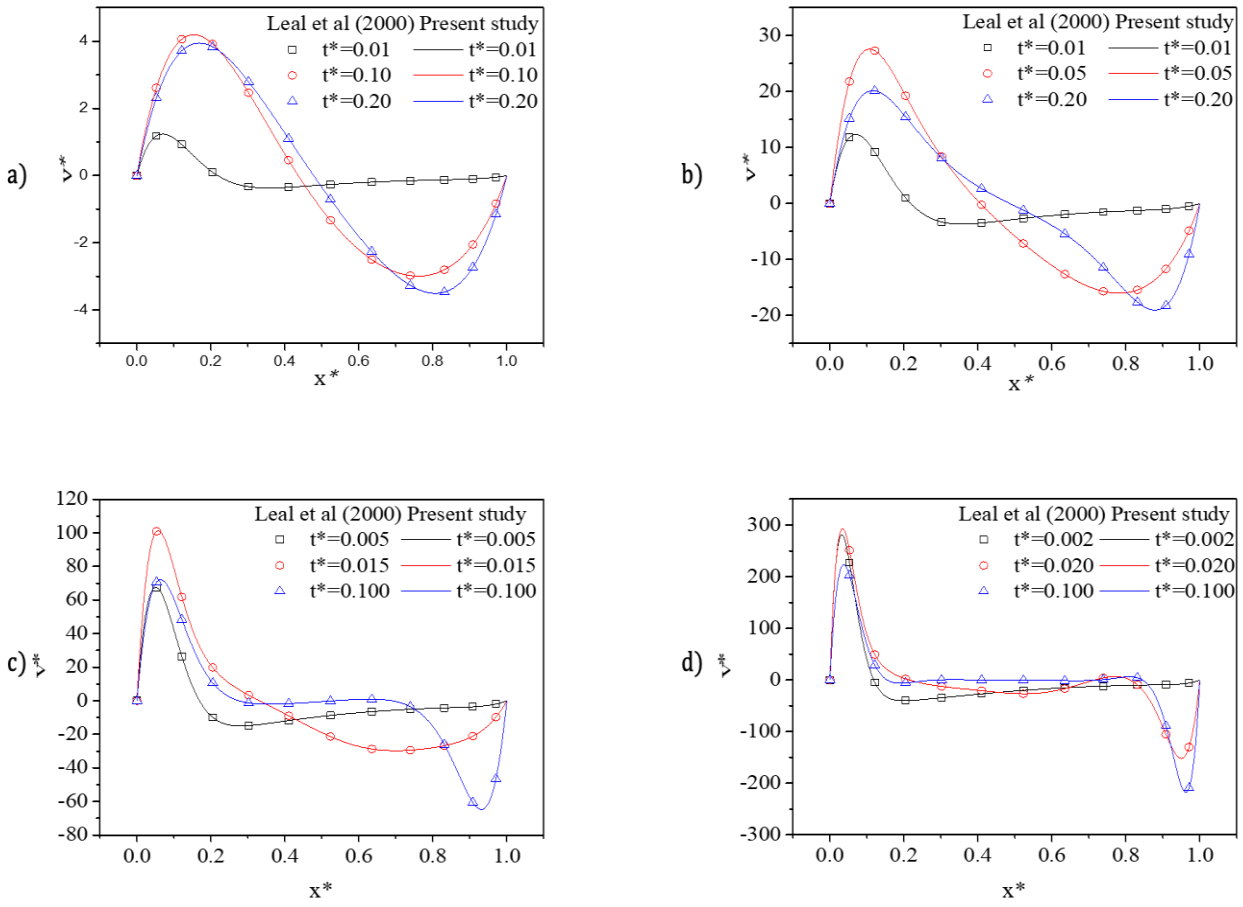

Figure 3.9 Comparison of vertical dimensionless velocity at half the horizontal plane for (a)Ra=10^3, (b)Ra=10^4, (c)Ra=10^5 and (d)Ra=10^6.

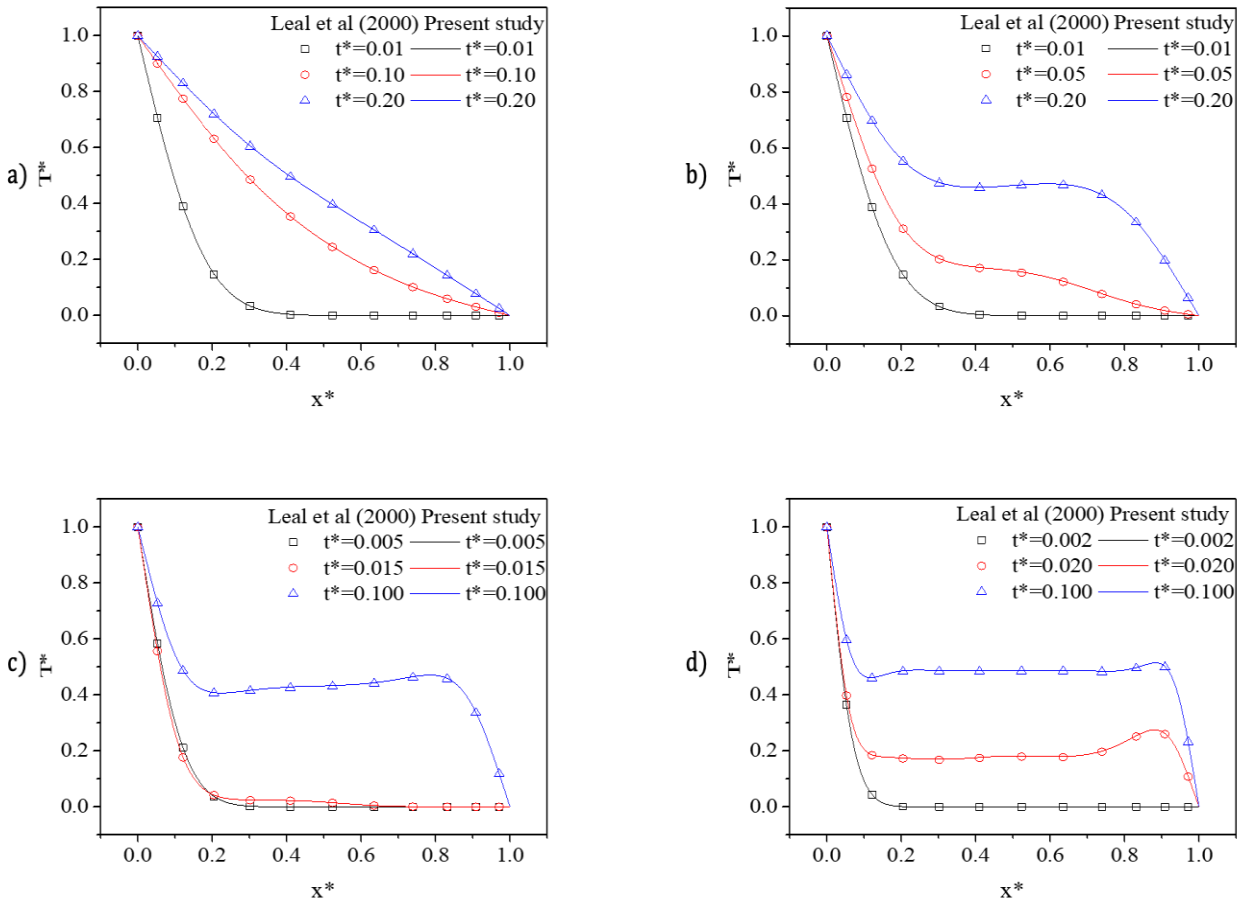

Figure 3.10 Comparison of dimensionless temperatures in the middle of the horizontal plane for (a)Ra=10^3, (b)Ra=10^4, (c)Ra=10^5 and (d)Ra=10^6.

Figures 3.9 and 3.10 show a good agreement between the results obtained in the present study and those reported in the literature with a maximum percentage deviation of 0.95% when compared with the one reported by **[82]**, so the conclusion is that the code developed for solving the problem in a transient state provides reliable information.

3.3.1.4 Heat transfer through a PCM wall

The following verification was performed to ensure that the PCM model is solved correctly. For this, the results of the present study are compared with the **Solomon [83]** analytical solution and the numerical results reported by **Arici et al. [84]**. A paraffin slab (n-eicosane) melting process with an initial temperature of 21 °C is the verification problem solved from the literature. One side of the slab was at a constant temperature of 95 °C. After 3600 *s* of the fusion process using a time step of ls, the temperature variation in the slab was compared with the analytical and numerical solution reported in the literature by **Solomon [83] and Arici**. **[84]** Based on the comparison of the results in Table 3.5, the results show good qualitative and quantitative

agreement with a maximum percentage difference of 1.28% and 9.47% regarding **Solomon [83]** and **Arici [84]**, respectively.

Table 3.5 Quantitative comparison of the temperature distribution throughout the PCM.

x(m)	Present study	Solomon (1979)	Error (%)	Arici et al. (2018)	Error (%)
0.000	95.00	95.00	0.00	95.00	0.00
0.002	86.77	86.78	0.01	86.60	0.20
0.004	78.60	78.60	0.00	78.21	0.50
0.006	70.57	70.52	0.07	69.84	1.03
0.008	62.72	62.58	0.22	61.51	1.92
0.010	55.11	54.83	0.51	53.22	3.43
0.012	47.73	47.29	0.92	44.95	5.82
0.014	40.54	40.02	1.28	36.70	9.47
0.016	36.04	35.72	0.89	35.32	1.99
0.018	34.50	34.18	0.93	33.96	1.55
0.020	33.04	32.73	0.94	32.65	1.19
0.022	31.68	31.38	0.95	31.39	0.93
0.024	30.42	30.13	0.95	30.20	0.74
0.026	29.27	28.99	0.96	29.09	0.63
0.028	28.23	27.95	0.99	28.07	0.58
0.030	27.28	27.01	0.99	27.13	0.54
0.032	26.42	26.17	0.95	26.29	0.48
0.034	25.66	25.42	0.94	25.54	0.46
0.036	24.98	24.75	0.92	24.87	0.43
0.038	24.38	24.17	0.86	24.28	0.39
0.040	23.85	23.66	0.80	23.77	0.34
0.042	23.39	23.21	0.77	23.32	0.30
0.044	22.99	22.83	0.70	22.93	0.25
0.046	22.65	22.51	0.62	22.60	0.22
0.048	22.37	22.23	0.63	22.32	0.23
0.050	22.12	22.00	0.54	22.08	0.19
0.052	21.92	21.81	0.50	21.88	0.20
0.054	21.75	21.65	0.46	21.71	0.19
0.056	21.61	21.52	0.42	21.57	0.19
0.058	21.50	21.41	0.42	21.45	0.21
0.060	21.42	21.32	0.47	21.36	0.28
0.062	21.36	21.25	0.51	21.28	0.35
0.064	21.31	21.20	0.52	21.22	0.41
0.066	21.29	21.15	0.66	21.17	0.55
0.068	21.29	21.12	0.80	21.13	0.73

3.3.1.5 Heat transfer through a semi-transparent wall

For the verification of the mathematical model, a 6mm glass sheet was used, and from the results, the heat fluxes to the interior and exterior were analyzed, as well as the temperatures at the center of the cavity. Figure 3.11 shows the temperature variation through a glass sheet for different outdoor air temperatures ($T_0 = 0 - 50\,°C$ in 5 °C intervals) and an indoor air temperature of ($T_i = 21\,°C$). It can be seen that the temperature gradients become smaller as the outdoor air temperature approaches the indoor air temperature.

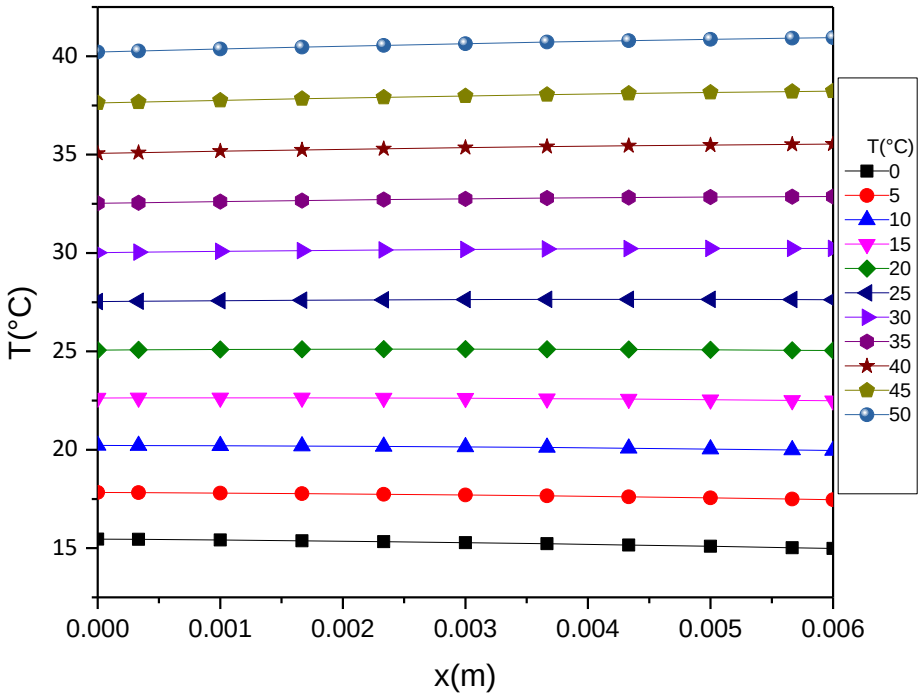

Figure 3.11 Temperature distribution through the semi-transparent wall

Table 3.6 shows the heat fluxes obtained on the surface in contact with the interior of the glass and the surface in contact with the exterior, where q_τ is the transmitted heat flux, q_α the absorbed heat flux by the system, q_ρ the heat flux reflected to the outside, q_i the heat flux to the inside by convection and radiation, q_0 the heat flux to the outside by convection and radiation, $q_i + q_\tau$ the total heat flux to the inside, $q_0 + q_\rho$ the heat flux to the outside total heat inside, the energy balance was made with the total heat fluxes inside and outside and a q_{total} was obtained, which was compared with the value of solar irradiation that falls on the glass and according to the table, an absolute percentage difference of 0.001 % was obtained. Therefore, it is concluded that the mathematical model for a semi-transparent wall was correctly developed in the computational code.

Table 3.6 Heat fluxes for the semi-transparent wall.

T(°K)	Heat fluxes (W/m^2)								
	Q_τ	q_α	q_ρ	q_i	q_o	$q_i + q_\tau$	$q_o + q_\rho$	q_{total}	G
0	585	105	60	-60	165.76	524.24	225.76	750	750
10	585	105	60	-8.68	113.68	576.32	173.68	750	750
20	585	105	60	45.58	59.42	630.58	119.42	750	750
30	585	105	60	102.18	2.82	687.18	62.82	750	750
40	585	105	60	161.27	-56.27	746.27	3.73	750	750
50	585	105	60	223.01	-118.01	808.01	-58.01	750	750

3.3.2 Global energy balance model

Below exercises of steady and unsteady state heat transfer solved by means of global energy balances are presented. These exercises consider different boundary conditions with the purpose of implement the method on the proposed system of the room. Each problem was compared and verified against its analytical solution.

3.3.2.1 One-dimensional heat conduction problem in steady state (convective boundary condition)

The physical model of the system under analysis is presented in Figure 3.12 which shows a concrete slab ($\lambda = 1.7\frac{W}{mK}$) with $H_x = 0.1m$ long and is subjected to heat flux $Q = 750W$ on the west boundary, also a convective heat loss $q_w^{conv} = h_w(T_w - T_1)$ where $h_w = 6\frac{W}{m^2K}$ and $T_w = 303\ K$. The east boundary is subjected to $T_e = 297\ K$

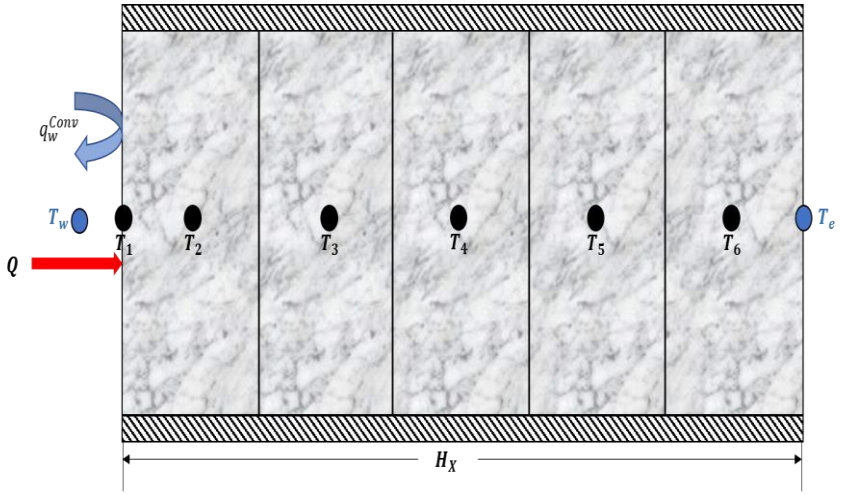

Figure 3.12 Physical model of the problem with convective boundary conditions.

To solve the problem an energy balance in each of the elements and the system boundaries is made, then an equation for each element and boundaries is obtained so a system of algebraic equations is formed which is solved by means of an iterative algebraic solution method. The development to obtain the equation that solves the temperature on the T_1 element is as follows:

$$Q + \frac{T_w - T_1}{a_1} = \frac{T_1 - T_2}{a_2}$$

$$(T_w - T_1)a_2 + a_1 a_2 Q = (T_1 - T_2)a_1 \tag{3.74}$$

$$(a_1 + a_2)T_1 - a_1 T_2 = a_2 T_w + a_1 a_2 Q$$

Where $a_1 = \frac{1}{h_{conv,w-1}}$ and $a_2 = \frac{Hx_1}{2\lambda}$

The energy balance for the T_2 element is:

$$\frac{T_1 - T_2}{b_1} = \frac{T_2 - T_3}{b_2}$$

$$(T_1 - T_2)b_2 = (T_2 - T_3)b_1 \tag{3.75}$$

$$-b_2 T_1 + (b_1 + b_2)T_2 - b_1 T_3 = 0$$

Where $b_1 = \frac{Hx_1}{2\lambda}$ and $b_2 = \frac{Hx_1}{2\lambda} + \frac{Hx_2}{2\lambda}$

The energy balance for the T_3 element is:

$$\frac{T_2 - T_3}{c_1} = \frac{T_3 - T_4}{c_2}$$

$$(T_2 - T_3)c_2 = (T_3 - T_4)c_1 \tag{3.76}$$

$$-c_2 T_2 + (c_1 + c_2)T_3 - c_1 T_4 = 0$$

Where $c_1 = \frac{Hx_1}{2\lambda} + \frac{Hx_2}{2\lambda}$ and $c_2 = \frac{Hx_2}{2\lambda} + \frac{Hx_3}{2\lambda}$

The energy balance for the T_4 element is:

$$\frac{T_3 - T_4}{d_1} = \frac{T_4 - T_e}{d_2}$$

$$(T_3 - T_4)d_2 = (T_4 - T_e)d_1 \tag{3.77}$$

$$-d_2T_3 + (d_1 + d_2)T_4 - d_1T_5 = 0$$

Where $d_1 = \frac{Hx_2}{2\lambda} + \frac{Hx_3}{2\lambda}$ and $d_2 = \frac{Hx_3}{2\lambda} + \frac{Hx_4}{2\lambda}$

The energy balance for the T_5 element is:

$$\frac{T_4 - T_5}{e_1} = \frac{T_5 - T_6}{e_2}$$

$$(T_4 - T_5)e_2 = (T_5 - T_6)e_1 \tag{3.78}$$

$$-e_2T_4 + (e_1 + e_2)T_5 - e_1T_6 = 0$$

Where $e_1 = \frac{Hx_3}{2\lambda} + \frac{Hx_4}{2\lambda}$ and $e_2 = \frac{Hx_4}{2\lambda} + \frac{Hx_5}{2\lambda}$

Finally, the energy balance for the T_6 element is:

$$\frac{T_5 - T_6}{f_1} = \frac{T_6 - T_e}{f_2}$$

$$(T_5 - T_6)f_2 = (T_6 - T_e)f_1 \tag{3.79}$$

$$-f_2T_5 + (f_1 + f_2)T_6 = f_1T_e$$

Where $f_1 = \frac{Hx_4}{2\lambda} + \frac{Hx_5}{2\lambda}$ and $f_2 = \frac{Hx_5}{2\lambda}$

The matrix arrangement is as follows:

$$\begin{bmatrix} (a_1 + a_2) & -a_1 & & & & & \\ -b_2 & (b_1 + b_2) & -b_1 & & & & \\ & -c_2 & (c_1 + c_2) & -c_1 & & & \\ & & -d_2 & (d_1 + d_2) & -d_1 & & \\ & & & -e_2 & (e_1 + e_2) & -e_1 & \\ & & & & -f_2 & (f_1 + f_2) & \end{bmatrix} \begin{bmatrix} T_1 \\ T_2 \\ T_3 \\ T_4 \\ T_5 \\ T_6 \end{bmatrix} = \begin{bmatrix} a_2T_w + a_1a_2Q \\ 0 \\ 0 \\ 0 \\ 0 \\ f_1T_e \end{bmatrix} \tag{3.80}$$

To verify the accuracy of the results these are compared with the analytical solution of the problem which is given by Equation (3.81).

$$T(x) = C_1 x + C_2 \tag{3.81}$$

Where $C_1 = \frac{Q+h_{conv,w-1}(T_w-T_e)}{\lambda+H_x*h_{conv,w-1}} x$ and $C_2 = T_e + \frac{H_x[Q+h_{conv,w-1}(T_w-T_e)]}{\lambda+H_x*h_{conv,w-1}}$

The Table 3.7 shows the obtained data from both methods (analytical and energy balances) and a comparison between them, also Figure 3.13 presents the temperature behavior of the given problem.

Table 3.7 Quantitative comparison of the temperature distribution for the problem with convective boundary condition.

Element	x(m)	Energy balances (°C)	Analytical solution (°C)
T_1	0.00	58.17	58.17
T_2	0.01	54.76	54.76
T_3	0.03	47.92	47.92
T_4	0.05	41.09	41.09
T_5	0.07	61.51	61.51
T_6	0.09	53.22	53.22

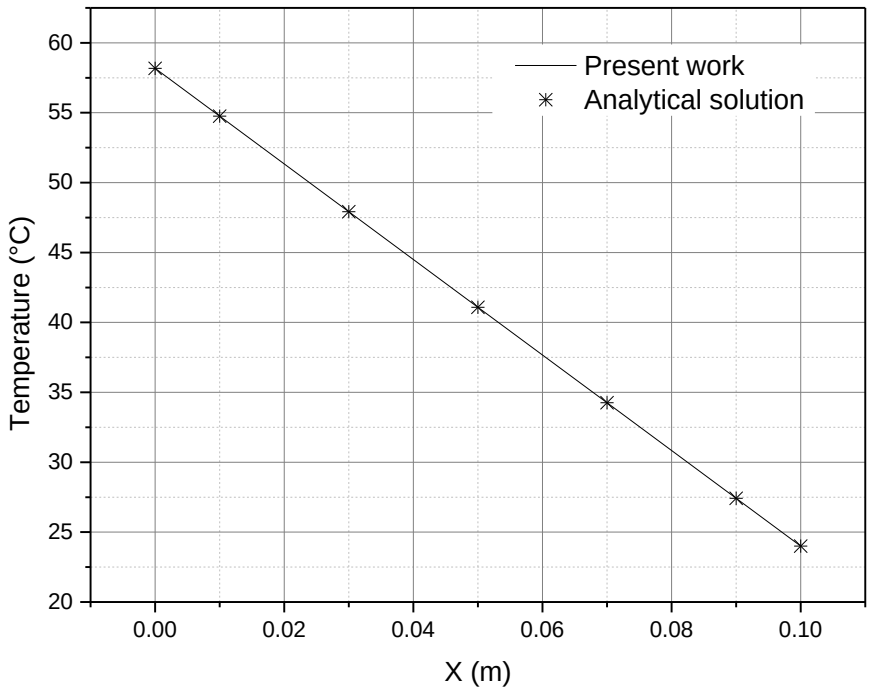

Figure 3.13 Qualitative comparation of the global energy balance method against the analytical solution.

By the qualitative and quantitative comparison of the results shown it can be concluded that the energy balance method was solved correctly.

3.3.2.2One-dimensional heat conduction problem in steady state (convective and radiative boundary condition

The physical model is presented by the Figure 3.14 which shows a concrete slab ($\lambda = 1.7\frac{W}{m°K}$) with $H_x = 0.1m$ long and is subjected to heat flux $Q = 750W$ on the west boundary, also a convective heat loss $q_w^{conv} = h_w(T_w - T_1)$ and a radiative heat loss $q_w^{rad} = \varepsilon\sigma(T_w^4 - T_1^4)$ where $h_w = 6\frac{W}{m^{2°}K}$, $\varepsilon = 0.90$, $\sigma = 5.67x10^{-8}$ and $T_w = 303\ °K$. The east boundary is subjected to $T_e = 297\ °K$

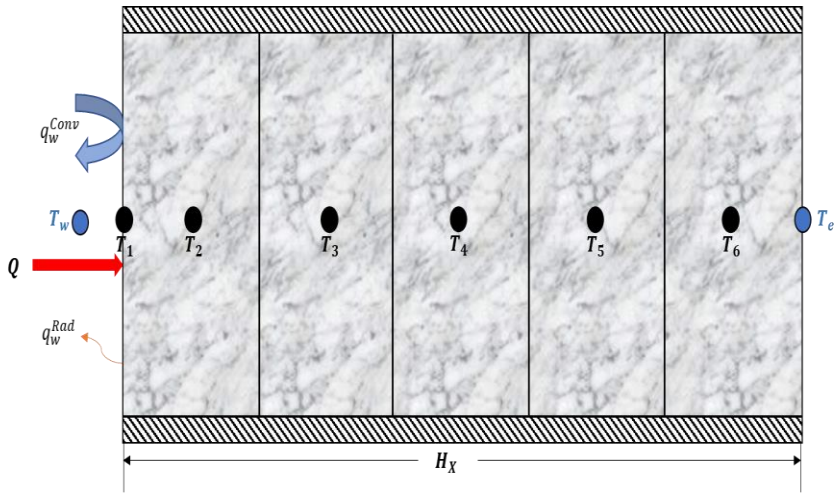

Figure 3.14 Physical model of the problem with convective and radiative boundary conditions.

Since the problem is similar to the previous one it is necessary to only carry out an energy balance on the west boundary element as follows.

$$\begin{aligned} Q + \frac{T_w - T_1}{a_1} &= \frac{T_1 - T_2}{a_2} \\ (T_w - T_1)a_2 + a_1a_2Q &= (T_1 - T_2)a_1 \\ (a_1 + a_2)T_1 - a_1T_2 &= a_2T_w + a_1a_2Q \end{aligned} \tag{3.81}$$

Where $a_1 = \frac{1}{h_{conv,w-1}h_{rad,w-1}}$ and $a_2 = \frac{Hx_1}{2\lambda}$

For this case, the radiative coefficient is determined by Equation 3.82.

$$\begin{aligned} q_w^{rad} &= \varepsilon\sigma(T_w^4 - T_1^4) \\ q_w^{rad} &= \varepsilon\sigma(T_w^2 - T_1^2)(T_w + T_1)(T_w - T_1) \end{aligned} \tag{3.82}$$

$$q_w^{rad} = h_{rad,w-1}(T_w - T_1)$$

The analytical solution for this problem is given by Equation (3.80). However, in this case C_1 and C_2 are determined by the nonlinear equations 3.83 and 3.84 as follows:

$$C_1 = \frac{T_e - C_2}{Hx} \tag{3.83}$$

$$(\varepsilon\sigma Hx)C_2^4 + \varepsilon\sigma(T_w^2 - T_1^2)(T_w + T_1)(T_w - T_1) \tag{3.84}$$

Table 3.8 shows the comparison of the obtained data, it is evident that the results obtained with the global energy balance method are the same as those obtained with the analytical solution, therefore, a satisfactory implementation of the method is concluded.

Table 3.8 Quantitative comparison of the temperature distribution for the problem with radiative and convective boundary condition.

Element	X (m)	Present study (°C)	Analytical solution (°C)
$\boldsymbol{T_1}$	0.00	52.09	52.09
$\boldsymbol{T_2}$	0.01	49.28	49.28
$\boldsymbol{T_3}$	0.03	43.67	43.67
$\boldsymbol{T_4}$	0.05	38.05	38.05
$\boldsymbol{T_5}$	0.07	32.43	32.43
$\boldsymbol{T_6}$	0.09	26.81	26.81

3.3.2.3 One-dimensional heat conduction problem in unsteady state

The considerations are a homogeneous slab as well as the previous exercises, however, for this case in unsteady state $T(x,t)$. The thermophysical properties $\lambda = 2.0\frac{W}{mK}$ $\rho = 1.0\frac{Kg}{m^3}$ and $C_p = 1.0\frac{J}{KgK}$ (Xamán y Gijón-Rivera, 2016) **[85]**. The system is subjected to first class boundary conditions $T_w = 0\,K$ for the west boundary and $T_e = 0\,K$ for the east boundary. The initial condition is $T_0 = 20 * \sin(\pi x)\,K$ and a time increment $\Delta t = 0.0001, 0.001, 0.01, 0.1s$ and the analytical solution for this problem is given by Ozisik **[86]** as follows:

$$T(x,t) = T_0 e^{-\alpha\beta t}\sin(\beta x) \tag{3.85}$$

Where $\alpha = \frac{\lambda}{\rho C_p}$ and $\beta = \frac{\pi}{Hx}$

To obtain the equations matrix for the global energy balance method, the transitory term must be introduced in the energy balance for each element, as example the energy balance for the element T_1 is shown below.

$$\frac{T_w - T_1}{a_1} - \frac{T_1 - T_2}{a_2} = \frac{\partial(\rho C_p T_1)}{\partial t} A * Hx \tag{3.86}$$

The transient term must be discretized.

$$\begin{gathered} \frac{\partial(\rho C_p T_1)}{\partial t} A * Hx \\ \frac{\rho C_p Hx}{\partial t}(T_1 - T_1^0) \end{gathered} \tag{3.87}$$

Then the discretized transitory term expression is:

$$a_p^0(T_1 - T_1^0) \tag{3.88}$$

So, the equation for the T_1 element is rewritten:

$$\left(a_1 + a_2 + a_1 a_2 a_p^0\right) T_1 - a_1 T_2 = a_2 T_w + a_1 a_2 a_p^0 T_1^0 \tag{3.89}$$

Also, the equations matrix is rewritten:

$$\begin{bmatrix} (AA) & -a_1 & 0 & 0 & 0 & 0 \\ -b_2 & (BB) & -b_1 & 0 & 0 & 0 \\ 0 & -c_2 & (CC) & -c_1 & 0 & 0 \\ 0 & 0 & -d_2 & (DD) & -d_1 & 0 \\ 0 & 0 & 0 & -e_2 & (EE) & -e_1 \\ 0 & 0 & 0 & 0 & -f_2 & (FF) \end{bmatrix} \begin{bmatrix} T_1 \\ T_2 \\ T_3 \\ T_4 \\ T_5 \\ T_6 \end{bmatrix} = \begin{bmatrix} a_2 T_w + a_1 a_2 a_p^0 T_1^0 \\ b_1 b_2 a_p^0 T_2^0 \\ c_1 c_2 a_p^0 T_3^0 \\ d_1 d_2 a_p^0 T_4^0 \\ e_1 e_2 a_p^0 T_5^0 \\ f_1 T_e + f_1 f_2 a_p^0 T_6^0 \end{bmatrix} \tag{3.90}$$

Where:

$$AA = a_1 + a_2 + a_1 a_2 a_p^0$$

$$BB = b_1 + b_2 + b_1 b_2 a_p^0$$

$$CC = c_1 + c_2 + c_1 c_2 a_p^0$$

$$DD = d_1 + d_2 + d_1 d_2 a_p^0$$

$$EE = e_1 + e_2 + e_1 e_2 a_p^0$$

$$FF = f_1 + f_2 + f_1 f_2 a_p^0$$

Figure 3.15 shows the results for the different time steps (Δt) and it is observed that the smaller the time step the more accurate are the results with respect to the analytical solution, so a reduction of the time step is needed also the replacement of the approximation type for one of a higher order to increase the accuracy of the numerical solution.

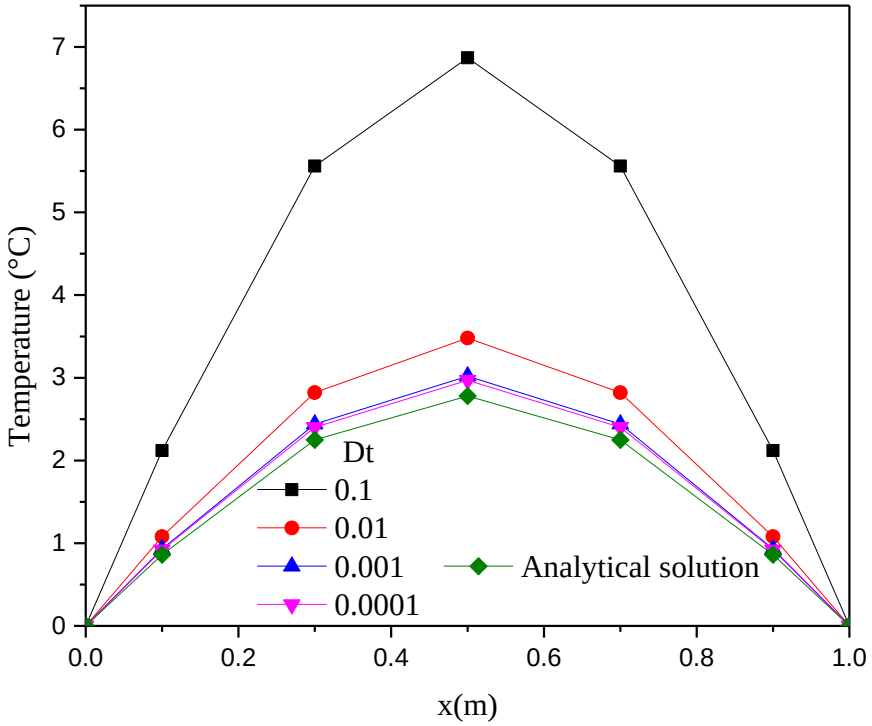

Figure 3.15 Temperature behavior of different time steps compared to the analytical solution.

3.4 General solution process of the developed computational code to solve the proposed system

1. The starting parameters and conditions are entered (dimensions, material, type of fluid, etc.)
2. The computational mesh is generated on which the equations of the mathematical model are solved.
3. View factors for radiative exchange in the cavity are calculated.
4. The temporal cycle starts (the cycle of each time step).
5. The weather conditions are introduced (Solar irradiance, ambient temperature and wind velocity).
6. The iterative process cycle starts (The iterative process in each time step)
7. The radiative exchange model is solved to determine the net radiative heat fluxes at the differential surfaces in the cavity.
8. The heat conduction in the semi-transparent wall is solved.
9. The physical properties of the PCM are calculated.

10. The heat conduction in the PCM wall is solved.
11. The velocity and pressure field are determined using the SIMPLE algorithm.
12. The energy equation for the cavity is solved.
13. The values of the convective heat transfer coefficient are calculated (with the correlations selected from the literature).
14. The coefficients of the equations of each element of the room are calculated to be later calculated in the matrix arrange.
15. The equations matrix is solved by means of the Gauss-Seidel numeric method.
16. The solutions are evaluated by means of a convergence criterion for each iteration and while this criterion is not met, steps 6 onwards are repeated.
17. If the criterion is met, then the result are printed.
18. The solutions are evaluated by means of a temporary convergence criterion for each time step, while this criterion is not met, steps 4 onwards are repeated.
19. If the temporal convergence criterion is met, the results are printed and the modelations ends.

Figure 3.16 presents the flowchart that represents the general solution procedure.

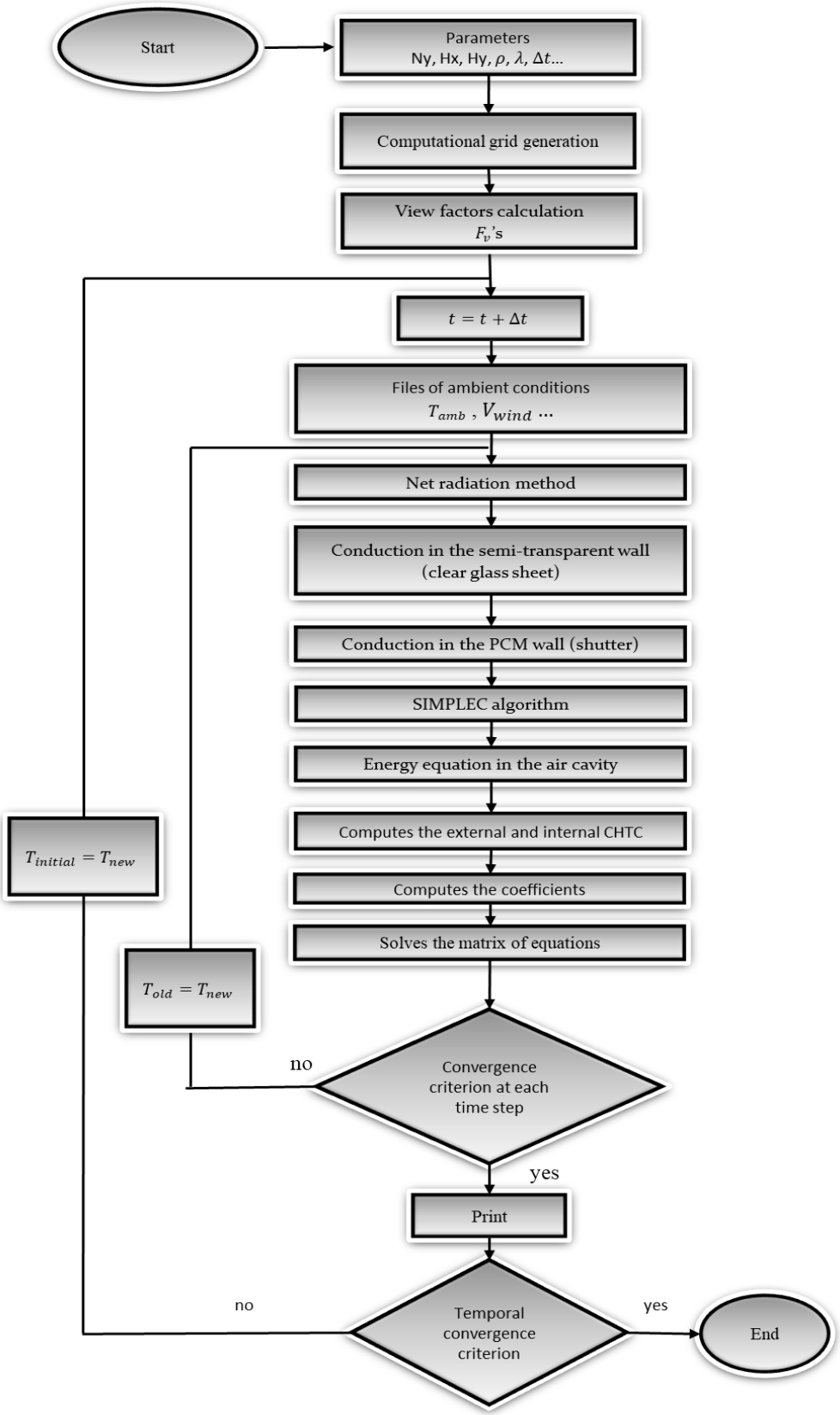

Figure 3.16 flowchart of the developed code general solution process.

3.5 Temporal and spatial grid independence analysis

Once the numerical code with the numerical modeling for the room system with a window with a phase change material is complete, an analysis is carried out to establish a numerical grid, which will be used in the modeling of the present study. The spatial grid independence purpose is to diminish the computational time without compromising the results accuracy. Also, because the code consists of a hybrid model conformed of a part that is solved employing an energy balance model (the room) and another part using a two-dimensional model in CFD (the window with the PCM), and since the energy balance model consists of only one node per room element; the independence grid analysis is carried out only on the CFD part of the code.

The temporal grid study consists of comparing the predictions of the numerical model for different time steps (Δ_t) to obtain a suitable Δ_t, for which the results obtained do not show a significant difference compared to other value of Δ_t. In the same way, the spatial study carried out by comparing the predictions of the numerical model for different grid sizes (number of computational nodes in both dimensions).

3.5.1 Conventional window system (clear glass)

To carry out the analysis, a fine spatial grid is proposed for the numerical model under study (conventional window), which is composed of 11x81 computational nodes. This grid is chosen so that the variation between the results depends only on the temporal part and is not affected by the spatial part. The time steps used were five, these are: 1, 3, 5, 10 and 15 seconds and the data that are compared are the total heat fluxes and temperature inside and outside the glass surface respectively. The system is subjected to the climate conditions of the city of Mérida, Yucatán, Mexico. The warmest day was selected (July 25, 2018), at a time of 13:00-14: 00 hours in which the initial temperature is 25 °C. The data of the phenomenon at 30 and 50 minutes are compared and the percentage deviation that exists between them is calculated for different time steps. The results obtained and their percentage deviation are shown in Table 3.9 below and it is observed that the percentage deviation that exists between the different time steps used for the analysis is practically 0%. Therefore, it is ensured that, if a time step of 10 seconds is used for the present study, the results that will be obtained will be reliable. Also, because it is a system in which only pure diffusion is modeled, the 11x81 grid is kept fixed to carry out the temporal and spatial grid analysis for the window system with a PCM.

Table 3.9 Comparison of results for the conventional window system at different time steps.

Time (minutes)	Δ_t (s)	$q_{Total,in}$ $\left(\frac{W}{m^2}\right)$	Error (%)	$q_{Total,out}$ $\left(\frac{W}{m^2}\right)$	Error (%)	$T_{S,in}$ (°C)	Error (%)	$T_{S,out}$ (°C)	Error (%)
	1	75.23		-47.62		34.72		34.98	
	3	75.23	0.00	-47.62	0.00	34.72	0.00	34.98	0.00
30	5	75.23	0.00	-47.62	0.00	34.72	0.00	34.98	0.00
	10	75.23	0.00	-47.62	0.00	34.72	0.00	34.98	0.00
	15	75.23	0.00	-47.62	0.00	34.72	0.00	34.98	0.00
	1	73.23		-45.54		34.74		34.73	
	3	73.23	0.00	-45.54	0.00	34.74	0.00	34.73	0.00
50	5	73.23	0.00	-45.54	0.00	34.74	0.00	34.73	0.00
	10	73.23	0.00	-45.54	0.00	34.74	0.00	34.73	0.00
	15	73.23	0.00	-45.54	0.00	34.74	0.00	34.73	0.00

3.5.2 Window system with a PCM-shutter

Likewise, the temporal grid independence analysis is carried out for the window system with the phase change material cover. To carry out this analysis, a fine spatial grid is proposed for the study system in which the cover with a PCM consists of 21x81 computational nodes for the x and y axes respectively, the air cavity consists of 61x81 nodes and the clear glass of 11x81. These grids are considered so that the data obtained are only affected by changes over time and not by the spatial part and in the same manner as in the conventional system, five time steps are used which are: 1, 3, 5, 10 and 15 seconds and the total heat fluxes, as well as the temperatures at the inner and outer surfaces respectively are compared. The analysis was carried out under the same climatic conditions as with the conventional window and the results obtained are analyzed in 10 minute intervals and the percentage deviation that exists between them in different time steps is calculated.

In Table 3.10 below is shown that the largest percentage deviations that exist between the time steps proposed for the analysis are of 0.003-0.317%. Therefore, it is ensured that, if a time step of 10 seconds is used for the window system with a PCM-shutter, the results to obtain will be reliable and the computational time is reduced.

Table 3.10 Comparison of results for the window system with a PCM at different time steps.

Time (minutes)	Δ_t (s)	$q_{Total,in}$ $\left(\frac{W}{m^2}\right)$	Error *(%)*	$q_{Total,out}$ $\left(\frac{W}{m^2}\right)$	Error *(%)*	$T_{S,in}$ (°C)	Error *(%)*	$T_{S,out}$ (°C)	Error *(%)*
10	1	24.41		42.29		28.56		40.09	
	3	24.41	0.04	42.23	0.08	28.56	0.00	40.08	0.01
	5	24.41	0.02	42.20	0.06	28.56	0.00	40.08	0.00
	10	24.42	0.08	42.04	0.26	28.56	0.00	40.07	0.03
	15	24.42	0.11	41.82	0.35	28.56	0.00	40.06	0.04
20	1	24.04		41.29		28.61		40.53	
	3	24.04	0.06	41.25	0.05	28.61	0.00	40.52	0.00
	5	24.05	0.03	41.23	0.04	28.61	0.00	40.52	0.00
	10	24.05	0.15	41.12	0.17	28.61	0.00	40.52	0.02
	15	24.06	0.20	40.99	0.22	28.61	0.00	40.51	0.02
30	1	23.57		38.77		28.67		39.92	
	3	23.58	0.07	38.75	0.04	28.67	0.00	39.92	0.00
	5	23.58	0.04	38.73	0.03	28.67	0.00	39.92	0.00
	10	23.58	0.18	38.64	0.14	28.67	0.00	39.91	0.01
	15	23.59	0.24	38.53	0.19	28.67	0.00	39.91	0.02
40	1	23.07		37.05		28.74		39.31	
	3	23.07	0.08	37.03	0.04	28.74	0.00	39.31	0.00
	5	23.07	0.05	37.01	0.03	28.74	0.00	39.31	0.00
	10	23.08	0.21	36.93	0.13	28.74	0.00	39.31	0.01
	15	23.09	0.28	36.83	0.18	28.74	0.00	39.30	0.02
50	1	22.54		36.19		28.81		39.71	
	3	22.55	0.09	36.16	0.04	28.81	0.00	39.71	0.00
	5	22.55	0.05	36.15	0.02	28.81	0.00	39.71	0.00
	10	22.55	0.23	36.08	0.12	28.81	0.00	39.70	0.01
	15	22.56	0.31	35.99	0.16	28.81	0.00	39.70	0.01

Once the time step is selected, a study of spatial grid independence in "x" direction is carried out for the air cavity between the glass and the cover with the PCM. Meanwhile, for the PCM and

the clear glass, the computational nodes are considered fixed on the "x" and "y" axis. The same number of nodes used for the temporal grid independence is used and the variation of the computational nodes for the air cavity in "x" direction was 31, 41, 51, 61 and 71 nodes. Based on the results obtained and shown in Table 3.11, 41 nodes in the "x" direction are chosen since it does not present a significant difference in the results and improves computational time.

Table 3.11 Spatial grid independence in x direction for window system with a PCM.

Time (minutes)	Grid size	$q_{Total,in}$ $\left(\frac{W}{m^2}\right)$	Error (%)	$q_{Total,out}$ $\left(\frac{W}{m^2}\right)$	Error (%)	$T_{S,in}$ (°C)	Error (%)	$T_{S,out}$ (°C)	Error (%)
	31x81	24.42		42.04		28.56		40.07	
	41x81	24.42	0.02	42.04	0.00	28.56	0.00	40.07	0.00
10	51x81	24.42	0.01	42.04	0.00	28.56	0.00	40.07	0.00
	61x81	24.42	0.00	42.04	0.00	28.56	0.00	40.07	0.00
	71x81	24.42	0.00	42.04	0.00	28.56	0.00	40.07	0.00
	31x81	23.58		38.64		28.67		39.91	
	41x81	23.58	0.02	38.64	0.00	28.67	0.00	39.91	0.00
30	51x81	23.58	0.01	38.64	0.00	28.67	0.00	39.91	0.00
	61x81	23.58	0.00	38.64	0.00	28.67	0.00	39.91	0.00
	71x81	23.58	0.00	38.64	0.00	28.67	0.00	39.91	0.00
	31x81	22.55		36.08		28.81		39.70	
	41x81	22.55	0.01	36.08	0.00	28.81	0.00	39.70	0.00
50	51x81	22.55	0.00	36.08	0.00	28.81	0.00	39.70	0.00
	61x81	22.55	0.00	36.08	0.00	28.81	0.00	39.70	0.00
	71x81	22.55	0.00	36.08	0.00	28.81	0.00	39.70	0.00

Next, spatial grid independence is carried out in the "y" direction and again only for the air cavity between the clear glass and the cover with the PCM. The variation of the computational nodes was 41, 51, 61, 71, 81, 91 and 101 nodes and the results presented in Table 3.12 show that the percentage deviations do not exceed 0.2%, but taking into account an aspect ratio of 2 to 1 for the dimensions of the cavity and taking into account the previous grid independence analysis, it was decided to choose a computational grid of 41x81 nodes for the air cavity with a time step of 10 seconds for the numerical modeling of the room with a window with a PCM system.

Table 3.12 Spatial grid independence in y direction for window system with a PCM.

Time (minutes)	Grid size	$q_{Total,in}$ $\left(\frac{W}{m^2}\right)$	Error (%)	$q_{Total,out}$ $\left(\frac{W}{m^2}\right)$	Error (%)	$T_{S,in}$ (°C)	Error (%)	$T_{S,out}$ (°C)	Error (%)
10	41x41	24.40		42.04		28.57		40.07	
	41x51	24.41	0.14	42.04	0.00	28.56	0.00	40.07	0.00
	41x61	24.41	0.10	42.04	0.00	28.56	0.00	40.07	0.00
	41x71	24.41	0.07	42.04	0.00	28.56	0.00	40.07	0.00
	41x81	24.42	0.05	42.04	0.00	28.56	0.00	40.07	0.00
	41x91	24.42	0.04	42.04	0.00	28.56	0.00	40.07	0.00
	41x101	24.42	0.03	42.04	0.00	28.56	0.00	40.07	0.00
30	41x41	23.57		38.64		28.67		39.91	
	41x51	23.58	0.13	38.64	0.00	28.67	0.00	39.91	0.00
	41x61	23.58	0.09	38.64	0.00	28.67	0.00	39.91	0.00
	41x71	23.58	0.07	38.64	0.00	28.67	0.00	39.91	0.00
	41x81	23.58	0.05	38.64	0.00	28.67	0.00	39.91	0.00
	41x91	23.59	0.03	38.64	0.00	28.67	0.00	39.91	0.00
	41x101	23.59	0.03	38.64	0.00	28.67	0.00	39.91	0.00
50	41x41	22.55		36.08		28.81		39.70	
	41x51	22.55	0.12	36.08	0.00	28.81	0.00	39.70	0.00
	41x61	22.55	0.08	36.08	0.00	28.81	0.00	39.70	0.00
	41x71	22.55	0.06	36.08	0.00	28.81	0.00	39.70	0.00
	41x81	22.55	0.04	36.08	0.00	28.81	0.00	39.70	0.00
	41x91	22.55	0.03	36.08	0.00	28.81	0.00	39.70	0.00
	41x101	22.55	0.02	36.08	0.00	28.81	0.00	39.70	0.00

3.6 Parameters and considerations for the study

For this study the ground temperature (T_{ground}) is considered a given value and according to Su et al. [**87**] ground temperature remains constant at or beyond 10 m which approaches the annual average ambient temperature.

It is considered that the length ($Hx = Hy = Hz = 4m$) corresponds to the typical dimension of a room in a glazed building, which room is filled with non-participant air (dry air). The vertical walls are considered opaque and consist of a concrete block of 0.15 m thickness [88]; the roof and floor elements are concrete slabs and have a thickness of 0.15 m and 0.20 m respectively, and the thermophysical and optical properties of the concrete are given by the official Mexican normative and Hernández-Pérez et al. [**89,90**]. The thickness of the glazed wall is considered of 0.006 m, the PCM and its thickness are yet to be selected, and heat conduction across the shutter shader that encapsulates the PCM is not considered because it is thin enough to be considered negligible. Also, the optical properties of this shader material made of aluminum are given by Bartl and Baranek [**91**]. Finally, the ground (soil) properties were reported by Rodriguez et al. [**92**]. Table 3.13 shows the thermophysical and optical properties of the materials used for this work.

Table 3.13 Thermophysical and optical properties of the materials used.

Material	ρ (kg/m)	λ $(W/m-K)$	C_P $(J/kg-K)$	ρ	τ^*	α^*	ε^*
Glass sheet	2500	1.4	750	0.08	0.78	0.14	0.85
Concrete	2300	1.74	920	0.33	-	0.67	0.87
Air	1.19	0.2563	1005	-	-	-	-
Ground (Soil)	1460	1.3	5059	-	-	-	-
Shutter (Alu)				0.9	-	-	0.1

The correlation proposed by Duffie and Beckman [**93**] was used to calculate the glazed wall exterior convective heat transfer coefficient (CHTC), which is shown in Equation (3.91), where V_{wind} is the air velocity in m/s and $h_{g,ext}$ is the exterior convective coefficient in W/m^2K.

$$h_{g,ext} = 3.0V_{wind} + 2.8 \quad (6.26)$$

For the opaque walls the exterior CHTC is shown in Equation (3.92) [**94**]

$$h_{ext,walls} = 1.44V_{wind} + 4.955 \quad (3.92)$$

The exterior CHTC for the opaque roof is $h_{ext,roof} = 13\ W/m^2K$ [**89**]. On the other hand, the glazed wall interior convective coefficient is $h_{room-g} = 2.5\ /Wm^2K$ [**95**] and for the interior opaque walls, floor and roof the CHTC are given by the Equations (3.93-3.95) [**96**], respectively.

$$h_{walls,room} = 2.35\Delta T^{0.21} \quad (3.93)$$

$$h_{room,floor} = 3.10\Delta T^{0.17} \quad (3.94)$$

$$h_{roof,room} = 2.72\Delta T^{0.13} \quad (3.95)$$

Finally, the sky temperature T_{sky} for the vertical and horizontal opaque walls that interact with the outside ambient temperature T_{amb} are shown in Equations (3.96, 3.97) **[97,98],** respectively.

$$T_{sky,walls} = 0.0552T_{amb}^{1.5} \quad (3.96)$$

$$T_{sky,roof} = 0.0553T_{amb}^{0.17} \quad (3.97)$$

3.7 Weather conditions data

For the present study, warm and cold weather conditions without significant changes in temperature between day and night and during the year was desired. Since the southeast of the Mexican republic has a tropical climate throughout most of the year **[99-101]**, the climate of Mérida, Yucatán (Aw) was selected as the warm weather representative of this country region (see Figure 3.17).

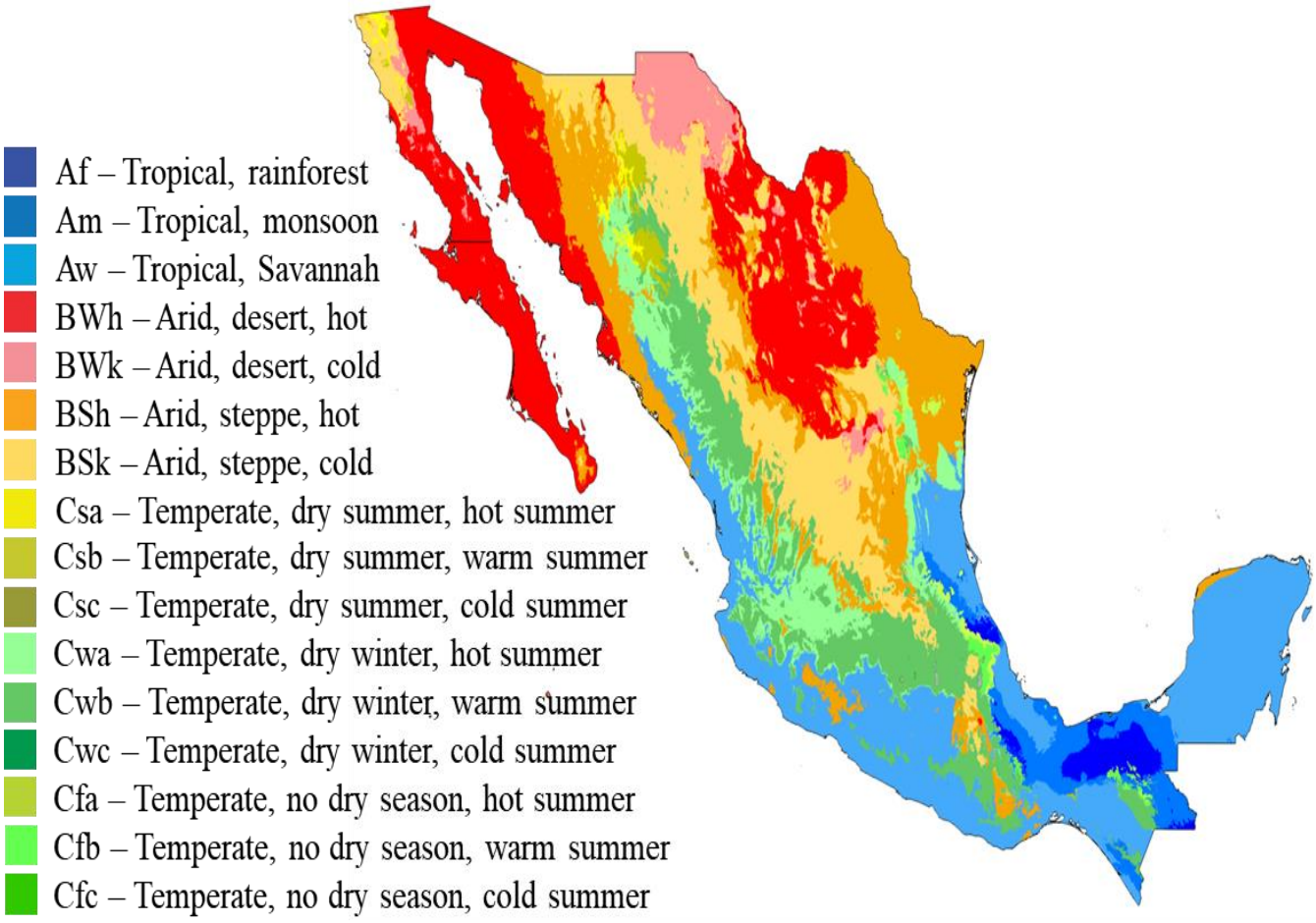

Figure 3.17 Köppen-Geiger climate classification for the Mexican Republic.

The climate data of Mérida, Yucatán was provided by Comisión Nacional del Agua (CONAGUA), and the data are from the year 2018. These data include wind speed, ambient temperature and solar radiation in 10-minute intervals for the 24 hours of the Day. For the present work, the coldest and warmest day of each month of the year were selected according to the minimum and maximum temperature values, these days are presented in Table 3.14 below.

Table 3.14 Warmest and coldest day of each month of the year.

Month	Warmest day	Coldest day
January	22	05
February	26	01
March	19	24
April	07	16
May	30	13
June	04	13
July	25	10
August	10	07
September	01	22
October	10	23
November	12	17
December	02	22

Since the radiation data obtained from CONAGUA are global horizontal, the vertical component of these values had to be calculated to carry out the numerical study. For this, it was developed a numerical code that uses the available radiation data, the date and geographic coordinates of the place for which the study is carried out, and with them the direct and diffuse solar radiation that reaches the vertical surface of both case studies was calculated using **Duffie and Beckman [93]** and **Kalogirou [102]** methodology, to obtain the vertical component of global solar radiation for different orientations **[103, 104]**. Once the vertical component for each orientation (south, north, west and east) is obtained, the one with the lowest solar radiation incidence was chosen, since this orientation is the optimal one chosen typically in the geographic zone of the ambient data. This process was carried out for all the days selected for the study and Figure 3.18 shows one of the selected days as an example and it can be observed that the south orientation has the lowest solar radiation. This also happens for most of the selected days; hence, it was decided that the south orientation will be used for the parametric study of the proposed problem. The rest of the figures for selected warmest and coldest day of each season of the year are presented in the Appendix C.

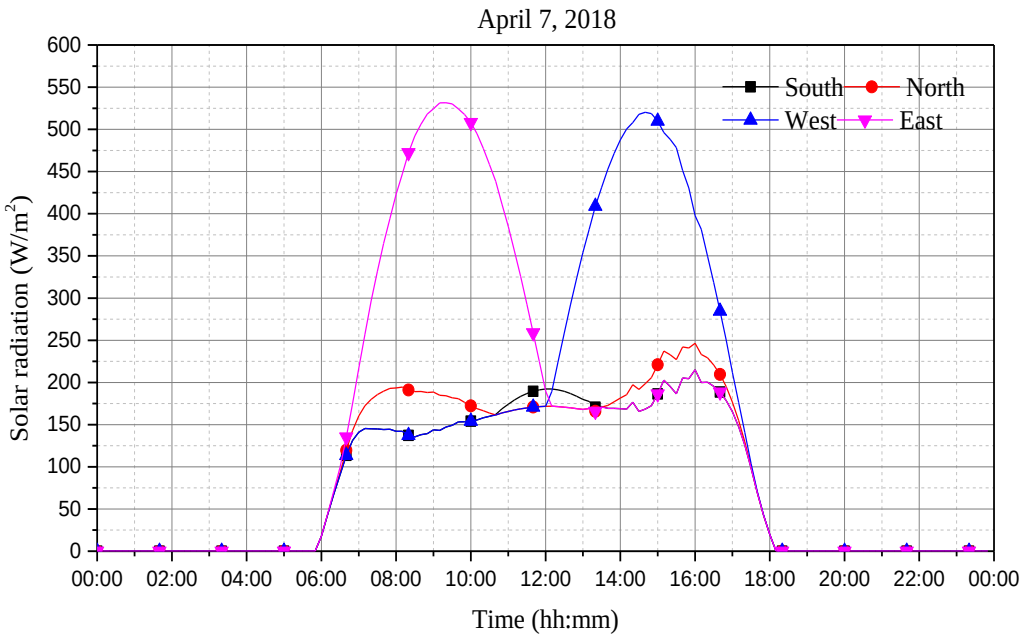

Figure 3.18 Normal average solar radiation on a vertical wall with different orientations.

3.7.1 Fitting equations for solar radiation and ambient temperature

For the analysis of the thermal performance of the room with the window with a PCM throughout its evolution over time, small modeling time intervals are required and because the data obtained from CONAGUA are for every 10 minutes, continuous mathematical expressions had to be developed as a function of time in seconds for both ambient temperature and solar radiation. On the other hand, the values every 10 minutes of the wind speed are considered constant since in the modeling the variation in these time intervals are negligible. The fitting equations of ambient temperature and solar radiation for the selected days are shown in the Appendix D.

In Figure 3.19 is presented the ambient temperature values for December 2, 2018, as an example of how the fitting equation for this day approaches the real ambient temperature values.

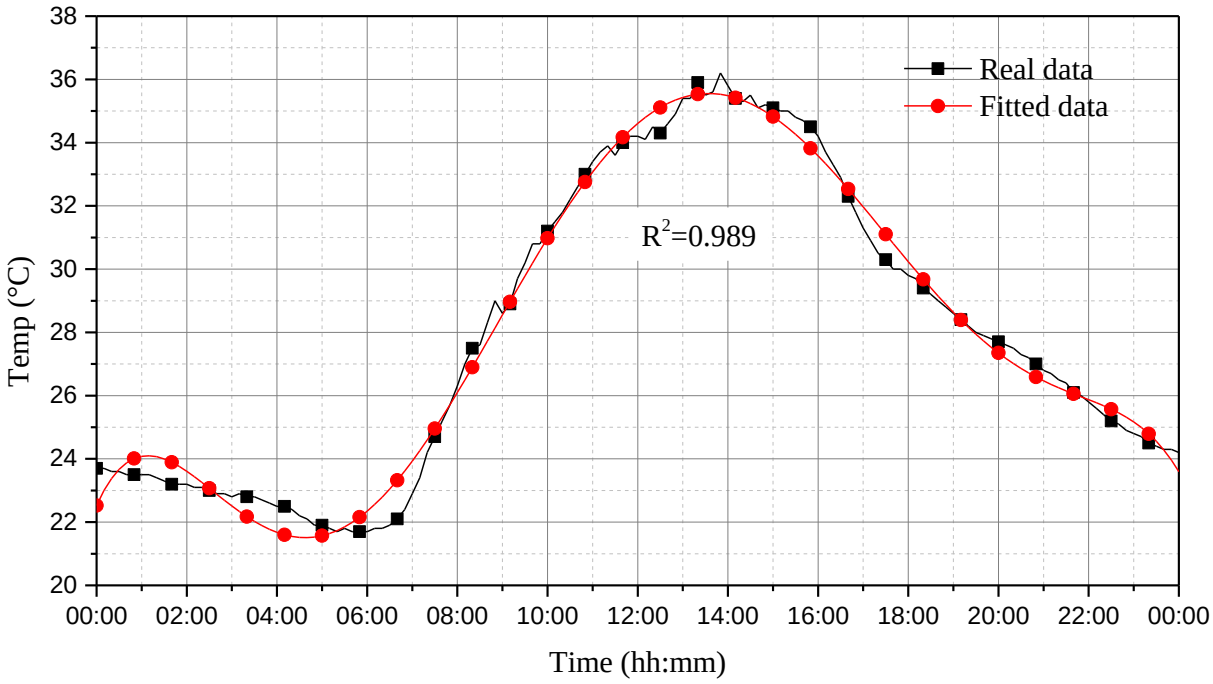

Figure 3.19 Comparison between the real data and fitted data for ambient temperature.

After describing the methods used to solve the governing equations and after verifying them; the numerical code was developed, the next step was to run the code and analyze the information obtained. Therefore, the results analysis was presented in Chapter 4.

Chapter 4

Results of the thermal evaluation

The thermal study consists in comparing the thermal performance of the window system with a PCM shutter against a conventional window system (clear glass only) for the coldest and the warmest day of each month of the year of the study. The simulations were performed from 05:00 to 07:00 hours to 24:00 hours, and it is worth mentioning that the starting hour of the simulations varies depending when the solar radiation starts in each of the selected days. It was carried out this way in order to reduce the computational time and because the variations in the ambient temperature are not significant at hours without solar radiation at the beginning of the day. However, at hours without solar radiation during the night, the simulations continued in order to verify the effectiveness of the delay in the thermal inertia caused by the use of the PCM shutter.

In order to know if the proposed window system adapts to the inside thermal comfort temperature conditions for the selected climate, a comfort temperature range is determined by means of an adaptive model, which is a linear model that takes into account the average ambient temperature to predict the inside comfort temperature, and is expressed by $T_c = 0.534T_{amb,ave} + 12.9$ **[105]**, where T_c is the comfort temperature inside the room, and $T_{amb,ave}$ is the average monthly outdoor ambient temperature, and the comfort zone is ± 2 to the comfort value of T_c.

Although twenty-four days was the total of days modeled, the temperatures behavior of the room and inner surface of the window are very similar in most days (See appendix E). This occurs to the peak temperatures of the envelope elements of the room (See appendix F). Therefore, the results discussion will be focused on the warmest and coldest day of each season of the year, considering that these days represent the worst climatic conditions of each season.

Below the behavior of the average inner surface temperatures of the window system with a PCM shutter compared against a conventional window system (without the PCM shutter) during the simulated hours for the warmest and coldest day of each annual seasons is shown as well as the temperature behavior in the room for both configurations.

4.1 Winter season

For the warmest day, Figure 4.1a shows the behavior of the average temperature at the inner surface of the window (T_g) and the inside room temperature (T_{room}) for both configurations. It is observed that the maximum and minimum average inner surface temperatures of the window system with the PCM were 44.08 and 20.5 °C at 14:19:50 and 06:00:00 hours, respectively, which shows a difference between them of 23.58 °C, while for the conventional window configuration, these temperatures were 37.53 and 19.17 °C at 14:17:40 and 06:00:00 hours respectively so the difference between them was 18.36 °C. This means that the conventional windows configuration performed better with lower temperatures through the simulated hours, also, the window with the PCM shutter raised the maximum and minimum inner surface temperatures by 6.55 and 1.33 °C, respectively. In the same way, the maximum and minimum temperatures of the room were 45.3 and 20.17 °C at 14:19:30 and 06:00:00 hours when the PCM shutter was implemented in the window, and for the room with the conventional window, these temperatures were 44.55 and 19.97 °C at 14:19:10 and 06:00:00 hours which represents a rise in the maximum and minimum temperatures of the order of 0.75 and 0.2 °C, respectively, when the PCM shutter was implemented. This behavior of the room temperatures corresponds to those shown by the window and indicates that the implementation of the PCM shutter did not benefit the inside temperatures as desired. This result is because the room was also affected by the other elements of its envelope, but this matter will be discussed later.

Besides, the comfort zone of the warmest day went from 26.5 to 30.5 °C, and the room temperatures reached this zone at 07:24:40 hours for the configuration with the PCM and at 07:28:30 hours with the conventional window. Then the comfort zone was exceeded at 08:01:30 and 08:08:10 hours by the PCM shutter and conventional configurations, respectively. Later in the day, when the temperatures tend to decrease due to the lack of solar radiation, the room temperatures reach the comfort zone again at 17:28:10 and 17:26:30 hours by both configurations and go below it at the same time at 18:33:10 hours, so both configurations were in the comfort zone for a total of 01:41:30 and 01:46:20 hours with and without the PCM shutter respectively. This shows that when the PCM shutter was implemented, the room temperatures at the beginning of the day increased slightly faster and later in the day decreased slightly slower when compared with the conventional window configuration, but despite this, the conventional window made the room temperatures to stay longer in the comfort zone.

For the coldest day (05-01-18) in the same way, the Figure 4.1b shows the behavior of the inner surface average temperature for both configurations, and these had a maximum and minimum of 31.30 (13:29:50 hours) and 14.83 °C (07:00:00 hours) with the PCM shutter, respectively, so the difference was 16.47 °C. And without the shutter, these temperatures were 25.04 (13:29:50 h) and 12.39 °C (07:00:00 h); thus, the difference between them was 12.65 °C, which means that without the shutter, the

variation between the maximum and minimum temperatures was lower. Also, when the PCM shutter was implemented, the maximum and minimum temperatures were 6.26 and 2.44 °C higher when compared with the performance of the conventional window. This behavior corresponds to those shown by the room temperatures with the window system with the PCM shutter, which presented maximum and minimum temperatures of 32.11 (13:29:50) and 14.85 °C (07:00:00) against the 31.25 (13:29:50) and 14.42 °C (07:00:00) shown by the room with the conventional window, which means that the PCM shutter elevated the temperatures of the room by 0.86 and 0.43 °C and although is desirable to raise the temperatures inside the room when the ambient temperatures are low, these are just slightly above of those of the conventional window configuration which were already too high for most of the day, when the comfort temperature is considered.

For this matter, the comfort zone for the coldest day went from 21.5 to 25.5 °C and the room temperatures reach it for the first time in the day at 08:44:50 and 08:55:40 hours by the PCM shutter and the conventional configurations, respectively, and exceed it at 10:03:40 and 10:28:00 hours. Then when the ambient conditions change again, the room temperatures of both configurations drop to the comfort zone at 15:56:20 and 15:43:40 hours and stay there until it goes below the comfort zone at 16:46:40 and 16:39:20 hours, which means that for the PCM shutter and conventional window maintain the room temperatures within the comfort zone for a total of 01:59:10 and 02:28:00 hours through the simulated hours. This indicates that the proposed system of the window with the PCM shutter did not benefit the room temperatures, and the reason why this happened will be discussed below.

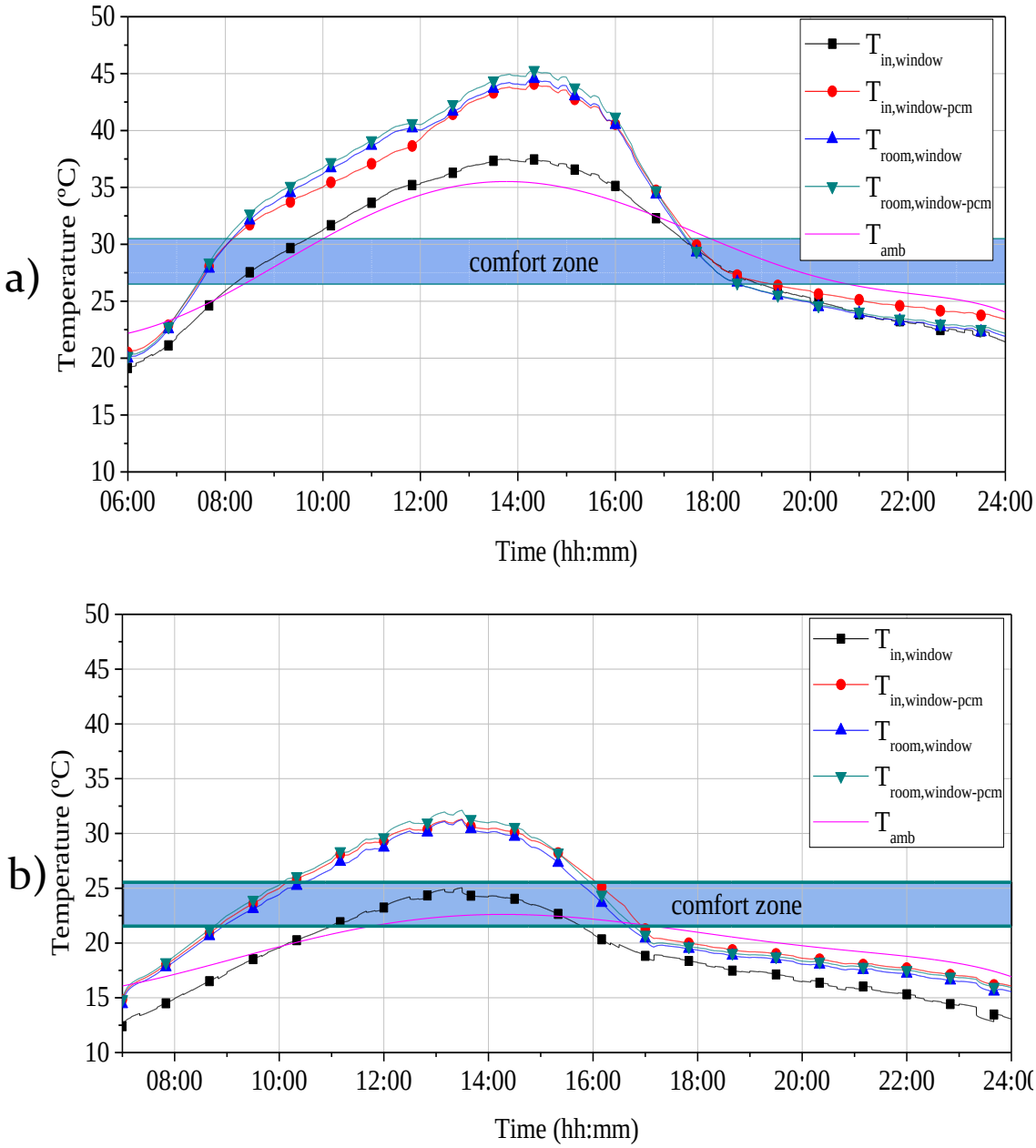

Figure 4.1 Comparison between the behavior of the inner surface average temperature and room inside temperature for both configurations for the a) warmest and b) coldest day of the winter season.

As Figure 4.2a shows, for the warmest day of the winter, the maximum temperature values for each envelop component of both evaluated configurations indicate that the roof element has the highest temperature with 62.02 and 61.9 °C for the PCM shutter and the conventional window configuration, then was followed by the east and west walls with temperatures around 53 °C, and for the window temperatures are 37.53 °C with the conventional window and when the PCM shutter was implemented its temperature was raised 2 °C above the north wall temperatures which are around 42 °C. This occurs because when the PCM shutter was implemented the entry of the solar

radiation into the room was blocked. However, the output of the energy provided by the rest of the elements of the envelope (which had higher temperatures) was also blocked. In addition, the PCM starts to release the stored energy when the temperatures decrease as the solar radiation disappear, causing the window to have higher temperatures than those of the conventional window. This caused a slight increase in the temperature inside the room as discussed in Figure 4.1. For the case of the coldest day, Figure 4.2b shows that for this day, the elements of the envelope with the highest temperature values were the north, east, and west walls with temperatures around 35 °C for both window configurations, next the roof temperatures, which were 30.6 °C for both systems and regarding the window temperatures, for the conventional window is appreciated was even lower than the floor temperature (27.37 °C) with a peak of 25 °C. On the contrary, the temperature value reached when the PCM shutter was implemented was 31.30 °C, and this value was higher than the roof temperature of 30.7 °C, which confirms that the PCM shutter did not accomplish its purpose of maintaining the temperature values uniform throughout the day.

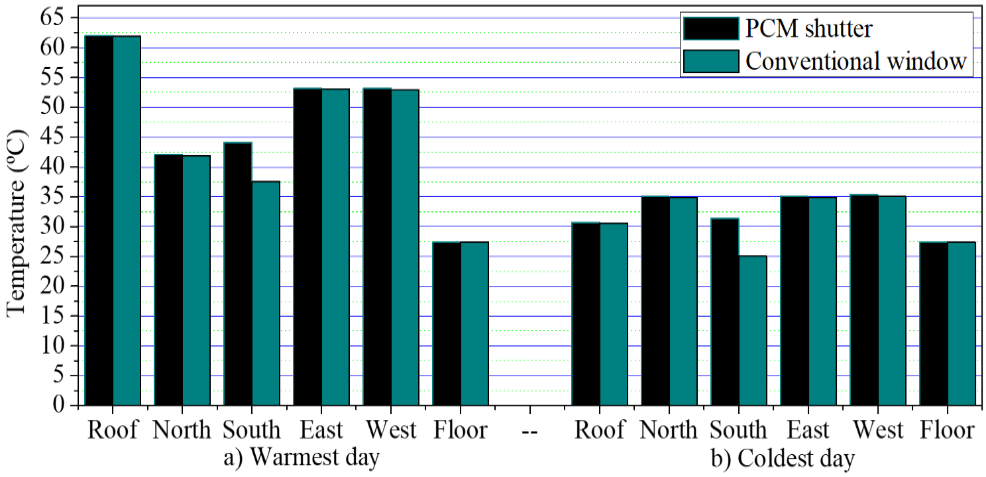

Figure 4.2 Comparison between the behavior of maximum temperatures of the envelope elements of the room for both configurations for the a) warmest and b) coldest day of the winter season.

For the following discussion of the heat fluxes in the inner surface of the window it must be mentioned that for the present study the negative values represent energy losses for the proposed system, ergo, the energy flowing from the room to the outside ambient, and the contrary occurs when the heat flux values are positive. Then Figure 4.3a shows the heat fluxes of the warmest day of the winter season and is observed that for both study cases the heat fluxes are negative the majority of the modeled hours. This behavior is due to the energy gains through the rest of the envelope elements of the room, which have higher temperatures (shown in Figure 4.2a) than the inner surface of the window in both configurations. This means that the energy added to the room through the walls and roof is directed towards the outside ambient through the window. However, when the PCM shutter is implemented the heat fluxes

tend to behave linearly, meaning that energy gains or losses are minimum, when compared with the conventional window system. Therefore, when the ambient temperature reaches its peak at around 14:00 hours, the conventional window dissipates the energy gains towards the outside, reaching the highest negative value of -61.43 Wh/m^2. While the heat flux value of the window with the PCM shutter at this hour is -11.85 Wh/m^2, meaning that this configuration doesn't let the energy leave the room. Which causes a rise in the room and window inner surface temperature, as shown in Figure 4.1a.

After solar radiation starts to diminish rapidly after 14:00 hours, and since the ambient temperature diminishes at a slower pace, the heat fluxes of the conventional window tend to have positive values reaching values around four Wh/m^2at 18:00 hours. The behavior is caused by the energy gained by de conventional window just by the ambient temperature. On the other hand, the window with the PCM shutter keeps raising the heat fluxes after 18:00 hours due to the energy stored in the PCM, from which a fraction is dissipated towards the inner surface of the window and the room, causing higher temperature values than those shown with the conventional window.

Similar behavior is shown in Figure 4.3b for the coldest day. Although the conventional window configuration never reaches the same heat fluxes values of the window with the PCM shutter and is due to the lower ambient temperatures of this day. On the coldest day, the heat fluxes of the window with the PCM shutter varied from -7.68 to 7.15 Wh/m^2 at 13:30 and 16:30 hours, respectively, with a difference of -0.53 Wh/m^2. While for the conventional window, these values varied from -52.41 to -6.40 Wh/m^2 at 13:30 hours and 17:10 hours with a difference of -56.01. Hence the conventional window varied -55.48 Wh/m^2 more than de window with the PCM shutter. This behavior proves the attenuation given by the PCM due to its capability to store energy, although it caused a rise in the temperatures, as discussed in Figure 4.1.

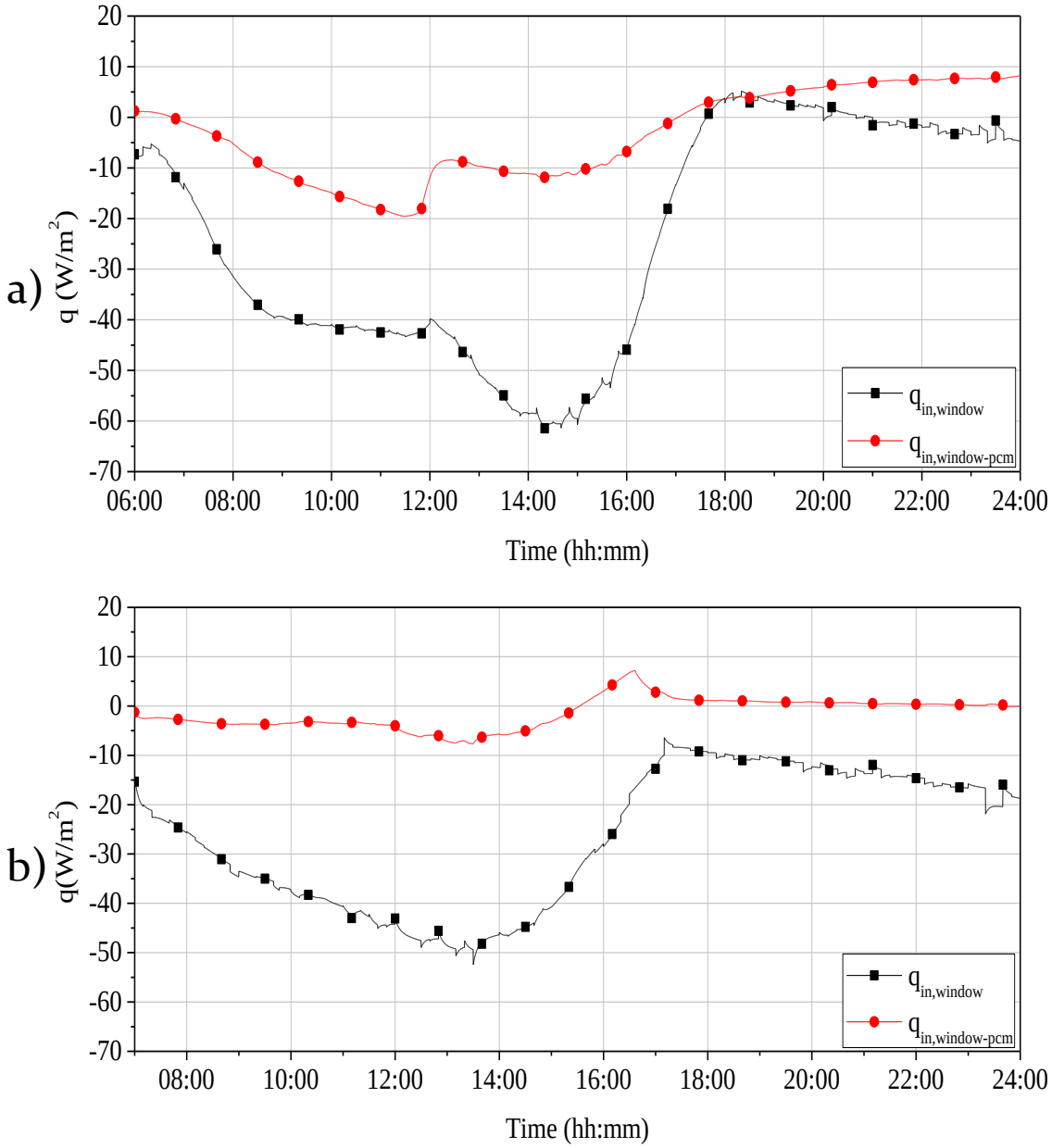

Figure 4.3 Comparison between the behavior of the inner surface heat fluxes during both configurations for the a) warmest and b) the coldest day of the winter season.

4.2 Spring season

Figure 4.4a shows the inner surface average temperature behavior for both configurations of the warmest day and the room temperatures. For this day, the maximum temperatures for the PCM shutter and conventional window systems were 44.98 and 40.23 °C at 14:08:30 and 13:38:30 hours, respectively. The minimum values of both configurations reached 21.8 and 20.88 °C at 06:00:00 hours, which indicates that when compared with the conventional window, the implementation of the PCM

shutter raised the maxim and minimum temperatures of the window inner surface by 4.75 and 0.92 °C respectively. Meanwhile, the room maximum temperatures of this day were 45.69 and 45.03 °C reached at 14:08:40 and 13:39:40 hours for the PCM shutter and the conventional cases, and the minimum temperatures reached were 21.44 and 21.31 at 06:00:00 hours. Hence, the PCM shutter configuration raised these values by 0.66 and 0.13 compared to the conventional window. These results are congruent with those shown by both windows cases and indicate that for the warmest day of the spring season, the proposed system with the PCM shutter did not perform well, but it was because of other factors, which in graphs will be shown and explained later.

Regarding the comfort zone on the warmest day, its upper and lower temperatures were 31.7 and 27.7 °C, respectively. The times in which it was reached were as follows: when the PCM shutter was implemented, it was reached and surpassed it at the beginning of the day at 07:03:00 and 07:44:40 hours, respectively, and at noon when the solar radiation ends and the ambient temperatures drop, the comfort zone was again reached at 17:39:20 and then was left behind at 18:38:10. For the case of the conventional window these hours were 07:07:10 and 07:51:10 hours for the first time in the morning, and at noon the second time at 17:38:30 and 18:38:30 hours. This gives a total of hours in the comfort zone of 01:40:30 hours for the PCM shutter case and 01:44:00 hours for the conventional window case, which means that throughout the day, the conventional window configuration kept the room temperature 00:03:30 hours longer in the comfort zone than the proposed system of the PCM shutter. It is also noticeable that in the morning with the PCM shutter, the room gained energy sooner than with the conventional window, and in the noon with the conventional window, the room freed the energy earlier than when the PCM shutter was implemented.

In the case of the coldest day, Figure 4.4b presents the inner surface average temperature for both cases under study, and their maximum temperatures hit 41.52 (13:59:20 hours) and 35.75 °C (13:54:50 hours) for the proposed and the conventional configurations. The figure also shows the minimum temperatures, which were 17.62 and 15.69 °C, reached at 06:00:00 hours. Therefore, when the shutter was implemented, the maximum and minimum temperatures were elevated by 5.77 and 1.93 °C compared to the conventional window. This behavior also occurred with the room temperatures since with the implementation of the PCM shutter, the maximum temperature (42.45 °C at 13:59:10 hours) was raised by 0.69 °C from the 41.76 °C (13:58:40 hours) of the conventional window, and the same happened to the minimum temperature (17.47 °C at 06:00:00) which elevated 0.25 °C compared to the temperature of 17.22 °C (06:00:00) presented by the conventional window configuration.

The comfort temperature analysis showed that on the coldest day, the upper and lower temperatures of the zone were 29.5 and 25.5 °C. When the PCM shutter was implemented, these values were reached at 07:23:40 hours and surpassed at 08:00:00

hours, then again at noon; the comfort zone was reached at 17:29:50 hours and left behind at 18:18:10 hours. In the case of the conventional window, these hours were 07:30:00 and 08:08:50 hours in the morning and 17:27:00 and 18:16:00 hours at noon. This adds up to a total of 01:24:40 hours in the comfort zone for the PCM shutter case and 01:27:50 hours for the conventional window case, which means that through the day, the conventional window configuration kept the room temperature 00:03:10 hours longer in the comfort zone than the proposed system of the PCM shutter.

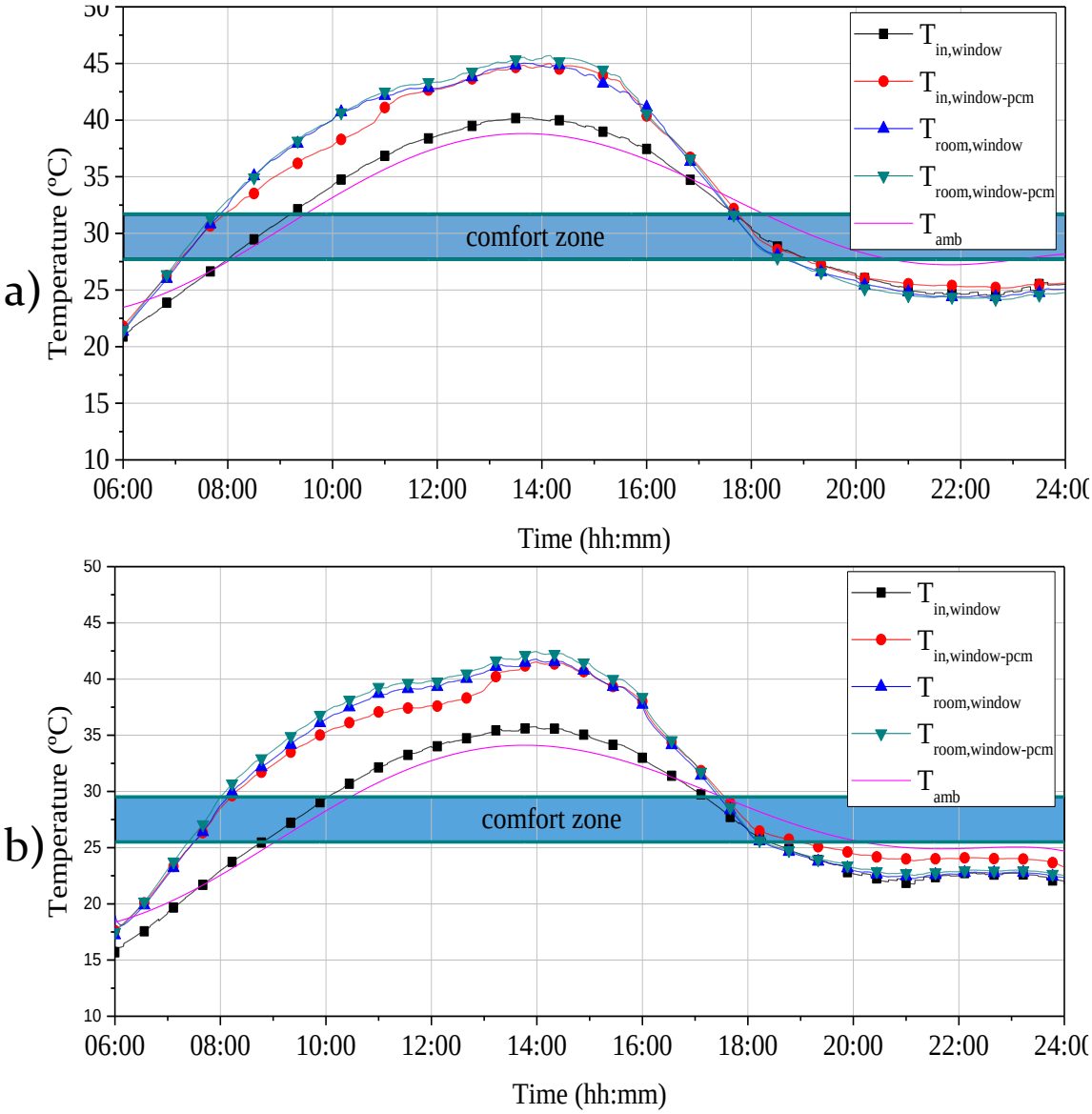

Figure 4.4 Comparison between the behavior of the inner surface average temperature and room inside temperature for both configurations for the a) warmest and b) coldest day of the spring season.

Figure 4.5a shows the maximum temperatures of the envelope components of the room for the warmest day of the spring season; it is evident that again the roof temperature was the highest with a temperature of 66 °C presented by both cases

under study, then the west wall follows with temperatures of 56.58 and 55.67 °C for the PCM shutter and the conventional cases, which were just one-degree difference from each other. The east wall temperatures also showed one degree of difference between the PCM and the conventional cases with values of 48.02 and 49.18, but the conventional case was higher in this wall. For the north wall, the temperatures between both configurations are close, around 45 °C. Finally, the south wall showed temperatures of 44.98 and 40.23 °C, meaning a rise in room temperatures of 4.75 °C when the PCM shutter was implemented. These results explain why the proposed system did not meet its goal since the temperatures of almost all the other envelope elements are higher and add energy to the room, and this energy could have gone out through the window if not blocked by the shutter. For the coldest day, Figure 4.5b shows that the envelope elements of the room tended to behave like on the warmest day, since also for this day, the roof temperatures were higher, hitting values around 61 °C, then the west wall presented temperatures of 52 °C for both configurations, next the east wall temperatures which were of 44 °C in both cases, and the north wall temperatures were 40 °C, this last was surpassed by the window (south wall) with the PCM shutter with a temperature of 41.52 °C which was 5.77 °C higher than the one reached by the conventional window configuration.

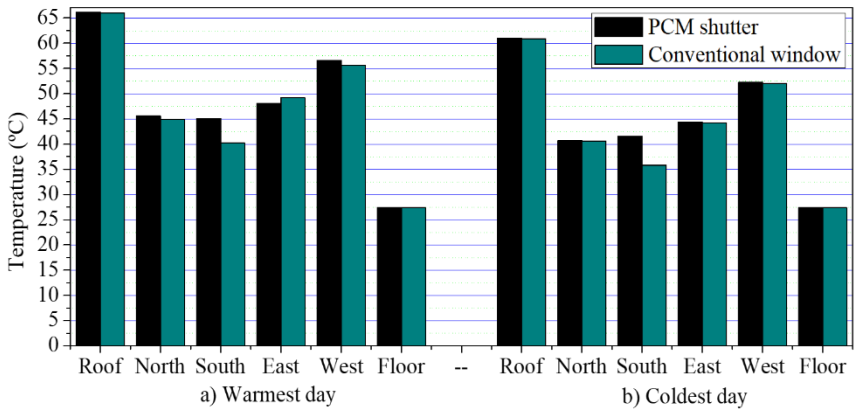

Figure 4.5 Comparison between the behavior of maximum temperatures of the envelope elements of the room for both configurations for the a) warmest and b) coldest day of the spring season.

The heat fluxes in the spring season are presented in Figure 4.6a for the warmest day and it shows a similar behavior as the one discussed in Figure 4.3. For the warmest day the heat fluxes of the window with the PCM shutter varied from -21.96 to 6.93 Wh/m^2 at 10:40 and 21:30 hours respectively, with a difference of -15.03 Wh/m^2. While for the conventional window these values varied from -50.58 to 7.12 Wh/m^2 at 10:00 hours and 18:20 hours with a difference of -43.46 Wh/m^2. Hence the variations are -28.43 Wh/m^2 higher with the conventional window. Figure 4.6b shows that in the coldest day of the spring the window with the PCM shutter varied from -19.89 to 8.68 Wh/m^2 at 11:30 and 20:40 hours respectively, with a difference of -11.12 Wh/m^2.

While for the conventional window these values varied from -57.68 to 2.28 Wh/m^2 at 10:10 hours and 18:10 hours with a difference of -55.40 Wh/m^2.

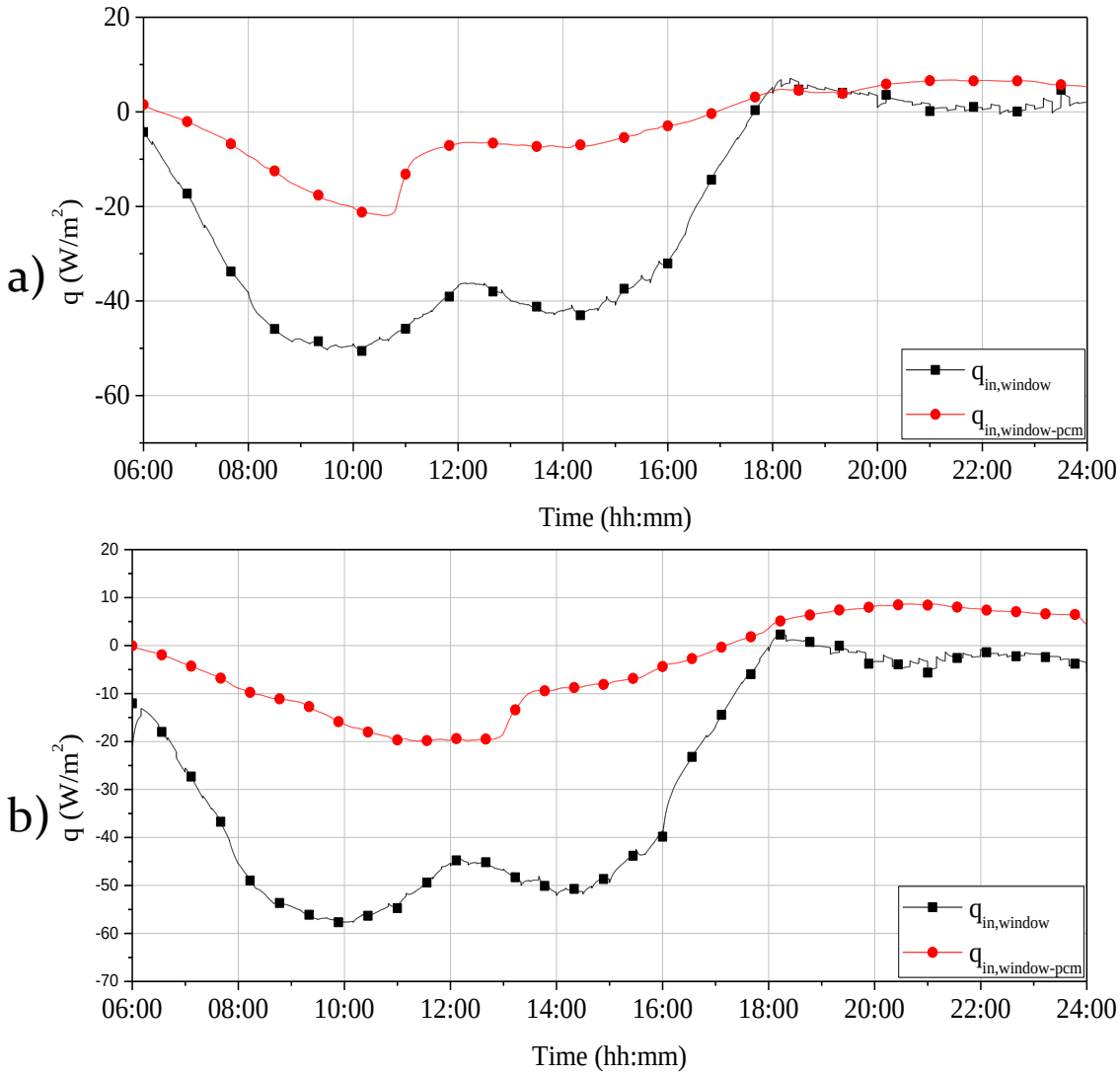

Figure 4.6 Comparison between the behavior of the inner surface heat fluxes for both configurations for the a) warmest and b) coldest day of the spring season.

4.3 Summer season

Figure 4.7a shows the inner surface average temperature behavior of the window for both configurations of the warmest day and the room temperatures. For his day the maximum temperatures for the PCM shutter and conventional window systems were 46.46 and 41.72 °C at 13:58:40 and 13:42:30 hours, respectively. The minimum values of both configurations reached 23.64 and 22.84 °C at 05:00:00 hours, which indicates that when compared with the conventional window, the implementation of the PCM shutter raised the maxim and minimum temperatures of the window inner surface by

4.74 and 0.80 °C respectively. Meanwhile the room maximum temperatures of this day were 49.65 and 46.32 °C reached at 13:55:50 and 13:39:40 hours, for the PCM shutter and the conventional cases, and the minimum temperatures reached were 23.16 and 23.03 °C at 05:00:00 hours. Therefore, the PCM shutter configuration raised these values by 3.33 and 0.13 °C when compared with the conventional window. These results are congruent with those shown by both windows cases and indicate that for the warmest day of the summer season, the proposed system with the PCM shutter did not perform well, but it was because of other factors, which in graphs will be shown and explained later.

Regarding the comfort zone of the warmest day, its upper and lower temperatures were 32.5 and 28.5 °C respectively. The times in which it was reached were as follows: when the PCM shutter was implemented, it was reached and surpassed it at the beginning of the day at 06:25:20 and 07:05:20 hours, respectively, and at noon when the solar radiation ends and the ambient temperatures drop, the comfort zone was again reached at 17:33:30 and then was left behind at 18:33:30. For the case of the conventional window these hours were 06:28:50 and 07:10:00 hours for the first time in the morning, and at noon the second time at 17:32:20 and 18:35:20 hours. This gives a total of hours in the comfort zone of 01:40:00 hours for the PCM shutter case and 01:44:10 hours for the conventional window case, which means that through the day, the conventional window configuration kept the room temperature 00:04:10 hours longer in the comfort zone than the proposed system of the PCM shutter. Is also noticeable that in the morning with the PCM shutter the room gained energy sooner than with the conventional window and in the noon was with the conventional window, the room freed the energy earlier than when the PCM shutter was implemented.

In the case of the coldest day, the Figure 4.7b presents the inner surface average temperature for both cases under study, and their maximum temperatures hit 41.85 and 36.79 °C (11:39:50 hours) for the proposed and the conventional configurations. The figure also shows the minimum temperatures, which were 21.08 °C (00:00:00 hours) and 18.27 °C (19:59:50 hours). Hence, when the shutter was implemented the maximum and minimum temperatures were elevated by 5.06 and 2.81 °C compared to the conventional window. This behavior also occurred with the room temperatures since with the implementation of the PCM shutter the maximum temperature (42.63 °C at 11:36:40 hours) was raised by 0.63 °C from the 42.00 °C (11:36:20 hours) of the conventional window, and the same happened to the minimum temperature (20.39 °C at 20:59:50) which elevated 0.52 °C when compared to the temperature of 19.87 °C (19:59:50) presented by the conventional window configuration.

The comfort temperature analysis showed that in the coldest day, the upper and lower temperatures of the zone were 30.1 and 26.1 °C. When the PCM shutter was implemented, these values were reached at 06:31:40 hours and surpassed at 07:08:20 hours, then again at noon the comfort zone was reached at 16:54:10 hours and left behind at 17:27:20 hours. In the case of the conventional window, these hours were

06:34:10 and 07:13:20 hours in the morning, and, 16:49:40 and 17:24:20 hours at noon. This adds up to a total of 01:10:50 hours in the comfort zone for the PCM shutter case and 01:13:30 hours for the conventional window case, which means that through the day, the conventional window configuration kept the room temperature 00:02:40 hours longer in the comfort zone than the proposed system of the PCM shutter.

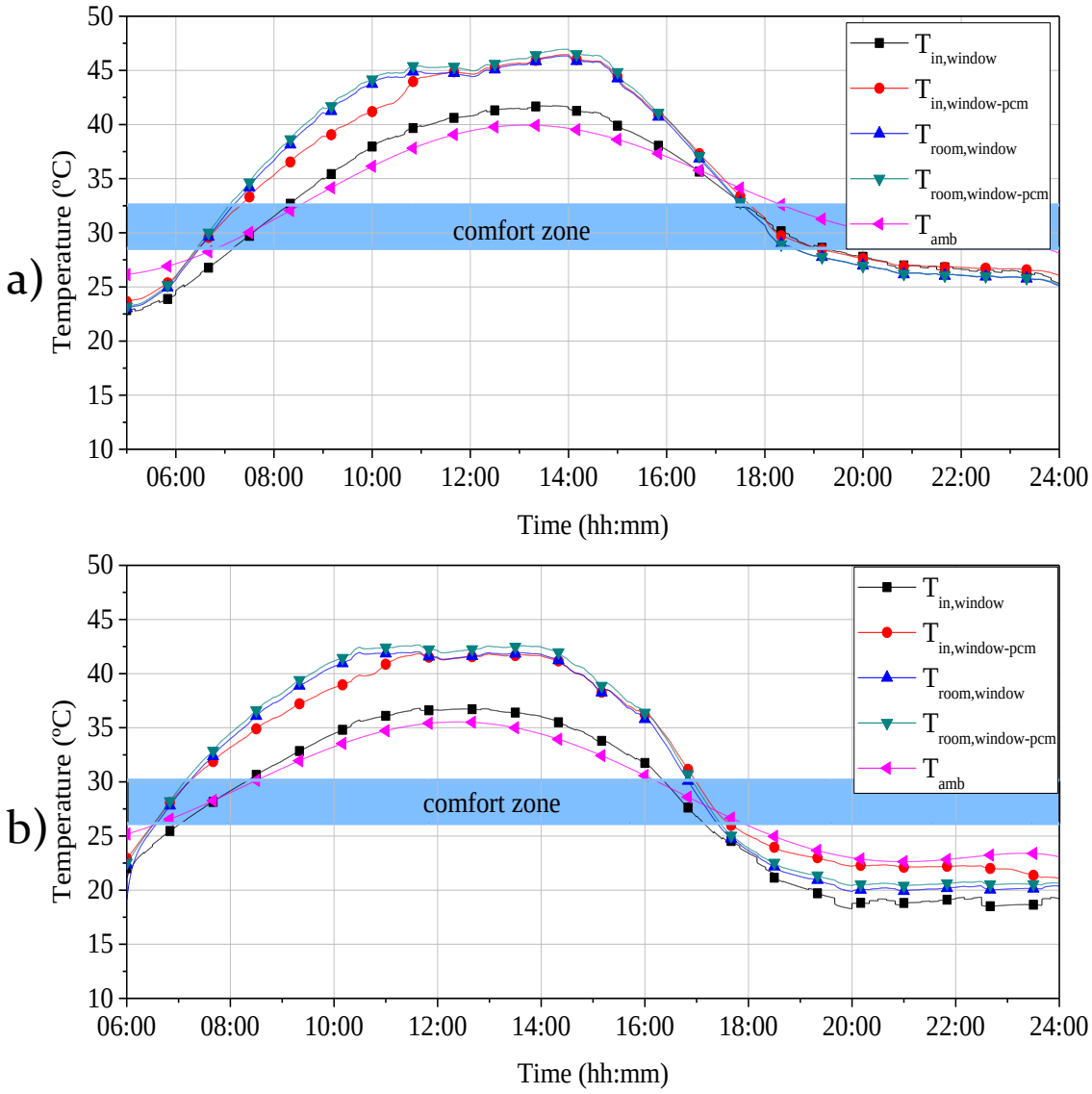

Figure 4.7 Comparison between the behavior of the inner surface average temperature and room inside temperature for both configurations for the a) warmest and b) coldest day of the summer season.

Figure 4.8a shows the maximum temperatures of the envelope components of the room for the warmest day of the summer season; it is evident that the roof temperature was the highest with a temperature of 66 °C presented by both cases under study, then the west wall follows with temperatures of 58 °C, next the east wall temperatures also showed similar values which were around 56 °C, then for the north wall the maximum temperatures between both configurations are close with

temperatures around 47 °C and finally the south wall showed temperatures of 46.46 and 41.72 °C which means a raise in the room temperatures of 4.74 °C when the PCM shutter was implemented. These results explain why the proposed system did not benefit the room temperatures, since almost all the other envelope elements presented higher temperatures and added energy to the room, which handicapped the performance of the PCM shutter because, instead of act as a blocker of the input energy of the outside ambient temperatures; the shutter did block the high temperatures of the other envelope elements which transferred its energy to the room, from escaping through the window. For the coldest day the Figure 4.8b shows that the envelope elements of the room tended to behave like in the warmest day, since also for this day, the roof temperatures were higher, hitting values around 64 °C, but in this day the east wall with 51 °C for both configurations, had higher temperatures than the west wall which presented temperatures of 50.5 °C for both configurations, the north wall temperatures were 41.6 °C, this last was surpassed by the window (south wall) with the PCM shutter with a temperature of 41.85 °C which was 5.06 °C higher than the one reached by the conventional window configuration.

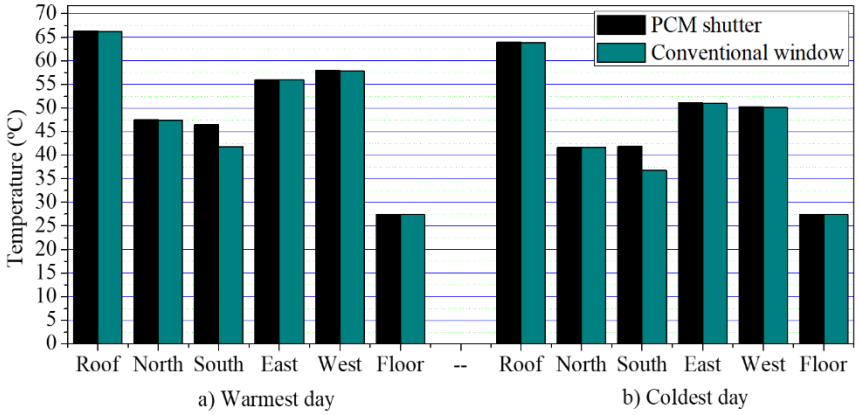

Figure 4.8 Comparison between the behavior of maximum temperatures of the envelope elements of the room for both configurations for the a) warmest and b) coldest day of the summer season.

Figure 4.9a shows the heat fluxes of the warmest and coldest day of the summer season which shows a similar behavior as the one discussed in Figure 4.3 and Figure 4.6. For the warmest day the heat fluxes of the window with the PCM shutter varied from -26.92 to 6.38 Wh/m^2 at 10:10 and 24:00 hours respectively, with a difference of -21.36 Wh/m^2. While for the conventional window these values varied from -65.86 to 7.12 Wh/m^2 at 09:10 hours and 18:10 hours with a difference of -58.74 Wh/m^2. Hence the variations are -37.38 Wh/m^2 higher with the conventional window. Figure 4.9b shows that in the coldest day of the spring the window with the PCM shutter varied from -23.20 to 12.14 Wh/m^2 at 10:30 and 20:00 hours respectively, with a difference of -11.06 Wh/m^2. While for the conventional window these values varied from -54.34 to 13.63 Wh/m^2 at 10:30 hours and 06:00 hours with a difference of -40.71 Wh/m^2.

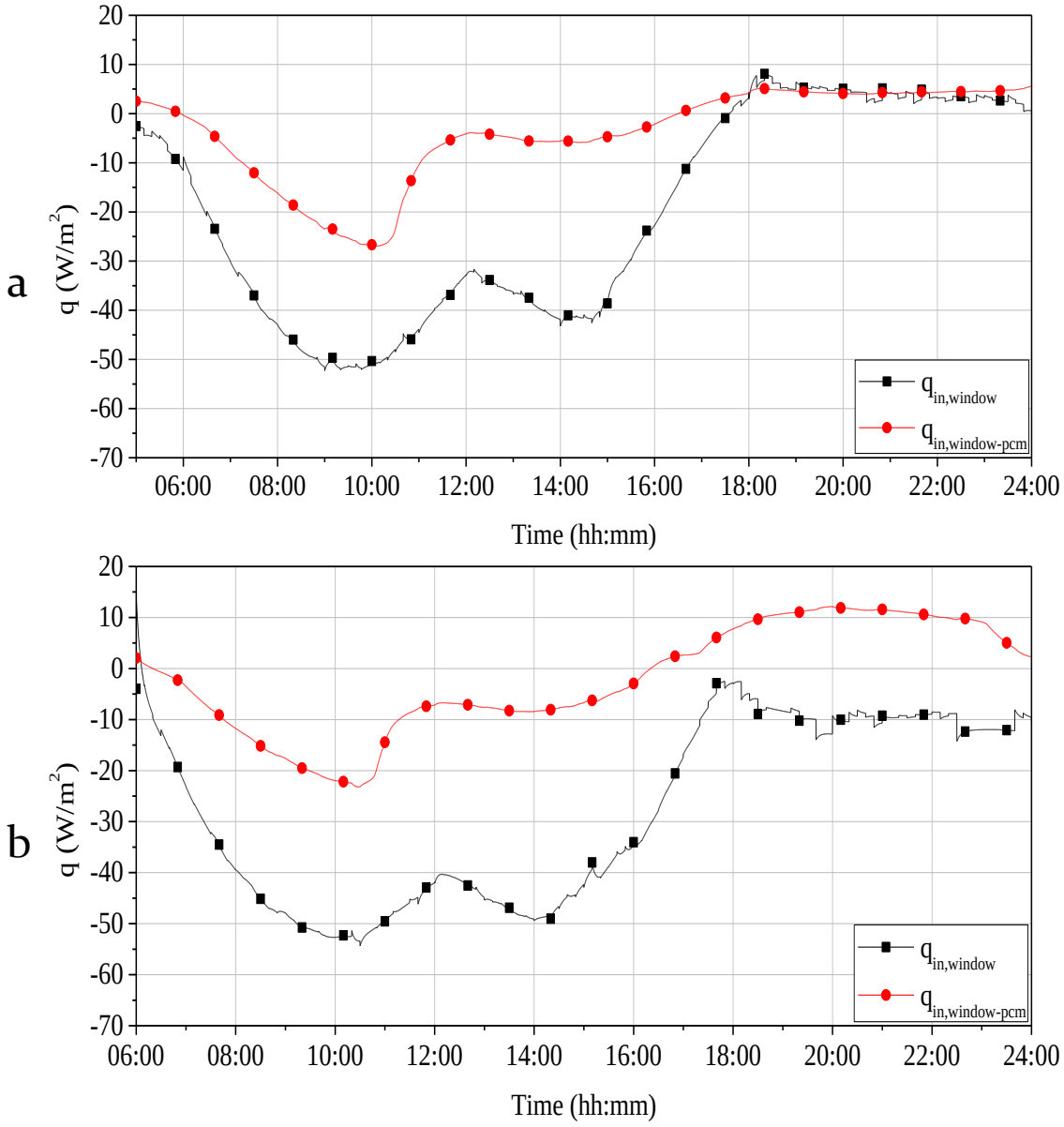

Figure 4.9 Comparison between the behavior of the inner surface heat fluxes for both configurations for the a) warmest and b) coldest day of the summer season.

4.4 Fall season.

For the warmest day Figure 4.10a shows the behavior of the average temperature at the inner surface of the window and the inside room temperature for both configurations. It is observed that the maximum and minimum average inner surface temperatures of the window system with the PCM were 44.62 and 22.34 °C at 14:09:50 and 06:00:00 hours, respectively, while for the conventional window configuration these temperatures were 39.04 and 21.03 °C at 14:08:20 and 06:00:00 hours, which means that the conventional windows configuration performed better with lower

temperatures through the simulated hours, also, the window with the PCM shutter raised the maximum and minimum inner surface temperatures by 5.58 and 1.31 °C when compared with the conventional window. In the same way for the room the maximum and minimum temperatures were 45.11 and 21.98 °C at 14:09:50 and 06:00:00 hours when the PCM shutter was implemented in the window, and for the room with the conventional window these temperatures were 44.45 and 21.81 °C at 14:09:50 and 06:00:00 hours which represents a raise in the maximum and minimum temperatures of the order of 0.66 and 0.17 °C respectively, when the PCM shutter was implemented. This behavior of the room temperatures corresponds to those shown by the window and indicate that the implementation of the PCM shutter did not benefit the inside temperatures as desired, and the possible cause of this behavior will be discussed later in the Figure 4.11.

As for the comfort zone, in the warmest day it went from 27.4 to 31.4 °C and the room temperatures reach this zone at 06:45:50 hours for the configuration with the PCM and at 06:48:50 hours with the conventional window. Then the comfort zone was exceeded at 07:19:00 and 07:22:40 hour by the PCM shutter and conventional configurations respectively. Later in the day when the temperatures tend to decrease due to the lack of solar radiation, the room temperatures reach again the comfort zone at 16:47:40 and 16:45:20 hours by both configurations and go below it at the same time at 18:02:30 hours so both configurations were in the comfort zone for a total of 01:47:40 and 01:51:00 hours with and without the PCM shutter respectively.

For the coldest day, Figure 4.10b shows the behavior of the inner surface average temperature for both configurations and these had a maximum and minimum of 37.30 (13:45:30 hours) and 16.52 °C (06:00:00 hours) with the PCM shutter respectively, and without the shutter these temperatures were 31.88 (13:29:50) and 13.61 (06:00:00). Also, when the PCM shutter was implemented the maximum and minimum temperatures were 5.42 and 2.91 °C higher when compared with the performance of the conventional window. This behavior corresponds to those shown by the room temperatures with the window system with the PCM shutter which presented maximum and minimum temperatures of 39.33 (13:09:50) and 16.47 °C (06:00:00) against the 38.66 (13:09:50) and 16.09 °C (06:00:00) shown by the room the conventional window, which means that the PCM shutter elevated the temperatures of the room by 0.67 and 0.38 °C and although is desirable to raise the temperatures inside the room when the ambient temperatures are low, these are just slightly above of those of the conventional window configuration which were already too high for most of the day, when the comfort temperature is considered.

For this matter, the comfort zone for the coldest day went from 23.8 to 27.8 °C and the room temperatures reach it for the first time in the day at 06:53:30 and 06:59:10 hours by the PCM shutter and the conventional configurations respectively and exceed it at 07:31:30 and 07:40:30 hours. Then again when the ambient conditions change the room temperatures of both configurations drop to the comfort zone at 16:06:30 and 16:01:20 hours and stay there until it goes below the comfort zone at

16:47:30 and 16:42:20 hours, which means that for the PCM shutter and conventional window configuration maintain the room temperatures in the comfort zone for a total of 01:25:00 and 01:22:20 hours through the simulated hours. This indicates that the proposed system of the window with the PCM shutter, did not benefit the room temperatures although it kept longer the room temperatures in the comfort zone, and the reason as to why this happened will be discussed below.

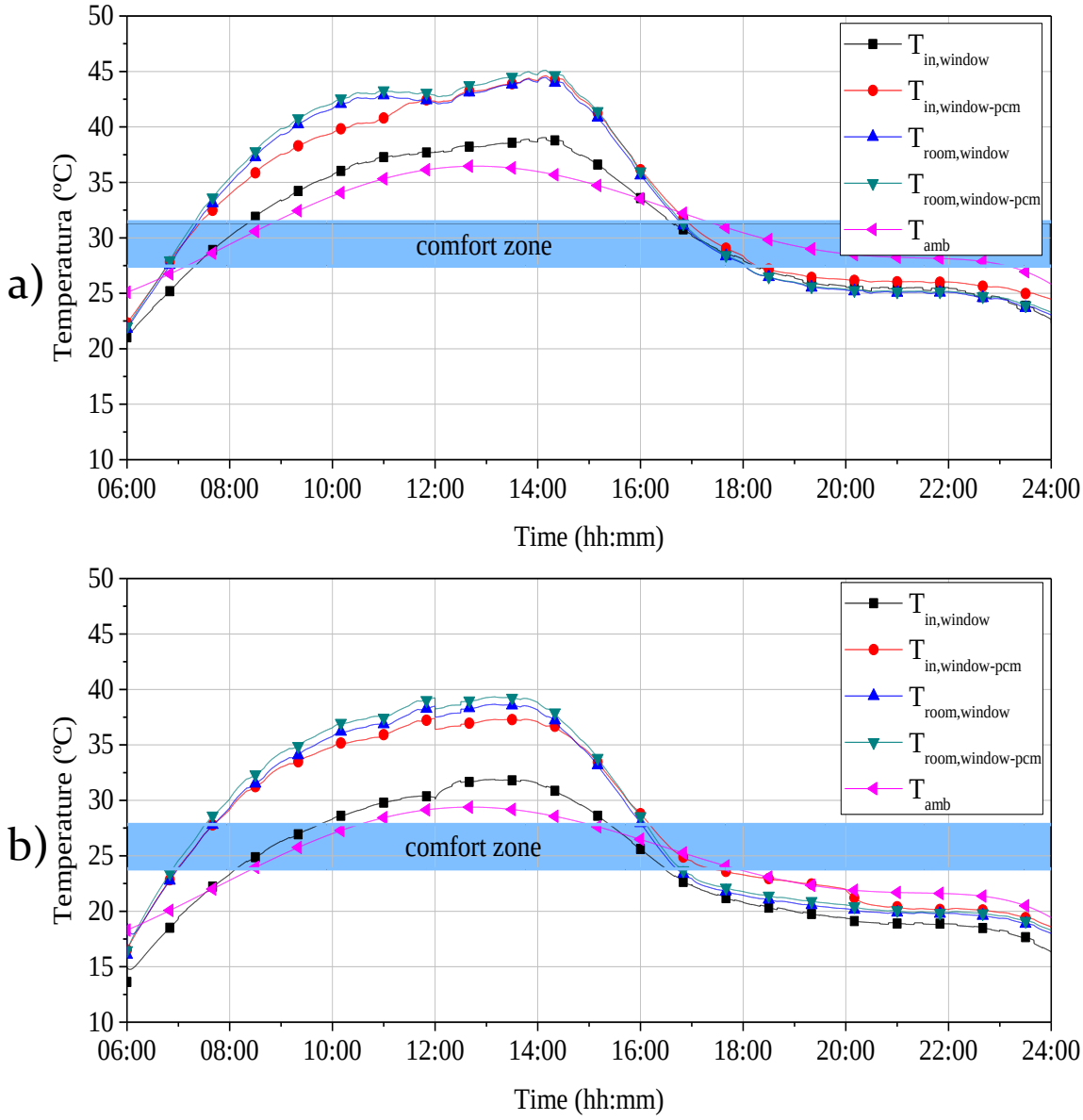

Figure 4.10 Comparison between the behavior of the inner surface average temperature and room inside temperature for both configurations for the a) warmest and b) coldest day of the fall season.

As Figure 4.11a shows, for the warmest day of the fall season the maximum temperature values for each envelop component of the both evaluated configurations indicate that the roof element has the highest temperature with 62.46 and 62.34 °C for the PCM shutter and the conventional window configuration, then was followed

by the west and east walls with temperatures around 55 and 52.5 °C, then the north wall presented temperatures around 49 °C and for the window the temperatures were 39.04 °C with the conventional window and when the PCM shutter was implemented its temperature was raised 5.58 °C. This occurs because with the shutter the way out of the energy transferred to the room by the rest of the elements of the envelope (which had higher temperatures) were blocked, and, although very little margin it causes an increase in the temperature inside the room as discussed in the **Figure 4.10**, and when the temperatures decrease as the solar radiation disappears, the PCM because of its energy store capacity causes the window temperatures to augment when compared to the conventional window. For the case of the coldest day the Figure 4.11b shows that for this day the elements of the envelope with the highest temperature values were the roof with 56 °C for both cases under study, next the west, east and north walls with temperatures around 45-42 °C, for both window configurations and the window temperatures, for the conventional windows is appreciated that was even 5.42 °C lower than the temperature reached when the PCM shutter was implemented which was 37.3 °C. This confirms that the PCM shutter did not accomplish its purpose to maintain the temperature values uniform through the day, but on the contrary, it did raise the temperature values of the room and its envelope elements all together.

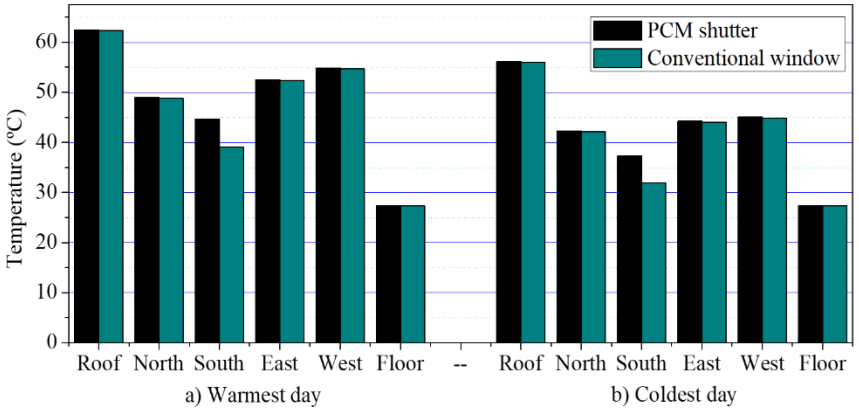

Figure 4.11 Comparison between the behavior of maximum temperatures of the envelope elements of the room for both configurations for the a) warmest and b) coldest day of the fall season.

The heat fluxes in the fall season are presented in Figure 4.12a for the warmest day and it shows a similar behavior as the one discussed in Figure 4.3 and Figure 4.6. For the warmest day the heat fluxes of the window with the PCM shutter varied from -24.67 to 7.74 Wh/m^2 at 10:30 and 24:00 hours respectively, with a difference of -16.93 Wh/m^2. While for the conventional window these values varied from -52.18 to 4.03 Wh/m^2 at 09:45 hours and 18:20 hours with a difference of -48.15 Wh/m^2. Hence the variations are -31.22 Wh/m^2 higher with the conventional window. Figure 4.9b shows that in the coldest day of the spring the window with the PCM shutter varied from -18.30 to 10.50 Wh/m^2 at 13:00 and 18:40 hours respectively, with a difference of -7.80

Wh/m^2. While for the conventional window these values varied from -61.95 to -4.27 Wh/m^2 at 10:10 hours and 17:10 hours with a difference of -57.68 Wh/m^2.

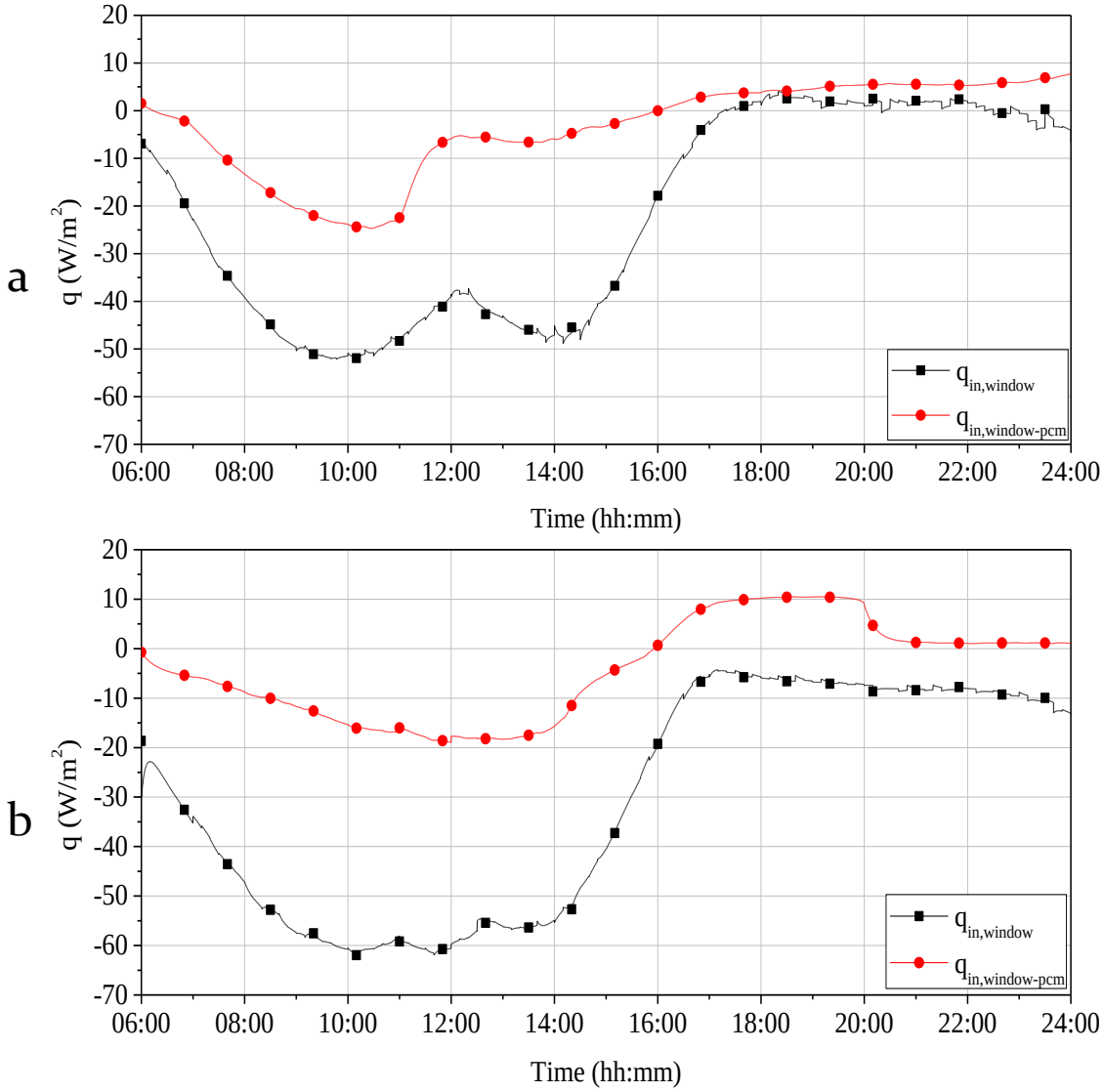

Figure 4.12 Comparison between the behavior of the inner surface heat fluxes for both configurations for the a) warmest and b) coldest day of the fall season.

4.5 Total heat fluxes on the inner surface of the window

To quantify the differences between the window with de PCM shutter against the conventional window, a trapezoidal integration was performed on the heat fluxes through all hours oof each of the days analyzed. It was considered a heat flux per square meter and the integration is expressed as follows:

$$\int_{t=1}^{t=n} q_{tot,int}(t)dt = \frac{\Delta t}{2}\left[q_{tot,int}(1) + \sum_{t=2}^{t=n-1} 2 * q_{tot,int}(t) + q_{tot,int}(n)\right] \quad (4.1)$$

Table 4.1 show the total heat flux of the warmest days of the twelve months for both study cases. According to Figures 4.3, 4.6, 4.9, 4.12 the heat fluxes of the eight analyzed days had very similar behaviors, ergo, when the PCM shutter is implemented, the heat fluxed tend to be linear, which causes an attenuation in the energy gains and losses in the room and in the window for both configurations. That is why in Table 4.1 it is appreciated that for all the evaluated days, whit the PCM shutter the total heat flux in the window inner surface is lower than the total heat flux of the conventional window in all months. It is also observed that the greater decrease in the total heat fluxes occurs on December with a 92.11 % due to the low temperatures during that day. On the other hand, the smallest decrease occurs on July with 81.58 %, caused by the higher temperatures of the summer season. The total heat flux reduction on the warmest days of the twelve months was 86.64%, when the PCM shutter is implemented.

Table 4.1 Total heat fluxes per square meter of the warmest days of each month of the year for both study cases.

Month	$\int_{t=1}^{t=n} q_{tot,int}(t)dt$ (kWh/m^2)		Dif (%)
	PCM Shutter	Conventional window	
January	0.05	0.47	89.36
February	0.06	0.43	86.05
March	0.03	0.36	91.67
April	0.05	0.39	87.18
May	0.05	0.40	87.50
June	0.09	0.51	82.35
July	0.07	0.38	81.58
August	0.06	0.38	84.21
September	0.07	0.45	84.44
October	0.06	0.39	84.62
November	0.04	0.40	90.00
December	0.03	0.38	92.11
Total	0.66	4.94	86.64

Table 4.2 presents the total heat flux of the coldest days of the twelve months for both study cases. It is shown that in all the coldest days the implementation of the PCM

shutter, provokes a decrease in the total heat flux, being the day of January the one with the highest decrease of 95.56% and the day of May the one with the smallest decrease with 82%. Then the total heat flux reduction obtained in the twelve coldest days modeled was 86.96% which is higher than the one presented on the warmest days. This behavior is due to the ambient temperature curves of those days, because are by themselves more attenuated than de curves of the ambient temperature of the warmest days.

Table 4.2 Total heat fluxes per square meter of the coldest days of each month of the year for both study cases.

Month	$\int_{t=1}^{t=n} q_{tot,int}(t)dt\ (kWh/m^2)$		Dif (%)
	PCM Shutter	Conventional window	
January	0.02	0.45	95.56
February	0.06	0.52	88.46
March	0.07	0.49	85.71
April	0.08	0.58	86.21
May	0.09	0.50	82.00
June	0.17	0.98	82.65
July	0.07	0.47	85.11
August	0.04	0.43	90.70
September	0.03	0.50	94.00
October	0.06	0.46	86.96
November	0.07	0.54	87.04
December	0.09	0.60	85.00
Total	0.85	6.52	86.96

After discussing and comparing the results, it is time to conclude. Chapter 5 describes the final conclusions and the work to carry on in future work to complement the present research work.

Chapter 5

Conclusions

The study of the thermal performance of a PCM shutter implemented in a window and how it affects the temperatures inside a room was carried out. The proposed system was subjected to the climate conditions of Mérida Yucatán in the Mexican Republic and the obtained results were compared against a conventional window thermal performance. For the study, the warmest and coldest day of each month of the year were selected to model the proposed system.

Then based on the obtained data it can be concluded that:

- The behavior of the temperatures of the window with the PCM shutter compared to those of the conventional window, as well as the temperatures inside the room; were very similar regardless of the season of the year or whether it was the hottest or coldest day of the season.
- The added time from all days that both cases of study kept the room temperatures inside the comfort zone were 12:49:20 hours for the PCM shutter case and 13:36:40 hours for the conventional window configuration. Which means that with the conventional window the room temperatures stayed 00:47:20 hours longer in the comfort zone through the eight analyzed days.
- The highest room temperature rise, occurred in the warmest day of the summer season, with a value of 3.33 °C, when the PCM shutter was implemented. Also, in that day the lowest room temperature rise was found with a value of 0.13 °C.
- In all analyzed days, the heat fluxes tended to be linear when the PCM shutter was implemented. Therefore, preventing the energy from flowing towards the outside ambient, provoking a rise in the temperatures on the inner surface of the window and the room.
- The PCM shutter is a promising technology since, because of the thermal storage capability of the PCM, it was able to reduce the total heat flux by around 87%. However, it raised the temperatures in the room and the inner surface of the window; therefore, its adequate thermal properties or thickness are to be further investigated for the implementation proposed in the present study.
- The PCM shutter alone cannot benefit the temperatures inside the room since the rest of the room envelope elements showed higher temperatures than the window system for all the analyzed day and in both cases under study.

The general conclusion is that the performance of the PCM shutter was not satisfactory since its purpose was to decrease the room temperatures and the contrary occurred. This is because the shutter alone cannot influence the room temperatures since the temperatures of the rest of the envelope elements were too high in comparison, also the orientation (south) in which the proposed system was located had the lowest solar radiation incidence among the other elements. Therefore, investigations implementing the proposed system in all orientations are needed. Also, it is concluded that the PCM shutter could be used as a calefaction passive tool for colder climates. Following, it is recommended for future investigations to:

- Evaluate the PCM shutter in all the orientations to better asses its thermal performance.
- Evaluate the optimal width between the glass sheet and the PCM shutter.
- Carry out a parametric study to choose the suitable phase change material for the modeled climate conditions as well as its optimal thickness.
- Evaluate the performance of the PCM shutter including another passive technology to improve the comfort temperatures inside the room.
- Validate the numerical code with experimental data of a similar physical model.
- Subject the PCM shutter system to different climate conditions of the Mexican Republic.

Bibliographic references

[1] Balance Nacional de Energía, Dirección General de Planeación Energética. https://www.gob.mx/cms/uploads/attachment/file/707654/BALANCE_NACIONAL_ENERGIA_0403.pdf, Accessed 08/10/2022.

[2] Comisión Nacional para el Conocimiento y Uso de la Biodiversidad (CONABIO). (2022). Available: http://www.conabio.gob.mx/informacion/gis/?vns=gis_root/clima/climas/climaImgw, Accessed 08/10/2022.

[3] A. Ruiz-Pardo, S. Alvarez-Domínguez, J. A. Saenz-Fernández, Revision of the Trombe wall calculation method proposed by UNE-EN ISO 13790. Energy and Buildings, 42 (2010) 763–773.

[4] S. Jabber, S. Ajib, Optimum design of Trombe wall system in Mediterranean region. Solar Energy, 85 (2011) 1891–1898.

[5] I. Hernández-López, J. Xamán, Y. Chávez, I. Hernández-Pérez, R. Alvarado-Júarez, Thermal Energy Storage and losses in a Room-Trombe Wall System located in México. Energy, 109 (2016) 512-524.

[6] W. Stec, A. van Paassen, A. Maziarz, Modelling the double skin facade with plants., Energy and Buildings, 37 (2005) 419-427.

[7] N. M. Nahar, P. Sharma, M. M. Purohit, Performance of different passive techniques for cooling of buildings in arid regions. Building and Environment, 38 (2003) 109-16.

[8] G. Villi, W. Pasut, M. De Carli, CFD modelling and thermal performance analysis of a wooden ventilated roof structure. Building Simulation, 2-3 (2009) 215-228.

[9] L. Susanti, H. Homma, H. Matsumoto, A naturally ventilated cavity roof as potential benefits for improving thermal environment and cooling load of a factory building. Energy and Buildings, 43 (2011) 211-218.

[10] I. Hernández-Pérez, G. Álvarez, J. Xamán, I. Zavala-Guillén, J. Arce, E. Simá, Thermal performance of reflective materials applied to exterior buildings components-A review. Energy and Buildings, 80 (2014) 81-105.

[11] Y. Y. Huang, C. T. Chen, Y. C. Tsai, Reduction of temperatures and temperature fluctuations by hydroponic green roofs in a subtropical urban climate. Energy and Buildings, 129 (2016) 174–185.

[12] M. Chagolla-Aranda, E. Simá, G. Álvarez, J. Xamán, I. Hernández-Pérez, E. Téllez-Velázquez, Effect of irrigation on the experimental thermal performance of a green roof in a semi-warm climate in Mexico. Energy and Buildings, 154 (2017) 232-243.

[13] J. Xamán, J. Cisneros-Carreño, I. Hernández-Pérez, I. Hernández-López, Aguilar-K. M. Castro, E. V. Macias-Melo, Thermal performance of a hollow block with/without insulating and reflective materials for roofing in Mexico. Applied Thermal Engineering, 123 (2017) 243–255.

[14] D. Morillón Gálvez, (1993). Bioclimática, Sistemas Pasivos de Climatización, Ed. Universidad de Guadalajara.

[15] J. Xamán, C. Pérez-Nucamendi, J. Arce, J. Hinojosa, G. Álvarez, I. Zavala Guillén, Thermal analysis for a double pane window with a solar control film for using in cold and warm climates, Energy and Build. 76 (2014) 429–439.

[16] J. Aguilar, J. Xamán, G. Álvarez, I. Hernández, C. López, Thermal performance of a double pane window using glazing available on the Mexican market. Renewable Energy, 81, (2015) 785-794.

[17] J. Xamán, Y. Olazo, Y. Chávez, J. Hinojosa, I. Hernández, I. Hernández, I. Zavala, Computational fluid dynamics for thermal evaluation of a room with a double glazing window with a solar control film. Renewable Energy, 94 (2016) 237-250.

[18] J. Xamán, C. Jiménez, G. Álvarez, I. Zavala I., Hernández I., Aguilar J., Thermal performance of a double pane window with a solar control coating for warm climate of Mexico. Applied Thermal Engineering, 106 (2016) 257-265.

[19] J. Xamán, Y. Olazo, I. Zavala, I. Hernández, J. Aguilar, J. Hinojosa, Thermal evaluation of a room coupled with a double glazing window with/without a solar control film for Mexico. Applied Thermal Engineering, 110 (2017) 805-820.

[20] W. J. Hee, M. A. Alghoul, B. Bakhtyar, O. Elayeb, M. A. Shameri, M. S. Alrubaih, K. Sopian. The role of window glazing on daylighting and energy saving in buildings, Renewable and Sustainable Energy Reviews. 42 (2015) 323-343.

[21] T. Silva, R. Vicente, F. Rodrigues, Literature review on the use of phase change materials in glazing and shading solutions, Renewable and Sustainable Energy Reviews. 53 (2016) 515-535.

[22] J. Kosny, (2015). PCM-Enhanced building components, Ed. Springer.

[23] K. A. R. Ismail, J. R. Henriquez, PCM Glazing Systems. International Journal of Energy Research. 21 (1997) 1241-1255.

[24] K. A. R. Ismail, J. R. Henriquez, Parametric study on composite an PCM glass systems. Energy Conversion and Management. 43 (2002) 973-993.

[25] K. A. R. Ismail, C. T. Salinas, J. R. Henriquez, Comparison between PCM filled glass windows and absorbing gas filled windows, Energy and Buildings. 40 (2008) 710-719.

[26] Y. A. Kara, A. Kurnuc, Performance of coupled novel triple glass and phase change material wall in the heating season: An experimental study, Solar Energy. 86 (2012) 2432-2443.

[27] B. L. Gowreesunker, S. B. Stankovic, S. A. Tassou, P. A. Kyriacou, Experimental and numerical investigations of the optical and thermal aspects of a PCM-glazed unit, Energy and Buildings. 61 (2013) 239-249.

[28] F. Goia, M. Zinzi, E. Carnielo, V. Serra, Spectral and angular solar properties of a PCM-filled double glazing unit, Energy and Buildings. 87 (2015) 302-312.

[29] L. Changyu, Y. Yumeng, L. Dong, Q. Hangbin, L. Xiaoyan, A model to determine thermal performance of a non-ventilated double-glazing unit with PCM and experimental validation, Procedia Engineering. 157 (2016) 293-300.

[30] S. Li, G. Sun, K. Zou, X. Zhang, Experimental research on the dynamic thermal performance of a novel triple-pane building window filled with PCM, Sustainable Cities and Society. 27 (2016) 15-22.

[31] D. Li, Y. Wu, C. Liu, G. Zhang, M. Arici, Energy investigation of glazed windows containing Nano-PCM in different seasons, Energy Conversion and Management, 172 (2018) 119-128.

[32] D. Li, Y. Wu, C. Liu, G. Zhang, M. Arici, Numerical investigation of thermal and optical performance of window units filled with nanoparticle enhanced PCM, Heat and Mass Transfer. 125 (2018) 1321-1332.

[33] C. Liu, Y. Wu, Y. Zhu, D. Li, L. Ma, Experimental investigation of optical and thermal performance of a PCM-glazed unit for building applications, Energy and Buildings. 158 (2018) 794-800.

[34] C. Liu, Y. Wu, J. Bian, D. Li, X. Liu, Influence of PCM design parameters on thermal and optical performance of multi-layer glazed roof, Applied Energy, 212 (2018) 151-161.

[35] E. M. Alawadhi. Effect of an incompletely closed window shutter on indoor illuminance level and heat gain, Energy and Buildings. 110 (2016) 112-119.

[36] E. M. Alawadhi. Using phase change materials in window shutter to reduce the solar heat gain. Energy and Buildins. 47 (2012) 421-429.

[37] Q. Wang, C.Y. Zhao. Parametric investigation of using PCM curtain for energy efficient buildings, Energy and Buildings. 94 (2015) 33-42.

[38] T. Silva, R. Vicente, F. Rodrigues, A. Samagaio, C. Cardoso. Performance of a window shutter with phase change material under summer Mediterranean climate conditions, Applied Thermal Engineering. 84 (2015) 246-256.

[39] T. Silva, R. Vicente, F. Rodrigues, A. Samagaio, C. Cardoso. Development of a shutter window with phase change materials: Full scale outdoor experimental approach, Energy and Buildings. 88 (2015) 110-121.

[40] T. Silva, R. Vicente, C. Amaral, A. Figueiredo. Thermal performance of a window shutter containing PCM: Numerical validation and experimental analysis, Applied Energy. 179 (2016) 64-84.

[41] Y. Li, J. Darkwa, G. Kokogiannakis. Heat transfer analysis of an integrated double skin facade and phase change material blind system, Building and environment. 125 (2017) 111-121.

[42] Y. Li, J. Darkwa, G. Kokogiannakis, S. Weiguang. Phase change material blind system for double skin facade integration: System development and thermal performance evaluation. Applied energy. 252 (2019) 113376.

[43] F. Goia, M. Perino, M. Hase. A numerical model to evaluate the thermal behaviour of PCM glazing system configurations. Energy and Buildings, 54, (2012) 141-153

[44] D. Li, Z. Li, Y. Zheng, C. Liu, H. A. Kadhim, X. Liu. Thermal performance of a PCM-filled double-glazing unit with different thermophysical parameters of PCM. Solar Energy, 133 (2016) 207-220.

[45] S. Zhang, W. Hu, D. Li, C. Chang, M. Arici, C. Yildis, X. Zhang, Y. Ma. Energy efficiency optimization of PCM and aerogel-filled multiple glazing windows. Energy. 222 (2021) 119916.

[46] R. Yang, D. Li, S. L. Salazar, Z. Rao, M. Arici, W. Wei. Photothermal properties and photothermal conversion performance of nano-enhanced paraffin as a phase change thermal energy storage material. Solar Energy Materials and Solar Cells 219 (2021) 110792.

[47] W. Jiang, B. Liu, X. Zhang, T. Zhang., D. Li, L. Ma. Energy performance of window with PCM frame. Sustainable Energy Technologies and Assessments. 45 (2021) 101109.

[48] L. Pei-Chun, B. Ford, D. Etheridge. A modeling study of segmentation of naturally ventilated tall office buildings in a hot and humid climate, International Journal of Ventilation, 11:1 (2012) 29-42

[49] S. Grynning, F. Goia, E. Rongvik, B. Time, Possibilities of characterization of a PCM window system using large scale measurements, International Journal of Sustainable Built Environment, 2 (2013) 56-64.

[50] L. Sanati, M. Utzinger. The effect of window shading design on occupant use of blinds and electric lighting. Building and Environment. 64 (2013) 67-76.

[51] M. Gijón-Rivera, J. Xamán, G. Álvarez, J. Serrano-Arellano. Coupling CFD-BES Simulation of a glazed office with different types of windows in México City. Building and Environment. 68 (2013) 22-34.

[52] F. Goia, M. Perino, V. Serra. Experimental analysis of the energy performance of a full-scale PCM glazing prototype. Solar Energy. 100 (2014) 217-233.

[53] L. Shuhong, K. Zhong, Y. Zhou, X. Zhang. Comparative study on the dynamic heat transfer characteristics of PCM-filled glass window and hollow glass window. Energy and Buildings. 85 (2014) 483-492.

[54] G. Gorgolis, D. Karamanis. Solar energy materials for glazing technologies, Solar Energy Materials and Solar Cells, 144 (2016) 559-578.

[55] J. Aguilar, J. Xamán, G. Álvarez, I. Hernández, C. López. Thermal performance a room with a double glazing window using glazing available in Mexican market. Applied Thermal Engineering. 119, (2017) 505-515.

[56] S. Omrani, V. Garcia-Hansen, B. Capra, R. Drogemuller. Natural ventilation in multi-storey buildings: Design process and review of evaluation tools. Building and Environment. 116 (2017) 182-194.

[57] I. Vigna, L. Bianco, F. Goia, V. Serra. Phase change materials in transparent building envelopes: A strengths, weakness, opportunities and threats (SWOT) analysis. Energies. 11 (2018) 111.

[58] B. Duraković, S. Mešetović. Thermal performances of glazed energy storage systems with various storage materials: An experimental study. Sustainable Cities and Society. 45 (2019) 422-430.

[59] D. Li, Y. Wu, B. Wang, C. Liu, M. Arıcı. Optical and thermal performance of glazing units containing PCM in buildings: A review. Construction and Building Materials. 233 (2019) 117327.

[60] C. C. Leyva. (2000). Estudio de la transferencia de calor en ventanas con vidrios duovent. (tesis de maestría en ciencias en ingeniería mecánica). Centro Nacional de Investigación y Desarrollo Tecnológico (CENIDET), Cuernavaca, Morelos.

[61] F. Noh-Pat, J. Xamán, G. Álvarez, Y. Chávez, J. Arce. Thermal analysis for a double-glazing unit with and without a solar control film (SnS-Cu_xS) for using in hot climates. Energy and Buildings, 43 (2011) 704-712.

[62] C. P. Nucamendi. (2012). Análisis térmico de una ventana de vidrio doble. (tesis de maestría en ciencias en ingeniería mecánica). Centro Nacional de Investigación y Desarrollo Tecnológico (CENIDET), Cuernavaca, Morelos.

[63] C. J. Xamán. (2015). Aplicación del método de multimallas a problemas de transferencia de calor. (tesis de maestría en ciencias en ingeniería mecánica). Centro Nacional de Investigación y Desarrollo Tecnológico (CENIDET), Cuernavaca, Morelos.

[64] Y. Olazo. (2015). Análisis térmico de una habitación con una ventana de vidrio doble. (tesis de maestría en ciencias en ingeniería mecánica). Centro Nacional de Investigación y Desarrollo Tecnológico (CENIDET), Cuernavaca, Morelos.

[65] E. González (2017). Evaluación térmica de vidrios de control solar disponibles en el mercado mexicano para ventanas de vidrio doble. (tesis de maestría en ciencias en ingeniería mecánica). Centro Nacional de Investigación y Desarrollo Tecnológico (CENIDET), Cuernavaca, Morelos.

[66] H. Versteeg, W. Malalasekera (2008). An Introduction to computational fluid dynamics, the finite volume method. Pearson, Prentice Hall, England.

[67] R. Siegel, J. Howell (1981). Thermal Radiation Heat Transfer. Hemisphere Publishing Co., Mc. Graw Hill Co., New York.

[68] S. Nasser, Al-Saadia, Z. Zhai. Systematic evaluation of mathematical methods and numerical schemes for modeling PCM-enhanced building enclosure, Energy and Buildings, 92 (2015) 374-388.

[69] C. Bonacina, G. Comini, A. Fasano, M. Primicerio. Numerical solution of phase change problems. International Journal of Heat and Mass Transfer, 16 (1973) 1825-1832.

[70] Y. C. Liu, L. S. hao, Modified effective specific heat method of solidification problems, Materials Transactions. 47 (2006) 2737-2744.

[71] V.R. Voller, C.R. Swaminathan, Fixed grid techniques for phase change problems: a review, International Journal of Numerical Methods in Engineering., 30 (1990) 875-898.

[72] J.P. Van Doormal, G.D. Raithby. Enhancements of the simple method for predicting Incompressible fluid flows, Numerical Heat Trans, 7 (1984) 147-163

[73] J. Ferziger, M. Perk (1997). Computational Methods for Fluid Dynamics, Springer.

[74] J. Xamán, G. Álvarez, J. Hinojosa, J. Flores. Conjugate turbulent heat transfer in a square cavity with a solar control coating deposited to a vertical semitransparent wall. International Journal of Heat and Fluid Flow, 30 (2009) 237–248.

[75] S.V. Patankar (1980). Numerical heat transfer and fluid flow. Hemisphere Publishing Corporation, Taylor & Francis Group, New York.

[76] J. Xamán, Y. Olazo, Y. Chávez, J. F. Hinojosa, I. Hernández-Pérez, I. Hernández López, I. Zavala-Guillén. Computational fluid dynamics for thermal evaluation of a room with a double glazing window with a solar control film. Renewable Energy, 94 (2016) 237–250.

[77] J. Van Doormaal, G. Raithby. Enhancements of the SIMPLE Method for Predicting Incompressible Fluid Flow, Numerical Heat Transfer, 7, 147-163, 1984.

[78] **S.** Patankar**,** D. Spalding. A Calculation Procedure for Heat Mass and Momentum Transfer in Three-Dimensional Parabolic Flows, Int. J. Heat Mass Transfer, 15 (1972) 1787-1806.

[79] Y. Cengel & A. Ghajar (2011). Heat and mass transfer. McGraw Hill.

[80] G. De Vahl Davis. Natural convection of air in a square cavity a benchmark numerical solution, Int. J. Numerical Meth. Fluids, 3 (1983) 249-264.

[81] D. A. Kaminskiand & C. Prakash. Conjugate natural convection in a square enclosure: effect of conduction in one of the vertical walls, Int. J. Heat Mass Transfer, 29 (1986) 19291988.

[82] M. Leal, H. Machado, R. Cotta. Integral transform solutions of transient natural convection in enclosures with variable fluid properties, International J. Heat Mass Trans. 43 (2000) 3977-3990.

[83] A.D. Solomon. An easily computable solution to a two-phase Stefan problem, Solar Energy, 23 (1979) 525-528.

[84] M. Arıcı, F. Bilgin, S. Nizetic, A.M. Papadopoulos. Phase change material based cooling of photovoltaic panel: a simplified numerical model for the optimization of the phase change material layer and general economic evaluation, J. Clean. Prod. 189 (2018) 738-745.

[85] J. Xamán, M. Gijón-Rivera (2016). "Dinámica De Fluidos Computacional Para Ingenieros", Palibrio.

[86] N. M. Özisik (1985). Heat transfer a basic approach, Mc. Graw Hill Co., USA.

[87] H. Su, L. Xiao-Bing, M. Jing-Yu. A numerical model of a deeply buried air-earth-tunnel heat exchanger. Energy and Buildings, 48 (2012) 233-239.

[88] HM Bloques adocretos S.A. DE C.V. la nacionalista. Productos de Concreto de Alta Calidad. http://www.hmbloques.mx/faltantes%20HM/BS%2015.pdf (accessed 06-12-2021)

[89] Norma Oficial Mexicana NOM-020-ENER-2011, Eficiencia energética en edificaciones. - Envolvente de edificios para uso habitacional, Diario Oficial de la Federación, Estados Unidos Mexicanos, 2011. http://www.dof.gob.mx/normasOficiales/4459/sener1.htm (accessed 06-12-2021)

[90] I. Hernández-Pérez, J. Xamán, E.V. Macías-Melo, K.M. Aguilar-Castro, I. Zavala-Guillén, I. Hernández-López, E. Simá. Experimental thermal evaluation of building roofs with conventional and reflective coatings, Energy and Buildings, 158 (2017) 569-579.

[91] J. Bartl, M. Baranek. Emissivity of aluminum and its importance for radiometric measurement, Measurement Science Review, 4 (2004) Section 3.

[92] M. K. Rodriguez, F. S. Coswig, K. R. Camargo, L. A. Isoldi, R. S. Brum, J. V. A. Ramalho, J. Vaz, L. A. O. Rocha, E. D. dos Santos. Thermal performance simulations of earth-air heat exchangers for different soils of a coastal city usinin-situ data. Sustainable Energy Technologies and assessments, 30 (2018) 224-229.

[93] J. A. Duffie & W.A. Beckman (2013). Solar Engineering of Thermal Processes. Wiley, Hoboken.

[94] S. E. G. Jayamaha, N. E. Wijeysundera, S. K. Chou. Measurement of the heat transfer coefficient for walls. Building Environment, 31 (1996) 399-407.

[95] International Standard ISO 15099, 2003, Thermal Performance of Windows, Doors and Shadings Devices – Detailed Calculations.

[96] A. J. N. Khalifa, Marshall R. H., Validation of heat transfer coefficients on interior building surfaces using a real-sized indoor test cell, International Journal of Heat and Mass Transfer, 33 (1990) 2219-2236.

[97] M. Daguenet (1985), Les séchoirs solaries: theorie et practique, UNESCO, France.

[98] H. Nowak, The sky temperature in net radiant heat loss calculations from low-sloped roofs. Institute of Building Science. Technical University of Wroclaw Poland, 29 (1989) 231-232.

[99] M.C. Peel, B.L. Finlayson, T.A. McMahon, Updated world map of the Köppen-Geiger climate classification, Hydrol. Earth Syst. Sci. 11 (2007) 1633-1644, https://doi.org/10.5194/hess-11-1633-2007

[100] B. L. Finlayson, M. C. Peel, T. A. McMahon, (2014) Climate and rivers, Elsevier Inc, University of Melbourne, Australia.

[101] H. E. Beck, N. E. Zimmermann, T. R. McVicar, N. Vergopolan, A. Berg, E. F. Wood. Present and future Köppen-Geiger climate classification maps at 1-km resolution. Sci. Data, 5 (2018) 180214.

[102] K. Soteris, (2009) Solar energy engineering: processes and systems. Academic Press, Primera edición.

[103] D. G. Erbs, S. A. Klein, J. A. Duffie. Estimation of the diffuse radiation fraction for hourly, daily and monthly-average global radiation. Solar Energy, 28 (1984) 293-302.

[104] J. F. Orgill, K. G. T. Hollands, Correlation equation for hourly diffuse radiation on a horizontal surface. Solar Energy. 19 (1977) 357-359.

[105] F. Nicol, Adaptive thermal comfort standards in the hot-humid tropics, Energy Build. 36 (2004) 628–637.

.

Appendix

A. Technical sheets of the reviewed literature

In this appendix the literature reviewed through the doctorate thesis development are presented. The review includes papers from the beginning of the implementation of PCM into glazed systems, to the most relatively current studies. The technical sheets are sorted based on the year of publication.

Ismaíl and Henríquez (1997) conducted a theoretical-experimental study of the thermal performance of windows with phase change material (PCM). In the analysis, a double glass window with a specific spacing was used, which was filled with a PCM between the glass sheets. The phase change material used was a glycol mixture. Commercially available glass samples in Brazil of different thicknesses were optically evaluated to determine absorptivity, transmittance and reflectance. Also, the double glass sheets were tested to establish the thickness of the glass, spacing, the color of the inner air layer and finally the proposed PCM, in a wave length of 300-2800 *nm* covering part of the ultraviolet, the visible and part of the infra-red wave. The results showed 50% reductions in the energy transmitted through the PCM window compared to the other configurations, especially in the infra-red and ultraviolet regions. The authors concluded that the proposed concept is effective to reduce incoming solar radiation.

Ismail and Henríquez (2002) conducted a numerical and experimental study of windows with PCM. To carry out the numerical study, they took a one-dimensional model of a double-glazed window system with a separation space between them, in which the PCM and air are located for the proposed and reference system respectively. In the experimental analysis a characterization of the optical properties of different glass sheets was carried out varying their thicknesses from 3 to 8 *mm* and spacing between them from 3 to 20 *mm*, in addition the study for blue and green PCM was made. The used material was a glicol mixture. The results showed that for a window filled with air with glass thicknesses of 8 *mm* and with a spacing of 3 *mm* the transmitted energy is reduced by 25% and that the increase of this space does not produce notable reductions in the transmitted energy, however, when the same system is implemented by the PCM, the reduction of this energy shows improvements in the order of 50% and this increases when colored materials are used. The authors concluded that the implementation of PCMs to windows is a viable and thermally effective option.

Ismail et al. (2008) conducted a comparative study of double glass windows filled with PCM against windows filled with absorbent gas. To model the window with PCM a one-dimensional radiation-conduction formulation was used, and for the window with absorbent gas a radiation-convection-conduction model and a radiation-

conduction model were used, in addition 3 gas mixtures were used, a highly absorbent gas mixture, one with intermediate absorptivity and one transparent to infrared radiation (air). The glasses used are 6mm thick and the spacing between glasses varied from 0.8 to 4 *cm*. The results showed that the windows filled with absorbent gases and with a reflective interior glass are more efficient to reduce the total heat gain in a range of 55 to 65%, while the window system with the PCM shows a reduction in the range of 65 to 80%. It was concluded that for the systems that use absorbing gases the influence of reflective glass is important.

Goia and Perino (2012) developed A numerical model that describes the thermo-physical behavior of a PCM layer in combination with other transparent materials (i.e. glass panes) to perform numerical analyses on various PCM glazing systems configurations. The authors illustrate the structure of the model, the main equations implemented and the hypotheses adopted for the model development. The comparison between numerical simulations and experimental data of a simple PCM glazing configuration is also presented to show the potentials and the limitations of the numerical model. While a good agreement between simulations and experimental data can be shown for the surface temperature of the glazing, the comparison between simulated and measured transmitted irradiances and heat fluxes does not always reach the desired accuracy. However, the numerical tool seems to predict well the thermo-physical behavior of the system and may therefore represent a good starting point for simulations on different configurations of PCM glazing systems.

Kara and Kurnuc (2012) conducted an experimental study of the thermal performance of new triple glass (NTG) coupled to walls with a PCM. The experiment was developed over a period of one year. On the south facade of a test room, two wall systems with a PCM were built for comparison. A plasterboard with an encapsulated PCM was applied to the outer surface of each wall, and it was covered with NTG. The PCMs that were used were Rubitherm GR35 and GR41 which are an encapsulated granulated paraffin. The results show that the total daily efficiency of the wall with GR35 varies in a range of 22 to 37%, while for the wall with GR41 it varies in a range of 20 to 33%. The authors concluded that the wall with GR35 performed better than the wall with GR41. Also, it was concluded that the solar transmittance of the NTG decreased almost 100% during the summer compared to winter, and that it fulfilled its purpose by preventing the PCM wall from overheating during the summer.

Pei-Chun et al. (2012) proposed a segmentation approach for a double skin façade (DSF) envelope design on naturally ventilated non-residential tall buildings in the hot and humid climate of Taiwan. The authors adopted two modelling approaches to investigate the segmentation effects. Firstly, the single-cell envelope flow model (EFM) is evaluated under the steady state condition for evaluating the off-design conditions of three types of building configuration. Secondly a segmented atrium and ventilated double skin façades are adopted using a multi-cell airflow network model (AFN). Dynamic thermal modelling is used, because of the particular importance of the thermal behaviour of the DSF. The results indicate that when using single-cell

EFM the isolated cases tend to have stable flow rates across floors and are relatively easier for flow pattern control. It is found that the segmentation case demonstrates the feasibility of comfort ventilation for over 60% of mid-seasons. In general, optimum segmentation could offer a major advantage for reducing the overall variation of flow rates across floors

Alawadhi (2012) performed a theoretical analysis of the thermal performance of a window blind with a phase change material (PCM). A two-dimensional model for the system to be studied was presented and the numerical solution was obtained with the finite element method. The geometry of the system consists of glass, an air spacing, and the blind with a PCM which is on the inner part of the system. The outer surface of the window is subjected to time-dependent solar radiation and forced convection boundary condition, while the inner surface of the glass is subjected to free and time-independent convection boundary conditions. Also, the author conducted a parametric study to assess the effect of using different types and amounts of PCM. The phase change materials that were used were the paraffins, n-octadecane, n-eicosane and P116. The results showed that the heat gain through the window was reduced by 23.29% when the blind was used with PCM P116 with a thickness of 0.03 m. The author concluded that the melting temperature and amount of PCM used in the blind has a significant effect on its thermal performance.

Gowreesunker et al. (2013) performed a numerical and experimental evaluation of the thermal performance of PCM glazing systems. To do it, the authors performed a characterization of the thermal and radiative properties of the PCM during the phase change process (solid-liquid) and its thermal performance was evaluated in a double glass window system and compared against a standard double glass window system. The used PCM was the organic paraffin RT27. The results showed that under stable conditions visible transmittance values of 90 and 40% are obtained for the liquid and solid phases respectively, that the dispersion effects are greater in the solid phase and the absorption in the liquid phase. It was concluded that after the phase change the window with PCM despite providing a transmittance value similar to that of a standard window, the absorption process is dominant in the PCM window compared to the reflection in a standard window, therefore, when using PCM in windows, the overheating effect must be taken into account once the PCM melts completely.

Grynning et al. (2013) conducted a parametric study for the characterization of a dynamic window system with PCM using large-scale measurements. For this, a weather simulator was used, which is composed of two test chambers separated by a window system consisting of a 4-glass window with a prismatic glass in the cavity closest to the outside, the second cavity contains argon and the cavity closest to the interior is filled with a PCM (wax paraffin) with an approximate thickness of 23 mm. The results showed that, even for climates similar to warm Nordics, the latent heat capacity of the PCM came into full action, requiring long periods of solar incidence with high outside temperatures. It was concluded that for systems containing PCM, which have high thermal inertia, it is important to ensure that the time intervals

between the cycles are sufficient so that the phase change can occur, for this case, intervals of 10 to 12 hours were not enough for the material to reach a stable state between time intervals.

Sanati and Utzinger (2013) examined the effect of an interior light shelf system on occupants use of venetian blinds and electric lighting. For the investigation an open plan studio space at the School of Architecture and Urban Planning, University of Wisconsin-Milwaukee was selected as the case study. The room is located on the 4th floor of the 4-story building and measures 12.2 by 24.4 m with windows facing south, west and north. The double-glazed clear glass windows measure 2.4 by 2.7 m and have a visible transmittance of 70%. There are 40 workstations with computers in this room. For this study, the room was divided into two sections along the south-north axis: The light shelf zone and the original window zone. For the light shelf zone case study a subdivided window is used. Occupants control the blinds on the lower half of the subdivided window and the upper half of the subdivided window has fixed light shelves. The results suggest that in identical environmental conditions, occupants whose workstations were located within the light shelf zone demonstrated a lower window occlusion (by about 20-30% less) than those who were located in the area with conventional windows. Additionally, occupants in the light shelf zone used 25% less electric lighting than those in regular window design area. The authors concluded that the window shading design affects occupant shade control behavior and their use of electric lighting.

Gijón-Rivera et al. (2013) carried out a theoretical study of a room on top of a building with three different glazed configurations in Mexico City with the purpose to show the advantages of using coupling models (CFD-BES) instead stand-alone solutions. For the study was considered a cavity which is formed by an adiabatic lower wall, two opaque conductive walls (left and upper), and a vertical semitransparent conductive wall with three different configurations: clear glass, clear glass with a solar control coating adhered inside (SnS-Cu_xS) and a reflective commercial glass (reflectasol). The CFD model was simulated as a 2D cavity considering conjugate heat transfer and solving the governing equations by the finite volume method. The BES model was carried out to assess the thermal performance of the room. Heat transfer coefficients obtained from CFD were supplied to the BES model to perform more accurate energy requirements in the room. Results showed that the reflective window configuration had the less necessity for using a coupled model and the glass-film window configuration presented the higher necessity for using a coupled model. Cooling energy loads in summer showed higher energy requirements of about 250 times more than for heating but during the winter, cooling loads were only 25 times more than heating loads. The reflective glass was the best configuration to achieve lower energy requirements (4%) inside room. It can be concluded that the thermal loads are higher in favour of the coupled solution in all cases. As a practical implication, a set of heat transfer coefficients correlations were presented for future implementations in buildings modelation programs.

Goia et al. (2014) Experimentally studied the thermal performance of a double glass window, to which a PCM was fitted between glasses. For this, a comparison was made of the performance of the proposed system against a conventional double glass window, which is filled only with air, both installed on the south face of a test chamber subjected to summer, autumn and winter weather conditions for sunny and rainy days. The composition of the windows consists of an 8 mm thick glass, a 15 mm cavity and the second 6mm glass, for the proposed system a wax paraffin with a melting temperature of 35 °C and melting enthalpy of 171 J/s (in a temperature range of 26 to 41 °C). The results showed that the Window with PCM reduced the total daily input energy in a range of 20 to 55% compared to the reference system, it was also observed that the higher the solar incidence the greater the benefit obtained from the proposed system. It was concluded that the PCM system provided significantly better performance during the summer. However, its behavior during the winter is more complex since its ability to control solar energy gains, as well as storing and redistributing it over time is affected by the incomplete use of the latent heat of fusion of the material due to the low temperature of outside air.

Shuhong et al. (2014) conducted a numerical-experimental study of the thermal performance of a double glass window filled with PCM (PCMW). They conducted a comparative analysis of the proposed system against a hollow double window system (HW) under winter and summer weather conditions in Nanjing China. For the numerical analysis a transient one-dimensional model was considered without taking into account convection. For the experimental part two thermally insulated rooms were used under the same conditions and within each room there is a test chamber to which their internal temperature was controlled by means of a cooling and heating system. The PCM used was inorganic (Glauber salt). The results showed that for the sunny summer days the temperature on the inner surface of PCMW is 10.2 °C lower than in HW, as well as a 39.5% reduction in the energy transmitted to the interior. On the rainy summer day, the peak temperature of the PCMW is 0.6 °C lower than in HW, and the energy transmitted inside increased by 43.5%. On the sunny winter day, the peak temperature for PCMW is about 9 °C lower than that of the HW and the energy transmitted to the interior decreased by 78.9%. During the rainy winter day, the peak temperature is 0.8 °C lower compared to HW and the energy transmitted outside the building increased by 5.8%. It was concluded that in the sunny days of summer the use of the proposed window system shows potential in terms of energy saving and improvement of thermal comfort inside the buildings, however, for the rainy days of summer, as well as sunny rainy days of winter the performance of the window with PCM is not satisfactory. In general, the annual energy consumption due to air conditioning can be reduced by 40.6% with the PCMW compared to the HW.

Hee et al. (2015) conducted a study of the impact on thermal comfort of windows with semi-transparent (glazed) elements for natural lighting in sustainable buildings. The study analyzed previous research regarding the different glazing techniques, revealing the impact that these techniques can cause visually and energetically in buildings in order to optimize them. Among the newest techniques are windows that

implement phase change materials (PCM), this technology is expected to provide more glazing options. However, the use of PCM in glass is still in the research and evaluation stage so these cannot be considered valid sustainable design options. It was concluded that the climate is important to select an optimal glazing of buildings

Aguilar et al. (2015) performed a numerical study of a double pane window (DPW) with three types of commercial glass available in México. The DPW consist of two vertical semitransparent walls separated by an air gap. The authors analyzed the effect of varying the gap width between glasses, the room temperature and the incident solar radiation. There were three configurations; case 1: clear glass-air gap-clear glass; case 2: clear glass-air gap-absorbent glass; and case 3: clear glass-air gap-reflective glass. Optical transmittance and specular reflectance of each case were measured under warm and cold climatic conditions. The results showed that, in order to increase or reduce the indoor heat gains, from b 0.02 m, the heat fluxes remain almost constant for both climate conditions. For cold climate, the case 1 reached the highest energy savings (~10.5 and ~28.5% higher than cases 2 and 3, respectively), however in warm climate it had the worst behavior (~105 and ~177% higher than cases 2 and 3, respectively). Finally, considering the case 1 as reference, the case 3 had the best combined energy saving ($17.64 $USD - kWh/year$) and case 2 presents a combined energy saving of $7.16 $USD - kWh/year$. Therefore, is highly recommended the use of reflective double pane window, like to case 3, in Mexican warm and cold climates.

Wang and Zhao (2015) [**37**] performed a numerical analysis of the thermal behavior of a window system with an inner curtain containing phase change material (PCM). For the study, a two-dimensional model of a window with a height of 1.5 m and a thickness of 5 mm was presented. The curtain thickness and the glass-curtain separation space as well as the melting temperature of the PCM were varied to assess its effects on the thermal performance of the system. The PCM used in the study was the RT28 paraffin and the n-eicosan with melting temperatures of 28 and 37 °C, respectively. Also, it was proposed to use two virtual PCMs with the same thermophysical properties as RT28 by changing the melting temperatures to 29 (PCM29) and 30 °C (PCM30). The results showed that with a glass-curtain spacing of 5 cm the PCM29 with a thickness of 5 mm has the best thermal performance by reducing the energy gain by 16.2% and can be further reduced by increasing the thickness of the PCM, while the RT28 and PCM30 reduced the energy gain by 13.5 and 13.9% respectively; on the other hand, the n-eicosano did not show any benefit due to its high melting temperature. It was concluded that the thicker the PCM more heat can store, but, the amount of the PCM that is effective is also reduced. Also, it was proposed to design a removable curtain system to be installed during sunny days and to be able to remove it when necessary.

Silva et. Al. (2015a) Experimentally analyzed the thermal performance of a window blind with PCM subjected to the Mediterranean summer climate. A test chamber was built with dimensions of length, width and height of 7, 2.35 and 2.58 m, respectively. The chamber is divided into 2 compartments both of equal dimensions with ceilings

and thermally insulated walls and both compartments have two windows on the south face. The blind is composed of hollow aluminum blades located behind a double glass window, which, its external and internal glass have a thickness of 5 *mm* and the space between them is 12 *mm*, with dimensions of 1.8 *m* long and 2.28 *m* high, with the difference that in one of the compartments of the test chamber the aluminum blades contain PCM filler. The phase change material used was the organic paraffin RT28HC. The results showed that the compartment with PCM reduced the maximum and minimum temperature values by 6 and 11% compared to the compartment without PCM. It was concluded that the use of PCM is an alternative for thermal conditioning inside buildings.

Silva et. Al. (2015b) [39] Experimentally analyzed the thermal performance of a window blind that contains PCM subjected to the winter climate of the Mediterranean. A test chamber was built with dimensions of length, width and height of 7, 2.35 and 2.58 *m*, respectively. The chamber is divided into 2 compartments of equal dimensions each, with thermally insulated ceilings and walls. Each compartment has two double glass windows with a thickness in the inner, outer glass and glass spacing of 6 x 6 x 12 *mm*, respectively and the blinds are installed behind the glazing system, the blinds are made up of an aluminum structure, the hollow aluminum blades and an insulating material, with the difference that in one of the compartments the hollow blades of the blinds contain PCM. The phase change material that used was the RT28HC. The results showed that the compartment with the blind that contains PCM reached a maximum temperature reduction of 90% during the period in which the PCM is storing energy. On the other hand, when the exterior and interior temperature fall below the solidification temperature of the PCM, it releases the stored energy and improves the internal temperature by 35%. It was concluded that the maximum peak of interior temperature of the compartment with the blind that contains PCM improved above 30%, but for the minimum temperature the improvements were practically null, this showed that other features such as the large size of the windows or Thermal bridge losses come into play, therefore, a study of the compatibility and optimization of these features is necessary.

Changyu et al. (2016) conducted a theoretical-experimental study of the thermal performance of two double glazed windows without ventilation with a PCM filling between them. The arrangement consists of 4 sheets of glass which are arranged like this: exterior glass, air, glass, PCM, glass, air, interior glass. A homogeneous one-dimensional mathematical model was presented in a transitory state with convective and radiative boundary conditions in the glasses in contact with the exterior and interior environment, and radiation and convection in the glasses in contact with the PCM were omitted. The experimental part was carried out in a test room with high, wide and long internal dimensions of 2.66, 1.46 and 1.65 *m* respectively, the glasses have a thickness of 4.5 *mm* and the air and PCM spaces measure 45 *mm*. The arrangement was compared with the RT27 paraffin phase change material against an arrangement without PCM. The results showed that at dawn the temperature inside the room with the arrangement containing the PCM was 7 °C lower than the room

with the arrangement without the PCM and at sunset it was 2 to 4 °C higher. It was concluded that the arrangement with PCM is effective by reducing energy gains inside the room.

Goia et al. (2015) [28] Analyzed the spectral and angular solar properties of a PCM-filled double glazing unit. The spectral and angular behaviour of different PCM glazing samples, characterised by different thicknesses of PCMs, were investigated by means of commercial spectrophotometer and by means of a dedicated optical test bed that includes a large integrating sphere with a diameter of 0.75 *m*. The results show that the light transmittance in the solid state is about 50% for the three samples, which though lower than an equivalent DGU without PCM in the gap, still provides adequate daylighting. Moreover, the PCM has high scattering/diffusing properties in the solid state, thus providing more uniform lighting distribution inside the building.

Shuhong et al. (2016) conducted an experimental study of the thermal performance of a triple-pane glass window, which was filled with a PCM. The study was carried out in two identical test rooms, the first with the proposed arrangement of triple-pane glass window with a PCM (TW + PCM) in the cavity closest to the outside and the second with the same arrangement with the difference of that this one is filled with air and not with a PCM (TW), it also has another double glass window arrangement filled with a PCM (DW + PCM). The three window arrangements are square with a length and width of 0.5 *m* and the three have a glass thickness of 5 *mm* and with air cavities of 14 *mm*. The PCM that was used was the paraffin MG29. The results showed that on a sunny summer day the temperature on the inner surface of the TW + PCM was 2.7 and 5.5 °C lower than DW + PCM and TW, respectively. Also, it was observed that for a rainy summer day the temperature on the inner surface of the TW + PCM was 0.74 and 1.65 °C lower than DW + PCM and TW, respectively, however, on the rainy day, the heat transferred to the interior of the test room was reduced by 14.7 and increased 4.5% compared to DW + PCM and TW, respectively. It was concluded that for sunny days the TW + PCM arrangement is effective by reducing overheating and the heat transferred to the interior by 16.6 and 28% compared to the DW + PCM and TW arrangements, respectively. For the rainy days it was concluded that the TW + PCM arrangement was not effective reducing the heat flow.

Gorgolis and Karamanis (2016) They carried out a literature review of the new technologies and materials for building glazed areas. Mention was made of the phase change materials (PCM) and how they have been used as insulating materials in buildings. These materials can be organic, inorganic or a combination of both (eutectic), for building glazing usually organic paraffins are used due to their transparency as liquids and their translucent property as solids. These materials have been incorporated with the intention of reducing near infrared radiation and allowing the passage to visible radiation, the main characteristic of the PCM is its high latent heat capacity allowing them to change phase when their melting temperature is exceeded by absorption of large amounts of energy, and releasing this energy during the solidification process, however, when the PCM changes from solid to liquid state

completely it shows an unwanted thermal performance and causes optical discomfort, so the amount of PCM needed so as its melting temperature are important characteristics to consider in choosing a suitable PCM according to the climatic conditions where they can be used.

Li et al. (2016) investigated the effect of thermophysical parameters of PCM on thermal performance of a PCM-filled double-glazing unit was investigated. The results show that the temperature time lag of the PCM-filled double-glazing unit increases and the temperature decrement factor decreases with the increase of density, thermal conductivity, specific heat capacity, latent heat, and melting temperature of PCM. Increasing density, latent heat, and melting temperature of PCM are effective to enhance the thermal performance of PCM-filled double-glazed units; however, enhancing thermal conductivity and specific heat capacity are ineffective when thermal conductivity is beyond 2.1 $W/(m\,K)$ and specific heat capacity is < 4460 $J/(kg\,K)$.

Alawadhi (2016) conducted an experimental study of the thermal and optical effects that occur when a window blind is partially open. The system consists of a glass window of 1.35 m high and 2.9 m long, with a thickness of 2 cm that is inside the room, the blind with a thickness of 0.75 cm is in contact with the outside environment and a 20 cm air space that separate it from the glass inside. For the study, the thermal performance of the window was analyzed with the partially open shutter with opening lengths of 10, 20 and 30 cm, comparing it to a window with the shutter fully closed. The results showed that when the blind is completely closed the window reaches a temperature of 26.7 °C, and when the blind has openings of 10, 20 and 30 cm the window reaches temperatures of 31.1, 33.8 and 36.5 °C, respectively. Therefore, a window with the blind partially open presents an increase in heat gain from 11.15 to 73.4% compared to a window with the shutter fully closed. It was concluded that when opening the 30 cm blind, adequate natural lighting is achieved, but the heat gains are very high, so it is more efficient to keep the blind completely closed and artificially illuminate the room.

Silva et al. (2016) conducted an experimental theoretical study of the thermal behavior of a window blind that contains a PCM. A test chamber was built with dimensions of length, width and height of 7, 2.35 and 2.58 m, respectively. The chamber is divided into 2 compartments both of equal dimensions with thermally insulated ceilings and walls and both compartments have two windows on the south face, the exterior and interior glass are 5 mm thick and the space between them is 12mm, with dimensions 1.8 m long and 2.28 m high. The blinds are installed behind the glaze, formed by an aluminum structure, and hollow aluminum blades with the difference that in one of the compartments the hollow blades of the blinds contain PCM. The PCM that was used was the paraffin RT28HC. For the theoretical part, two two-dimensional models were presented, one for the PCM compartment and the other for the reference compartment. The results showed that the maximum temperatures for the reference compartment and the one containing PCM the

differences between the numerical and experimental data were 2.97 and 3.54 °C, respectively. Also, it was observed that the average temperature inside the reference compartment varies from 15 to 46 °C and for the compartment with PCM it varies from 18 to 42 °C. It was concluded that the numerical results are in good agreement with the experimental results and that the compartment with PCM showed an improvement in the regulation of the indoor temperature of 8.7% for the heating period and 16.7% for the night period.

Aguilar et al. (2017) presented the theoretical thermal evaluation of a double glass window (DGW) coupled to a room, under climatic conditions of the Mexican Republic. The DGW consists of two glass sheets separated by a 12mm thick air cavity. They also analyzed the effect of varying the ambient temperature and incident solar radiation. The authors performed numerical modelations for four DPW configurations, the reference case, Case 1 (clear glass), Case2 (clear glass and absorbent glass), Case 3 (clear glass and low emissivity glass) and Case 4 (clear glass and reflective glass). The results showed that Case 4 reduces heat flows inwards by 73% compared to Case 1, while Cases 2 and 3 showed a similar behavior since they reduced heat flows to the interior by 33.5%. Based on the results, they concluded that Case 4 is the best option for energy savings in hot climates in the Mexican Republic because savings of up to 20.29 USD per KWh can be perceived with respect to Case 1. Additionally, the period of return on investment is 3.7 years.

Xamán et al. (2017) performed the numerical evaluation of the thermal performance of a double glass window (DGW) with / without solar control film coupled to a room (R). The numerical evaluation of the DGW was carried out under the climatic conditions of the Mexican Republic. The right wall of the room is partially adiabatic and is where the DGW is placed. The DGW consists of a sheet of glass (g1) in contact with the air inside the room, an air cavity and another sheet of glass (g2) in contact with the outside ambient air. The solar control film (SCF) is adhered to g1 for cold weather conditions and in warm weather conditions the SCF is adhered to g2. For the evaluation of R-DGW a numerical code was developed using the finite volume method. The authors considered three case studies: Case 1 which is the case of R-DGW without SCF (reference case) and Case 2 and 3 which are the cases for R-DPW with SCF under hot and cold weather conditions, respectively. The results showed that with the Case 2, a reduction of 62% was obtained compared to Case 1. For Case 3 the average temperature inside the room is similar to Case 1. Based on the results, the authors concluded that under warm weather conditions the use of Case 2 is recommended.

Omrani et al. (2017) presented an investigation review of the advantages and limitations of the methods currently being used to quantify natural ventilation performance focusing only on literature involving multi-storey buildings examining natural ventilation performance in cooling climates. For the investigation the authors divided the methods identified in the literature in three main categories: 1- Analytical and empirical methods,2- Computational modelation, and 3- Experimental methods.

For the computational modelation category the authors reported that A number of modelation approaches are identified within literature including the combination of CFD models with Building Energy Simulation (BES) models. The results shown that the amount and variation of detailed information that can be extracted from CFD are far greater than other methods but computational costs can be an issue depending on how complex is the case, on the other hand the required time for BES modelations is less than the required time for CFD modelations for the same building also provide information on a building's energy consumption in addition to thermal performance and can, therefore, be used for thermal performance studies. However, cannot provide detailed information such as airflow pattern inside. The authors concluded that it is not common to use costly experiments in natural ventilation design of regular multi-storey buildings so the combination of the accuracy of CFD with BES models is an viable alternative for specifics cases of study.

Li et al. (2018) proposed a configuration of triple-pane window (TW+ PCM),where the outer cavity is filled with PCM. The experiment was conducted in the summer days. Experimental systems of two reference windows (DW+ PCM and triple-pane window (TW)) are also set up successively. The results show that compared with DW+ PCM and TW, the peak temperature on the interior surface of TW+ PCM reduces by 2.7 °C and 5.5 °C respectively, which means the overheating risk is avoided effectively, and heat entered the building through the TW+ PCM reduces by 16.6% and 28% respectively in the sunny summer day. In the rainy summer day, the TW+ PCM shows advantageous performance on reducing the temperature fluctuation of the interior surface and the heat entered the building.

Li et al. (2018) developed a model to evaluate the thermal and optical performances of window units filled with nanoparticle enhanced PCM (NePCM). The effect of different types of nanoparticles, volume fractions of nanoparticles and sizes of nanoparticles on the thermal and optical performances of windows such as temperature, heat flux, solar transmittance, absorptance and reflectance were numerically investigated and compared with the referent case (i.e. pure PCM). The results showed that the optical and thermal performances of window units filled with nanoparticle dispersed paraffin wax are improved compared to that of with pure paraffin. However, the improvement is nearly the same regardless of nanoparticle type. The effect of volume fraction and size of nanoparticle is significant during the sunset and sunrise periods. Considering both thermal and optical performances of window units, it is recommended to disperse CuO nanoparticles with the volume fraction of below 1% and nanoparticle size of below 15 *nm* in PCM.

Liu et al. (2018) experimentally investigated the optical and thermal performances of a PCM-glazed unit and compared with that filled with air, and the influences of solar irradiance, melting temperature and PCM layer thickness on three parameters were analyzed including the transmittance, the temperature difference between upper and

bottom surfaces, and the interior surface temperature of the glazed unit. The results show that the thermal performance of glazed unit filled with PCM is improved compared with that of air, and transmittance of glazed unit is 50% when the PCM is liquid. Solar irradiance and PCM layer thickness both have effects on the optical and thermal performance of glazed unit, but the effect of melting temperature on thermal performance can be neglected. Increasing the PCM thickness can effectively decrease the heat loss of glazed unit filled with PCM, but the PCM thickness in the glazed unit is not beyond 16 *mm* considering the optical performance of glazed unit.

Liu et al. (2018) developed a numerical model to provide a tool to determine thermal and optical performance of a multi-layer glazed roof filled with phase change material for developing engineering analyses. The model was validated by the experimental results measured in a multi-layer glazed roof test facility. The influences of air convection and PCM design parameters on thermal and optical performance of the multi-layer glazed roof filled with PCM were also investigated by the model. The results show that a good agreement was obtained between experimental data and simulations. The influence of air convection on the thermal and optical performance of multi-layer glazed roof is weak for different PCM melting temperatures and thicknesses, except for its effect on the interior temperature. Considering that the maximum and minimum interior temperatures are key parameters to analyze the thermal performance of multi-layer glazed roof, the air convection process should be considered. The influences of PCM thickness and melting temperature on optical performance are big. The PCM thickness has also serious influences on the thermal performance, which include interior temperature, temperature time lag, temperature difference of the interior surface and the upper surface of air layer, and total transmitted energy. With the PCM thickness increasing, the variation of temperature difference of the interior surface and the upper surface of air layer in one day experiences multiple peaks and troughs. Considering influence of PCM design parameters on both thermal and optical performance of glazed roof, thickness of 12–20 *mm* and melting temperature of 16–18 °C was recommended.

Ilaria Vigna et al. (2018) made a literature review, classification and detailed analysis focused on experimental works from 1998 to 2018, to identify the main possible integrations of PCMs in transparent/translucent building envelope components in order to draw a global picture of the potential and limitations of these technologies. The envelopes with PCMs have been classified from the simplest "zero" technology, which integrates the PCM in a double glass unit (DGU), to more number of glass cavities (triple glazed unit TGU), different positions of the PCM layer (internal/external shutter), and in combination with other materials (TIM, aerogel, prismatic solar reflector, PCM curtain controlled by an electric pump). The results of the analysis show that the main strengths of integrating PCMs in transparent building envelopes are related to an enhancement, in terms of performance, of the technology from the energy, thermal, and comfort points of view. Benefits, which show an

increase in the thermal mass and the heat storage capacity of the building envelope, have also been revealed. However, different weaknesses still need to be overcome, at both the technological and chemical level. In addition, the energy performance should also be evaluated accurately during winter. Another critical aspect pertains to the visual and thermal behavior of the dynamic envelope during the transition phase of the material, when the PCM is not completed liquid. The authors concluded that some research on the subject still needs to be carried out in order to achieve cost-effective solutions and a higher technology readiness level. The review has also highlighted the need to develop and/or integrate numerical models in building performance modelation tools, as well as performance metrics, and standardized test procedures.

Duraković and Mešetović (2019) tested experimentally conventional, water and PCM glazing systems simultaneously in natural environment using test chambers. Experimental setup uses a three-chamber box (Chamber #1, Chamber #2 and Chamber #3) to resemble living room state with windows facing south. The box is subdivided into three smaller chambers in order to test three samples at the same time. Furthermore, the chamber is made out of 5 *cm* thick Styrofoam having dimensions width, length, and height of 150x50x50 *cm* respectively, while small chambers share same material property but, each has a size of width, length and height of 50x50x50 *cm* respectively. The glazing samples used had dimensions of width, length and height of 30x41 *cm*, while the glass pane thickness was 4 *mm* each with the cavity space between panes of 12 *mm*. Time lag, temperature damping and average temperature for each glazing system were comparatively analyzed. In the results it was observed that compared to a conventional glazing system, water and PCM filled glazing systems are significantly different. Water filled glazing system has increased specific heat capacity of water by resulting in one hour time lag. Statistically, it is observed that temperature damping is significant but average temperature is significantly higher. PCM filled glazing system has statistically significant temperature dumping over three hour period during melting process and four hour period during solidification process. Total temperature dumping period was about seven hours within temperature range of 24–28 °C. Therefore, it was found that water glazing system has most promising temperature damping properties, but significantly unfavorable average temperature, while PCM glazing system has significantly promising average temperature and temperature dumping properties.

Dong Li et al. (2019) made a literature review on experimental and modelation researches about the optical and thermal performance of glazing units containing phase change materials (PCM). For the analysis it was discussed the employed research methods, mathematical models and important conclusions drawn with the purpose to identify the application of PCMs in various types of glazing units, such as conventional vertical windows, double glazing facades and glazing roofs. Finally, the challenges and future works of glazing units containing PCM addressed were: a) The solar heat gain will be sharply reduced when PCM is applied in building glazing systems in cold climates, because PCM such as paraffin remains in the solid state due to the lower temperature of ambient environment, so its visual transmittance

decreases from 90% in liquid state to 40% in solid state, and the amount of solar energy entering indoor decreases. To solve this problem can be considered to add nano-sized reinforcement medium to strengthen the thermal conductivity of paraffin and accelerate phase transition process, However, few studies have explored the impact of nanoparticle size, volume concentration and nanoparticle type on the photothermal characteristics of paraffin under scattering effect. b) Limited works comprehensively investigate the spectral characteristics of thermal radiation properties of material and the spectral distribution of solar energy in detail, especially in numerical modeling, since it is the basement for accurate calculation of the optical and thermal transfer model of glazing unit filled with PCM. c) Most of the researchers have regarded paraffin as a homogeneous material without considering its porous structure which further affects the optical and thermal transfer of glazing unit filled with PCM.

Dong Li et al. (2019) studied the implementation of a Phase change material (PCM) blind system for double skin facade. A novel laminated composite PCM blind system with high thermal energy storage capacity was developed and evaluated in a typical DSF building. The results showed that the integrated PCM blind system was able to keep the average air temperature in the DSF below 35 °C during the monitored period in summer and showed no significant increase as compared with the ambient temperature. The surface temperature of the inner skin of the DSF was also reduced up to about 2.9 °C as compared with the external skin surface temperature thus reducing heat transfer into the building. By using validated numerical models, the PCM blind was found to perform thermally better than a conventional aluminum blind. Finally, design and operational parameters of the PCM blind including the blind tilt angle and its position were optimized. Further comparative studies against other integrated DSF systems are however being encouraged to establish the full effectiveness of the developed PCM blind system.

Dong Li et al. (2020) carried out the numerical investigation of the thermal performance of glass window composed of glass, silica aerogel and phase change material (PCM). To assess the glass window thermal behavior, a numerical model describing the heat transfer mechanism occurring in the PCM layer in combination with the other transparent wall layers was established and verified. Also, the influence of factors such as thermal conductivity, density, specific heat and thickness of silica aerogel on the thermal performance of the glass window was analyzed. The results show that the most significant controlling parameters are the thermal conductivity and thickness of silica aerogel, while the impact of density and specific heat of silica aerogel on the thermal performance of glazing unit is marginal. A proper thickness of aerogel that maximizes the exploitation of latent heat of PCM should be identified, which is between 20 and 30 *mm* for the studied climatic conditions. It was concluded that integrating silica aerogel insulation into PCM-glass window system is an effective technology in cold regions, solving the problem that PCM cannot effectively exploit latent heat, while retaining the advantages of PCM in winter.

Dong Li et al. (2020) made a review of the experimental and simulation researches on the optical and thermal performance of glazing units containing PCM and discusses the employed methods, mathematical models and important conclusions drawn. Finally, the challenges and future works of glazing units containing PCM are addressed. The authors concluded that further developments and future works for the optical and thermal performance of glazing units containing PCM in buildings can focus on the possible remedies for: 1. The reduction of solar heat gain when the PCM is applied in buildings glazing systems in cold climates, 2. The characterization of thermal radiation properties of materials and spectral distribution of solar energy, also the non-gray model of optical and thermal transfer should be improved since it is the basement for accurate calculation of the optical and thermal transfer model of glazing unit filled with PCM, 3. The scattering effect caused by the presence of porous structure of paraffin in the solid state and the process of phase transition which further affects the optical and thermal transfer of glazing unit filled with PCM.

Zhang.et al. (2021) numerically investigated the energy performance of ten different glazing configurations in the severe cold climate of China. Furthermore, the thermal behavior of the glass windows filled with silica aerogel or PCM was analyzed and compared with traditional glass windows filled with air. In addition, to ensure the efficient functioning and minimize the heat loss through the PCM-filled window in the severe cold climate, three configurations of the triple-glazing selected for optimization and filled with silica aerogel and PCM were evaluated based on optical properties of the glass, thickness of the silica aerogel layer and melting point of the PCM. The transient solution for the simplified models of glazing units also included the radiative heat transfer. The results show that adding PCM into the glass window results in degradation of thermal performance of glass windows in winter. However, as the silica aerogel is used together with a PCM having a suitable melting temperature in triple pane windows, the thermal comfort can be improved. On the other hand, setting appropriate optical parameters of the glass for the radiation above 2.5 mm significantly enhances the energy efficiency of the glass window coupled with the silica aerogel and PCM.

Yang R. et al. (2021) numerically investigated the energy performance of ten different glazing configurations in the severe cold climate of China. Furthermore, the thermal behavior of the glass windows filled with silica aerogel or PCM was analyzed and compared with traditional glass windows filled with air. For the study, three configurations of the triple-glazing selected for optimization and filled with silica aerogel and PCM were evaluated based on optical properties of the glass, thickness of the silica aerogel layer and melting point of the PCM. The transient solution for the simplified models of glazing units also included the radiative heat transfer. The results show that adding PCM into the glass window results in degradation of thermal performance of glass windows in winter. However, as the silica aerogel is used together with a PCM having a suitable melting temperature in triple pane windows, the thermal comfort can be improved. On the other hand, setting appropriate optical

parameters of the glass for the radiation above 2.5 μm significantly enhances the energy efficiency of the glass window coupled with the silica aerogel and PCM.

Jiang et al. (2021) investigated the energy consumption of various windows in the rural residence of severe cold climate on the basis of the thermal performance analysis of glass and frames. Based on Energy Plus multi-objective gradual exploration, the energy consumption of the test room with various windows during heating period was simulated, and the windows configuration was optimized considering daylighting performance. There are three steps to explore the energy consumption of four kinds of glass, four frame materials and three kinds of frame configuration, and nine groups of WWR. The results show that the triple pane glass PCM frame of one mullion-one transom type is the best comprehensive scheme. In order to meet the requirements of lighting performance, and under the constraints of building height and structure, the design with large size of south side window and small size of north side window has obvious energy-saving effect. It saves about 20% energy than the original one. The conclusions are proposed for the window design and application of PCM frame in severe cold areas.

Background of studies concerning windows carried out in CENIDET

Cortina. (2000) conducted a theoretical-experimental study of the thermal performance of double-glazed windows (duovent). Three window arrangements were studied, all arrangements consisted of two glass panes 6 *mm* thick each and a 12 *mm* air gap. In one arrangement only clear glass was considered, in the second one a solar control film (filtrasol) was placed on the glass that is in contact with the outside and the third arrangement had reflectaplata as a control film. For the theoretical part, a one-dimensional model of heat transfer in the transient state was presented considering convective and radiative boundary conditions. The experimental part consisted of mounting the different window arrangements to an experimental device that measures the thermal efficiency of the glass and comparing the results with the theoretical model. In the results it was observed that the arrangement with reflectaplata was the best reducing the energy gain inside the compartment, allowing only 17% of the incident energy to pass compared to a single clear glass of 3 *mm*, it was also found that the results of the Theoretical part have a percentage of error in a range of 1.1 to 4.7% for different arrangements. It was concluded that the theoretical model provided results satisfactorily and that the glasses evaluated are an alternative for the control of solar energy inside the rooms.

Noh-Pat. et al (2011) analyzed the thermal performance of a double ventilated glass window with and without the solar control film SnS-Cu_xS under hot weather conditions. A two-dimensional model was considered for both cases of the window with and without control film, the solar control film is considered in contact with the air in the cavity and adhered to the exterior glass. The dimensions of the window are 1 *m* high for both glasses with a temperature inside the room of 24 °C and temperature of the outside environment of 32 °C. The effect of varying the separation between

glasses [$1 \leq b\ (cm)\ \leq 10$] was analyzed. The results showed that the lowest heat flow was achieved with a 6 cm glass gap with and without the control film and that from the radiation incident with the solar control film the energy gain is 17% and without the solar control film the gain is 72%. It was concluded that the window with the solar control film was effective reducing energy gains by 55% compared to the window without the solar control film, it was also concluded that the optimal distance between glasses is 6 cm for the solar control film used in the analysis.

Pérez. (2012-2014) performed a numerical analysis of the conjugate heat transfer in double-glazed windows with a solar control film for warm and cold weather. A two-dimensional model was presented in permanent state with transitory formulation and in laminar regime. For the analysis, 3 configurations were considered, the first consists of the double glass window with solar control film (C1), the second is the double glass window without the control film (C2) and the third is the single glass window (C3), the glasses are 80cm high and 6 mm thick, the separation between glasses was varied from1 to 10 cm, the indoor temperature was also varied from 15 to 30 °C for warm weather and 20 to 35 °C for cold weather with constant outside temperatures of 35 and 15 °C respectively. The results showed that for warm weather the configuration that transmits the least amount of heat is C1 and the one that transmits the highest is C3, the average total flow values being more than triple than for C1, and for cold weather the configuration that transmits more total energy inside is C2. It was concluded that the optimal setting for warm weather is C1 and for cold weather it is C2, in addition the optimum opening for the air cavity between glass is 6cm.

Jiménez. (2015) Performed a pseudo-transitory numerical study of the application of the additive corrections multi-mesh method (ACM) for the problem of a double glass window with conjugate heat transfer in steady state. For this, computational runs were made every 5 seconds, so it was necessary to perform 14400 runs to obtain the results of the pseudo-transitory from 8:00 am to 6:00 pm. Numerical meshes of 61x41, 71x51, 81x61, 91x71, 101x81 and 111x91 were established. The results showed that the mesh that provides acceptable results is 81x61, also that the ACM coupling reduced the computation time by 47%. It was concluded that a window with the solar control film reduces by 57% the heat flow to the interior with respect to a window without the control film and that the ACM technique determines the error components efficiently guaranteeing the convergence of the numerical solution and reducing the computation time.

Olazo. (2015-2016) conducted a numerical study of the conjugate heat transfer in steady state of a room with a double glass window. She proposed a two-dimensional model for the window taking it as an elongated cavity and coupled it as a boundary condition to the room model which is also two-dimensional and considered it as a square cavity with turbulent flow. The modeling was done for a full day (24hrs) of warm and cold weather. For the warm weather, a comparison was made between a room with double glazed windows (C1) and a room with a double glass window with a solar control film adhered to the glass in contact with the outside environment (C2),

for the Cold weather was compared C1 with a configuration in which the room window has a solar control film on the glass in contact with the indoor environment (C3). The solar control film that was used was SnS-Cu_xS _xS with a thickness of 6 μm. The height of the room and the window is 3 and 0.8 m respectively and the thickness of the glass is 6 mm and the distance between them was 6cm. In the results it was observed that for warm weather throughout the day the temperatures in the room for C1 were 36 °C and for C2 they were 32 °C, while for cold weather the temperatures for C1 only differ by 1 °C with respect to C3. It was concluded that for warm weather C2 reduces the incoming heat by 62% with respect to C1 and for cold weather it is concluded that the thermal performance of C1 and C3 is similar.

Gonzáles. (2017) conducted a numerical study of the conjugated heat transfer in a double glass window system using glazing elements available in the Mexican market. A two-dimensional model was presented in a permanent state and in a laminar regime in which the window is 80 cm high and the glasses are 6 mm thick and 2 cm apart between them. A single clear glass was taken as a reference case (C1) and different cases were compared such as a double glass window with clear glasses (C2), a double glass window with a reflective glass (C3) and a double glass window with a low emissivity glass (low-ε) (C4). The results showed that with respect to C1 that generates an annual cost for electric energy consumption of $ 783.11, C2 reduces the annual cost for energy consumption by 12%, C3 reduces it by 72.6% generating an annual cost per consumption of $ 214.95 and C4 reduces it by 28.6%. It was concluded that C3 showed the best thermal performance in warm weather conditions, generating greater savings by recovering the investment through reflective windows over a period of 3.5 years.

B. Energy balance development for the envelope elements

In this appendix the development of the energy balances performed on the envelope elements is presented, and the final equation in lumped coefficient notation, for each envelope element is also shown.

B.1.- Energy balance on the north wall element

The west wall T_{W_3} element is interacting with the T_{ext}, T_{sky}, G and the T_{room} so considering an energy flux with a right to left direction the balance takes the form shown in Eq. (B.1) below:

$$q_{in} = \frac{T_{sky} - T_{W_3}}{\frac{1}{h_{sky-W_3}^{rad}}} + \frac{T_{ext} - T_{W_3}}{\frac{1}{h_{ext-W_3}} + \frac{H_{x,W_3}}{2\lambda_{W_3}}} + \alpha_{W_3} G$$

$$q_{out} = \frac{T_{W_3} - T_{room}}{\frac{H_{x,W_3}}{2\lambda_{W_3}} + \frac{1}{h_{W_3-room}}} + q_{W_3}^{rad} \tag{B.1}$$

considering that $q_{in} - q_{out} = q_{stored}$ then:

$$\left(\frac{T_{sky} - T_{W_3}}{\frac{1}{h_{sky-W_3}^{rad}}} + \frac{T_{ext} - T_{W_3}}{\frac{1}{h_{ext-W_3}} + \frac{H_{x,W_3}}{2\lambda_{W_3}}} + \alpha_{W_3} G \right) - \left(\frac{T_{W_3} - T_{room}}{\frac{H_{x,W_3}}{2\lambda_{W_3}} + \frac{1}{h_{W_3-room}}} + q_{W_3}^{rad} \right)$$

$$= a_p^0 (T_{W_3} - T_{W_3}^0)$$

$$\left(\frac{T_{sky} - T_{W_3}}{b_0} + \frac{T_{ext} - T_{W_3}}{b_1} + \alpha_{W_3} G \right) - \left(\frac{T_{W_3} - T_{room}}{b_2} + q_{W_3}^{rad} \right) = a_p^0 (T_{W_3} - T_{W_3}^0) \tag{B.2}$$

$$\left(\frac{b_1 T_{sky} - b_1 T_{W_3} + b_0 T_{ext} - b_0 T_{W_3}}{b_0 b_1} + b_0 b_1 \alpha_{W_3} G \right) - \left(\frac{T_{W_3} - T_{room}}{b_2} + q_{W_3}^{rad} \right)$$

$$= a_p^0 (T_{W_3} - T_{W_3}^0)$$

$$b_1 b_2 T_{sky} - b_1 b_2 T_{W_3} + b_0 b_2 T_{ext} - b_0 b_2 T_{W_3} + b_0 b_1 b_2 \alpha_{W_3} G - b_0 b_1 T_{W_3} \quad \text{(B.3)}$$
$$- b_0 b_1 T_{room} + b_0 b_1 b_2 q_{W_3}^{rad} = b_0 b_1 b_2 a_p^0 (T_{W_3} - T_{W_3}^0)$$

Developing the equation, the mathematical model for the window element is as shown in Eq (B.4):

$$\left(b_1 b_2 + b_0 b_2 + b_0 b_1 + b_0 b_1 b_2 a_p^0\right) T_{W_3} - b_0 b_1 T_{room}$$
$$= b_1 b_2 T_{sky} + b_0 b_2 T_{ext} + b_0 b_1 b_2 \alpha_{W_3} G + b_0 b_1 b_2 q_{W_3}^{rad} \quad \text{(B.4)}$$
$$+ b_0 b_1 b_2 a_p^0 T_{W_3}^0$$

B.2.- Energy balance on the glass element (south face of the room)

The glass element is interacting with the T_{ext}, T_{sky}, G and the T_{room} so considering an energy flux with a right to left direction the balance takes the form shown in Eq. (B.5) below:

$$q_{in} = \frac{T_{room} - T_g}{\frac{1}{h_{room-g}} + \frac{H_{x,g}}{2\lambda_g}} + q_g^{rad}$$
$$q_{out} = \frac{T_g - T_{ext}}{\frac{H_{x,g}}{2\lambda_g} + \frac{1}{h_{ext-g}}} + \frac{T_g - T_{sky}}{\frac{1}{h_{sky-g}^{rad}}} + \alpha_g G \quad \text{(B.5)}$$

considering that $q_{in} - q_{out} = q_{stored}$ then:

$$\left(\frac{T_{room} - T_g}{\frac{1}{h_{room-g}} + \frac{H_{x,g}}{2\lambda_g}} + q_g^{rad}\right) - \left(\frac{T_g - T_{ext}}{\frac{H_{x,g}}{2\lambda_g} + \frac{1}{h_{ext-g}}} + \frac{T_g - T_{sky}}{\frac{1}{h_{sky-g}^{rad}}} + \alpha_g G\right)$$
$$= a_p^0 (T_g - T_g^0) \quad \text{(B.6)}$$
$$\left(\frac{T_{room} - T_g}{d_1} + q_g^{rad}\right) - \left(\frac{T_g - T_{ext}}{d_2} + \frac{T_g - T_{sky}}{d_0} + \alpha_g G\right) = a_p^0 (T_g - T_g^0)$$

$$\left(\frac{T_{room}-T_g}{d_1}+q_g^{rad}\right)-\left(\frac{d_0T_g-d_0T_{ext}+d_2T_g-d_2T_{sky}}{d_2d_0}+d_2d_0\alpha_gG\right)$$

$$=a_p^0(T_g-T_g^0)$$

$$d_2d_0T_{room}-d_2d_0T_g+d_2d_0q_g^{rad}-d_1d_0T_g-d_1d_0T_{ext}+d_1d_2T_g-d_1d_2T_{sky} \quad \text{(B.7)}$$

$$+d_1d_2d_0\alpha_gG=d_1d_2d_0a_p^0(T_g-T_g^0)$$

Developing the equation, the mathematical model for the window element is as shown in Eq (B.8):

$$-d_2d_0T_{room}+\left(d_2d_0+d_1d_0+d_1d_2+d_1d_2d_0a_p^0\right)T_g$$

$$=d_1d_0T_{ext}+d_1d_2T_{sky}+d_1d_2d_0\alpha_{roof}G+d_2d_0q_g^{rad} \quad \text{(B.8)}$$

$$+d_1d_2d_0a_p^0T_g^0$$

B.3.-Energy balance on the floor element

The floor element is interacting with the T_{room} and the T_{earth} so considering an energy flux with a downwards direction the balance takes the form shown in Eq. (B.9) below:

$$q_{in}=\frac{T_{room}-T_{floor}}{\frac{1}{h_{room-floor}}+\frac{H_{x,floor}}{2\lambda_{floor}}}+q_{floor}^{rad}$$

$$q_{out}=\frac{T_g-T_{earth}}{\frac{H_{x,floor}}{2\lambda_{floor}}} \quad \text{(B.9)}$$

considering that $q_{in}-q_{out}=q_{stored}$ then:

$$\left(\frac{T_{room}-T_{floor}}{\frac{1}{h_{room-floor}}+\frac{H_{x,floor}}{2\lambda_{floor}}}+q_{floor}^{rad}\right)-\left(\frac{T_{floor}-T_{earth}}{\frac{H_{x,floor}}{2\lambda_{floor}}}\right)=a_p^0(T_g-T_g^0) \quad \text{(B.10)}$$

$$\frac{T_{room} - T_{floor}}{e_1} - \frac{T_{floor} - T_{earth}}{e_2} = a_p^0 (T_{floor} - T_{floor}^0)$$

$$e_2 T_{room} - e_2 T_{floor} + e_1 e_2 q_{floor}^{rad} - e_1 T_{floor} - e_1 T_{earth} \tag{B.11}$$

$$= e_1 e_2 a_p^0 (T_{floor} - T_{floor}^0)$$

Developing the equation, the mathematical model for the floor element is as shown in Eq (B.12):

$$-e_2 T_{room} + \left(e_1 + e_2 + e_1 e_2 a_p^0\right) T_{floor} = e_1 T_{earth} + e_1 e_2 q_{floor}^{rad} + e_1 e_2 a_p^0 T_{floor}^0 \tag{B.12}$$

B.4.- Energy balance on the east wall element

The west wall T_{W_4} element is interacting with the T_{ext}, T_{sky}, G and the T_{room} so considering an energy flux with a right to left direction the balance takes the form shown in Eq. (B.13) below:

$$q_{in} = \frac{T_{sky} - T_{W_4}}{\frac{1}{h_{sky-W_4}^{rad}}} + \frac{T_{ext} - T_{W_4}}{\frac{1}{h_{ext-W_4}} + \frac{H_{x,W_4}}{2\lambda_{W_4}}} + \alpha_{W_4} G$$

$$q_{out} = \frac{T_{W_4} - T_{room}}{\frac{H_{x,W_4}}{2\lambda_{W_4}} + \frac{1}{h_{W_4-room}}} \tag{B.13}$$

considering that $q_{in} - q_{out} = q_{stored}$ then:

$$\left(\frac{T_{sky} - T_{W_4}}{\frac{1}{h_{sky-W_4}^{rad}}} + \frac{T_{ext} - T_{W_4}}{\frac{1}{h_{ext-W_4}} + \frac{H_{x,W_4}}{2\lambda_{W_4}}} + \alpha_{W_4} G \right) - \left(\frac{T_{W_4} - T_{room}}{\frac{H_{x,W_4}}{2\lambda_{W_4}} + \frac{1}{h_{W_4-room}}} \right) \tag{B.14}$$

$$= a_p^0 (T_{W_4} - T_{W_4}^0)$$

$$\left(\frac{T_{sky} - T_{W_4}}{f_0} + \frac{T_{ext} - T_{W_4}}{f_1} + \alpha_{W_4} G \right) - \left(\frac{T_{W_4} - T_{room}}{f_2} \right) = a_p^0 (T_{W_4} - T_{W_4}^0)$$

$$\left(\frac{b_1 T_{sky} - b_1 T_{W_4} + b_0 T_{ext} - b_0 T_{W_4}}{f_0 f_1} + f_0 f_1 \alpha_{W_4} G\right) - \left(\frac{T_{W_3} - T_{room}}{f_2} + q_{W_4}^{rad}\right)$$

$$= a_p^0 (T_{W_4} - T_{W_4}^0)$$

$$f_1 b_2 f_{sky} - f_1 f_2 T_{W_4} + f_0 f_2 T_{ext} - f_0 f_2 T_{W_4} + f_0 f_1 f_2 \alpha_{W_4} G - f_0 f_1 T_{W_4} - f_0 f_1 T_{room} \quad \text{(B.15)}$$

$$+ f_0 f_1 f_2 q_{W_4}^{rad} = f_0 f_1 f_2 a_p^0 (T_{W_4} - T_{W_4}^0)$$

Developing the equation, the mathematical model for the window element is as shown in Eq (B.16):

$$\begin{aligned} &\left(f_1 f_2 + f_0 f_2 + f_0 f_1 + f_0 f_1 f_2 a_p^0\right) T_{W_4} - f_0 f_1 T_{room} \\ &= f_1 f_2 T_{sky} + f_0 f_2 T_{ext} + f_0 f_1 f_2 \alpha_{W_4} G + f_0 f_1 f_2 a_p^0 T_{W_4}^0 \end{aligned} \quad \text{(B.16)}$$

B.5.- Energy balance on the west wall element

The glass element is interacting with the T_{ext}, T_{sky}, G and the T_{room} so considering an energy flux with a right to left direction the balance takes the form shown in Eq. (B.17) below:

$$\begin{aligned} q_{in} &= \frac{T_{room} - T_{W_2}}{\frac{1}{h_{room-W_2}} + \frac{H_{x,W_2}}{2\lambda_{W_2}}} \\ q_{out} &= \frac{T_{W_2} - T_{ext}}{\frac{H_{x,W_2}}{2\lambda_{W_2}} + \frac{1}{h_{ext-W_2}}} + \frac{T_{W_2} - T_{sky}}{\frac{1}{h_{sky-W_2}^{rad}}} + \alpha_{W_2} G \end{aligned} \quad \text{(B.17)}$$

considering that $q_{in} - q_{out} = q_{stored}$ then:

$$\left(\frac{T_{room} - T_{W_2}}{\frac{1}{h_{room-W_2}} + \frac{H_{x,W_2}}{2\lambda_{W_2}}}\right) - \left(\frac{T_{W_2} - T_{ext}}{\frac{H_{x,W_2}}{2\lambda_{W_2}} + \frac{1}{h_{ext-W_2}}} + \frac{T_{W_2} - T_{sky}}{\frac{1}{h_{sky-W_2}^{rad}}} + \alpha_{W_2} G\right) \quad \text{(B.18)}$$

$$= a_p^0 (T_{W_2} - T_{W_2}^0)$$

$$\left(\frac{T_{room}-T_{W_2}}{g_1}\right)-\left(\frac{T_{W_2}-T_{ext}}{g_2}+\frac{T_{W_2}-T_{sky}}{g_0}+\alpha_{W_2}G\right)=a_p^0(T_{W_2}-T_{W_2}^0)$$

$$\left(\frac{T_{room}-T_{W_2}}{g_1}\right)-\left(\frac{d_0T_{W_2}-d_0T_{ext}+d_2T_{W_2}-d_2T_{sky}}{g_2g_0}+g_2g_0\alpha_{W_2}G\right)$$

$$=a_p^0(T_{W_2}-T_{W_2}^0)$$

$$g_2g_0T_{room}-g_2g_0T_{W_2}+g_2g_0q_{W_2}^{rad}-g_1g_0T_{W_2}-g_1g_0T_{ext}+g_1g_2T_{W_2} \quad \text{(B.19)}$$

$$-g_1g_2T_{sky}+g_1g_2g_0\alpha_{W_2}G=g_1g_2g_0a_p^0(T_{W_2}-T_{W_2}^0)$$

Developing the equation, the mathematical model for the window element is as shown in Eq (B.20):

$$-g_2g_0T_{room}+\left(g_2g_0+g_1g_0+g_1g_2+g_1g_2g_0a_p^0\right)T_{W_2}$$

$$=g_1g_0T_{ext}+g_1g_2T_{sky}+g_1g_2g_0\alpha_{roof}G+g_1g_2g_0a_p^0T_{W_2}^0 \quad \text{(B.20)}$$

C. Figures of solar radiation decomposition

a)

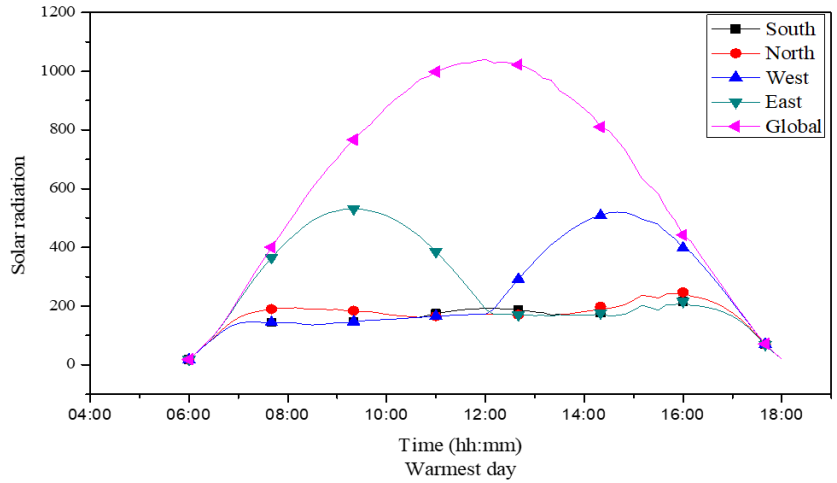

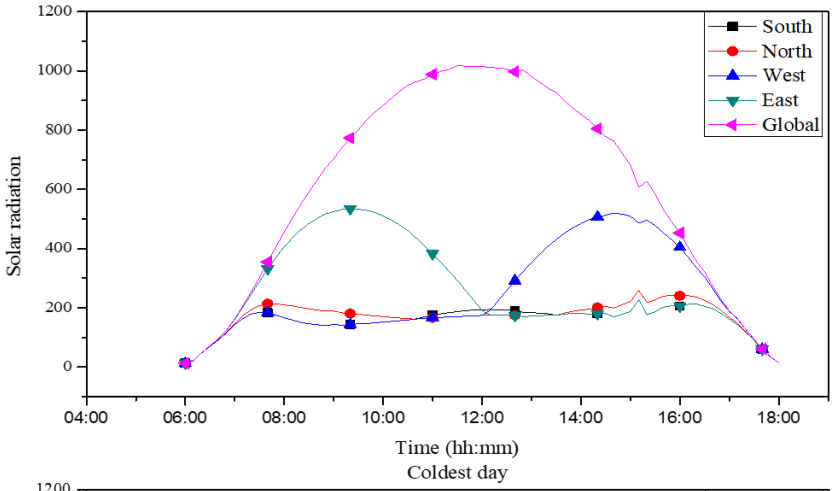

b)

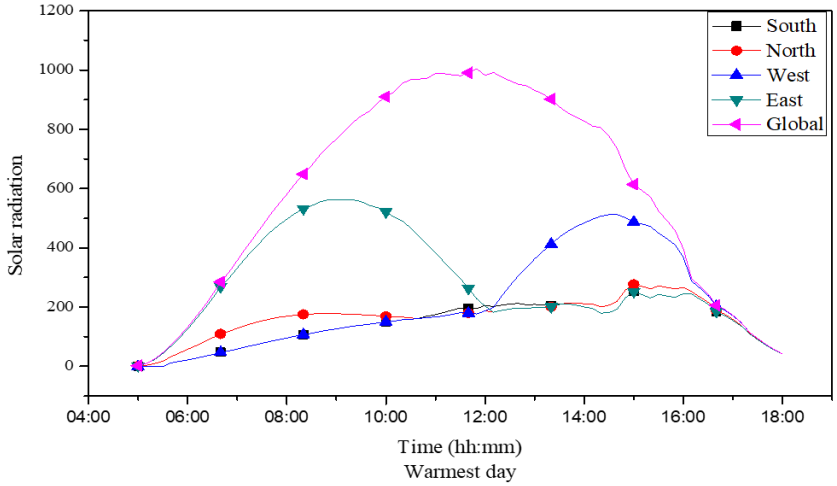

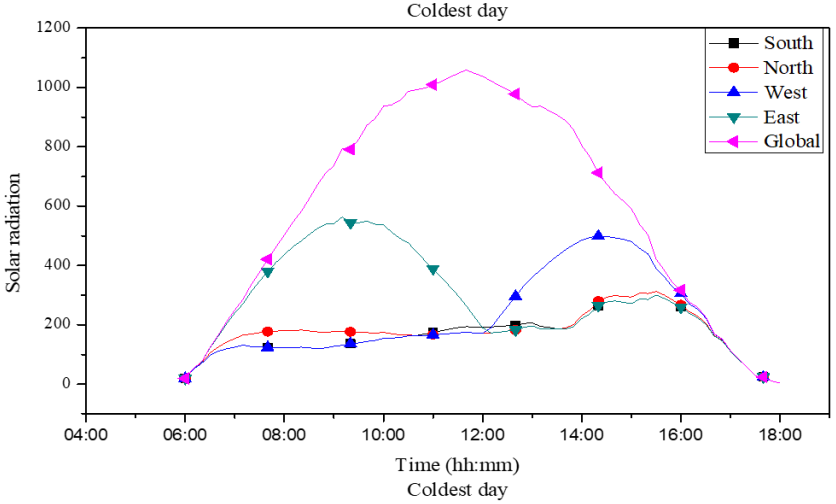

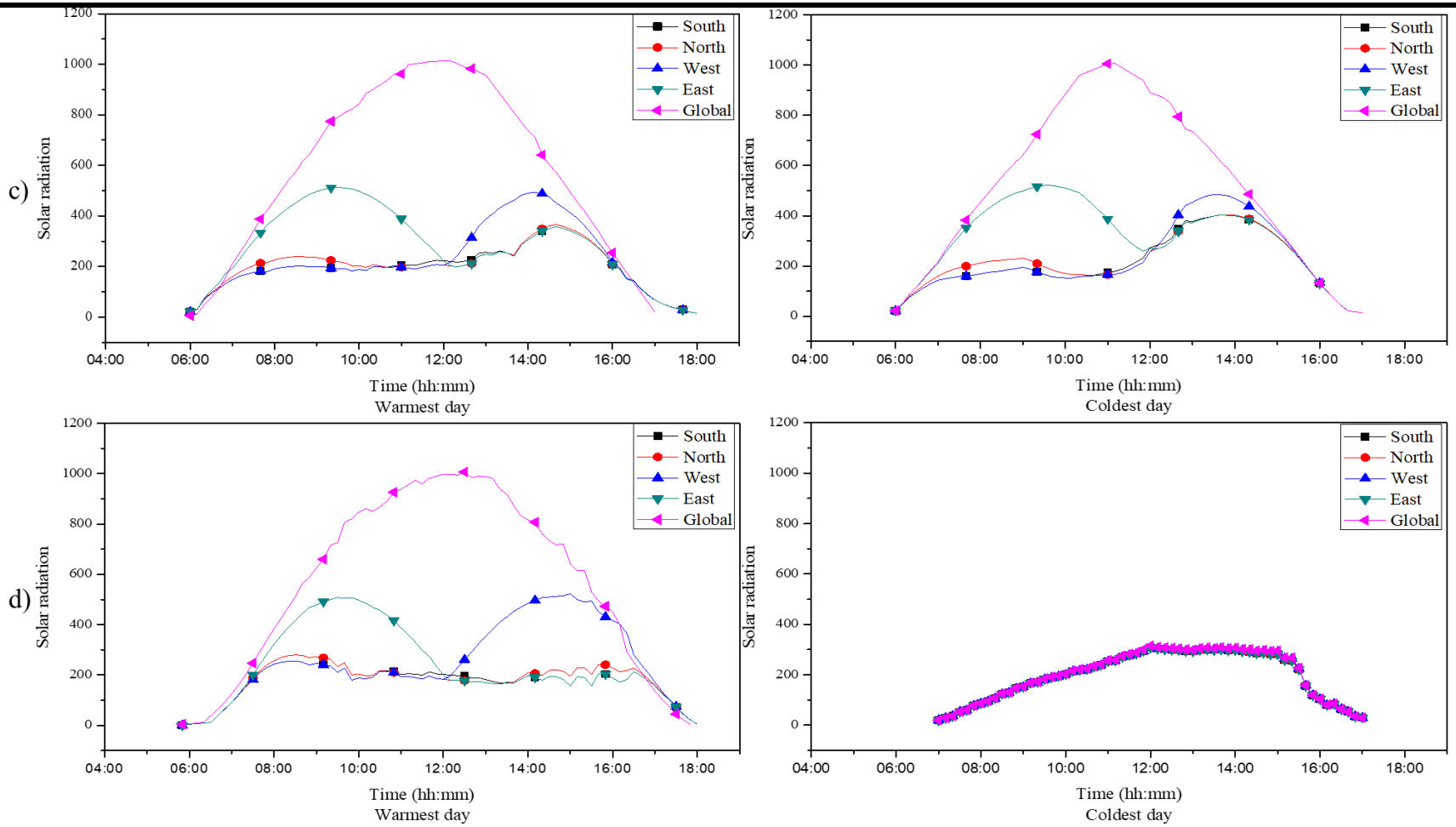

Figure C.1 Solar radiation decomposition of the warmest and coldest day for a) spring, b) summer, c) fall and d) winter.

D. Fitting equations for ambient temperature and solar radiation

Table D.1 Fitting equations for ambient temperature.

Date	Fitting equations
January 22	$t(x) = -8.657040873600240E-28x^6 + 4.590066652915770E-22x^5 - 6.894028896243320E-17x^4 + 4.084863552635670E-12x^3 - 9.345396137028570E-08x^2 + 6.933189108799810E-04x + 2.173784277826050E+01$
January 05	$t(x) = -3.115081171979400E-27x^6 + 8.497623105434400E-22x^5 - 8.528757039835970E-17x^4 + 3.702329736223820E-12x^3 - 5.928416712533070E-08x^2 + 1.265036904989360E-04x + 1.784797387498470E+01$
February 26	$t(x) = -6.916297056646530E-27x^6 + 1.931459294714890E-21x^5 - 1.992264761392410E-16x^4 + 9.078717698509140E-12x^3 - 1.686870184235310E-07x^2 + 9.739404002750970E-04x + 2.334300530709150E+01$
February 01	$t(x) = -7.602725173840940E-27x^6 + 2.133971858872230E-21x^5 - 2.209932082081500E-16x^4 + 1.013172195166820E-11x^3 - 1.914678960011040E-07x^2 + 1.185238552224630E-03x + 1.733351103420860E+01$
March 19	$t(x) = -6.916297056646530E-27x^6 + 1.931459294714890E-21x^5 - 1.992264761392410E-16x^4 + 9.078717698509140E-12x^3 - 1.686870184235310E-07x^2 + 9.739404002750970E-04x + 2.334300530709150E+01$
March 24	$t(x) = -7.965309022591080E-27x^6 + 2.218419397809690E-21x^5 - 2.275738062496380E-16x^4 + 1.028411806404070E-11x^3 - 1.884185301041610E-07x^2 + 1.078176887723710E-03x + 1.926808710963810E+01$
April 07	$t(x) = -7.333191164735770E-27x^6 + 2.081364783897500E-21x^5 - 2.164857738006480E-16x^4 + 9.847678591272880E-12x^3 - 1.792618772623880E-07x^2 + 9.588972055993850E-04x + 2.523114292776880E+01$
April 16	$t(x) = -3.651745996197070E-27x^6 + 9.405523523726400E-22x^5 - 8.514872607832360E-17x^4 + 2.986184083042240E-12x^3 - 2.239496434521330E-08x^2 - 2.646107583217370E-04x + 2.073790716067010E+01$
May 30	$t(x) = -1.035055662357710E-26x^6 + 2.710578818888920E-21x^5 - 2.611270086183710E-16x^4 + 1.111595622178680E-11x^3 - 1.966086582705360E-07x^2 + 1.220342420232610E-03x + 2.426021167149880E+01$
May 13	$t(x) = -8.060796508392980E-27x^6 + 2.162391664495140E-21x^5 - 2.124293325436880E-16x^4 + 9.097922912982430E-12x^3 - 1.551467824468210E-07x^2 + 8.417664916748890E-04x + 2.252090557415800E+01$
June 04	$t(x) = -4.678099999950510E-27x^6 + 1.301621589370200E-21x^5 - 1.311301046032150E-16x^4 + 5.628641584464720E-12x^3 - 9.066065150085260E-08x^2 + 3.979570714314210E-04x + 2.579569544846890E+01$
June 13	$t(x) = -5.764155893542740E-27x^6 + 1.418471553054900E-21x^5 - 1.248490122641320E-16x^4 + 4.534808712458120E-12x^3 - 5.418553474401820E-08x^2 + 3.829854181347510E-05x + 2.491460306443330E+01$
July 25	$t(x) = -7.334403072151750E-27x^6 + 1.987096675152630E-21x^5 - 1.970775743006390E-16x^4 + 8.502295265127630E-12x^3 - 1.447402152281870E-07x^2 + 7.345887213716650E-04x + 2.741928364450000E+01$
July 10	$t(x) = -4.901756079178620E-27x^6 + 1.368610478969660E-21x^5 - 1.396384329642400E-16x^4 + 6.203251566127150E-12x^3 - 1.110028039529380E-07x^2 + 7.266045004605810E-04x + 2.280046935073190E+01$

August 10	$t(x) = -3.917689635530650E-27x^6 + 1.1187790011296l0E-21x^5 - 1.171432838772330E-16x^4 + 5.328757136921390E-12x^3 - 9.450621092383510E-08x^2 + 4.745042428773160E-04x + 2.659048576856000E+01$
August 07	$t(x) = -1.042330588391630E-26x^6 + 2.739857487809040E-21x^5 - 2.647126112070570E-16x^4 + 1.130787664429380E-11x^3 - 2.020692761420420E-07x^2 + 1.278587847973970E-03x + 2.462415009426330E+01$
September 01	$t(x) = -5.373467020043490E-27x^6 + 1.492577455786470E-21x^5 - 1.518235847658630E-16x^4 + 6.707348557621850E-12x^3 - 1.164536173703210E-07x^2 + 6.246030991263750E-04x + 2.463695755570370E+01$
September 22	$t(x) = -7.739408216012230E-27x^6 + 2.074536311916410E-21x^5 - 2.025691690780600E-16x^4 + 8.578059086915470E-12x^3 - 1.446852958852420E-07x^2 + 7.518147020633140E-04x + 2.512452692128140E+01$
October 10	$t(x) = -6.238568503484140E-27x^6 + 1.617296979221180E-21x^5 - 1.516231003000380E-16x^4 + 6.007048870603940E-12x^3 - 8.624153766947570E-08x^2 + 3.407769460146430E-04x + 2.346304564073220E+01$
October 23	$t(x) = -4.484695274270760E-27x^6 + 1.232832427116330E-21x^5 - 1.220024112082080E-16x^4 + 5.025801347342220E-12x^3 - 6.897770296783460E-08x^2 + 3.932298035991270E-05x + 2.364778459079390E+01$
November 12	$t(x) = -6.187365233947550E-27x^6 + 1.673138307994860E-21x^5 - 1.655148216235740E-16x^4 + 7.092567021838670E-12x^3 - 1.179473948565750E-07x^2 + 5.512217361065550E-04x + 2.411867419927880E+01$
November 17	$t(x) = -5.368943063454350E-27x^6 + 1.361344133864220E-21x^5 - 1.228563463213420E-16x^4 + 4.484902486539950E-12x^3 - 4.888816544082120E-08x^2 + 2.197054755015420E-06x + 1.675555097496180E+01$
December 02	$t(x) = -7.008855640192870E-27x^6 + 1.923012154158220E-21x^5 - 1.945050769215750E-16x^4 + 8.654109569481310E-12x^3 - 1.556177892151310E-07x^2 + 8.900495548260780E-04x + 2.252243481548070E+01$
December 22	$t(x) = -6.478156101765250E-27x^6 + 1.748811472407670E-21x^5 - 1.720170954618100E-16x^4 + 7.286078215445710E-12x^3 - 1.202731688904400E-07x^2 + 7.638401825325050E-04x + 9.992105776145760E+00$

Table D.2 Fitting equations for solar radiation.

Date	Fitting equations
January 22	$t(x) = -2.036159260544150E-24x^6 + 1.1121685346091l0E-19x^5 + 2.635237170141320E-14x^4 - 3.191604096272980E-09x^3 + 1.348643513854730E-04x^2 - 2.440781883533850E+00x + 1.597376685542820E+04$
January 05	$t(x) = 1.659976645168580E-22x^6 - 5.294341333263040E-17x^5 + 7.002344644709770E-12x^4 - 4.916803355962110E-07x^3 + 1.933450027972190E-02x^2 - 4.037839585272080E+02x + 3.499608232170570E+06$
February 26	$t(x) = 1.006040152516000E-23x^6 - 2.542441247138560E-18x^5 + 2.626212253897110E-13x^4 - 1.420524595994930E-08x^3 + 4.242199201083910E-04x^2 - 6.611123616671840E+00x + 4.190863110159270E+04$
February 01	$t(x) = -2.910913835687570E-18x^5 + 4.803248653697600E-13x^4 - 3.119238865042130E-08x^3 + 9.942274742460970E-04x^2 - 1.551214841304230E+01x + 9.467973987196370E+04$

March 19	$t(x)= 1.277920191659140E-22x^6 - 4.104521178211500E-17x^5 + 5.483095399149150E-12x^4 - 3.900074026827260E-07x^3 + 1.557910933054890E-02x^2 - 3.313465264982130E+02x + 2.931347836007720E+06$ $t(x) = -3.772774073223500E-22x^6 + 7.532467578749950E-17x^5 - 6.172337316531000E-12x^4 + 2.653014126186170E-07x^3 - 6.302110333628690E-03x^2 + 7.843965664198290E+01x - 3.998741233371l0E+05$ $t(x) = 3.584643324737050E-24x^6 + 3.264687811810940E-19x^5 - 2.512437765387560E-13x^4 + 3.314220096781910E-08x^3 - 1.945038167905260E-03x^2 + 5.463803688419320E+01x - 5.996520646167350E+05$
March 24	$t(x) = -2.720661486983280E-24x^6 - 4.2924761600069l0E-19x^5 + 1.318163249474660E-13x^4 - 1.067176802726920E-08x^3 + 3.921398107837660E-04x^2 - 6.773176016820060E+00x + 4.450967072418600E+04$ $t(x) = 1.723583579815840E-22x^6 - 5.565745649215350E-17x^5 + 7.453563667538870E-12x^4 - 5.299520052202010E-07x^3 + 2.110255479212670E-02x^2 - 4.462743622205930E+02x + 3.916592648397160E+06$
April 07	$t(x) = 4.652073283347690E-23x^6 - 9.670041676749950E-18x^5 + 8.373836309168750E-13x^4 - 3.861263264056320E-08x^3 + 9.942186294517590E-04x^2 - 1.342175104704040E+01x + 7.365621331136560E+04$ $t(x) = 8.954323844769470E-23x^6 - 2.861308951756140E-17x^5 + 3.787503329390520E-12x^4 - 2.659136886272370E-07x^3 + 1.044684477704990E-02x^2 - 2.178177060431490E+02x + 1.883733721322690E+06$
April l6	$t(x) = 2.447134827877590E-23x^6 - 5.041335899533980E-18x^5 + 4.364840454602420E-13x^4 - 2.029244187146980E-08x^3 + 5.286809914286750E-04x^2 - 7.188894990653190E+00x + 3.936419761143790E+04$ $t(x) = 6.663348569569840E-23x^6 - 2.204771711449370E-17x^5 + 3.016403173925470E-12x^4 - 2.184984155451910E-07x^3 + 8.841456250977070E-03x^2 - 1.895614035570680E+02x + 1.683132024258740E+06$
May 30	$t(x) = -2.574213487125550E-23x^6 + 5.491841453818370E-18x^5 - 4.802588794137410E-13x^4 + 2.210265138443360E-08x^3 - 5.662267238295440E-04x^2 + 7.679322394763400E+00x - 4.308250445200140E+04$ $t(x) = 2.186911202858340E-21x^6 - 7.478615404451930E-16x^5 + 1.062615916263400E-10x^4 - 8.028916239204510E-06x^3 + 3.402029970721280E-01x^2 - 7.663922715179540E+03x + 7.170495178703800E+07$
May l3	$t(x) = 5.599815132643380E-23x^6 - 1.029096105906060E-17x^5 + 7.834291870650690E-13x^4 - 3.170309022200250E-08x^3 + 7.172601259837870E-04x^2 - 8.508815171708640E+00x + 4.097153720697190E+04$ $t(x) = 4.860653304272300E-23x^6 - 1.457625746712640E-17x^5 + 1.812830936988850E-12x^4 - 1.198919880189980E-07x^3 + 4.455529617591610E-03x^2 - 8.839180331395030E+01x + 7.328802057514250E+05$
June 04	$t(x) = -2.861431372395080E-23x^6 + 5.774019630290080E-18x^5 - 4.622529118839550E-13x^4 + 1.869833765555330E-08x^3 - 4.031851904463190E-04x^2 + 4.450810442128040E+00x - 1.993253515094520E+04$ $t(x) = 1.621673714323420E-22x^6 - 5.246413694736030E-17x^5 + 7.034974054319460E-12x^4 - 5.005351201590490E-07x^3 + 1.993278338973200E-02x^2 - 4.213161791937840E+02x + 3.693491983865120E+06$
June l3	$t(x) = -4.400220400658500E-23x^6 + 9.011340678960820E-18x^5 - 7.401518851870600E-13x^4 + 3.110187290828750E-08x^3 - 7.056994352413130E-04x^2 + 8.267886557067100E+00x - 3.940366285884640E+04$ $t(x) = 8.066275812438520E-23x^6 - 2.547420484197750E-17x^5 + 3.336088454535400E-12x^4 - 2.320171696905020E-07x^3 + 9.042827270490730E-03x^2 - 1.873699272632770E+02x + 1.613531905042180E+06$

July 25	$t(x) = 1.128750844182770E-23x^6 - 1.328591363029190E-18x^5 + 5.426496675342920E-14x^4 - 9.055358742901790E-10x^3 + 6.069374293982130E-06x^2 - 1.292735338029160E-02x + 3.015236636099870E+00$ $t(x) = 1.426039722141270E-22x^6 - 4.470929522974070E-17x^5 + 5.810069997514060E-12x^4 - 4.006626438524490E-07x^3 + 1.546684050710290E-02x^2 - 3.169645035052560E+02x + 2.694683363481050E+06$
July 10	$t(x) = 1.412701723292810E-23x^6 - 1.746297669818040E-18x^5 + 7.691244326648580E-14x^4 - 1.456924823410810E-09x^3 + 1.191436565101120E-05x^2 - 3.548921282265380E-02x + 2.018384312430860E+01$ $t(x) = 4.402151211217520E-23x^6 - 1.455788152788060E-17x^5 + 1.982884289656260E-12x^4 - 1.425824795664190E-07x^3 + 5.715106775513070E-03x^2 - 1.211898783377900E+02x + 1.063181760125830E+06$
August 10	$t(x) = 1.562632781367110E-21x^6 - 2.803858266297510E-16x^5 + 2.077394052169060E-11x^4 - 8.136027708874370E-07x^3 + 1.776668546215420E-02x^2 - 2.050988905422630E+02x + 9.777751316339620E+05$ $t(x) = 1.834662678794350E-23x^6 - 6.187921841052720E-18x^5 + 8.805417956617880E-13x^4 - 6.748689477851120E-08x^3 + 2.925085713848550E-03x^2 - 6.761926702071290E+01x + 6.483066914360500E+05$
August 07	$t(x) = -6.300806791646300E-23x^6 + 1.300109087218960E-17x^5 - 1.084502220347100E-12x^4 + 4.672376886693650E-08x^3 - 1.097245529366110E-03x^2 + 1.338771510592610E+01x - 6.677331665827150E+04$ $t(x) = 2.908256353521180E-21x^6 - 1.040306649278530E-15x^5 + 1.547206737795570E-10x^4 - 1.224558365972780E-05x^3 + 5.439453938415030E-01x^2 - 1.285672673440540E+04x + 1.263212575762540E+08$
September 01	$t(x) = 3.326129922500880E-22x^6 - 6.546227331016830E-17x^5 + 5.300471247218010E-12x^4 - 2.257728229321800E-07x^3 + 5.329747409661460E-03x^2 - 6.603590052194400E+01x + 3.352201184024070E+05$ $t(x) = -6.439590877693980E-24x^6 + 2.328428674824830E-18x^5 - 3.389011472836830E-13x^4 + 2.562346036231720E-08x^3 - 1.071177554563440E-03x^2 + 2.372959817586630E+01x - 2.198457205901420E+05$
September 22	$t(x) = 7.216845810810190E-24x^6 - 1.414250654656220E-18x^5 + 1.245523319855650E-13x^4 - 6.243967376716640E-09x^3 + 1.792050482800410E-04x^2 - 2.634429353633340E+00x + 1.503990755738340E+04$ $t(x) = -1.047745278197580E-22x^6 + 3.631881417624940E-17x^5 - 5.191460048240090E-12x^4 + 3.918380088819760E-07x^3 - 1.647756887648850E-02x^2 + 3.662096516641670E+02x - 3.362000480355650E+06$
October 10	$t(x) = 1.465227861287350E-23x^6 - 2.803131817987190E-18x^5 + 2.316705196627570E-13x^4 - 1.062582244409230E-08x^3 + 2.804466462823250E-04x^2 - 3.905510485293500E+00x + 2.187720915934000E+04$ $t(x) = -3.574971787995560E-22x^6 + 1.162549041154200E-16x^5 - 1.566761548137960E-11x^4 + 1.120064423032550E-06x^3 - 4.479931436284540E-02x^2 + 9.506231462343150E+02x - 8.361795050442240E+06$
October 23	$t(x) = 7.667295003782570E-23x^6 - 1.558469982081330E-17x^5 + 1.316568592011320E-12x^4 - 5.912686264622690E-08x^3 + 1.483407032629590E-03x^2 - 1.957780191319450E+01x + 1.055484763863620E+05$ $t(x) = -2.706358068742100E-22x^6 + 8.650374311788690E-17x^5 - 1.146423132385110E-11x^4 + 8.060944415690350E-07x^3 - 3.170942908125270E-02x^2 + 6.615804069249850E+02x - 5.719267982810540E+06$
November 12	$t(x) = 3.121312808946990E-23x^6 - 6.053547861826900E-18x^5 + 4.912020497308660E-13x^4 - 2.132706926982310E-08x^3 + 5.185610498168240E-04x^2 - 6.585869306732190E+00x + 3.362758399707360E+04$

	$t(x) = -2.545238902559440E\text{-}22x^6 + 8.302524196991410E\text{-}17x^5 - 1.120858731142730E\text{-}11x^4 + 8.018183704531760E\text{-}07x^3 - 3.206664096952600E\text{-}02x^2 + 6.800195202809540E+02x - 5.976076920041150E+06$
November 17	$t(x) = 1.819753347867370E\text{-}22x^6 - 3.446749382524660E\text{-}17x^5 + 2.700018144718450E\text{-}12x^4 - 1.120436889781990E\text{-}07x^3 + 2.596146583101780E\text{-}03x^2 - 3.175954676798010E+01x + 1.597630823591860E+05$
	$t(x) = 1.894837418228100E\text{-}22x^6 - 5.768575330405290E\text{-}17x^5 + 7.310454534947640E\text{-}12x^4 - 4.935964997657730E\text{-}07x^3 + 1.872131856812580E\text{-}02x^2 - 3.779925629504340E+02x + 3.172071041977160E+06$
December 02	$t(x) = 3.288273474413380E\text{-}23x^6 - 7.864883832030590E\text{-}18x^5 + 7.691585296137290E\text{-}13x^4 - 3.928474274322600E\text{-}08x^3 + 1.100900059326290E\text{-}03x^2 - 1.595802865309550E+01x + 9.317849936024870E+04$
	$t(x) = 2.379776463221480E\text{-}24x^6 + 7.381964286490630E\text{-}19x^5 - 2.641931638937210E\text{-}13x^4 + 2.824099884591120E\text{-}08x^3 - 1.422429035901580E\text{-}03x^2 + 3.499053519996610E+01x - 3.398348999705780E+05$
December 22	$t(x) = 7.932065737863420E\text{-}23x^6 - 1.647987815937000E\text{-}17x^5 + 1.423534772200650E\text{-}12x^4 - 6.533166233761690E\text{-}08x^3 + 1.674122832321430E\text{-}03x^2 - 2.257839227640910E+01x + 1.245854066659270E+05$
	$t(x) = -9.992136526307970E\text{-}23x^6 + 3.333405123680890E\text{-}17x^5 - 4.581657903913510E\text{-}12x^4 + 3.324328678005850E\text{-}07x^3 - 1.344271064758050E\text{-}02x^2 + 2.875150685093400E+02x - 2.542948074694610E+06$

E. Temperature graphs of the room and window for each month

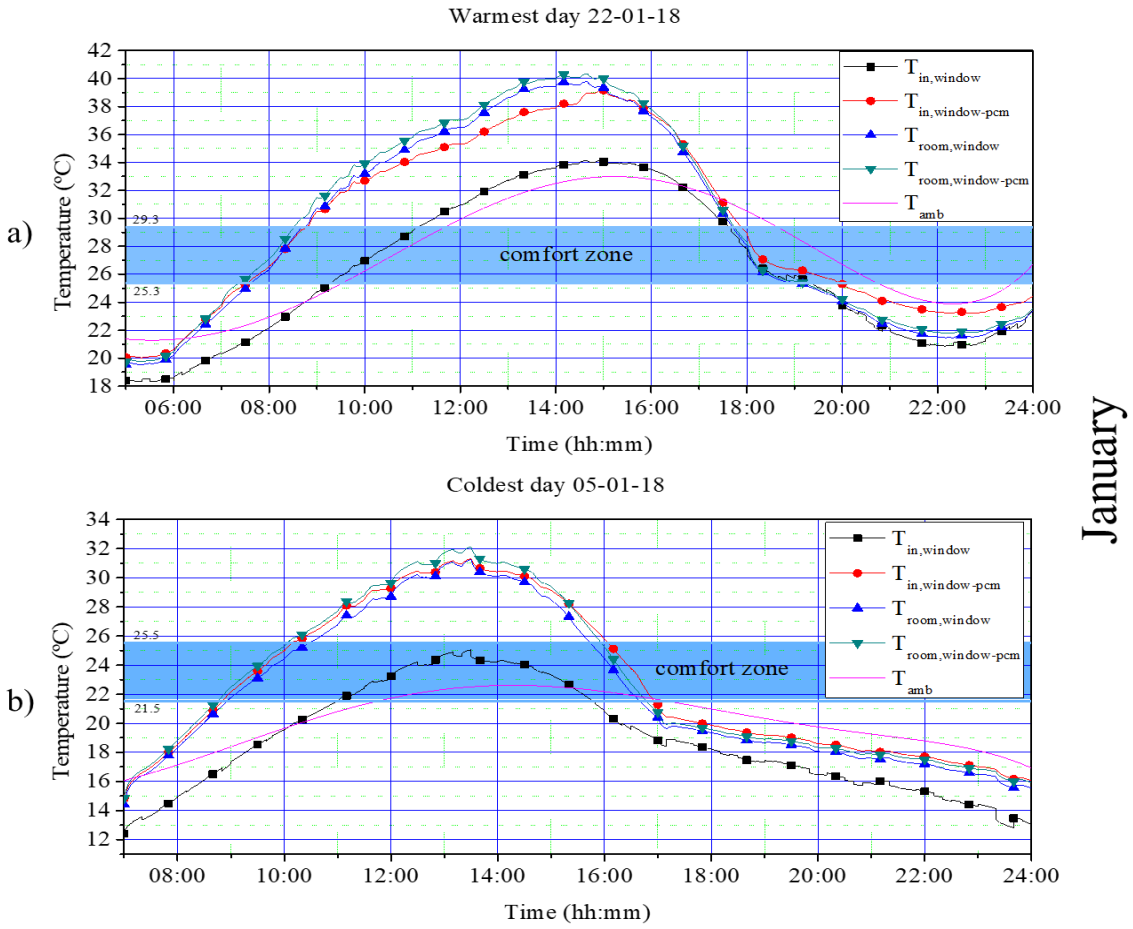

Figure E.2 Comparison between the behavior of the inner surface average temperature and room inside temperature for both configurations for the a) warmest and b) coldest day of January.

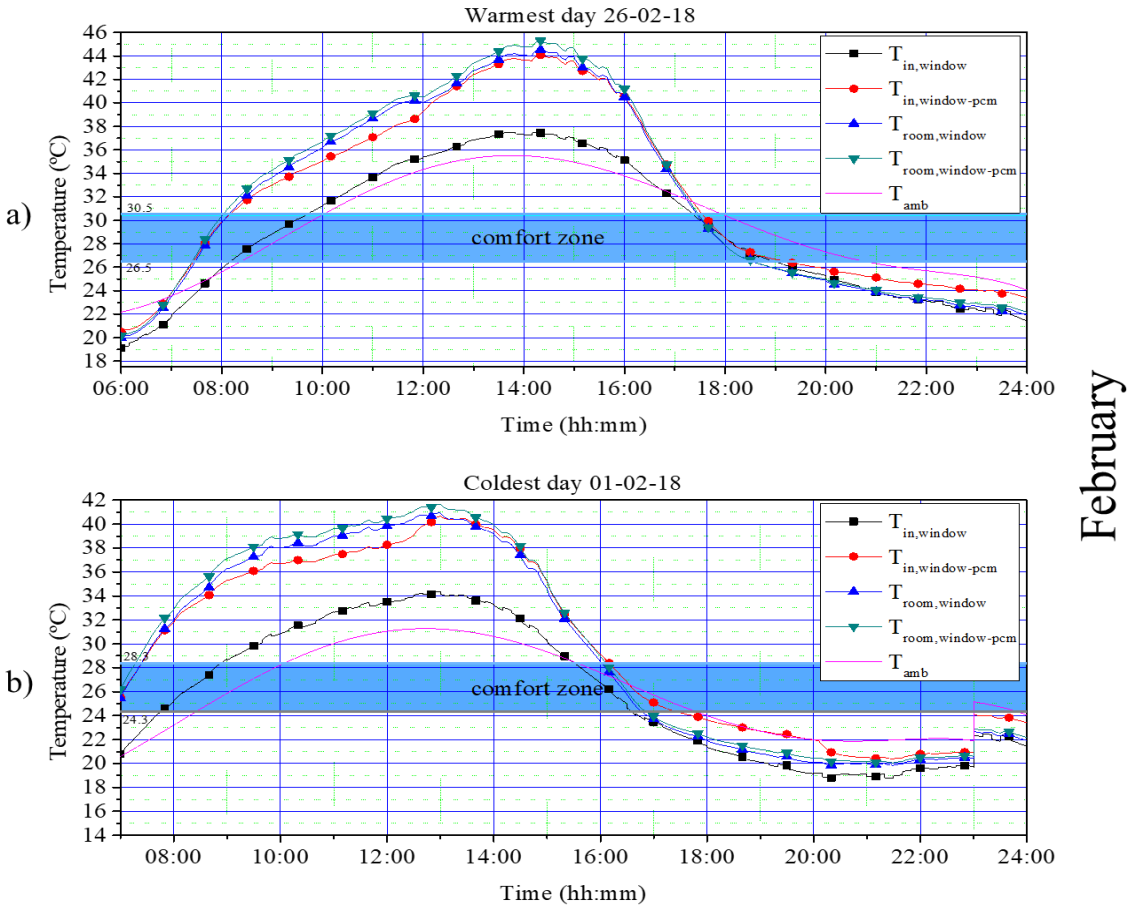

Figure E.3 Comparison between the behavior of the inner surface average temperature and room inside temperature for both configurations for the a) warmest and b) coldest day of February.

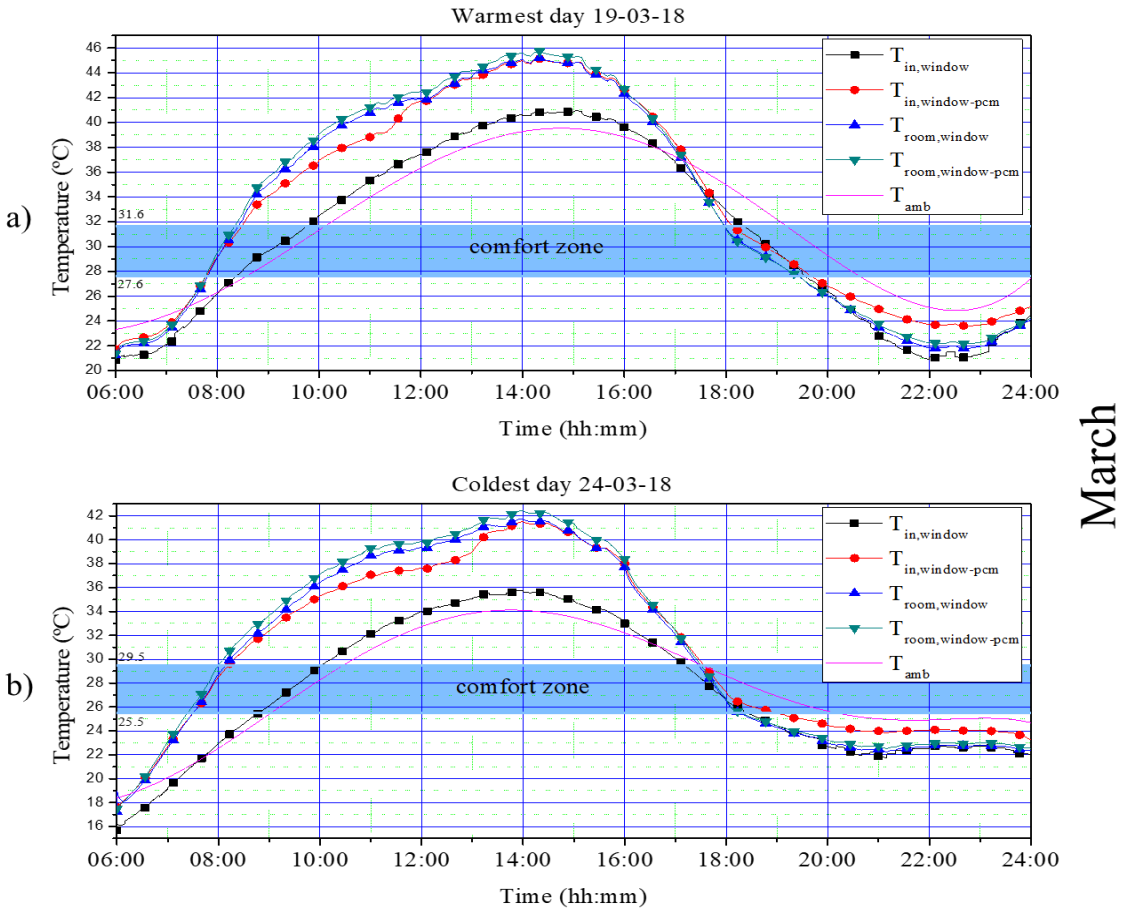

Figure E.4 Comparison between the behavior of the inner surface average temperature and room inside temperature for both configurations for the a) warmest and b) coldest day of March.

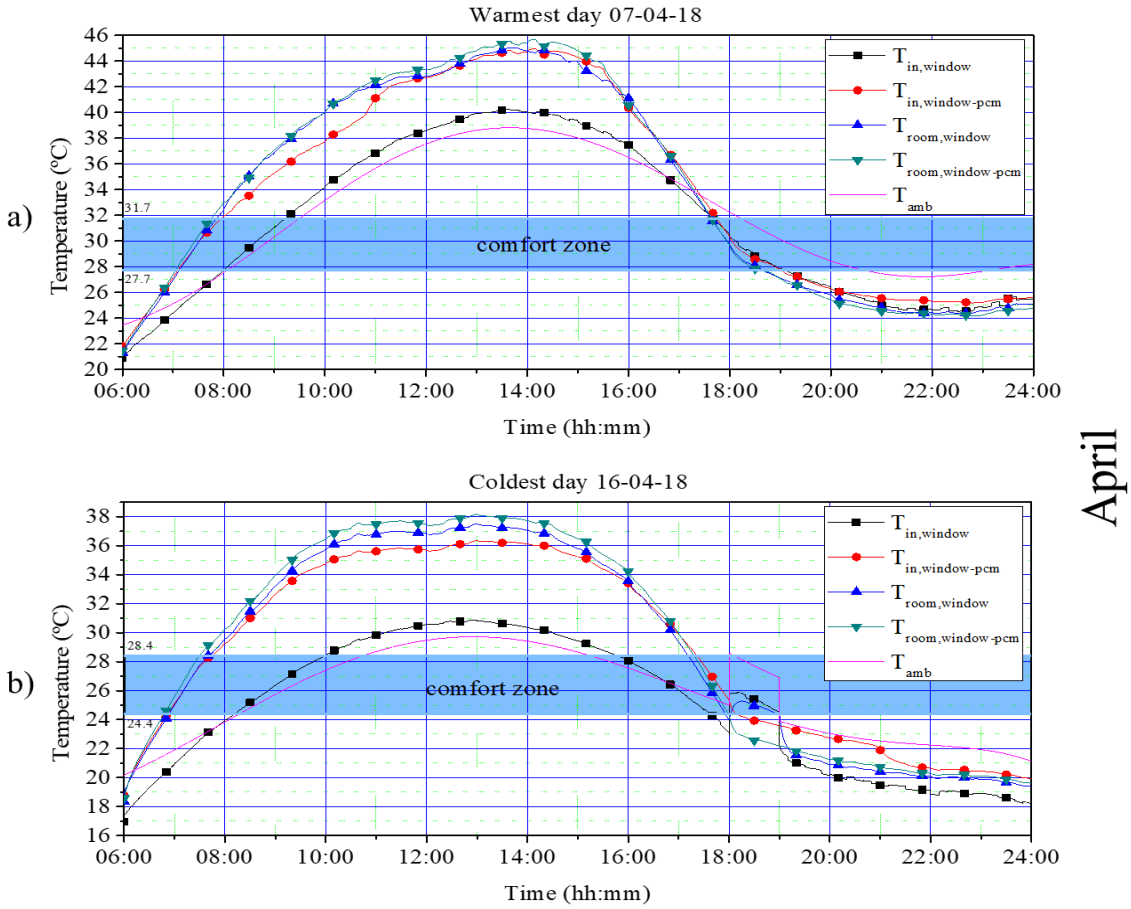

Figure E.5 Comparison between the behavior of the inner surface average temperature and room inside temperature for both configurations for the a) warmest and b) coldest day of April.

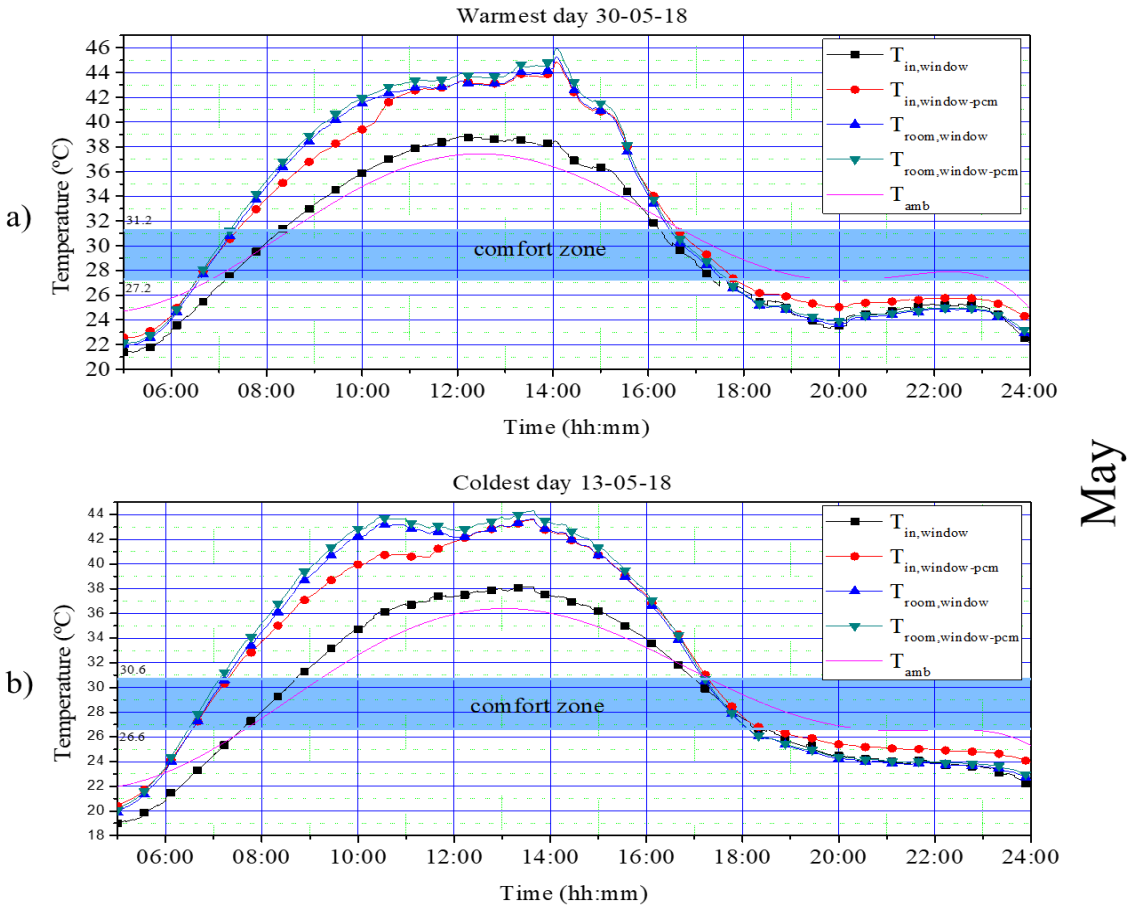

Figure E.6 Comparison between the behavior of the inner surface average temperature and room inside temperature for both configurations for the a) warmest and b) coldest day of May.

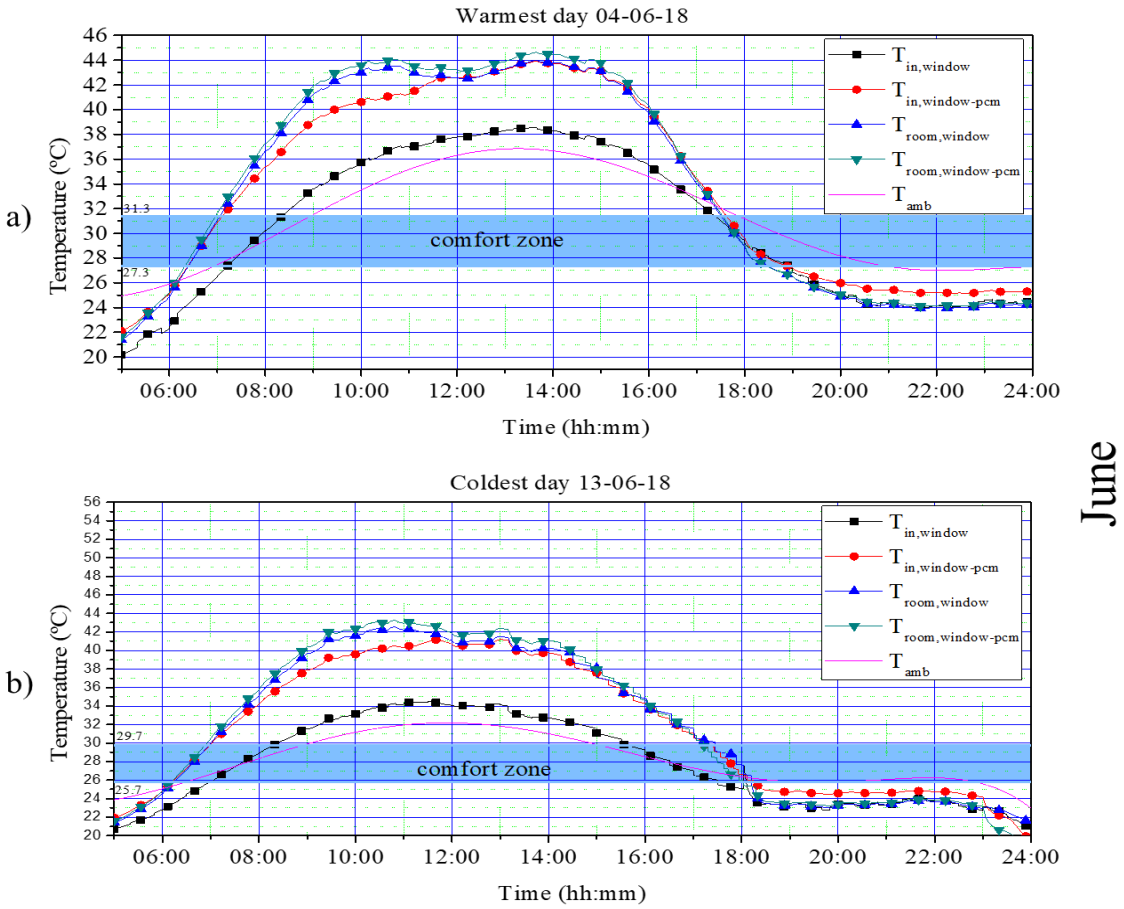

Figure E.7 Comparison between the behavior of the inner surface average temperature and room inside temperature for both configurations for the a) warmest and b) coldest day of June.

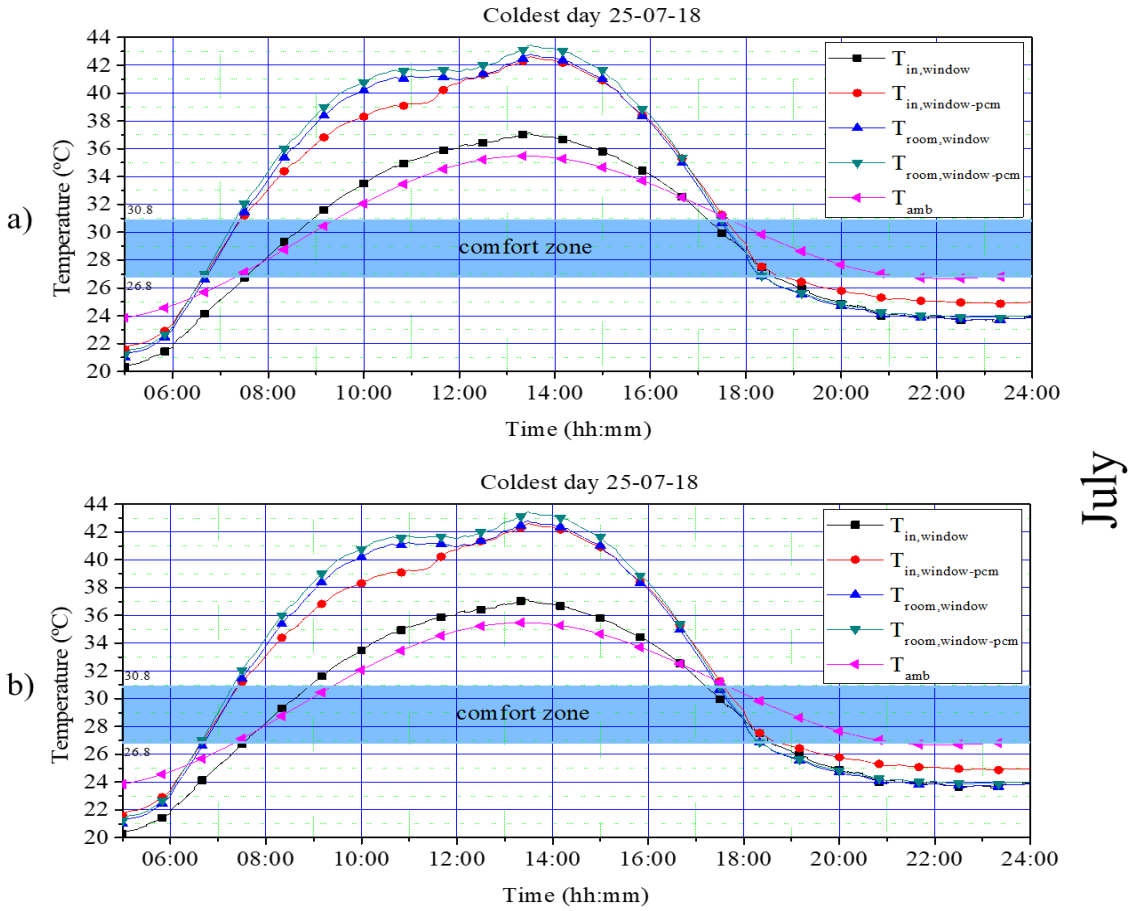

Figure E.8 Comparison between the behavior of the inner surface average temperature and room inside temperature for both configurations for the a) warmest and b) coldest day of July.

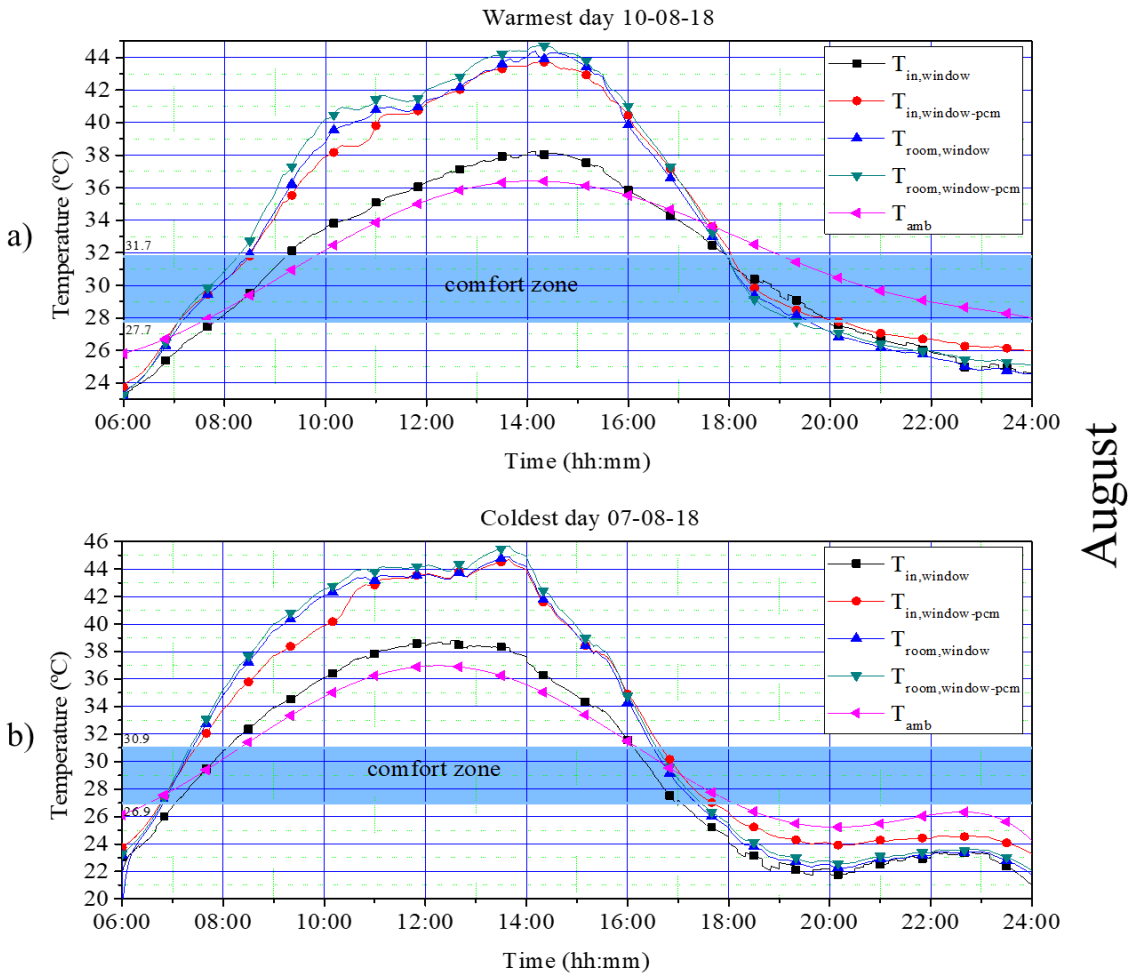

Figure E.9 Comparison between the behavior of the inner surface average temperature and room inside temperature for both configurations for the a) warmest and b) coldest day of August.

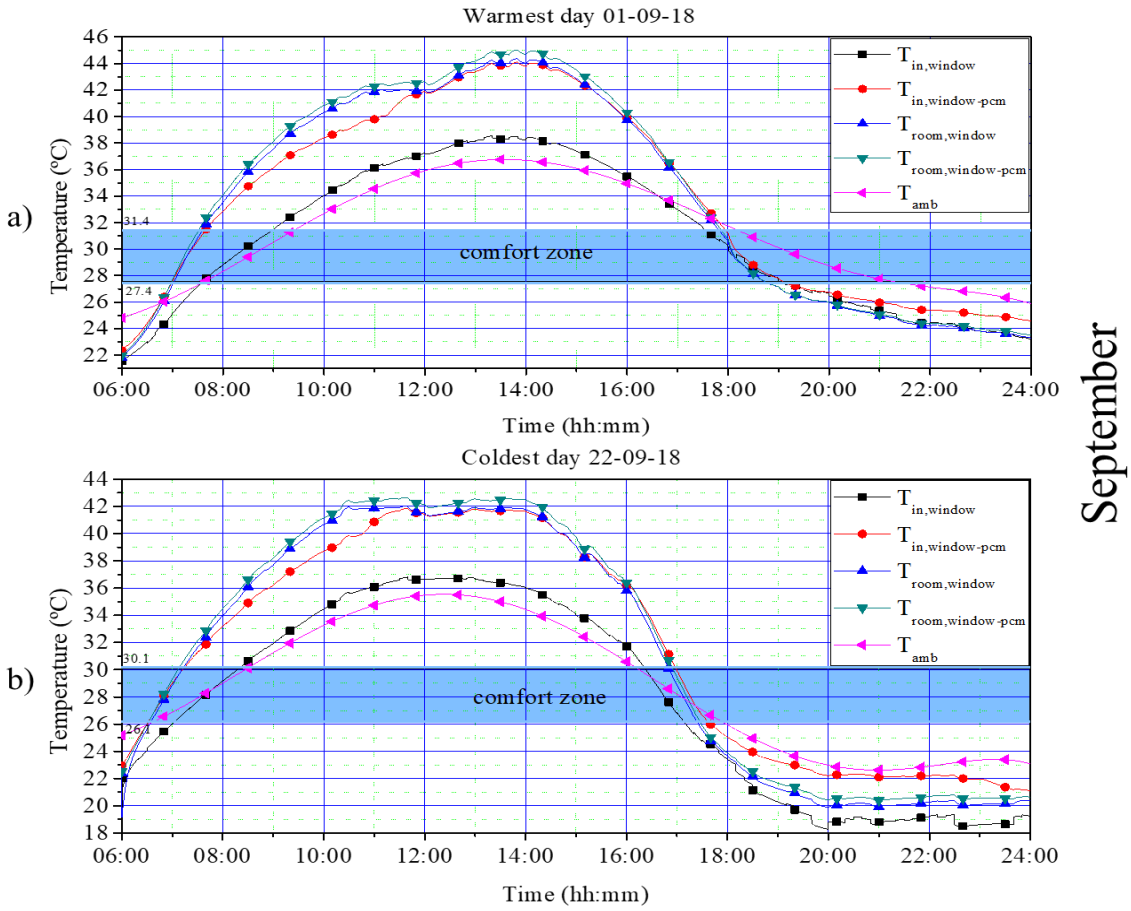

Figure E.10 Comparison between the behavior of the inner surface average temperature and room inside temperature for both configurations for the a) warmest and b) coldest day of September.

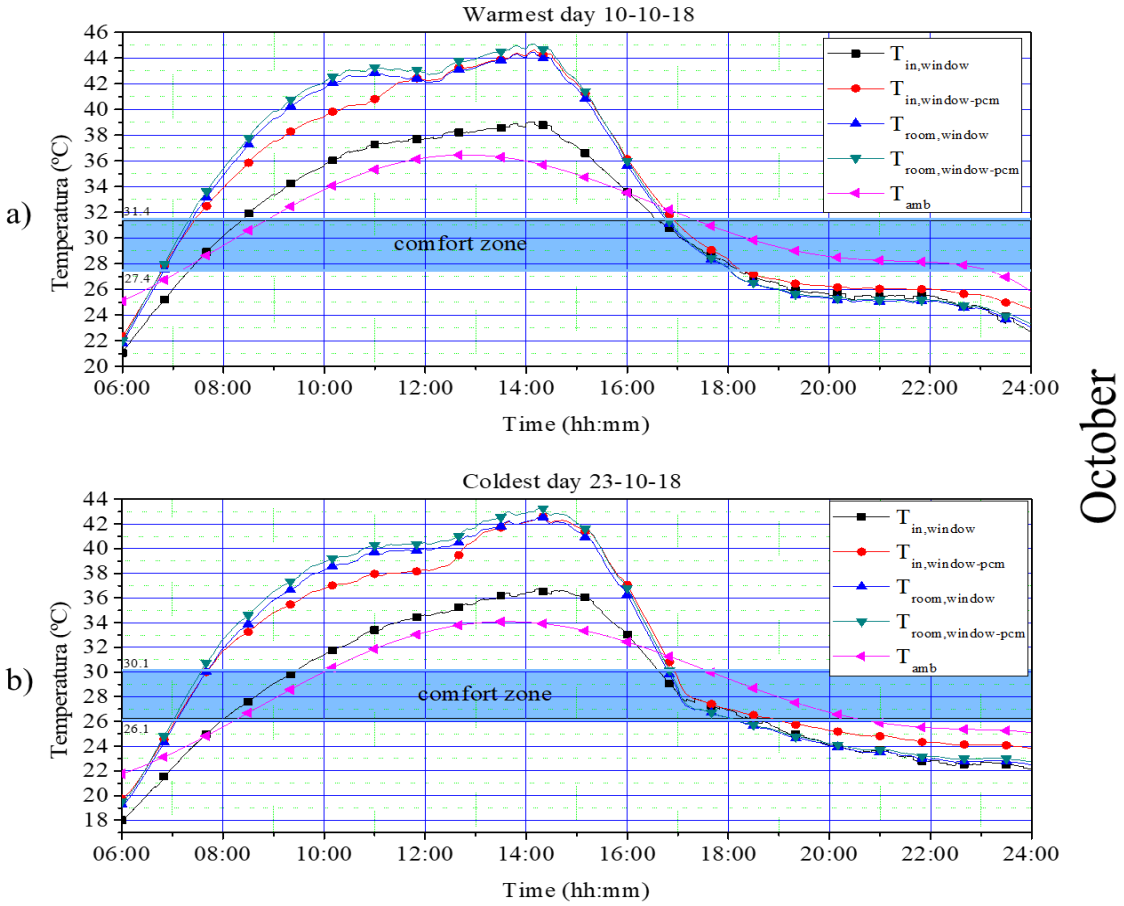

Figure E.11 Comparison between the behavior of the inner surface average temperature and room inside temperature for both configurations for the a) warmest and b) coldest day of October.

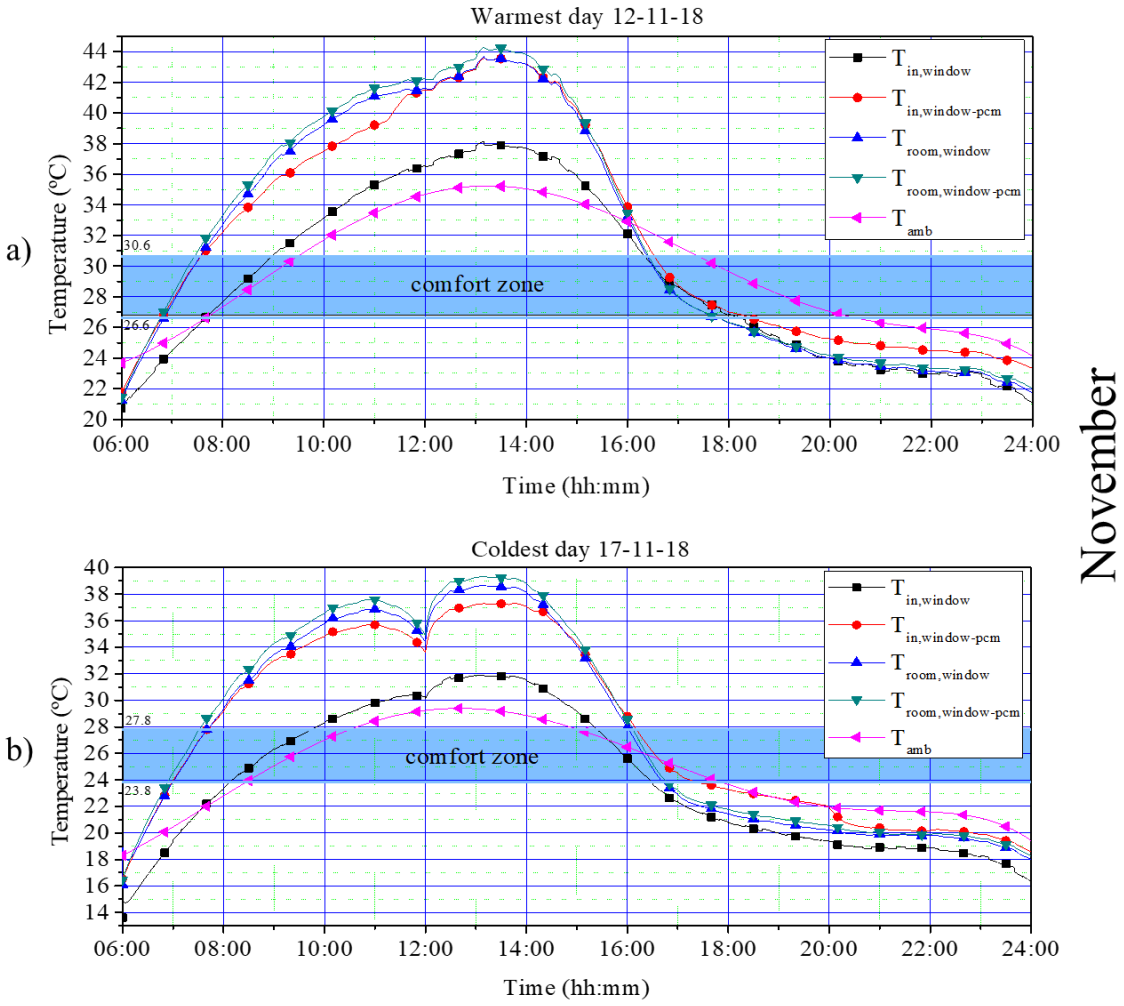

Figure E.12 Comparison between the behavior of the inner surface average temperature and room inside temperature for both configurations for the a) warmest and b) coldest day of November.

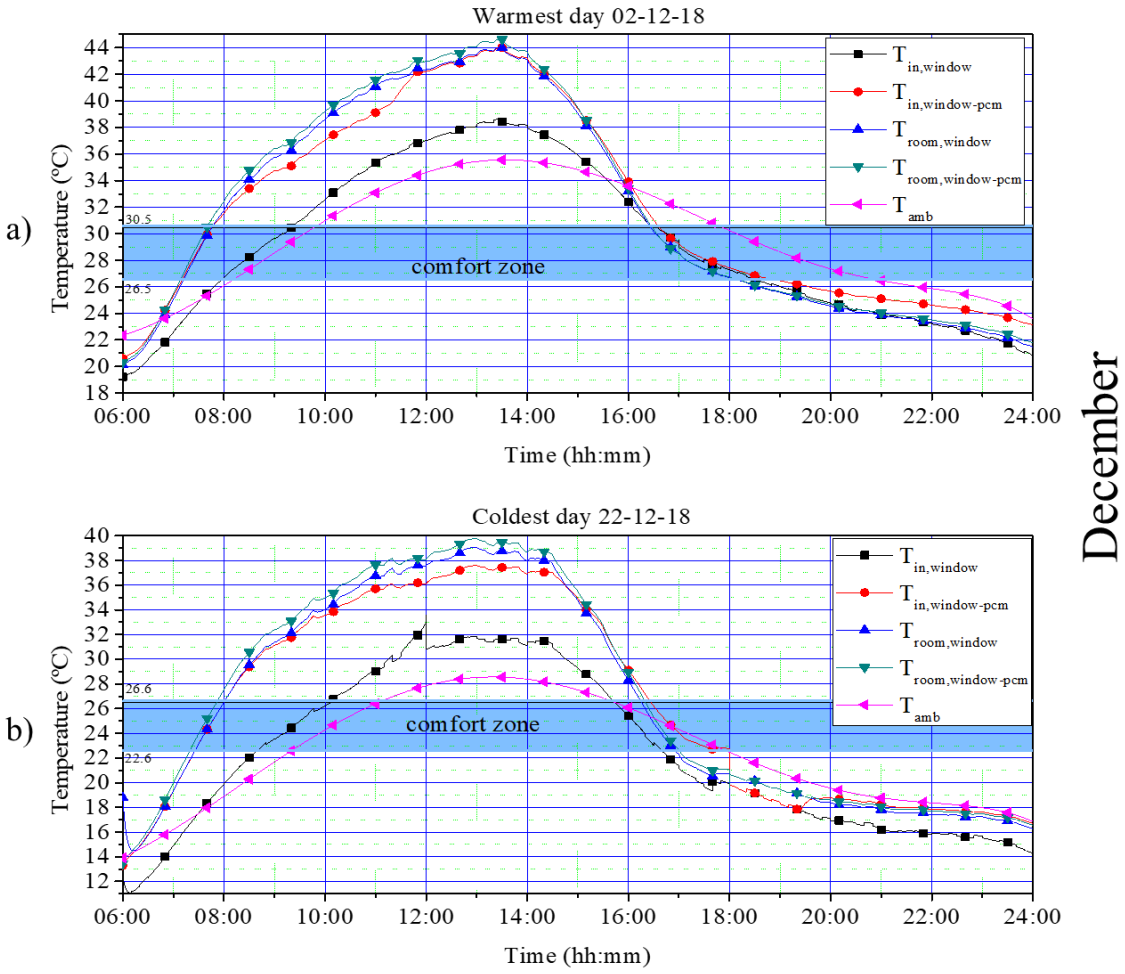

Figure E.13 Comparison between the behavior of the inner surface average temperature and room inside temperature for both configurations for the a) warmest and b) coldest day of December.

F. Peak temperatures graphs of the envelope elements for each month

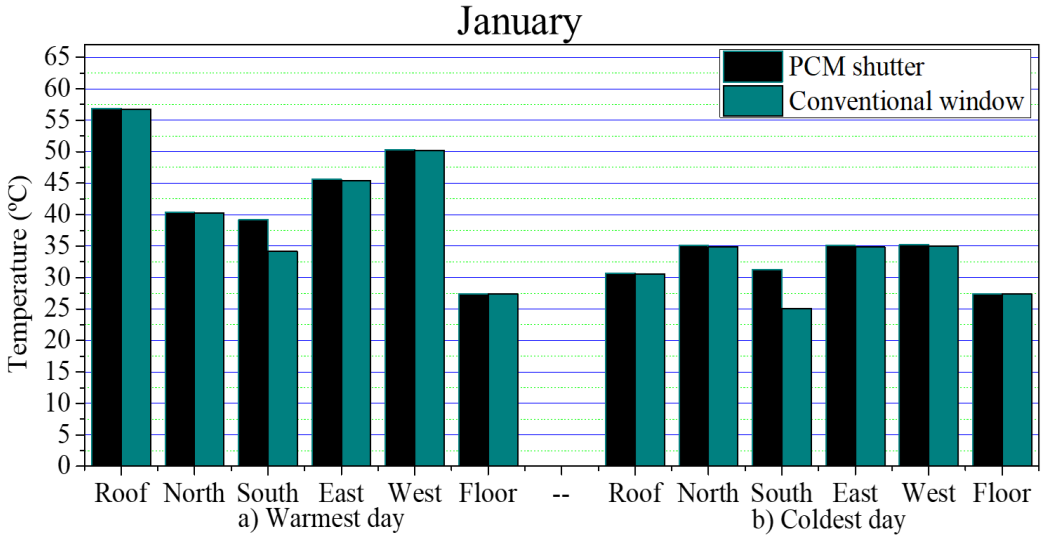

Figure F.1 Comparison between the behavior of maximum temperatures of the envelope elements of the room for both configurations for the a) warmest and b) coldest day of January.

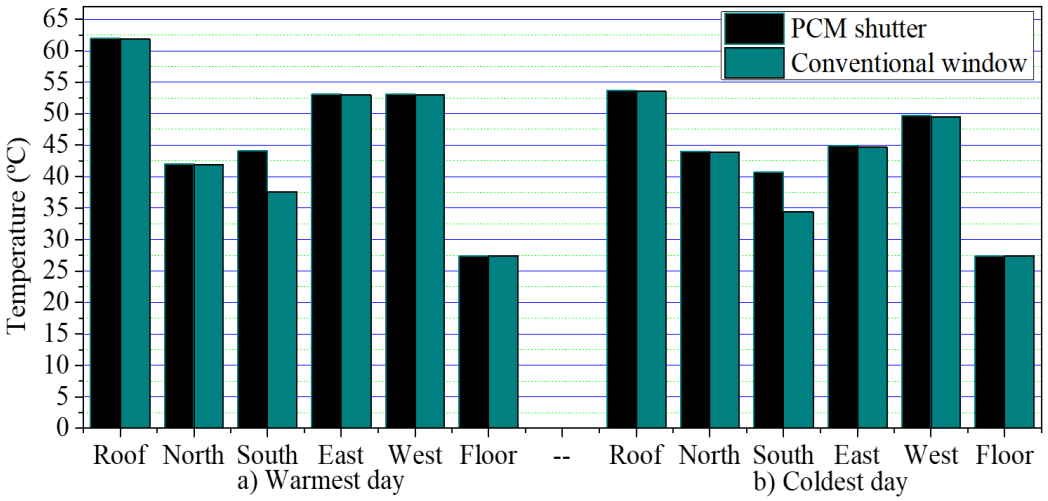

Figure F.2 Comparison between the behavior of maximum temperatures of the envelope elements of the room for both configurations for the a) warmest and b) coldest day of February.

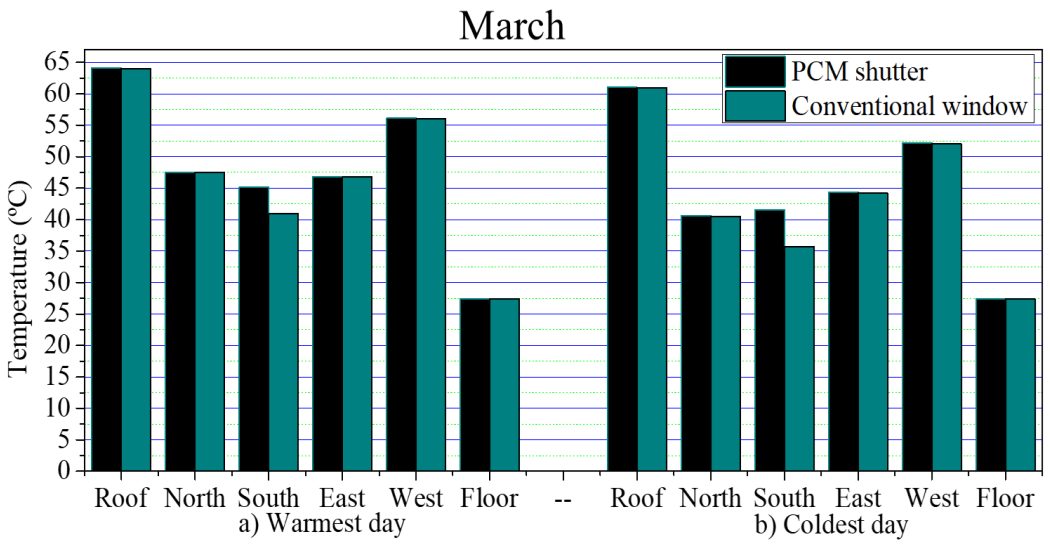

Figure F.3 Comparison between the behavior of maximum temperatures of the envelope elements of the room for both configurations for the a) warmest and b) coldest day of March.

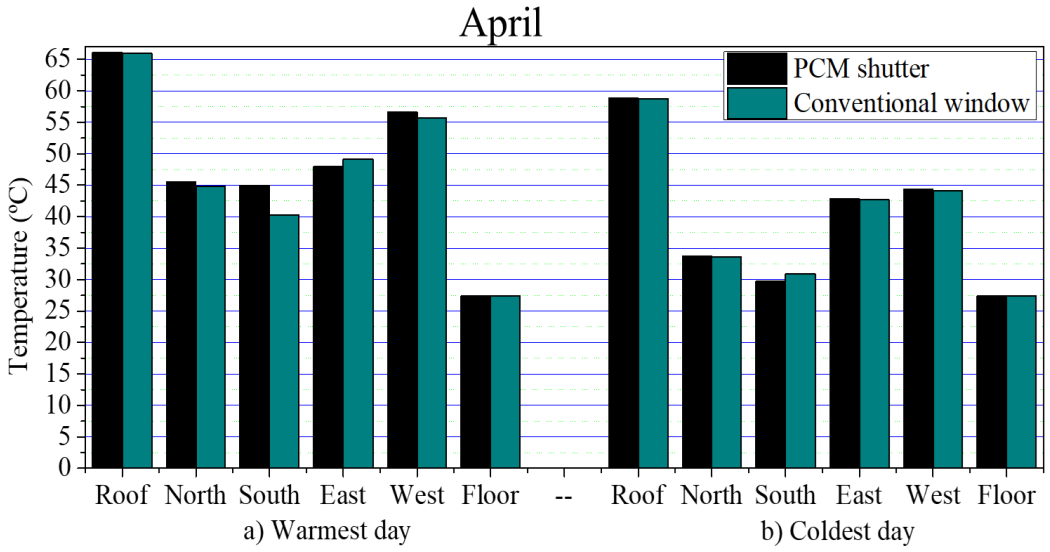

Figure F.4 Comparison between the behavior of maximum temperatures of the envelope elements of the room for both configurations for the a) warmest and b) coldest day of April.

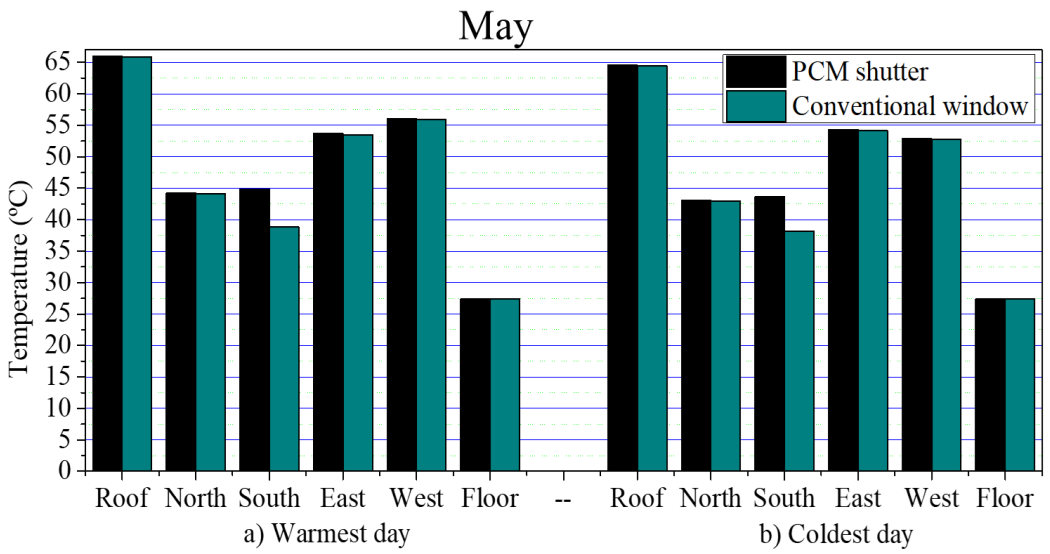

Figure F.5 Comparison between the behavior of maximum temperatures of the envelope elements of the room for both configurations for the a) warmest and b) coldest day of May.

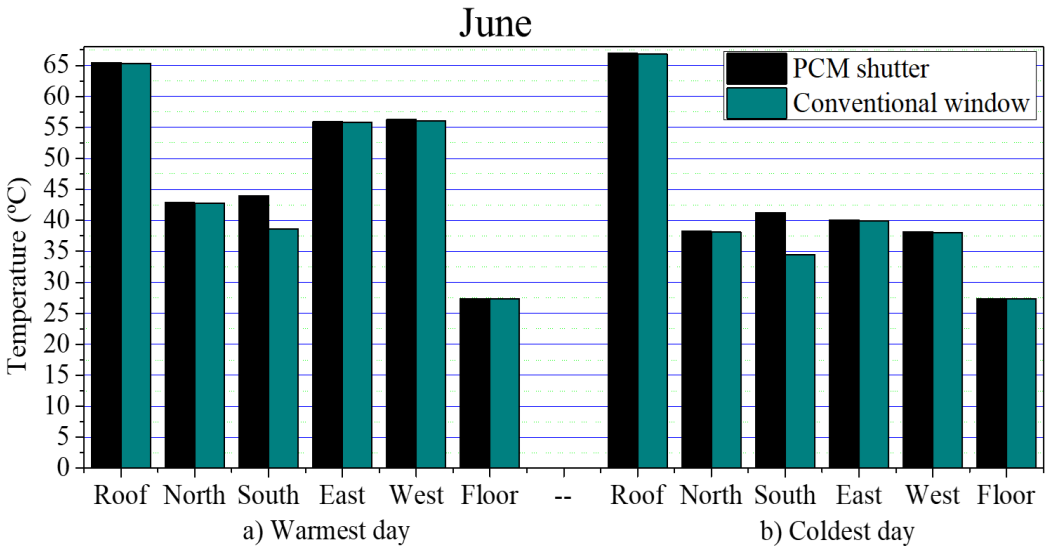

Figure F.6 Comparison between the behavior of maximum temperatures of the envelope elements of the room for both configurations for the a) warmest and b) coldest day of June.

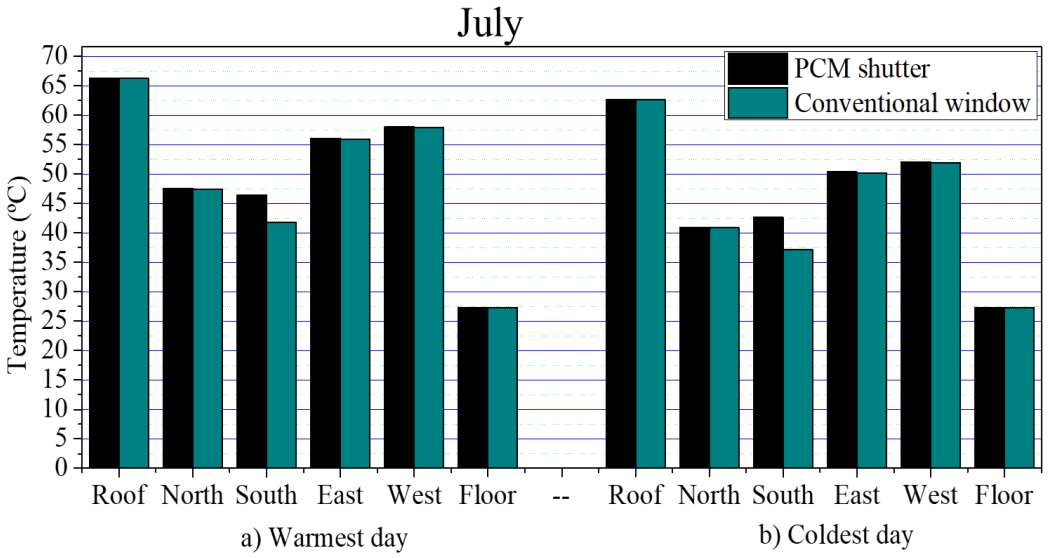

Figure F.7 Comparison between the behavior of maximum temperatures of the envelope elements of the room for both configurations for the a) warmest and b) coldest day of July.

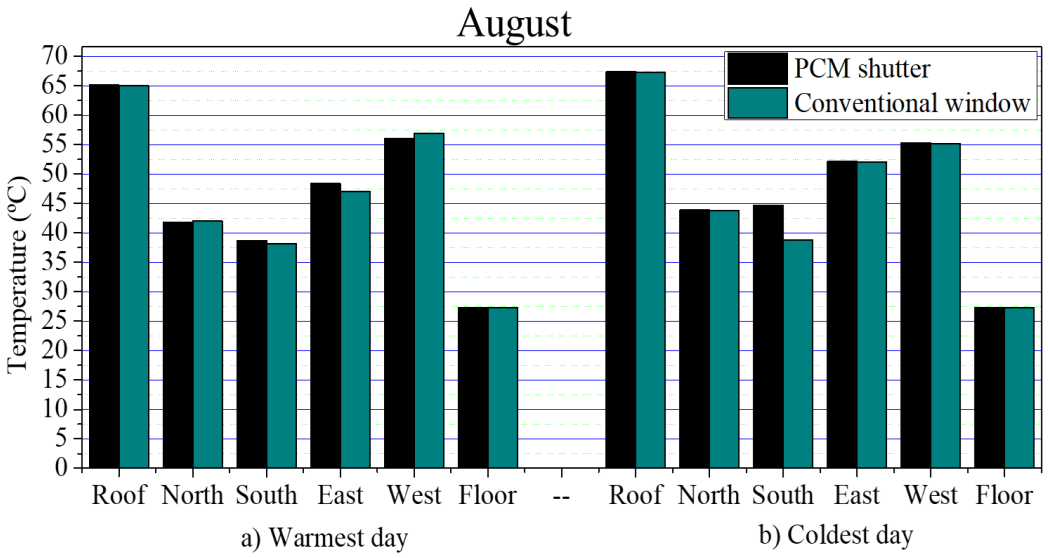

Figure F.8 Comparison between the behavior of maximum temperatures of the envelope elements of the room for both configurations for the a) warmest and b) coldest day of August.

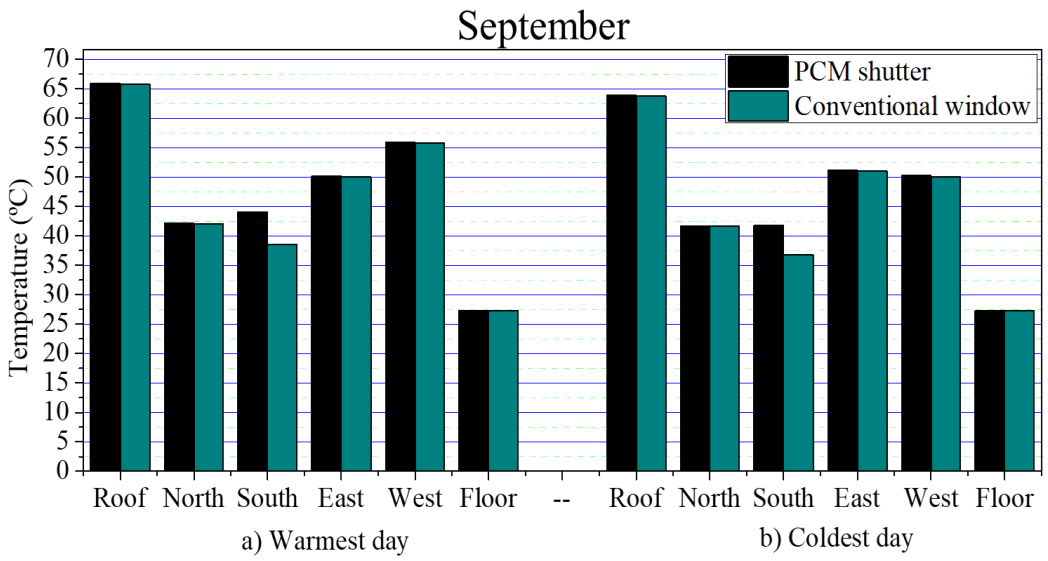

Figure F.9 Comparison between the behavior of maximum temperatures of the envelope elements of the room for both configurations for the a) warmest and b) coldest day of September.

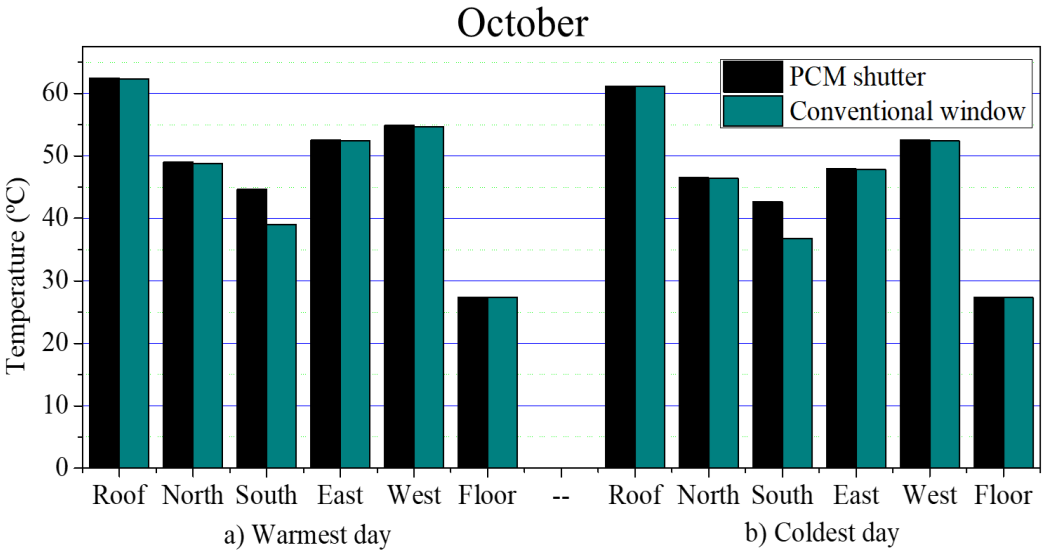

Figure F.10 Comparison between the behavior of maximum temperatures of the envelope elements of the room for both configurations for the a) warmest and b) coldest day of October.

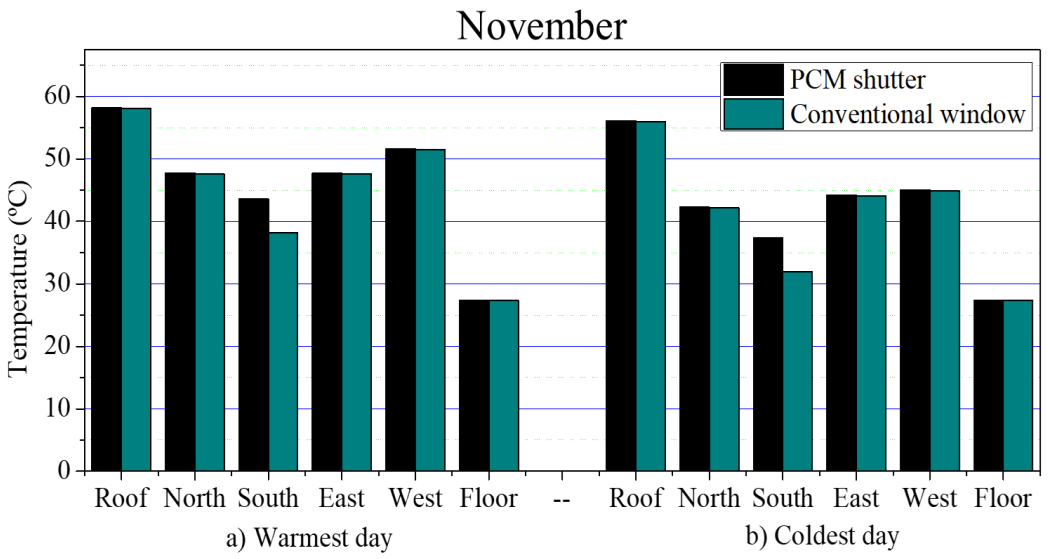

Figure E.11 Comparison between the behavior of maximum temperatures of the envelope elements of the room for both configurations for the a) warmest and b) coldest day of November.

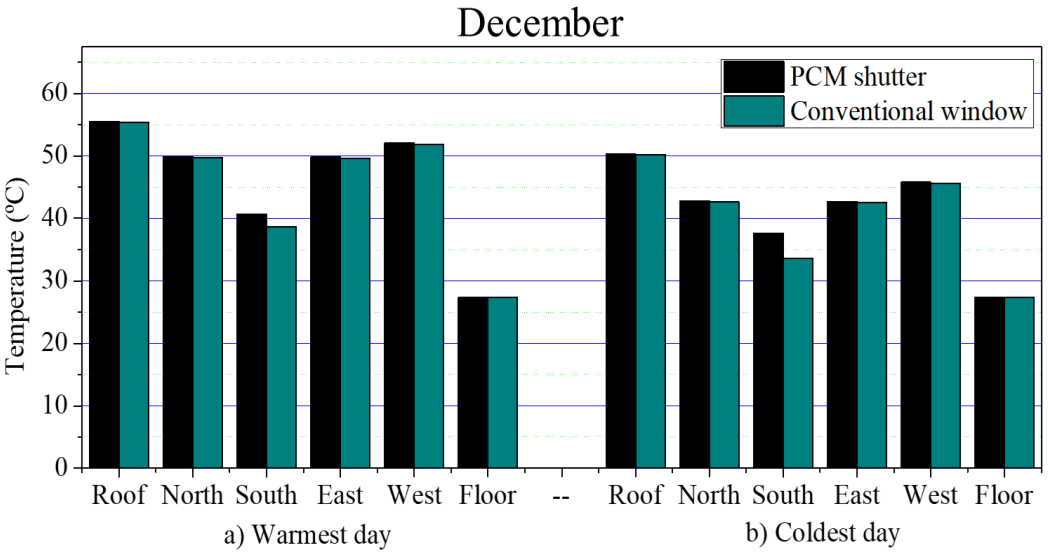

Figure E.12 Comparison between the behavior of maximum temperatures of the envelope elements of the room for both configurations for the a) warmest and b) coldest day of December.

G. Papers

Science of the Total Environment 856 (2023) 158978

Contents lists available at ScienceDirect

Science of the Total Environment

journal homepage: www.elsevier.com/locate/scitotenv

Review

Research and development of green roofs and green walls in Mexico: A review

A. Ávila-Hernández *, E. Simá, M. Ché-Pan

Tecnológico Nacional de México/CENIDET, Prol. Av. Palmira S/N. Col. Palmira, Cuernavaca, Morelos CP 62490, Mexico

HIGHLIGHTS

- The importance of green roofs is to reduce energy consumption in buildings and the UHI effect.
- Thermal and energy behavior of green roofs and walls in the different climates of Mexico.
- Analysis of the development and panorama that Mexico has on green roofs and walls compared to the rest of the world.
- Review of the rules, incentives, and regulations of green roofs and walls.

GRAPHICAL ABSTRACT

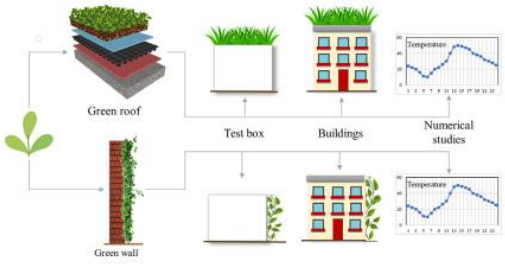

ARTICLE INFO

Editor: Huu Hao Ngo

Keywords:
Green roofs
Green walls
Urban heat island
Energy saving
Green infrastructure laws
Thermal comfort

ABSTRACT

The residential sector is one of the primary energy consumers and emitters of greenhouse gases. Given the environmental problem, one of the methods of mitigating electricity consumption and reducing the temperature in buildings is green infrastructure: green roofs and walls. This article presents a compilation of the studies carried out in México about green infrastructure; the energy, thermal and environmental benefits obtained were analyzed according to the vegetation, substrate, climate, and systems configuration. In addition, the development of policies, laws, regulations, and incentives in the field of green roofs in Mexico was also analyzed. The results indicate that using green infrastructure can help mitigate greenhouse gases since a green roof can reduce the indoor temperature up to 19.9 °C, save 28 % annually in electricity consumption and remove 80 % of rainwater pollutants. Finally, the results of this research can provide insight for researchers, legislators, and urban planners about the state in which Mexico is located, as well as help in decision-making.

Energy & Buildings 281 (2023) 112775

Contents lists available at ScienceDirect

Energy & Buildings

journal homepage: www.elsevier.com/locate/enb

Thermal performance of a window shutter with a phase change material as a passive system for buildings in warm and cold climates of México

M. Che-Pan [a,*], E. Simá [a], A. Ávila-Hernández [a], J. Uriarte-Flores [b], R. Vargas-López [c]

[a] Tecnológico Nacional de México / CENIDET, Prol. Av. Palmira S/N. Col. Palmira. Cuernavaca, Morelos CP 62490, Mexico
[b] Laboratorio de Combustión, División de Termometría, Área Eléctrica, Centro Nacional de Metrología, Km 4.5 Carretera a Los Cués, Municipio El Marqués, C.P. 76246 Querétaro, Mexico
[c] Universidad Autónoma de Guadalajara, Av. Patria 1201, Lomas del Valle, 45129 Zapopan, Jalisco, Mexico

ARTICLE INFO

Article history:
Received 15 October 2022
Revised 19 December 2022
Accepted 4 January 2023
Available online 7 January 2023

Keywords:
Thermal performance
Window shutter
Phase change material
Passive solar system

ABSTRACT

This paper shows the thermal performance of a window system with a shading cover made out of a phase change material (window-PCM shutter). The analysis was the numerical study where conjugated heat transfer was considered on the whole system window-PCM shutter. The modeling was conducted under warm (Merida) and cold weather (Toluca) conditions in México for the warmest and coldest day. Two different phase change materials (PCMs) were selected for the study: Paraffin wax - MG29 and *n*-octadecane. The results show that the *n*-octadecane and the MG29 were capable of keeping the inside comfort temperature for 14:35 and 16:23 h, respectively.

The *n*-octadecane and MG29 reduced the energy of the window-PCM shutter inside surface by 67.3 and 71.6%, respectively, compared to a conventional window. Under cold weather conditions also occurred reductions of heat fluxes by 87.2 (*n*-octadecane) and 83% (MG29) with the window-PCM shutter system compared to a conventional window, causing non-comfort temperatures. The use of a window-PCM shutter is highly recommended under warm weather conditions, given that it showed to be a viable option for energy savings in buildings; however, for its implementation under cold weather conditions of México, it becomes necessary further investigations with other PCMs.